DISSERTATION

Groundwater Contaminant Source Zone Identification at an Industrial and Abandoned Mining Site – A Forensic Backward-In-Time Modelling Approach

Submitted to the faculty of Natural Sciences III

of the

Martin Luther University Halle-Wittenberg

In partial fulfilment of the requirements for the award of the

degree of Doctor of Natural Sciences

By

Dipl.-Geol. Reiner Stollberg

Born on: 05-12-1981 in Wolfen, Germany

Committee: 1. Prof. Dr. rer. nat. Peter Wycisk

2. Prof. Dr. rer. nat. Holger Weiß

3. Prof. Dr. rer. nat. Rudolf Liedl

Submitted: Halle (Saale), 25-04-2012

Date of Defence: Halle (Saale), 28-01-2013

"All models are wrong but some are useful"

George E. P. Box

Declaration of Authorship

I, Reiner Stollberg hereby declare that this thesis and the work presented in it are entirely my own and have been generated by me as the result of my research. All the sources I have used or quoted are signed clearly by means of complete references.

Sign:

Date: 25-04-2012

Acknowledgment

It is a pleasure to thank the many people who contributed to make this thesis possible.

I would like to show gratitude to my advisor Dr. habil. Wolfgang Gossel of the Martin Luther University Halle-Wittenberg for his experiences on modelling he shared with me, the numerous discussions, comments, and his professional support throughout my whole Ph.D. time. With his inspiration and enthusiasm he kept me motivated from the beginning to the concluding level of the thesis, even in tough times. He is a brilliant tutor for students as well as for young scientists, and I am thankful for the excellent teaching content and working material he offered me.

I am indebted to my many student colleagues for providing a pleasant and creative working atmosphere as well as a fun environment. Therefore, I am especially grateful to Thomas Müller, Ronny Lähne, and Christian Wolfig who never grew tired concerning discussions and sudden inspirations even late at night.

A special thanks goes to Ralf Trabitzsch who helped me at all times with his organisation talent on formal urgent matters, on those I was too wearied to clarify or arrange myself.

I owe my deepest gratitude to my parents, grandmothers, and my sister who supported and encouraged me in pursuing my career. Without them, this would have been impossible.

Not to forget my close friends, who I really would like to thank for their support as well as the needed distraction during the hard times. They have always believed in me.

Lastly, I offer my regards and blessings to all of those I did not mention here, who supported me in any respect during the completion of the project.

Table of Contents

Abstract

When a contamination in groundwater is observed by groundwater monitoring or some appropriate exploration technique, the origin of pollution is not necessarily known, mostly unknown or only suspected. But dealing with contaminated sites, the zoning of contaminant source location(s) constitutes an essential component for an optimal site remediation management, for designing and implementing efficient remediation strategies, or for assigning liability with respect to the "polluter-pays" principle.

Numerical modelling of groundwater flow and solute transport provides a favourable approach for a model-based source localisation in hydrodynamic complex systems. This can be implemented either heuristically by using conventional transport modelling or by inverse modelling. Nevertheless, these methods mostly involve fundamental model simplifications and/or require numerous simulations due to their iterative behaviour. Therefore, retrospective transport modelling, initiated from an affected reference location, represents a further promising technique that has the major advantage of receiving information about prior transport pathways and a source indication from a single simulation run. This practise is widely applied by using reverse particle tracking.

This work introduces transient 3-D backward-in-time transport modelling for source identification problems, which is based conceptually on the adjoint model of the classic advection-dispersion equation for simulating solute transport in groundwater. Related to advective-based particle tracking, this technique additionally includes a dispersive transport mechanism being normally present due to material heterogeneities in the subsurface. Both approaches are applied to synthetic contamination scenarios to evaluate their accuracy for the source localisation procedure of previously assigned mass sources. The virtual studies specify (I) experimental simulations in a transient 2-D model environment and (II) a transient 3-D case study of the industrial and abandoned mining area Bitterfeld-Wolfen.

Obtained results indicate a significantly higher accuracy of forensic backward-in-time transport modelling for the localisation of mass sources than received from the commonly used reverse particle tracking technique. While the generated pathlines of the tracking technique tend to be consistently underestimated with respect to their pathline lengths and only indicate the direction of prior solute transport, backward location probability estimates of retrospective transport modelling enclose the source location(s) in most cases entirely. Here the usage of location probability estimates from multiple reference locations decreases the model uncertainty for the localisation additionally.

This work has shown that transient 3-D backward-in-time transport modelling provides a favourable and more accurate technique for source identification problems than the commonly utilised reverse particle tracking method.

Kurzfassung

Im Falle des Nachweises einer Grundwasserkontamination ist die verursachende Schadstoffquelle oftmals nicht bekannt, nicht eindeutig zuordenbar oder kann anhand lokaler Faktoren nur vermutet werden. Eine eindeutige Lokalisierung ist jedoch unabdingbar für die Planung, Dimensionierung und Implementierung von effizienten Sanierungsstrategien eines belasteten Aquifers. Zudem erfordern auch die Grundsätze der Zustandsstörer- bzw. Handlungsstörerhaftung im Rahmen der rechtlichen Nachsorgepflicht eine eindeutige Zuordnung des Quellherdes.

Die numerische Simulation von Strömungs- und Transportprozessen im Grundwasser eignet sich für eine modellbasierte Lokalisierung von potenziellen Schadstoffeintragspunkten in hydrodynamisch komplexen Systemen. Dies kann auf Basis einer rein heuristischen Simulation des Stofftransportes oder auch durch eine inverse Modellierung umgesetzt werden. Beide Techniken gehen jedoch zumeist einher mit starken Simplifikationen des zu untersuchenden Systems und/oder erfordern zahlreiche Simulationsläufe entsprechend ihrer iterativen Implementierung. Eine retrospektive Abbildung des Stofftransports, ausgehend von Referenzlokationen wie z.B. belasteten Grundwassermessstellen, stellt eine weitere vielversprechende Lösungsstrategie dar. Wesentliche Informationen wie z.B. frühere Austragspfade und potenzielle „Herkunftsgebiete" (Quellen) können dabei bereits durch einen einzelnen Simulationslauf abgebildet werden. Eine Umsetzung kann unter Verwendung der etablierten rückwärtigen Bahnlinienmethode (reverse particle tracking) erfolgen.

Die vorliegende Arbeit führt eine innovative und zugleich präzisere Technik zur Identifikation von „unbekannten" Schadstoffquellen ein und basiert auf dem klassischen Advektion-Dispersion-Ansatz zur Beschreibung von Stofftransportprozessen im Grundwasser. Im Vergleich zur advektiven Bahnlinienmethode berücksichtigt die advektiv-dispersive retrospektive Transportmodellierung (backward-in-time transport modelling) zusätzlich den dispersiven Anteil des Transportprozesses im Grundwasser. Zum Methodenvergleich wurden beide Verfahren auf synthetische Kontaminationsszenarien angewendet, um deren Eignung und Charakteristika für eine modellbasierte Lokalisierung der zuvor definierten Eintragsquellen zu untersuchen. Die virtuellen Szenarien beschreiben (I) experimentelle Simulationen eines instationären 2-D Problems und (II) eine instationäre, realitätsnahe 3-D Fallstudie in der ehemaligen Industrie- und Bergbauregion Bitterfeld-Wolfen.

Die Simulationsergebnisse der retrospektiven Transportmodellierung weisen eine generell höhere Genauigkeit für die Abbildung potenzieller Eintragsflächen auf als die der zu vergleichenden Bahnlinienmethode. Während die advektiven Bahnlinien, im Sinne gedeuteter Transportdistanzen, regelmäßig unterrepräsentiert waren und lediglich die Richtung des Stofftransportes indizierten, so konnten die zuvor definierten Eintragsflächen durch die forensische advektiv-dispersive Simulationstechnik mehrheitlich eindeutig ausgewiesen werden. Insbesondere die Berücksichtigung mehrerer Referenzlokationen reduzierte die bestehende Modellunsicherheit erheblich.

List of Figures

List of Tables

List of Symbols and Abbreviations

α_L	Longitudinal dispersion length	[L]
α_T	Transversal dispersion length	[L]
A	Area	[L²]
ADE	Advection-Dispersion-Equation	[-]
BC	Boundary condition	[-]
c	Leakage factor	[L²/T]
C	Solute concentration	[M/L³]
C_a	Sorbed phase	[1]
d	River bed thickness	[L]
D_d	Effective diffusion coefficient	[L²/T]
D_L	Longitudinal hydrodynamic dispersion coefficient	[L²/T]
D_T	Transversal hydrodynamic dispersion coefficient	[L²/T]
D_x	1-D dispersion coefficient	[L²/T]
Δh	Hydraulic head variation	[L]
Δt	Temporal variation	[T]
GUI	Graphical User Interface	[-]
h	Hydraulic head	[L]
h_{sw}	Hydraulic head of the surface water body	[L]
K_d	Henry distribution coefficient	[M/L³]
k_f	Hydraulic conductivity	[L/T]
K_F	Hydraulic conductivity tensor	[L/T]
k_{ij}	Hydraulic conductivity tensor element	[L/T]
L	Distance	[L]
$\vec{n}$	Area of surface normal	[L²]
n_e	Effective porosity	[-]
p	Backward location probability	[-]
P	Backward location probability distribution	[-]
PDE	Partial Differential Equation	[-]
Q	Volume of water	[L³/T]

R	Retardation factor	[-]
ρ_S	Density of dry matrix material	[M/L³]
S_0	Specific storage	[L^{-1}]
t	Time	[T]
t_0	Initial time	[T]
T	Tortuosity	[-]
T	Backward travel time probability	[T]
v	Specific discharge	[L/T]
v_a	Flow velocity	[L/T]
v_n	Specified water flux	[L³/T]
v_c	Reduced flow velocity (retardation)	[L/T]
vC	Specified mass flux rate	[M/L³]
x_0	Initial spatial coordinate	[L]
x	Spatial coordinate	[L]
y_0	Initial spatial coordinate	[L]
y	Spatial coordinate	[L]
z_0	Initial spatial coordinate	[L]
z	Spatial coordinate	[L]

1 Introduction

1.1 Introduction to forensic modelling

The presented forensic modelling concept provides an integrated and novel approach with respect to the remediation management optimisation of multi-source contaminated sites. Once a contamination has been detected within an aquifer system, the knowledge about the source location and release recovery is substantial for the implementation of an effective groundwater remediation strategy.

While plume management approaches such as pump-and-treat, reactive barriers, natural attenuation, and enhanced natural attenuation are feasible approaches for site remediation where the position of the source(s) is unknown or inaccessible (BECKER *et al.* 2006, TEUTSCH *et al.* 2001), these options appear partially ineffective, as the required timeframe for the in-situ depletion often is inestimable. Therefore, source removal by excavation or containment constitutes the more effective remediation strategy since it will lead to a significant and sustainable reduction of the contaminant emission (GRATHWOHL 1998). However, its application requires a clear source localisation! Moreover, with respect to the "polluter-pays" principle, the assignment of liability constitutes an essential part for the site remediation progress which is additionally based on a clear source zone localisation. The presented forensic modelling concept combines robust and accurate techniques for source identification problems under transient field scale conditions.

Numerical transport models, such as MT3DMS (ZHENG & WANG 1999), FEFLOW (DIERSCH 2009a), or e.g. FEMWATER (LIN *et al.* 1997), are applicable to simulate solute transport processes in systems of three-dimensional scale. Whereas future predictions on the plume development can be realized by classical advective-dispersion transport modelling (forward-in-time modelling), the forensic aspect, the estimation of probabilities on source locations and travel times, is a challenging concept. In principle, source identification can be done heuristically by using conventional transport modelling but is highly time-inefficient in regards to the numerous simulation runs needed. Thus this approach will fail at the scale of real-world model scenarios due to an extensive computational effort. Reverse particle tracking as well as backward-in-time modelling are promising alternatives regarding classical forward oriented transport modelling.

Reverse particle tracking is the classical approach for capture zone delineation of groundwater observation wells and was applied recently by VISSER *et al.* (2009), INOUE *et al.* (2009), MOUTSOPOULOS *et al.* (2008), ROCK & KUPFERSBERGER 2002, and VASSOLO *et al.* (1998). Its methodology is based on the placement of imaginary particles at observation well locations which are tracked subsequently backward in time, upgradient to the negative velocity field of the aquifer. As a result, particle pathways and end points define the probabilistic capture zone of the considered observation well. Conceptually, this approach is also applicable for contaminant source identification. For this purpose, particles are induced

at model locations which are characterised by contamination presence. From a conceptual point of view, particle tracking is only controlled by the advective transport process and does not account for dispersion effects caused by material heterogeneities of the aquifer. With respect to this, advective particle tracks theoretically often tend to follow a narrower and underestimated path and ultimately comprise some uncertainty for the process of source identification and travel time recovery.

Backward-in-time transport modelling is a promising and more accurate alternative to describe prior locations or travel time probabilities, since it is based on the classic formulation for describing solute transport processes in groundwater – the advection-dispersion equation (ADE). Theoretical foundations can be traced to the work of WILSON & LIU (1994, 1997), and NEUPAUER & WILSON (1999, 2001, 2004). In general, the backward-in-time transport model represents the adjoint model of the classical advection-dispersion equation (ADE). Since this model approach considers aquifer heterogeneities by the dispersion term, derived probability estimates are more accurate than probabilities obtained from reverse particle tracking. NEUPAUER & WILSON (2005) applied backward advective-dispersive modelling for capturing zone delineation of a pump-and-treat remediation system at the Massachusetts Military Reservation under steady-state flow conditions. Moreover, FRIND et al. (2006) used the method for the capture zone delineation of the Greenbook Wellfield, Waterloo, and considered steady-state flow conditions, too.

For the current study, the approach of reverse particle tracking as well as backward-in-time transport modelling were applied to source zone identification problems of a meanwhile obtained groundwater contamination of regional scale. Moreover, since real world scenarios are usually characterised by transient system conditions, the concept of backward-in-time transport modelling was modified and extended as being valid under non-uniform model characteristics.

1.2   Purpose and aim of the study

Under methodological aspects the focus is to implement an accurate and robust forensic concept for the identification of unknown contamination sources in the scale of real world scenarios. Therefore, based on numerical groundwater flow and transport models, a forensic modelling approach for source identification problems is applied exemplarily at the complex model scenario of the Bitterfeld-Wolfen megasite. For the numerical modelling procedure the finite element code FEFLOW (DIERSCH 2009) is used. With respect to the demands of the study site, this project focuses the following issues: (1) numerical modelling at a regional scale, (2) the reproduction of the transient and mining affected groundwater flow velocity fields within the regional aquifer system(s), (3) contaminant transport modelling, (4) the application of appropriate modelling techniques for source identification problems in transient model environments, and (5) the evaluation of the chosen techniques concerning their robustness and accuracy.

The Bitterfeld-Wolfen megasite had been affected by excessive impacts of open-cast lignite mining and related chemical industry for more than a century. Residuals from chemical production were deposited in multiple abandoned mining fields without having any base seal protection or respective securing measures. Today, a groundwater contamination of regional scale is present in the upper Quaternary and lower Tertiary aquifer system. The hydrochemical situation is characterised by a complex mixture of organic compounds, dominated by chlorinated aliphatic and aromatic hydrocarbons. Contaminant distribution patterns comprise a high diversity in lateral and vertical scale which cannot be compared to usual single source contaminant plumes. At the same time, within the 150-year-old mining history, the opening of various lignite mining fields and related groundwater withdrawal led to wide ranging changes of the natural groundwater flow regime. Various spatio-temporal changes of regional groundwater flow directions and gradients overlaid significantly the contaminant discharge originating from unsecured deposits and former production sites. In consequence, plume origins of the complex multi-source contaminant distribution cannot be clearly attributed anymore! Moreover, information about pollutant sources, chemical inventory or release history is rare to non-existent. These circumstances complicate substantially the implementation of an effective and sustainable site remediation concept which focuses primarily on effective source remediation options.

According to BECKER *et al.* (2006) and TEUTSCH *et al.* (2001), an accurate designation of unknown contaminant source areas enhances significantly the effectiveness of the local site management, monitoring and remediation strategies, and allows additionally appropriate risk assessment studies.

1.3   Previous work

The Bitterfeld-Wolfen region had been subject of environmental research since the beginning of the 1990s. As the chemical pollution affected various environmental compartments, numerous research disciplines are involved at this area.

The department of Hydro- and Environmental Geology of the Martin Luther University Halle-Wittenberg participated in the broadly based SAFIRA research project, which addressed the rehabilitation of regionally contaminated aquifers (WEIß *et al.* 1997 and WEIß *et al.* 2004). Therefore, the creation of high-resolution geological/hydrogeological 3-D models of the Bitterfeld subsurface (WYCISK *et al.* 2009) as well as the 3-D visualisation of hydrochemical data made a contribution for applied remediation and risk assessment studies. Moreover, a regional long-term numerical flow model of the respective region was established by GOSSEL *et al.* (2009), which is applicable to reproduce mining induced variations of the groundwater flow regime within the historical time frame of 1840 to 2005.

Therefore, profound data was available for the site characterisation of the Bitterfeld-Wolfen case study area.

The general methodology of backward-in-time modelling was applied to contaminant transport problems previously by several techniques, such as stochastic random walk modelling, reverse particle tracking and continuum approaches, which involve an advection-dispersion transport mechanism. Backward-in-time random walk simulations were used by UFFINK (1989), CHIN & CHITTALURU (1994), and KUNSTMANN & KINZELBACH (2000) for the capture zone delineation of pumping wells. Recently, VISSER *et al.* (2009), INOUE *et al.* (2009), and MOUTSOPOULOS *et al.* (2008) used the advective based reverse particle tracking method for capture zone delineation, too. NEUPAUER & WILSON (1999, 2001) showed that backward location and travel time probabilities of a conservative tracer, obtained from a backward advective-dispersive model, represent adjoint states of its resident concentration. NEUPAUER & WILSON (2005) as well as FRIND *et al.* (2006) applied backward advective-dispersive transport modelling for the capture zone delineation of pumping wells in multi-dimensional model domains under steady-state flow conditions.

Here the approach of backward-in-time transport modelling had never been applied before to contaminant source zone identification problems within a complex, three-dimensional, and transient model context.

2 Case study area: Bitterfeld–Wolfen

2.1 Regional Classification

Located in the southeast of Saxony-Anhalt, at the border to Saxony, Central Germany, the model domain Bitterfeld-Wolfen covers an area of approximately 330 km². Surrounded by the major cities Leipzig (distance: 40 km, Saxony), Erfurt (distance: 170 km, Thuringia), Halle (distance: 30 km, Saxony-Anhalt), Magdeburg (distance: 115 km, Saxony-Anhalt) and Berlin (distance: 155 km), the flattened landscape of the Bitterfeld region is characterised by several environmental units. The central part is characterised predominantly by industrial structures, abandoned mining fields, mining lakes, and urban areas.
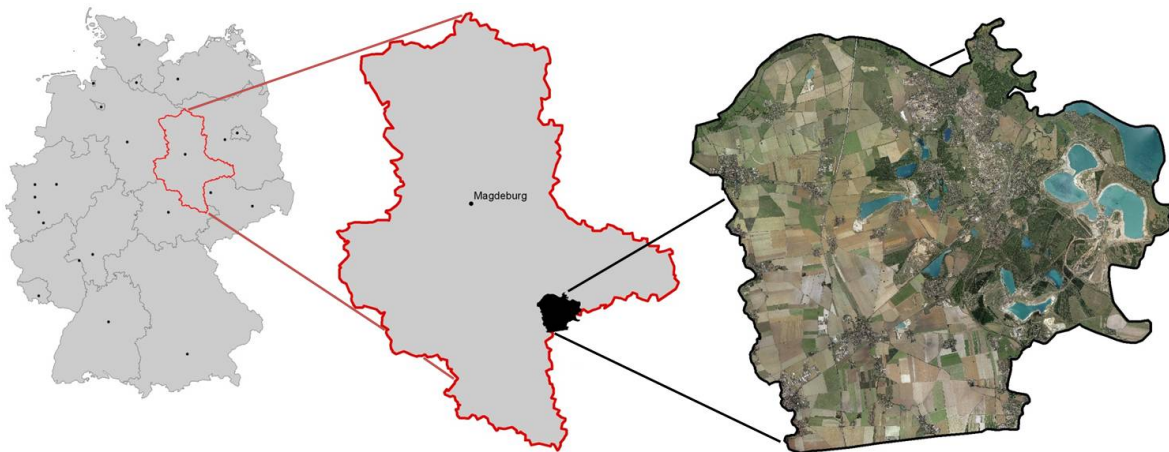
Figure 2-1: The figure illustrates the location of the Bitterfeld-Wolfen study site. The model domain is located in the southeast of Saxony-Anhalt, Central Germany.

Especially the western and southern part comprises loess-dominated areas and related agricultural fields. Expansive heath lands towards the north and the east close the environmental classification of the model domain.

The chosen model boundary is based on the regional surface water system by following individual river courses. In particular, the central part, dominated by the former industrial areas of Bitterfeld-Wolfen and adjacent urban areas, is subject of the numerical modelling procedure.

2.1.1 Climate

According to its meteorological aspects, the region is assigned to the climatic zone of the Leipzig Lowland Plain and is characterised by the continental influenced inland climate of Germany. The region is classified to the water-scarce areas of Germany (precipitation mean

550 mm/year; GRIMMER 2006) due to its eastern location of the Central German Arid Zone, in the rain-shadow area of the Harz Mountains. The annual average of precipitation ranges from 300 mm/yr in drought years to 600-700 mm/yr in rainy years.
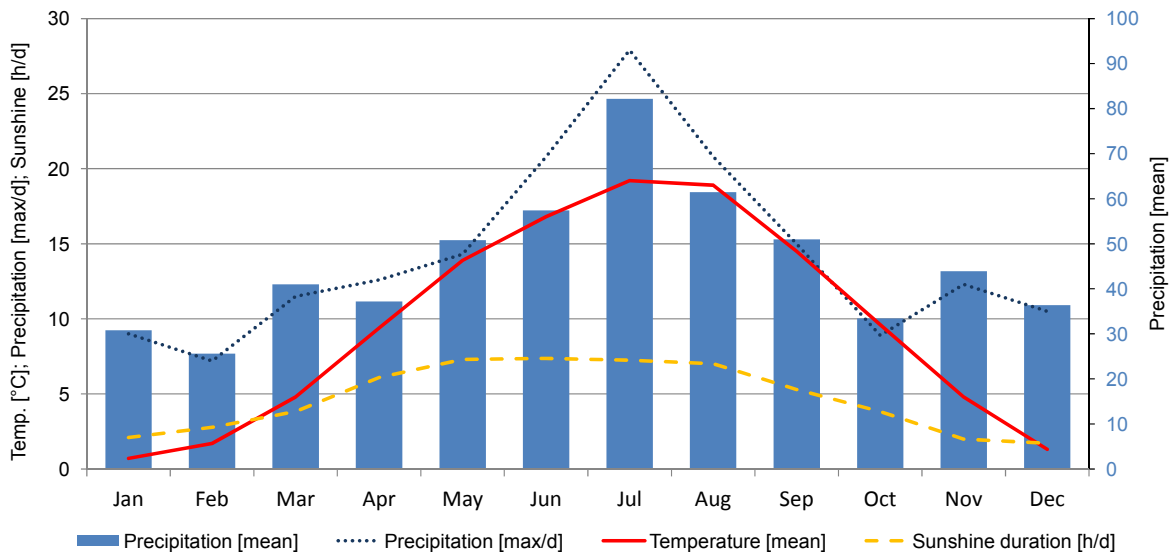
Figure 2-2: Monthly averages of the climatic setting of the Bitterfeld-Wolfen region; since 1991 meteorological data has been collected by the Schkeuditz/Leipzig station (ID: 10469) of the DWD (German Weather Service) on daily basis. The diagram was processed from climatic data of 1991 to 2010, provided by the DWD: www.dwd.de (06/11/2010)

In the course of one year, maximum monthly rain rates occur from June to August, which is associated directly with the rain events of high intensity. Lowest rain rates can be observed in February. The mean annual temperature is about 9.5 °C. In the winter months the mean temperature decreases in maximum down to 0 to -1.0 °C. In the summer months, July and August, the mean temperature is about 18.0 to 19.0 °C. Furthermore, the period of the longest sunshine duration is overlaid by the maximum annual rain rates. This implies a heightened evaporation. Evaporation rates of 400 to 500 mm (WOLFIG 2010) restrain significantly the groundwater recharge with respect to the annual precipitation mean of about 550 mm per year.

2.1.2 Surface Waters

The natural surface water system was severely influenced and restructured due to the extensive open-pit lignite mining activities in the Bitterfeld area. The natural river courses were modified to gain access to the local lignite deposits. The riverbeds of Lober, Strengbach, Leine as well as a large part of the Mulde were rearranged. An overview about the current river course situation is given in Figure 2-3.
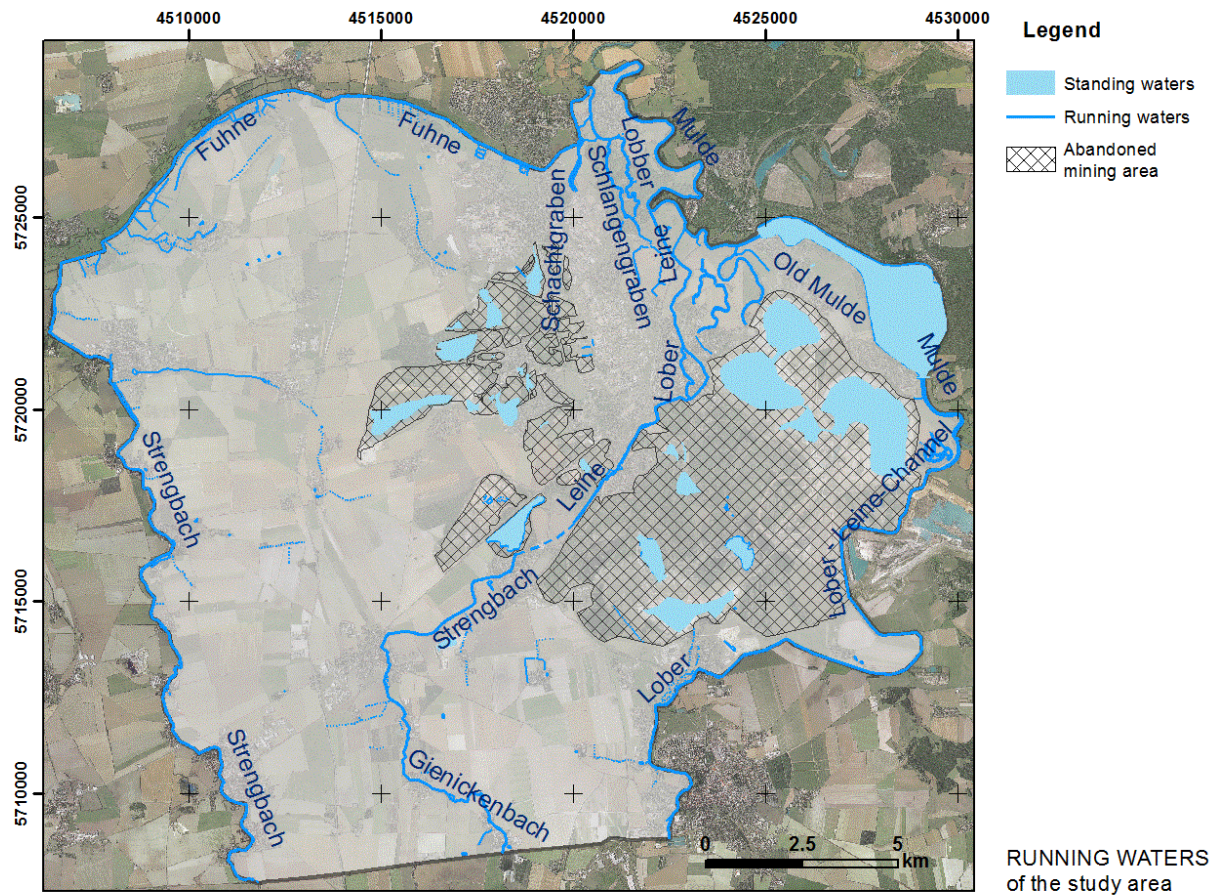
Figure 2-3: Active river system of the model domain; the general river system drains the area towards the north where all individual running waters join the river Mulde. The original river courses of the Strengbach/Lober/Leine system were rearranged due to the extensive mining activities. Background photograph source: http://www.bing.com/maps

In addition, mining induced wide ranging groundwater withdrawal led to enormous groundwater drawdown cones and ended up in a disorder of the natural waterway system. Therefore, partial running waters required an artificial water supply to ensure an ecological minimum runoff of the complete surface water system. With the end of active mining, dewatering was not necessary anymore and the remaining open-pits were flooded. Today, the risen mining lakes constitute a landscape feature of the Bitterfeld-Wolfen region.

The upper Saalian aquifers, embedded in the Saalian till complex, drain into the northern located Lober–Leine–Strengbach catchment area. Thus, the regional surface water system is loaded from the south. The main receiving water Mulde forms the north-eastern boundary. The flood plain area and the river course of the Fuhne bound the model area towards the north.

Several river bed arrangements had been realised in consequence of the lignite mining. Besides the major rearrangement of the Mulde river course, as a grand hydro-engineering solution, river courses of Leine, Lober, and Strengbach were also modified. The Lober was

7

turned from its natural catchment area into the Leine catchment area. In consequence, the pre-existing watershed between the two rivers collapsed (LUCKNER *et al.* 1995).

Running Waters

The *Strengbach*, having its origin in Saalian glacial fluvial sands, drains into the model domain from the south. Indeed, two individual running waters named Strengbach are situated in the study area. The western joins the Fuhne in the north and characterises simultaneously the western model boundary (Figure 2-3). The inner river is initially named as Gienickenbach and passes the villages Roitzsch and Holzweißig towards the north. Its streambed is partially channelled and fades in two separate streams (Lober and Leine) in the area of Bitterfeld. Fading into the *Lober*, the channel crosses the inner city and ends up in a lake named *Großer Teich*. The natural stream course was interrupted due to the Goitzsche mining field opening and needed to be rearranged. In the following, Lober and Leine were loaded by drainage water of the open cast mine Goitzsche.

In addition to this, *Lobber* and the *Schlangengraben* cross the floodplain forest near Greppin. Their courses are almost natural and show meandering characteristics. Both streams join the *Spittelwasser* in the south of Jeßnitz.

This Spittelwasser creek is the linkage between Lobber/Schlangengraben and the main receiving water Mulde in the north. This shallow creek is characterised by partial swamp-like areas, which implies low stream flow velocities. In the past, the Spittelwasser creek came to the fore due to high concentrations of groundwater pollutants such as Dioxins and HCH isomers observed in the streambed (SCHWARTZ *et al.* 2006 and CONSOIL 2000). The entry of groundwater pollutants was caused by the discharge of industrial waters from the chemical Bitterfeld-Wolfen production site.

The *Fuhne* River is the northern boundary of the model domain and joins the Spittelwasser nearby Jeßnitz. Several small creeks join the Fuhne from the south and the north. Adjacent areas characterise a swampy environment which indicates effluent groundwater conditions (GOSSEL *et al.* 2009).

The *Lober-Leine-Channel* is an artificially created channel system which represents the south-eastern model boundary. The channel generally drains in northern direction and joins the Mulde River in the eastern model area.

The *Mulde* is the largest and major receiving surface water of the study domain. Based on the confluence of two sub-streams, *Zwickauer Mulde* and *Freiberger Mulde*, the origin of the so-called *Untere Mulde* (Lower Mulde) is located in the Erzgebirge Mountains, Saxony. Its catchment contains wide parts of Saxony and joins the Elbe River in Saxony-Anhalt, near Dessau. The river course passes the *Muldestausee*, a former lignite mining field, in the northeast of the model area. Until 1990, the Mulde was loaded with a huge amount of chemical pollutants which originated from the chemical industrial production of the Bitterfeld-Wolfen site. Local pollutants had also been detected in the river Elbe (UMWELTBUNDESAMT

2010, BARTH *et al.* 2007, UMWELTBUNDESAMT 2006, and KALBITZ & POPP 1999) and could be traced up to the North Sea (UMWELTBUNDESAMT 2009).

Standing waters

More than 30 abandoned open pit fields remained in the region from the extensive lignite mining. A detailed overview about the mining complexes is given in chapter 2.2. Due to the lignite winning, overlaying sediments had been cut off which needed to be dumped in neighbouring or abandoned mining fields. The voluminous lignite outtake led to a significant mass deficit which could not be compensated by the remaining sediments and resulted in several mining hollows.

In 1995, Central Germany was characterised by 94 mining hollows of individual size (LUCKNER *et al.* 1995), of which 34 were prepared for flooding in the following 20 years.

The Goitzsche mining field has been the largest mining hollow in the Bitterfeld-Wolfen region. During its operation time, 850,000,000 m³ of overburden had been moved and approximately 317,000,000 tons of lignite was mined.

With the end of active lignite mining, a new environmental concept needed to be developed for the remaining post-mine landscape. In principle, all the mining hollows were organised for a controlled/uncontrolled flooding. Particular areas have been declared as inaccessible protectorates with no urban infrastructure. Other areas have been prepared for local recreation, which includes the infrastructure of Bitterfeld and adjacent villages. In consequence, a seascape of 25 km² as well as a related shoreline of 66 km emerged in the vicinity of Bitterfeld-Wolfen. The 15 km² wide lake *Goitzsche* resulted from the respective mining hollow. This water body is surrounded by several additional mining lakes such as Muldestausee, Mühlbeck, Niemegk, Döbern, Holzweißig-Ost, Holzweißig-West, Freiheit IV etc. (see Figure 2-4).

The major condition for an appropriate flooding process is the warranty of stable slope systems. Therefore, the open-pit peripherals were reconstructed by cutting and filling to create shallow and stable slope systems. Generally, the main objective of the complete renaturation concept for the post-mine landscape was the recreation of a self-regulating water system which additionally includes the interaction between surface waters and the groundwater.

As no water for the flooding process was accessible from mining related groundwater abstraction anymore and the natural groundwater rebound was temporally insufficient, the flooding process was speeded up locally by using additional water loads from nearby surface waters. Therefore, the Goitzsche mining lake was flooded with water of the Mulde River.
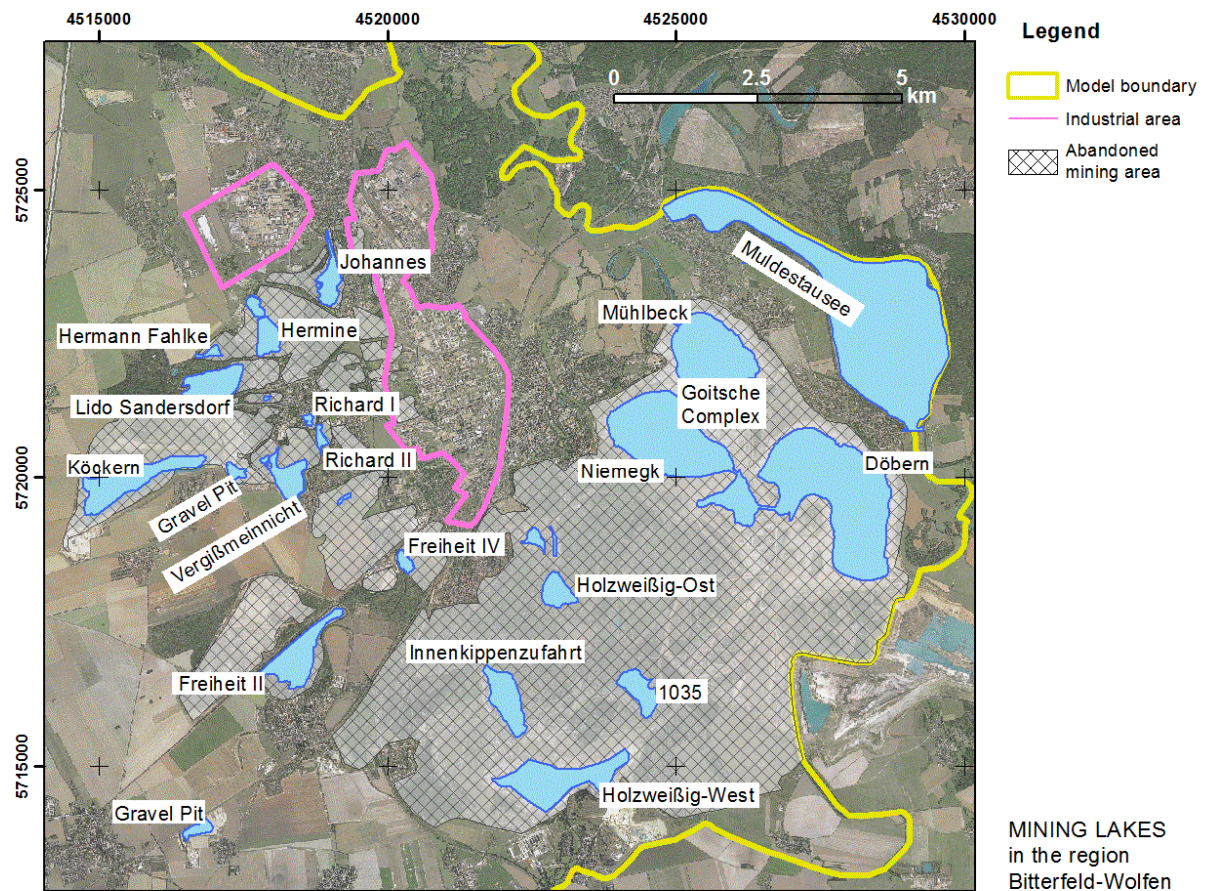
Figure 2-4: Several lakes resulted from the flooding process of former lignite mining hollows. The picture illustrates the mining lake situation in 2001.

2.1.3 Geomorphology

The terrain surface of the model domain is characterised by different environmental units. The western part is structured moderately by a plain of glacial outwash sediments. In contrast, the eastern domain is structured more intensively by different levels of flood plain areas of the Lower Mulde and the prior mining areas. Generally, the relief dips slightly from the south to the north.

The region was mainly formed during the Elsterian and Saalian glacial episode. The inland ice shields reached the area for several times from the north and left multiple intact glacial series. Thus, the region is ranked to the older moraine area of Germany. Particularly the outwash sediments of the Saalian formation form the upper part near the surface. The region was influenced by periglacial conditions during the Weichselian glacial episode, since the Weichselian inland ice shields did not reach the model domain.
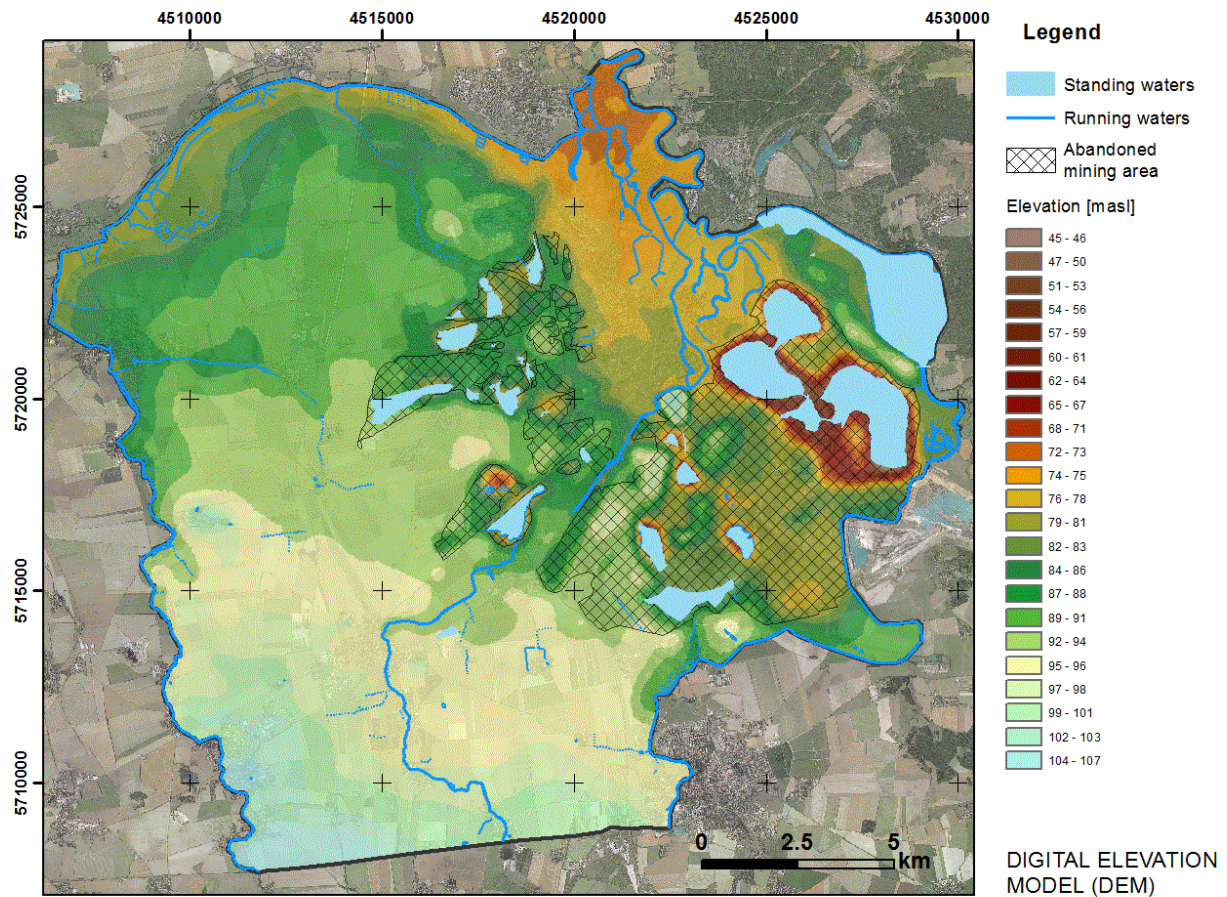
Figure 2-5: The digital elevation model (DEM) of the model was processed from laser scanning data in ArcMap©. The morphology dips slightly from +107.0 m in the south to about +72.0 m in the north. Lower terrain elevations occur in the former mining areas (< +45.0 m) and river valleys. DEM data source: http://srtm.csi.cgiar.org

The relief dips slightly from +107.0 masl in the south to about +72.0 masl in the north. The river courses of the Fuhne at the northern boundary and of the Mulde at the eastern boundary notched the model terrain significantly. Their flood plain elevations differ from +78.0 masl down to +72.0 masl. The Mulde river flood plain in the north and east can reach a width of four kilometres maximum. Its flanks drop away from approximately +90.0 masl down to +72.0 masl in the flood plain centre. Further surface waters such as smaller creeks and channels structured the terrain surface only marginally.

In addition to that, multiple mining fields in the surroundings of the urban areas of Bitterfeld-Wolfen reflect the extensive impacts on the natural terrain (see Figure 2-5). Wide ranging mining activities led to the devastation of the natural geological system and formed an anthropogenic landscape. More than 30 different mining fields of variable size had been opened during the 150-year-old mining history initiated in 1839 (LIEHMANN 1993). Local mining fields reached depths below +40.0 masl.

2.1.4 Geological Settings

The appearance of the Central German lignite mining area comprises a complex geological setting of a differentiated genesis. According to GLÄSEL (1955), the model domain has undergone a fantastic and gradual development in the course of several geological aeons: transgression and regression of the sea, orogeneses, the influence of deserts, spry volcanism, tropical to sub-tropical virgin forest vegetation as well as solidification under snow and ice.

65 million years ago, at the beginning of the Tertiary periods, Central Germany was characterised by favourable conditions for depositing lignite. The tropical to subtropical, wet-warm climate caused rampant vegetation which resulted in a high number of individual lignite seams of variable age. Due to the transgression of the prior North Sea into the Leipzig Bay, huge marine to brackish sediments were deposited and formed the major units of the Tertiary layer. At the turn of the Upper Oligocene to the Lower Miocene, a further regression of this Oligocene Sea led to the deposition of an additional lignite seam complex – *Bitterfelder Flözkomplex*. A following gradual siltation formed a massy clay layer, *Bitterfelder Decktonkomplex*, which overlays the lignite deposits.

The Quaternary period (1.8 million years to present) was characterised by an explicit cooling in north-western Europe since the Miocene. This period is dominated by climatic changes between glacial and interglacial stages. The Pleistocene in Central Germany is separated into three glacial episodes, including two interglacial phases in-between. The inland ice penetrated Central Germany from the north. In particular, the inland ice shields of the Elsterian and Saalian stage crossed and formed the landscape of the model area. Characteristic sediments such as massive gravel bodies, tills, and outwash sediments prove that glacial influence. The Weichselian inland ice did not reach the region of Central Germany. During this period, gravel accumulation in river plains as well as loess deposition took place. Limnic sediments of the Holstein and Eem interglacial episodes separate the glacial stages from each other. The Holocene is characterised by an accretion of river gravel and flood plain loam.

Pre-Tertiary

The Bitterfeld-Wolfen region is located in the area of the Northern-Saxonian-Anticline within the Central German Crystalline Zone and refers to the Bohemian Massif of Central Europe (WIMMER *et al.* 2006).

The basement consists of Pre-Variscan and Variscan folded rocks and is divided into several tectonic blocks. It is crossed and separated by a fault system characterised by a dominating Hercynian strike (Figure 2-6). These segments had been moved tectonically during the Saxonic Orogenesis in the Upper Cretaceous period as well as during the Tertiary period.
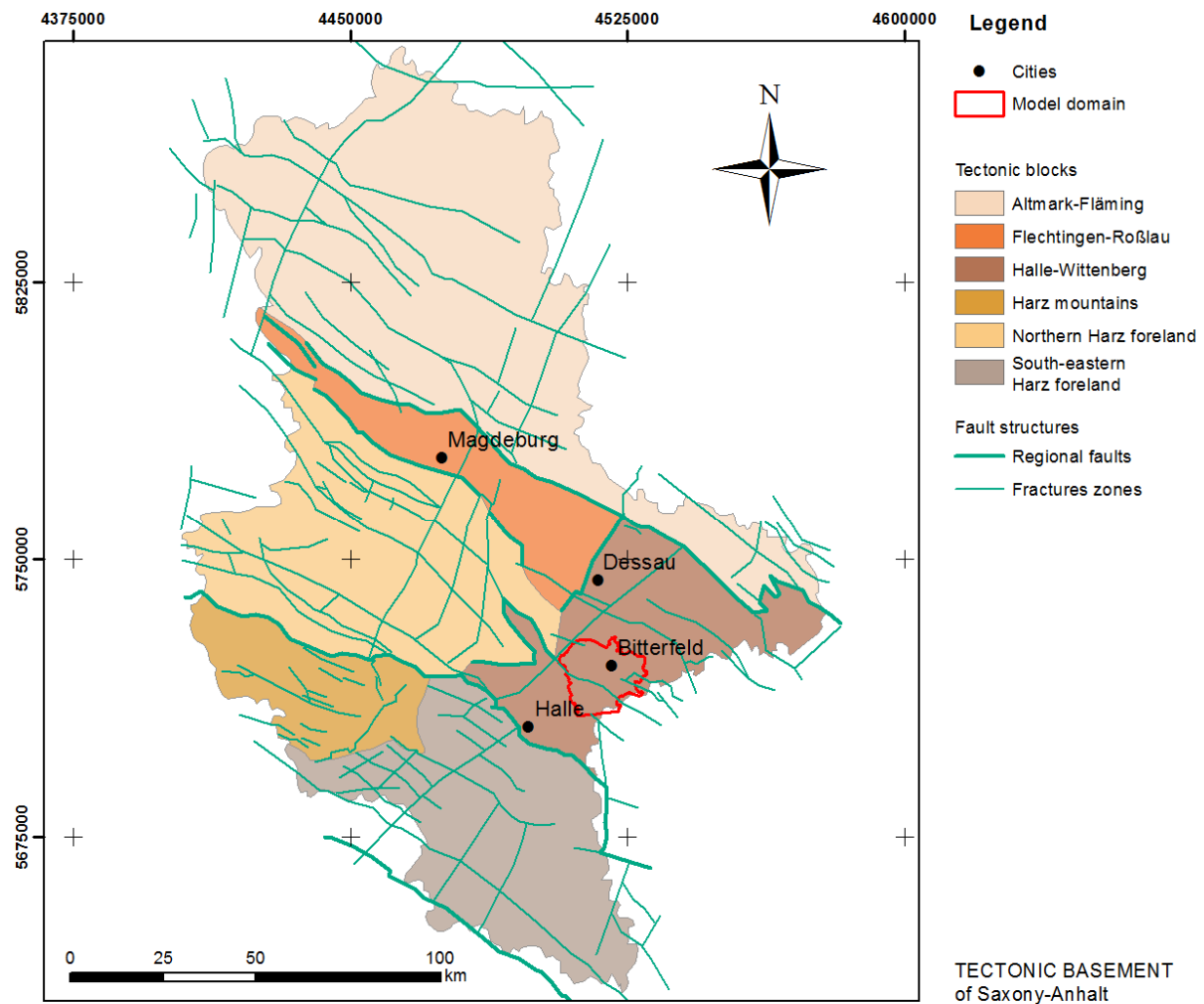
Figure 2-6: The Pre-Tertiary basement of Saxony-Anhalt is structured intensively in several regional geological units and tectonic blocks. (Simplified after LANGE & RAPPSILBER 2008)

Furthermore, the present basement setting was reshaped by halokinetic processes of the saliferous Zechstein formation. Subsequently, this saliferous unit induced upward and downward movements which affected the tectonic system and finally formed the present landscape of Saxony-Anhalt (EHLING 2008).

In general, the subsurface of the model domain is specified by the Halle-Wittenberg block. The Halle-Wittenberg segment is bounded by the Halle fault zone (*Hallesche Marktplatzverwerfung)* in the southwest, the Wittenberg-fault (*Wittenberger Abbruch*) in the northeast and further local fault systems. The major segments of the Halle-Wittenberg element are: the Halle segment, the Bitterfeld-Wolfen segment and the Dessau segment. The study site is assigned to the Bitterfeld-Wolfen segment (Figure 2-7). Primarily, the Pre-Tertiary basement of the surrounding model domain is characterised by Upper Proterozoic and Palaeozoic rocks. A detailed synopsis is given by EHLING 2008. The Proterozoic eon is represented by wide deposits of greywacke, mudstones and siltstones which reach the

hinterland of Leipzig towards the south and southeast. Furthermore, Cambrian rocks with a sand-silt facies form the western margin of the granodiorite massif near Delitzsch. This post-collisional intrusion is of Upper Proterozoic/Lower Palaeozoic age (WIMMER *et al.* 2006). Carboniferous rocks form the central and the northern zone of the Halle-Wittenberg block. These zones are characterized by conglomerates, sandstones, mudstones, greywacke, clay schist, vulcanites as well as thin coal seams (EISSMANN 1994).
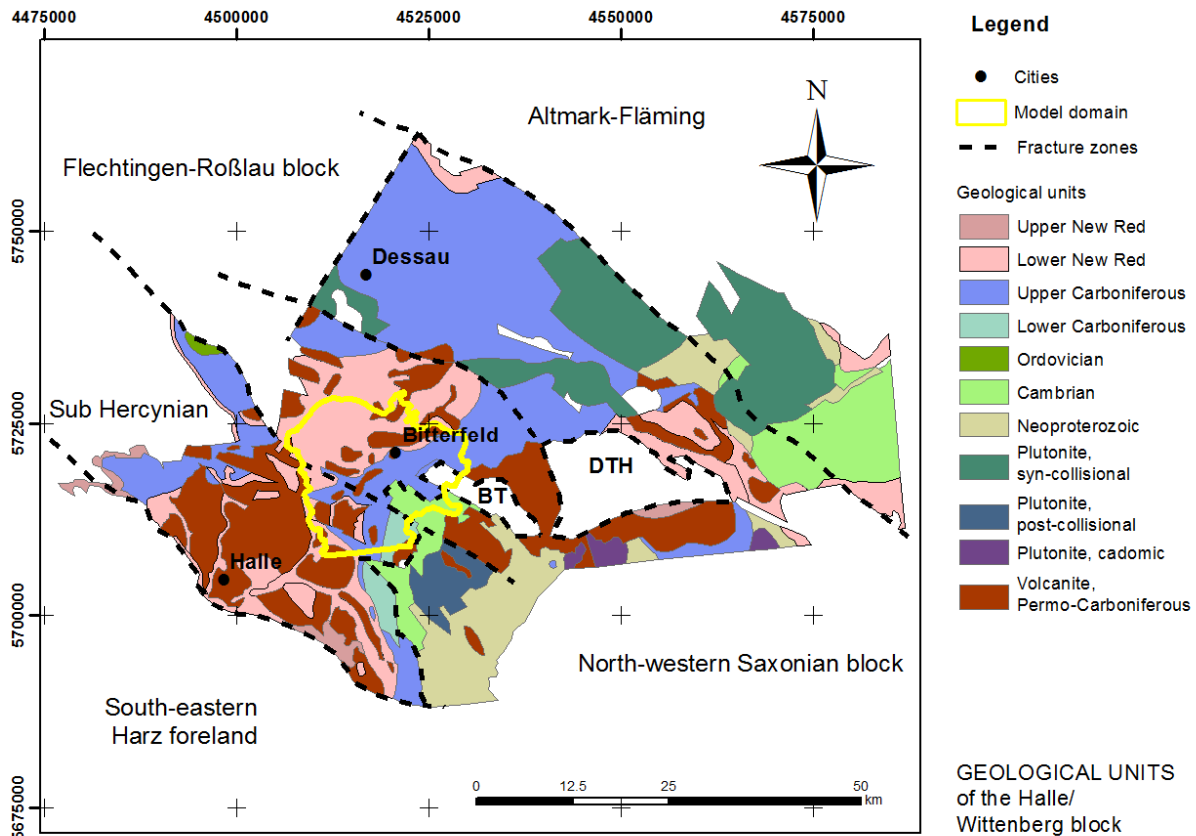
Figure 2-7: Bordered by the "Hallesche Marktplatzverwerfung" in the southwest and the "Wittenberger Abbruch" in the northeast, the tectonic Halle-Wittenberg element contains several rock types of different geological age. (Simplified after EHLING 2008)

Intensive Carbo-Permian volcanism led to a wide ranging occurrence of quartz porphyries which are assigned to the *Hallescher Vulkanitkomplex*. In some parts these vulcanites penetrate the terrain surface in form of porphyry outcrops. These locations can be found in the city of Halle, its neighbourhood, at the *Petersberg*, and the *Muldensteiner Berg* near Bitterfeld.

Zechstein deposits are handed down in trench-like depressions which are filled with carbonate rocks, mudstone, siltstone, anhydrite and gypsum. Especially gypsum and anhydrite units are subject of subrosion processes (lixiviation), which finally led to these

depressions. Subrosion effects were observed within the model domain in the area of Niemegk and near the Bitterfeld trench and cause geological dislocations in the overlaying Cenozoic formation (HAFERKORN 1999; see Figure 2-8). Additionally, large Tertiary brown coal deposits accumulated in these hollows. Prior to the Middle Eocene (Tertiary), the Pre-Tertiary land surface was subject of an intense kaolin alteration which led to a 15 to 35 meters thick kaolin layer at the bottom of the following Tertiary unit (EISSMANN 2002).
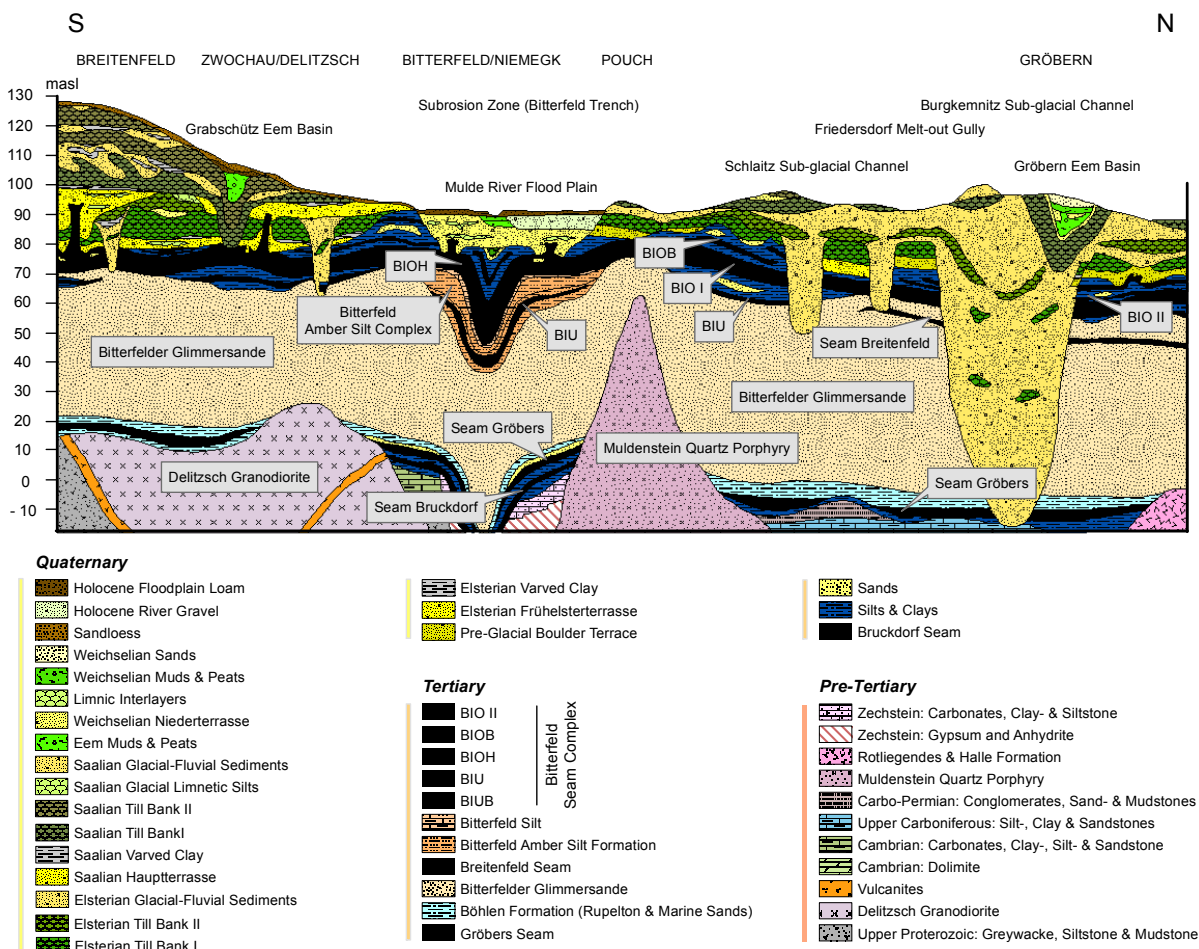
Figure 2-8: Geological cross section of Bitterfeld and its surrounding area; it illustrates schematically the structure of the Pre-Tertiary basement, the Tertiary unit, and the glacial/interglacial sediments of the Quaternary period at the top. Subrosion processes led to dislocations in the overlaying Tertiary/Quaternary sediments. (Simplified after EISSMANN 2002)

Tertiary

During the Paleocene and the Lower Eocene, Central Germany was the subject of several degradation and erosion processes (EISSMANN 1994). A first sediment accumulation is proven in local remains of Lower Eocene age which are linked to subrosion depressions in

the Pre-Tertiary unit. The total thickness of the Tertiary unit ranges from 70 to 80 meters. In local depressions the thickness increases up to 120 meters (STANDKE 2004).

In general, the Tertiary unit consists of sands, silts, clay and lignite seams which were deposited under fluvial (meander river system) and marine (transgression/regression) conditions. Based on this, differentiated sedimentation environments were present. Extensive peat formations were deposited in temporal coastal zones, leading to several seam horizons within the Tertiary unit. These lignite complexes provided the economic basis for the industrial development of the Bitterfeld-Wolfen region.

Associated with clays and sands, the seam horizon *Bruckdorf* is the oldest known lignite seam of the region. Its geological range is limited to depressions of the underlying Pre-Tertiary unit. Followed by a 15 to 20 meter sandy series, a further lignite seam occurs, the seam *Gröbers*. This seam horizon has a larger geological range than the older seam *Bruckdorf*. Its thickness varies between one and eight meters (KRAPP & RUSKE 1992).

A compact and massy silt-clay layer accrued due to a first sea transgression during the Lower Oligocene. The so-called *Rupelton* (Rupelian Clay) has an immense geological range and covers the Pre-Tertiary surface as well as the older Eocene sediments almost completely. This fine clastic layer can be found consistently in a depth of 50 to 60 meters. Its thickness ranges from 10 to 20 meters (KRAPP & RUSKE 1992). The *Rupelton* fades out or is missing in areas of Pre-Tertiary outcrops (e.g. *Muldensteiner Berg* and *Petersberg*). In general, this silt-clay layer is separated into three subunits: a lower silt unit at the basis, a more sandy middle part, and a silt dominated sediment unit at the top (STANDKE 2004). The *Rupelton* is overlaid by the up to 60 m thick marine to brackish sands of the *Bitterfelder Glimmersand* unit.

A representative overview about the Tertiary stratigraphy of the Bitterfeld-Wolfen region is given by drilling log data illustrated in Figure 2-9.

A detailed overview of the *Bitterfelder Glimmersand* (Bitterfeld Mica Sand) horizon is given in WIMMER *et al.* (2004). The sand sequence can be differentiated vertically into four individual sedimentation cycles. An increase of the coarser grain-size category is observed from the bottom to the top. The lowest sedimentation cycle is initiated by an alternate bedding of very fine sandy glauconitic silt, the so-called *Glaukonitschluff* (Glauconite Silt). It is followed by the *Glaukonitsand* (Glauconite Sand) unit consisting of glauconite, silt, and fine sand. The next sediment part contains mica enriched fine and middle sands. A carboniferous silt layer (*Breitenfelder Schluff;* Breitenfeld Silt) or a very thin lignite seam (*Breitenfelder Flöz;* Breitenfeld Seam) occurs locally and separates the Lower Bitterfeld Mica Sands from the Upper Bitterfeld Mica Sands. The top formation is characterised by glauconitic fine sands or alternatively by fine sandy middle sands. The top surface of the Bitterfeld Mica Sand Complex represents a Tertiary palaeo-relief with sedimentary crest and depression structures. It varies from +49 masl in depressions to +70 masl in the crest zones. According to EISSMANN (1994), these structures belong to a dune facies of a former coastal landscape.

A further thin lignite seam, the *Bitterfelder Unterbegleiter*, may occur locally in depression zones while it crops out simultaneously in the crest areas.

Geological Exploration Drilling

name: 2039/95 / location: Bitterfeld East / groundlevel: + 79,96 m

Depth		Description	Formation
			Holocene
6,40		blocking-up	
			Holocene Flood Plain Gravel Of The Muld River
15,30		coarse sand, middle sandy, fine gravelly	
			Lower Miocene Bitterfeld Seam (unsplittet)
24,00		lignite	Upper Bitterfeld Mica Sands (Lower Miocene to Upper Oligocene)
26,00		fine sand, middle sandy	Friedersdorf Amber Silt
26,90		silt, fine sandy	Lower Bitterfeld Seam
27,00		fine sand, silty	Zöckeritz Sands
28,10		lignite	Zöckeritz Amber Silt
29,80		fine sand, silty	
30,00		silt, clayey	
31,10		fine sand, silty, clayey	
31,30		middle sand, fine sandy, silty	
33,00		fine sand, middle sandy, silty	
33,50		middle sand, fine sandy	
			Upper Bitterfeld Mica Sands
			Breitenfeld Silt Horizon
40,40		fine sand, silty	
41,00		silt, fine sandy	
			Lower Bitterfeld Mica Sands (Upper Oligocene)
49,90		fine sand, silty	Glauconite Sand and Silt Complex (Upper Oligocene)
50,00		silt, clayey	
50,50		fine sand, silty	
50,70		silt, clayey, fine sandy	
53,00		fine sand, silty	
54,00		silt, clayey, fine sandy	

Figure 2-9: Exploration drilling: the drilling log provides a characteristic geological Tertiary sequence of the model domain starting from the Glauconite Complex and ending up with the Lower Miocene Bitterfeld Seam Complex. (Modified after WIMMER ET AL. 2006)

The top of the Oligocene Bitterfeld Mica Sand sequence is characterised by fine to coarse sands of the so-called *Bitterfelder Bernsteinschluff* (Bitterfeld Amber Silt). These sediments represent the Bitterfeld amber deposit. Its amber varieties are famous for their fortune of insects which was very important for the economy of the region. The latest information about the genesis of the deposit, different amber varieties, and its mining history is reported in WIMMER *et al.* (2009) and WIMMER *et al.* (2006).

Optimal conditions for formation of lignite prevailed in the northern part of the Leipzig Bay during the Miocene epoch. At the turning point Upper Oligocene/Miocene, a further seam-complex emerged, consisting of four individual lignite horizons. The *Bittferfelder Flözkomplex* (Bitterfeld Seam Complex) is structured into a lower seam (*BiU*), a main seam (*BiOI*), its accompanying seam (*BiOIH*) and an upper seam (*BiOII*). The interbeds range from limnic to fluvial sediments. This seam complex reaches averaged thicknesses between 10 to 13 meters and 20 meters in maximum (EISSMANN 2002). The *BiOI* has been the main subject of the local mining activities. An overview of the mining history is given in chapter 2.2.

The Bitterfeld Seam Complex is covered widely by the so-called *Bitterfelder Decktonkomplex* (Bitterfeld Clay Cover Complex). This complex is characterised by Miocene clays and silts where two or three sandy horizons can be embedded. According to EISSMANN (1994), this grey-blue, highly plastic pelite layer accumulated in a slowly sinking flood area which was reshaped permanently by the presence of a meander river system. The Bitterfeld Clay Cover Complex is the geologically youngest Tertiary unit of the region and closes the Tertiary layer series.

Quaternary

Generally, the Quaternary unit is more structured and geologically more complex than the Tertiary unit. A wide ranging mechanical degradation of the Tertiary sediments was initiated along the former river courses of Saale, Weiße Elster, and Mulde. Subsequently, the advance of Quaternary inland ice shields led to a significant reduction of the transport energy in rivers, which was followed by sediment aggradation of gravels and sands in associated river valleys. Thus, the Quaternary formation is initialised by the occurrence of three pre-glacial gravel terraces and the river gravel of the *Frühelsterterrasse* (Early Elsterian Terrace). The sediments of the Early Elsterian Terrace are mainly characterised by gravel-sands which range in thickness from 5 to 15 meters (EISSMANN 1994). The original geological setting of pre-glacial terraces was decimated for several times by younger Elsterian sub-glacial channel erosion as well as by fluvial erosion of the major receiving waters. Within the model domain, sediments of the Early Elsterian Terrace are handed down by a three to four kilometres wide gravel band along the south-eastern and eastern model boundary.

During the Elsterian Glacial Complex, the model area was run over by the inland ice shields for two times, which left two bulky and locally complete glacial series. These series consist of varved clay at the basis, a bulky till horizon in the middle and are closed by glacial-fluvial and glacial-limnic postglacial sediments. These glacial-fluvial sediments mostly consist of sandy gravels or gravely sands. In some cases, this horizon can be subdivided into a lower and upper part by interbedded limnic silts.

In general, The Elsterian glacial stage is separated into the *Zwickauer Phase* (1) and the younger *Markranstädter Phase* (2).

Initialised by the *Dehlitz-Leipziger Bänderton* (glacial varved clay), the *Zwickauer Phase* (1) is characterised by a Elsterian till of 5 to 10 meters, in maximum 35 meters, which is primarily of homogeneous composition and of grey to green-grey colour (EISSMANN 1994). The younger *Markranstädter Phase* (2) is characterised by its *Miltitzer Bänderton* (glacial varved clay) and a following dark grey till horizon of 2 to 10 meters. Both Elsterian glacial stages are covered individually by glacial-limnic sands and silts as well as by glacial to glacial-fluvial gravels and sands.

Deep and long ranging sub-glacial channels are characteristic for the upper phase of the Elsterian epoch. Such a complex sub-glacial channel system exists in the northeast of the prior Goitzsche mining field. Those glacial spillways notched the underlying Quaternary and Tertiary units down into the Bitterfeld Mica Sands or even reach down to the Pre-Tertiary relief (Figure 2-8). KNOTH (1995) mentioned thicknesses of about 50 to 70 meters, EISSMANN & MÜLLER (1978), even thicknesses of more than 100 meters. These structures are filled with fluvial to glacial-fluvial and glacial-limnic sediments. In addition, they contain erosion rests of Quaternary and Tertiary units such as till blocks and lignite. These melt-out sediments have a larger geological range outside the channel systems, especially in the south-eastern and northern part of the model domain. According to EISSMANN (1975), this sand-gravel horizon is named locally as *Krippehnaer Mischschotter*.

The Elsterian glacial complex is followed by the Holstein interglacial. It is assumed that the Holstein interglacial left locally limnic sediments (sands, silts, and peats) in morphological depressions. Those sediments have not been proven within the model area. It is most likely that these interglacial sediments were reduced significantly by several erosion processes of younger Saalian units.

A re-initialisation of prior existing river systems caused such wide ranging erosion processes of lower Quaternary and Tertiary sediments at the beginning of the Saalian glacial epoch. At the same time, a huge fluvial gravel layer, named *Saale-Hauptterrasse* (Saalian Main Terrace), was deposited by the rivers *Weiße Elster* and the *Untere Mulde*. This gravel layer covers the western part completely with a thickness between 6 and 13 meters. Besides its function as a major stratigraphical horizon of the Quaternary epoch, it contains an archaeological importance due to a high number of Palaeolithic finds (EISSMANN 1994).

The following Saalian glacial complex can be separated into three glacial series – *Zeitzer Phase* (1), *Leipziger Phase* (2) and *Fläminger Phase* (3).

Near *Delitzsch*, the Saalian Main Terrace is widely covered by the first Saalian till horizon of the *Zeitzer Phase* (1). This unit is accompanied by its basal varved clay (*Böhlener Bänderton)* and by glacial-fluvial sands and gravels on the top. These glacial-fluvial sediments can be separated into a lower and upper horizon by embedded glacial-limnic silts and clays.

According to EISSMANN (1994), ice edge oscillations of the Saalian inland ice shields during the *Leipziger Phase* (2) left two intact glacial sub-series: *Bruckdorfer Bänderton* (glacial varved clay), second Saalian till horizon (lower bank), recessional outwash sediments (2a);

Breitenfelder Bänderton (glacial varved clay), second Saalian till horizon (upper bank) and recessional outwash sediments (2b).

Glacial sediments of the *Fläminger Phase* (3) are not present in the study area. Moreover, periglacial redeposition and the accretion of aeolian sediments, such as sand loess and loess, took place (KNOTH *et al.* 1998).

The Saalian glacial complex was followed by another interglacial interval. Limnic sediments (muds, peats and silts) of the Eem interglacial have been found in local deposits near *Zwochau-Grabschütz* (WANSA & WIMMER 1990, see Figure 2-8).

The inland ice shields of the Weichselian glacial episode only reached the northern part of Central Germany and did not penetrate the model domain. Nevertheless, gravel aggradation took place again along the older river routes. The Weichselian *Niederterrasse* was deposited along the Mulde river valley. This gravel body is present in the subsurface of the industrial and urban area of Bitterfeld-Wolfen towards the east. This boulder terrace can be divided into an upper and lower formation with up to four embedded periglacial, silty interlayers (HILLER *et al.* 1991). Periglacial conditions led to aeolian loess and sand loess accumulation, material redeposition and frost-sediment interactions (ALTERMANN & RUSKE 1997).

Due to the Weichselian inland ice recession, its melting, and the defrosting of permafrost soil, a further stage of fluvial erosion was initialised. Based on this, an accretion of sand, gravel and boulder formed the Holocene gravel terrace of the *Untere Mulde*. This Holocene gravel horizon cut into the older Weichselian *Niederterrasse* in the east of Bitterfeld. Fine-clastic flood plain loom at the top of this horizon is common. According to EISSMANN (1994), mud and peat are present in areas of abandoned river courses and low moors. The Quaternary formation is completed by a Holocene pedogenesis.

Due to extensive anthropogenic impacts of open-cast lignite mining, the natural geological structure was destructed in many places. With respect to this, Holocene and Pleistocene units have been affected most. Moreover, wide ranging and inhomogeneous landfills were created by the redeposition of the lignite accompanying sediments.

2.1.5 Hydrogeological Settings

The hydraulic subsurface characteristics of the Bitterfeld-Wolfen area are relatively complex due to the regional geological settings. The hydraulic system is structured into a lower Tertiary aquifer system and an upper Quaternary aquifer system, where several geological sub- units can differ from each other. Primarily the lower aquifer system is almost sealed completely by the *Rupelton* which prevents a probable water exchange to deeper lying horizons. In contrast, multiple hydraulic connections exist between the lower and upper aquifer which provide shortcuts and pathways for groundwater flow and solute transport interactions. Quaternary sub-glacial channels which are located in the central part of the study domain represent high conductivity zones and signify preferential exchange pathways.

The redeposition of overburden at the former mining areas generated a new anthropogenic aquifer unit and led to fundamental changes in the natural groundwater flow regime.

Pre-Tertiary

The Pre-Tertiary basement consists primarily of Precambrian, Cambrian, Carboniferous, and Permian rocks which are traversed by several tectonic fault zones. The basement includes conglomerates and sandstones which need to be classified as potential pore aquifers. Groundwater exchange along crossing fault structures, between the Pre-Tertiary formation and younger geological units, seems to be plausible. The top part of the Pre-Tertiary basement is kaolinised intensively and is acting therefore as a consistent aquitard at the bottom of the Tertiary sequence. This low permeable layer is only missing locally in areas where post-collisional intrusions or Permo-Carboniferous volcanics penetrate the Pre-Tertiary top part. Hence, at a regional scale, a vertical water exchange between the Cenozoic formations and older geological units can be excluded almost completely. A feasible groundwater exchange might only be present along subrosion zones.

Tertiary

The Eocene lignite seams *Gröbers* and *Bruckdorf* in combination with their impermeable accompanying sediments constitute a hydraulic barrier effect at the bottom of the Tertiary unit. This lower sediment package is widely overlaid by the Oligocene *Rupelton* aquitard, which has a fundamental role in preventing a probable groundwater exchange between the Cenozoic aquifers and lower formations. Thus, potential occurring pollutant discharge into Pre-Tertiary units is limited. This aquitard is only missing in areas where Pre-Tertiary units, such as intrusion rocks, penetrate Cenozoic formations (Figure 2-8).

The following *Bitterfelder Glimmersand* aquifer constitutes the major aquifer unit of the model domain. This sand aquifer varies in its thickness from 30 to 50 meters and covers an area of several thousand square kilometres. According to KRAPP & RUSKE (1992), the hydraulic conductivity of the marine to brackish sands range from $1 \cdot 10^{-4}$ to 10^{-5} [m/s]. Related to its thickness and its hydraulic conductivity values, this sand layer is characterised by a high transmissibility and retention capacity. From a hydrogeological point of view, the *Bitterfelder Glimmersand*e can be separated into three sub-units. This is based on its characteristic sediment layering, where a significant increase in grain size is observed from the bottom to the top of the layer (see Figure 2-9). The aquifer remained almost unaffected by the long-term mining activities. However, safe lignite mining required a technical drainage of the overlaying hydrogeological units which was installed primarily in this *Glimmersand* horizon. As mentioned previously, existing hydraulic connections to overlaying younger units, e.g. by sub-glacial channels, suggest an active groundwater circulation in vertical direction.

Within the top section of these marine to brackish sands, a thin-banded seam *Breitenfeld* can be embedded. In combination with its impermeable accompanying sediments such as silt and clay, it serves as a confining aquitard.

The *Bitterfelder Glimmersand* aquifer is overlaid by the *Bitterfelder Flözkomplex,* including all its individual seam horizons, accompanying silts and clays, and intervening sand pockets.

This horizon can reach a thickness to about 20 meters and serves then as a consistent aquitard (hydraulic conductivity: $5 \cdot 10^{-5}$ - $1 \cdot 10^{-7}$ after WEIß *et al.* 2002) between the Tertiary aquifers and younger Quaternary units. Due to extensive lignite mining activities as well as natural erosion structures (e.g. glacial boulder terraces/sub-glacial channels), several aquitard gaps are present which provide favourable migration pathways (Figure 2-10).
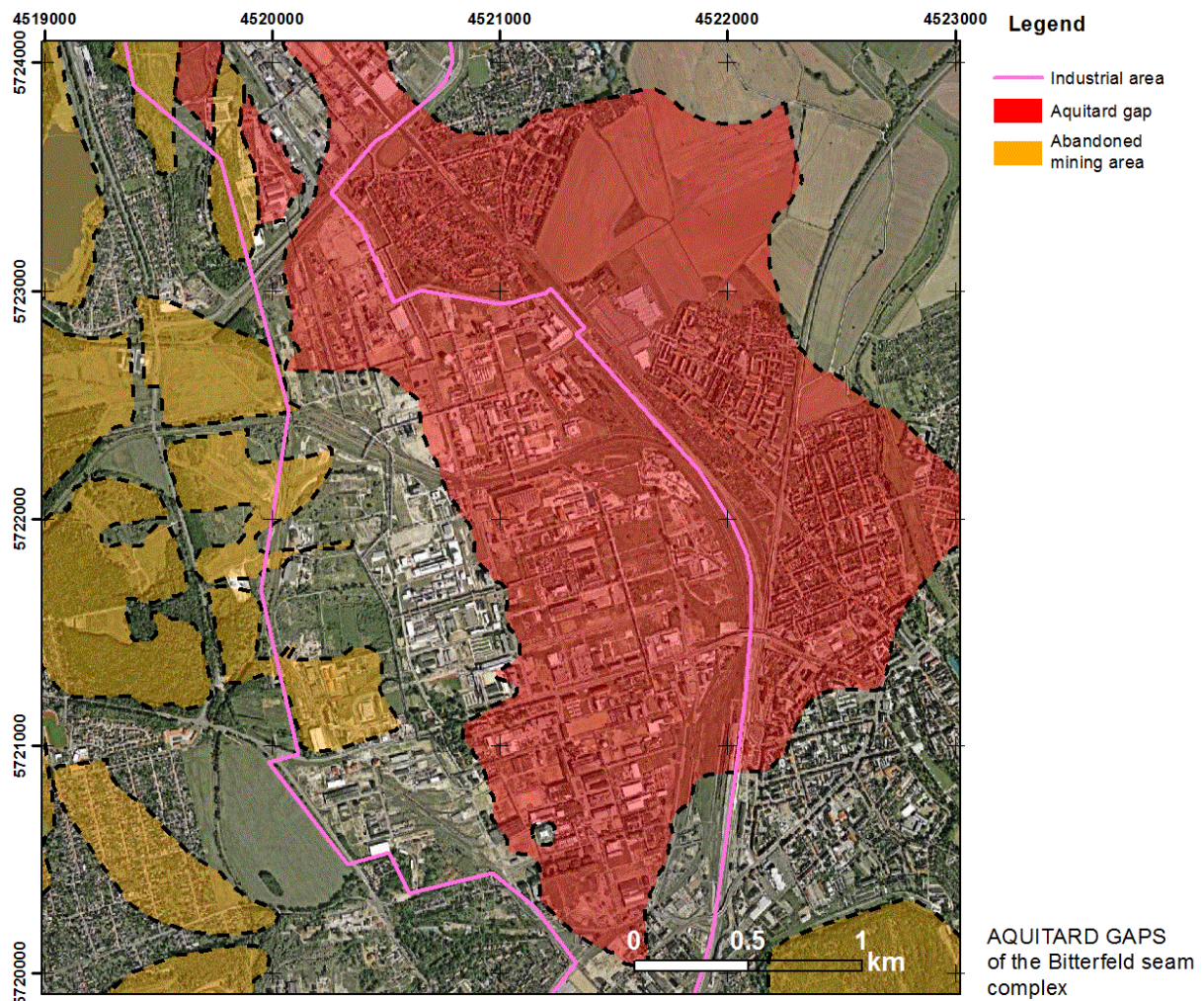
Figure 2-10: Hydraulic connections provide pathways and shortcuts for groundwater/contaminant exchange between the lower Tertiary and the upper Quaternary aquifer. Those aquitard gaps arose due to natural erosion processes as well as anthropogenic mining activities.

Miocene silts and clays of the *Bitterfelder Decktonkomplex* overlay the seam complex directly. Up to three different sand units can be embedded in this bulky clay horizon. Those sand units vary greatly concerning their lateral and vertical dimensions as well as sediment characteristics. Basically, the *Bitterfelder Decktonkomplex* represents a massy aquitard. Those embedded sand units join each other locally and provide some hydraulic connections between upper and lower aquifer units. Here, the *Roitzscher Flusssand Zone* near the village Roitzsch is mentioned where all these individual sand and gravel horizons merge. At this location they provide a hydraulic linkage between the Tertiary *Bitterfelder Glimmersand* aquifer and the Quaternary *Saale-Hauptterrasse*.

Quaternary

From a hydraulic point of view, the Quaternary hydrogeological system is much more structured than the lower Tertiary system. It consists of multiple lithostratigraphic units which are characterised by various hydraulic conductivity contrasts. Due to its geological genesis, those hydrogeological units are closely interrelated to each other. The system is treated as a joint aquifer due to its internal hydraulic connectivity. In addition, deep reaching sub-glacial channel structures and several wide ranging boulder terraces provide various hydraulic linkages to the lower Tertiary aquifer system.

The lowest Quaternary aquifer which is characterised by the pre-glacial gravel banks and the younger Elsterian Frühelsterterrasse only exist in the southern and south-western part of the model domain. This aquifer unit is overlaid only locally by an Elsterian till layer (aquitard). In addition to this, younger well permeable Elsterian sediments are present in the north-western part of the study site and provide hydraulic connections to lower Tertiary aquifers such as the *Bitterfelder Glimmersande* and *Roitzscher Flussande*.

A south-southeast/north-northwest oriented sub-glacial channel structure runs underneath the industrial and urban area of Bitterfeld-Wolfen. Filled with well permeable sediments (>$1 \cdot 10^{-4}$ [m/s]; GOSSEL *et al.* 2009) it characterises a significant hydraulic conductivity contrast to the surrounding hydrogeological units. In addition, its bottom layer reaches down to the Tertiary *Bitterfelder Glimmersande* and represents a hydraulically effective connectivity between the lower Tertiary aquifer system and the upper Quaternary aquifer units.

Sediments of the *Saale-Hauptterrasse* form the main Quaternary aquifer of the study area. This aquifer unit consistently covers the western, central and southern area of Bitterfeld-Wolfen. At the same time, hydraulic linkages to the lower Elsterian aquifer units exist. The main Quaternary aquifer is overlaid almost completely by the first Saalian till bank, which represents a typical aquitard horizon. Towards the north, in the vicinity of *Ramsin*, *Heideloh* and *Zörbig*, this till bank is followed by Saalian glacial-fluvial sediments, which characterise an overlaying aquifer again. Those sediments overlay directly the *Saale-Hauptterasse* along the northern model boundary, near the Fuhne river valley, and provide a hydraulic linkage to the lower Quaternary and Tertiary aquifers.

Younger river bank gravels of the Weichselian and Holocene stage cut the *Saale-Hauptterrasse* in the western part of the Bitterfeld-Wolfen industrial zone and characterise the Quaternary the main aquifer towards the east.

The Weichselian *Niederterrasse* horizon can be classified into an upper and a lower aquifer unit which are separated from each other by local occurring aquitards (periglacial sediments). Those riverbank sediments are characterised by hydraulic conductivities of about $1 \cdot 10^{-3}$ to $1 \cdot 10^{-4}$ (WYCISK *et al.* 2002). In contrast, hydraulic conductivity values of $4 \cdot 10^{-5}$ to $8 \cdot 10^{-9}$ [m/s] are representative for the interbedded periglacial sediments (WEIß *et al.* 2002).

Related to KRAPP & RUSKE (1992), the well permeable Holocene riverbank sediments are characterised by an averaged hydraulic conductivity of about $1 \cdot 10^{-3}$ [m/s].

In areas where those younger Weichselian and Holocene gravel banks are present, the underlying Tertiary *Bitterfelder Flözkomplex* (aquitard) is mostly decimated in its thickness or is eroded completely (RUSKE *et al.* 1999). Hydraulically, this led to the creation of wide ranging aquitard gaps which are illustrated exemplarily in Figure 2-10. Apart from the river bed, terrace sediments are overlaid by a less permeable flood plain loam of variable thickness.

The natural Quaternary sequence is closed by loess and sand-loess sediments of approximately one meter thickness in average (EISSMANN & MÜLLER 1978). Characteristic hydraulic conductivities values are in the range of 10^{-6} to 10^{-7} [m/s].

The redeposition of overburden formed lithologically complex landfills. The permeability of the refilled sediments is based on the material characteristics of the former geological units which are ranging from gravel sediments to till material. Typically, the landfill material characterises a mixed composition of local sediments and sediment material of adjacent mining fields. Due to this, hydraulic characteristics range from low to high permeable materials.

2.2   History of lignite mining

Comprehensive literature exists about the mining history of the Bitterfeld-Wolfen area, but it is available mostly in the German language. This includes the detailed manuscripts of LIEHMANN (1998, 2003, 2004, and 2006) - "*Chronik des Braunkohlenbergbaus im Revier Bitterfeld*".

The Bitterfeld lignite deposit was part of the Central German Lignite District which includes the lignite deposits of *Bitterfeld*, *Gräfenhainchen*, *Delitzsch*, *Brehna*, *Köthen* and *Wittenberg* (LIEHMANN 1996).

The local mining activities in the Bitterfeld-Wolfen area started at the beginning of the 19th century (1839) and were run extensively until the 90s of the 20th century.
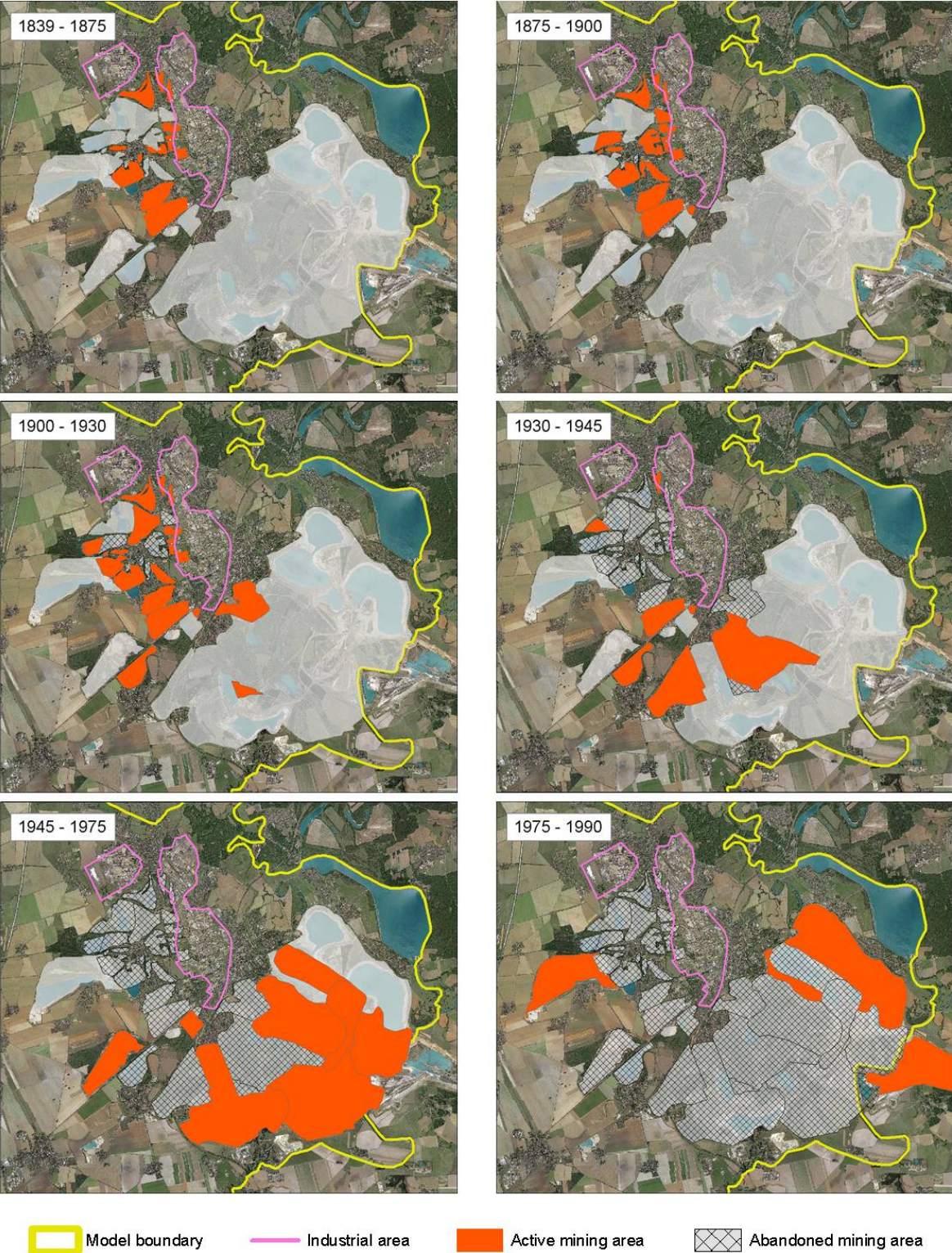
Figure 2-11: Spatio-temporal development of open-pit lignite mining in the Bitterfeld district from 1839 to 1992; the chronological development was characterised by an anticlockwise opening of open-pit mines which began in the west and ended in the east.

As a consequence of the German reunification in 1989/90, the mining activities in the Bitterfeld region were given up completely in year 1992. In its early years, the mining was started in pits and adits at the margins of outcropping lignite seams. Until 1890 the lignite mining was mainly characterised by using pick dug and shovel (SYNNATZSCHKE 2010). Subsequently, haulage mining was introduced, which failed initially due to the low depths to groundwater and the insufficient technical equipment for groundwater drainage.

In consequence of the technological progress and the development of the steam engine, the drainage of open-cast mines was no problem anymore. The first open-pit mine *Auguste*, opened in 1839, was drained technically by using a steam engine. At the same time new technologies for the mining process such as bucket-chain excavators were introduced. Since then, agricultural fields, forests, river plains, urban areas, even complete landscape sections have fallen victim to the excessive lignite mining in the region.

A new technology for groundwater hoisting was introduced in the early 1960s. The more effective *Filterbrunnen* technique enabled groundwater lowering to depths of more than 25 meters. With this it was possible to drain the Tertiary lignite basis, which led to effective lignite mining.

The permanent presence of natural high groundwater levels caused a general high water content of lignite from Bitterfeld which leads simultaneously to a lower heating value. This was a significantly competitive disadvantage against other lignite deposits!

Therefore, several briquette fabrics were installed to remedy this fact. According to LIEHMANN (1993), the first briquette manufactory was installed nearby the mining field *Deutsche Grube*, Sandersdorf, in 1872. Subsequently, further briquette facilities settled in the neighbourhood of the mining fields *Antonie*, *Louise* and *Holzweißig*.

During the 150-year old mining history, more than 40 different open-pit mines of individual size had been opened, and approximately 317,000,000 tons of lignite were extracted. In addition, 850,000,000 m³ of sediment/overburden were moved and significantly affected an area of more than 75 km² (HAFERKORN *et al.* 1999).

In consequence of the enormous available lignite resources, multiple related industries began to settle in the Bitterfeld-Wolfen region. Thus, the agriculturally characterised landscape was turned into an industrial centre, which offered simultaneously thousands of jobs.

First mining activities started regionally in the western part of Bitterfeld. In the course of time, active mining moved anticlockwise to the south, southeast and east. Open-pit mines got larger and deeper in time, which was progressively initiated by more powerful hoisting equipment and more effective mining technologies. The spatio-temporal development of the mining history is illustrated in Figure 2-11.

Different branches of the chemical industry settled in the Bitterfeld-Wolfen region, due to the general industrialisation at the end of the 19th century. Therefore, available lignite deposits were used as the major energy resource for production. After that the demand for lignite

increased rapidly. An overview of the annual lignite production is given in Figure 2-12. Official assignments were set between the operating companies and lignite suppliers to ensure their production. Already in those contracts, the dumping of ashes from power generation or chemical residuals from industrial production in abandoned mining hollows was regulated. This led to multiple hazardous dump-sites in the region.

The maximum of the annual lignite production volume was reached in the middle of the 20th century. The largest quantities of lignite were mined in the huge open-pit mine *Goitzsche,* which was opened in the southeast of Bitterfeld in year 1949 (Figure 2-11). This mine was run until the complete shutdown of all mining activities after the German reunification in 1989/90.
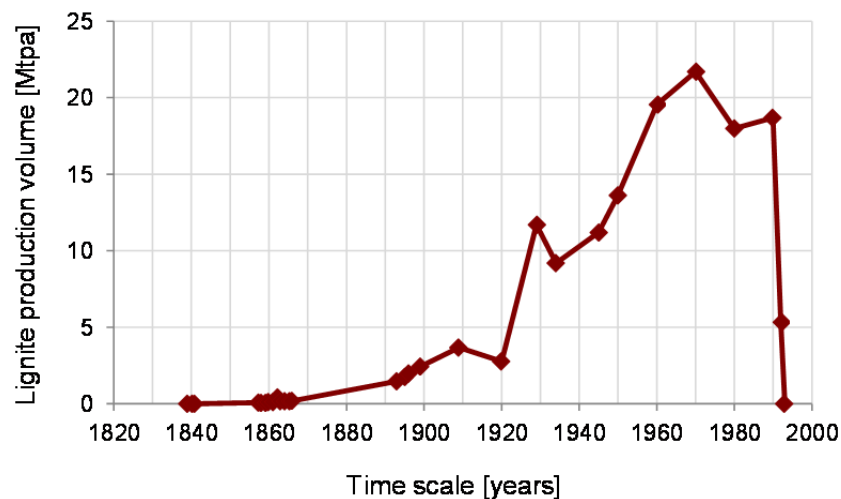
Figure 2-12: Overview about the annual lignite production volume in the Bitterfeld district; 8450 tons of lignite were mined in year 1840. This volume increased rapidly to a maximum production of about 21,700,000 tons in year 1970. Active lignite mining ended after the German reunification in 1989/90. Data source: LIEHMANN (1998)

Due to the long-term and excessive mining activities, huge areas had been destroyed in their natural geological and hydrogeological structure. Simultaneously, the natural groundwater system as well as the surface water system was affected significantly by the regional groundwater drawdown.

After the shutdown of active lignite mining in the region, a large-scaled renaturation process of the post-mined landscape followed. This process focussed on the restoration of an intact and self-regulating water system which includes surface waters and groundwater HAFERKORN *et al.* 2005). This concept involved the flooding of abandoned open-pit mines, the stabilisation of their embankments and the integration of the post-mined landscape into existing ecosystems and infrastructure.

2.3   Industrial history and production

In addition to the extensive mining impacts of more than 150 years, the Bitterfeld-Wolfen region is characterised by a 110-year-old history of industrial production. Since the end of the 19th century, the region has undergone a development from an agricultural area to one of the most important centres of chemical industry in Germany and worldwide. Together with the industrial centres near *Halle* and *Leipzig*, the region formed the so-called *Mitteldeutsches Industriedreieck* (Industrial Triangle of Central Germany).

In the middle of the 19th century, the opening of the railroad tracks *Halle-Wittenberg* and *Leipzig-Dessau* provided the basis for economic development. Furthermore, the Bitterfeld-Wolfen region had locational advantages which ultimately led an extensive industrial settlement at the end of the 19th century (KRETSCHMER 1993):

- The proximity to potassium salt deposits of the *Bernburg* and *Staßfurt* district;
- Clay deposits of lignite accompanying sediments (*Bitterfeld Decktonkomplex*);
- Sufficient water resources (*Untere Mulde*, hoisted mining-water);
- Favourable possibilities for sewage disposal;
- The usage of abandoned open-pit mines as disposals for industrial residuals;
- Land and labour prices were low (at the end of the 19th century);
- A well-developed construction industry.

Large lignite deposits had been the decisive reason for the industrial development of the region. In consequence, local mining activities were increased rapidly. Since 1872, several briquette facilities were installed to overcome the qualitative disadvantage of the local lignite resources due to its high water content. In addition, high-quality, plastic clays of the *Bitterfelder Decktonkomplex* (section 2.1.4) provided a basis for brickworks and potteries which produced mainly clay pipes, wall panels, floor plates and chimney top parts. Besides briquette factories and the local ceramic branch, the iron and steel industry settled.

An economic recession in all three branches led consequently to a decline of mined lignite at the end of the 19th century. In consequence, the low-priced lignite resources started the development of the chemical industry, which used the resource for power generation. According to KRETSCHMER (1993), the first chemical enterprises settled in 1893. The electrochemical sector was represented by the *Elektrochemische Werke Berlin*, and the *Griesheim-Elektron Plant (CFGE)*. In 1895, the *Greppiner Werke* (production of azocolourants and aniline inks) were founded by the *Aktiengesellschaft für Anilinfarben zu Berlin (AGFA),* which was later transformed into the *Farbenfabrik Wolfen* (ink factory). Moreover, noteworthy for the region, the film factory *Filmfabrik Wolfen* was built in the northwest of the industrial area in 1909. An overview about the production range of the listed manufactures is given in Table 2-1.

Table 2-1: Production assortment of the located chemical industries in the Bitterfeld-Wolfen area until 1945. Data sources: PLUMPE (1990), ALBRECHT & KRETSCHMER (1993), HENTZSCH (1996), FINGER (1996) and THIEKEN (2001).

Production site	Since	Production range	Location
Elektrochem-ische Werke Berlin	1893	- Inorganic products: chlorine, phosphorus - Organic substances: monochlorobenzene, mono-chloroacetic acid	Bitterfeld North
Griesheim-Elektron Plant (CFGE)	1893	- Inorganic products: chlorine, caustic soda, potassi-um hydroxide solution, phosphorus - Heavy and light metals (aluminium, magnesium) - Steel-nobles: chrome, wolfram, molybdenum etc. - Plastics: mainly polyvinyl chloride (PVC)	Bitterfeld South
Ink Factory Wolfen (AGFA)	1895	- Azocolourants and aniline inks - Organic substances: nitrobenzene, aniline, naph-thole - Acids: nitric acid, naphthylamine-sulfonic acid	Greppin/ Wolfen
Film Factory Wolfen (AGFA)	1909	- Film materials: black-and-white film, color film, sound film, magnetic tape - Synthetic fibres: nitrocellulose, viscose, acetate silk - Plastics: polyvinyl chloride, polyamide, polyacryloni-trile	Wolfen

Apart from the synthesis of chemical precursors, products such as soaps, papers, colours, and textiles rounded off the range of chemical production. Most of these production processes had been highly energy-intensive and were only profitable in the form of large-scale facilities. Due to missing energy networks at that time, the industrial complexes often settled close to the mining areas. With respect to this, lignite as an energy source and raw material was back in demand and set the linkage between lignite mining and chemical industry for more than a century.

At the beginning of the 20th century, the Bitterfeld-Wolfen industry was characterised by several chloro-alkali electrolysis plants which were introduced by CFGE in 1894. This technology enabled the production of caustic soda, potassium hydroxide solution, and chlorine gas which emerges from the electrification process of fossil fuels:

$$2 \text{ NaCl} + 2 \text{ H}_2\text{O} \rightarrow \text{Cl}_2 + \text{H}_2 + 2 \text{ NaOH}$$

$$2 \text{ KCl} + 2 \text{ H}_2\text{O} \rightarrow \text{Cl}_2 + \text{H}_2 + 2 \text{ KOH}$$
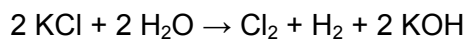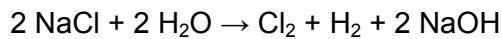
Most of the synthesised chlorine gas was used for processing lightly volatile hydrocarbons (LHKW) that were used to fabricate inks and pesticides (Lindane).

Pre-existing large companies such as the film and ink factory, *CFGE*, and affiliated divisions of the *Elektrochemische Werke Berlin* fused into a global *Farbenindustrie Aktiengesellschaft (IG Farben)* by 1945. Within this corporation, all incorporated plants were reorganised and associated in research fields. Production workflows were optimised and bundled. At this time, the German chemical industry dominated the world market in the ink sector, photographic materials and pharmaceuticals.

The chemical industry operated as a supplier for explosives, poison gases and armaments during the Second World War. In consequence of losing this war, all production facilities were taken over by the Soviet occupation power. The new leadership reorganised the internal structures of *IG Farben* into the *Elektrochemisches Kombinat Bitterfeld (EKB)*. Since then, the Bitterfeld-Wolfen region produced mainly for the Soviet Union until 1952. Later in that year, the *EKB* and the ink facility Wolfen were handed over to the German Democratic Republic (GDR).

According to HENTZSCH (1996), the *EKB* was the biggest producer for chlorine or chlorine related products of the former GDR. In addition to pesticides (Lindane and DDT), graphite, and aluminium production, up to 2700 individual marketable products originated from the Bitterfeld-Wolfen industry. As a result of merging the *EKB* with the ink facility Wolfen into the *Chemiekombinat Bitterfeld (CKB)* in year 1969, the production range increased to 4500 individual chemical products. That included dyestuffs, ion exchangers, chlorine products, inorganics, detergents, pesticides, and further consumer goods.

As a consequence of the German reunification in 1989/90, most of the chemical production sections broke down completely due to the omission of traditional markets and the low competiveness against other producers.

In 1990, compartments of the *CKB* were split up into the *Chemie AG Bitterfeld* and the *Filmfabrik Wolfen AG*. Due to the general decline of the chemical industry and lignite mining, a period of renaturation/remediation started which focussed on the environmental impacts of mining and chemical industry. This process is still in progress.

2.4   Environmental impacts from mining and industry

Due to long-term mining activities, huge areas had been widely destroyed in their natural geological settings. Simultaneously, the hydrogeological structure as well as the surface water system had been changed irreversibly. Extensive groundwater lowering affected the groundwater system at a regional scale. With respect to this, groundwater flow directions and gradients changed spatially in time with respect to the spatio-temporal mining development (Figure 2-11). Groundwater drawdown cones of adjacent mining fields overlapped on each other and intensified their effect into the groundwater system.

In addition, the chemical industry left toxic residuals by an improper waste management at unsecured production locations, unsealed dumps or depositions, from local sewage water systems and local disasters. These pollutant loads caused groundwater contamination on a regional scale. Dominated by aromatic hydrocarbons and chlorinated aliphatics, the contamination patterns are highly diverse in horizontal and vertical scale. In the past, the contaminant spreading was influenced significantly by the mining related groundwater withdrawal, which led to complex pollutant distribution patterns.

After the end of active lignite mining in the 1990s, the mining related groundwater lowering was not necessary anymore. Since then, the groundwater table has been rising naturally. In some areas and local open-pit mines, a passive groundwater hoisting has continued to ensure a controlled groundwater rebound or to limit the rebound process to a specified groundwater elevation level.

The groundwater uptake additionally influenced the migration of distributed groundwater contaminants. Besides a general dislocation of contamination plumes, the rising groundwater table is leading up polluted groundwater to near the surface zone.

The restructuring of natural geological bedding conditions

An area of more than 75 km² had been destroyed irreversibly in the surroundings of the Bitterfeld-Wolfen area. Lignite exploitation and redeposition of overburden modified drastically the natural geologic setup in horizontal and vertical dimension. This led to significant changes in the natural geological profile and affected the structure of the hydraulic groundwater system simultaneously. The outtake of lignite seams (aquitards) and lignite accompanying sediments (aquitards) resulted in the creation of hydraulic linkages between the lower Tertiary *Bitterfelder Glimmersand* aquifer and the upper Quaternary aquifer system.

Overburden was dumped in abandoned open-pit mines. In addition, terrain depressions were filled up by these sediments too. BURCHARDT & STROBEL (1992), differentiate three forms of anthropogenic landfills:

(1) Existing mining hollows were filled with overburden from adjacent open-pit mines, ashes and construction waste. The resulting landfills differ concerning their material composition in

horizontal and vertical scale. The redeposited sediments have a significant thickness and reach down to the depths of former mining activities.

(2) Mining fields were used as waste deposits for the dumping of chemical residuals from the local industrial production. Due to a missing base seal protection, these dump-sites harm and affect significantly the existing groundwater system by contaminant discharge.

(3) Materials such as natural sediments, construction waste, ashes and slugs were also used to compensate ground surface depressions and basins.

Abandoned open-pit mines which had not been refilled by overburden were prepared for flooding by natural groundwater and particularly by additional water form adjacent running waters. The flooding of the *Goitzsche* mining complex was initiated in 1999. This process was overlaid by the century flood event in August 2002. Due to a broken dike along the Mulde river course, several open-pit mines were flooded within a couple of days.

Environmental pollution – a groundwater contamination at a regional scale

Long-term chemical production at the Bitterfeld-Wolfen site affected environmental compartments such as air, soil, surface water and groundwater by a high variety of pollutants from the local industry. According to WALKOW (1996), an explicit environmental pollution has existed since the early stage of chemical production in 1893. Various production facilities, large industrial areas and the dumping of chemical residuals in former lignite mines formed a multi-source contaminant scenario.

Especially the former mining complexes, which had been filled with residuals from chemical production, constitute major pollutant sources of the current groundwater contamination. Moreover, the upper subsurface zone of the industrial complexes is contaminated highly in an area of about 11 km² and needs to be treated as a probable additional pollutant source.

Additional contaminant loads originated from the sewage water channels Spittelwasser und Schachtgraben. In the past, these channels drained industrial waters from the local production. Most of the dumped material resulted from industrial production after 1945, at the time when the production range was extended by chlorinated hydrocarbons and pesticides. An overview of the local waste dump locations is given in Figure 2-13.

The chemical inventory of the waste disposals is characterised mainly by chlorinated hydrocarbons, heavy metals, industrial sludge and HCH isomers (see Table 2-2). In a certain way, the hydrochemical spectrum of the groundwater contamination reflects the former production range of about 4500 to 5000 individual substances (HENTZSCH 1996, HEIDRICH *et al.* 2004) which includes various intermediate and end products. Additional chemical compounds need to be expected which can arises from proceeding metabolism processes.

The total contaminant discharge affected the aquifer system of an area of about 25 km². In consideration of an aquifer thickness of about 40 meters and an effective porosity of about 20%, the contaminated groundwater volume is estimated to approximately 200,000,000 m³.
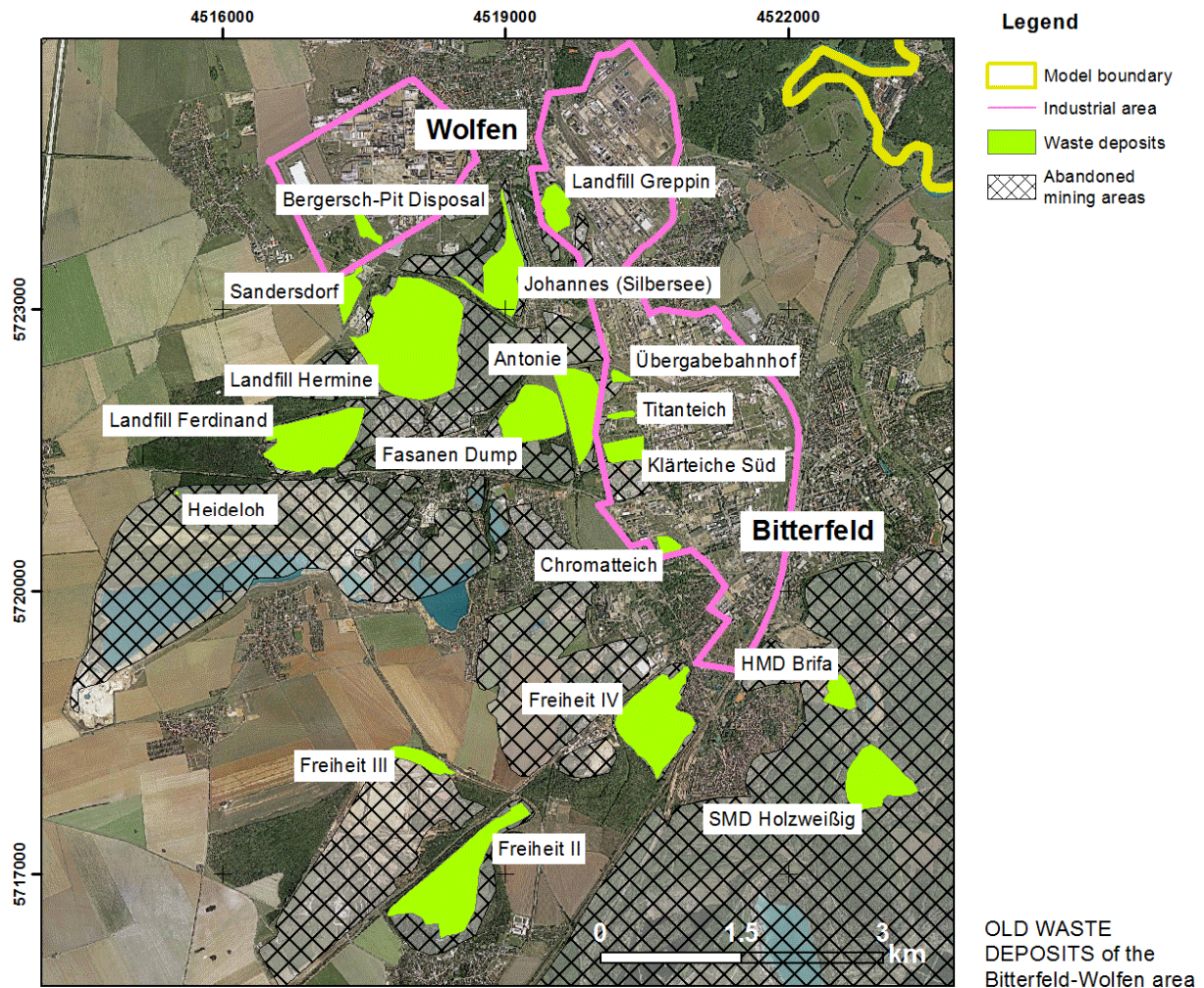
Figure 2-13: Existing dump-sites of the Bitterfeld-Wolfen region are filled with residuals from the chemical production, ashes, slugs, construction waste and domestic waste. Those dump-sites quantify a total volume of more than 15,000,000 m³.

Contaminant distribution patterns cover wide areas of the *CAG Bitterfeld* and the *Filmfabrik Wolfen* as well as parts of the neighboured urban areas. According to GROßMANN *et al.* (2003), the hydrochemical situation is dominated mainly by the following substances: chlorobenzene, lightly volatile hydrocarbons (LHKW), nitrochlorobenzene, BTEX (benzene), chloroaniline, cresolyl, hexachlorocyclohexane (HCH), tinorganic compounds, prometryn and dimethoate.

The contaminant distribution patterns are characterised by a high diversity in horizontal and vertical scale. Zones of high concentration levels are located directly near zones at the detection limit. With respect to the plume complexity, these distribution patterns cannot be compared to usual single source contamination plumes. Often, an explicit source allocation is not possible anymore.

33

Table 2-2: Landfill sites, operation time and their chemical inventory in the region Bitterfeld-Wolfen. Data sources: HILLE ET AL. (1992), WALKOW (1996) and THIEKEN (2001).

Dump site	Period	Inventory	Vol. [M m³]
Antonie*	1918 – n.d.	HCH, heavy metal sludge, ash, CKW	5 – 6
Greppin*	1931 – n.d.	Toxic organic sludge, CKW	2.5
Freiheit III	since 1964	Construction waste, industrial sludge, ash	2.0
Hermine	1958 – 1992	Heavy metal, ash, asbestos, CKW	4.0
Freiheit IV	after 1954	Ash/sludge (Cr, Hg), DDT, PAK	0.2
Johannes	1921 – 1991	Lignin sludge, heavy metal (Pb, Zn), CKW	2.0
Sandersdorf	1978 – 1990	Domestic waste, construction waste, LHKW	0.3
Grube Bergersch	1968 – 1978	LHKW, PAK, ash, sludge, construction waste	0.4
Heideloh	1965 – 1971	HCH, construction waste	0.7
Chromatteich	until 1954	Chromate	0.5
HMD Brifa	since 1960s	Construction and domestic waste	0.8
SMD Holzweißig	n.d.	Ash, heavy metal	1.5
Titanteich	1950 – 1964	Titanium, HCH, heavy metal	0.1
Übergabebahnhof	1951 – 1960s	HCH, heavy metal	0.5
Fasanen-kippe	1930 – n.d.	HCH, industrial sludge, excrement	-
Ferdinand	after 1914	Ash, construction waste, flushing dump	-
Freiheit II	after 1951	Domestic waste	-
Klärteich Süd	n.d.	Industrial sludge, heavy metal, LHKW	-

The contaminants have left their direct source zone and are meanwhile mixed up with other pollutant plumes. In consequence, the Quaternary aquifer, the Tertiary aquifer as well as the top of the *Rupelton* are highly contaminated by chemical compounds. Due to the huge volume of the affected groundwater, the groundwater itself is classified as a contamination source of second-order. According to GROßMANN *et al.* (2003), the situation is classified as the following:

 (1) Contamination plumes which originated from the production areas have been detected north of the *Filmfabrik* area, east of *Greppin*, and in the southeast of the centre of *Bitterfeld*. Towards the north, an additional plume is traceable in the downstream to the river *Mulde*.

(2) The highly contaminated area has the dimension of approximately eight kilometres from south to north and about six kilometres in west-east direction.

(3) The contaminant discharge within the lower aquifer units has progressed further than near the surface horizons. This is explainable by the long-term groundwater lowering which was mainly installed at the lower aquifer units (*Bitterfelder Glimmersande*) of the hydraulic system.

(4) In addition to the former production areas and existing waste disposals, further probable contamination sources have to be considered: *Schachtgraben* (AOX, ammonium, benzene), *Mulde* flood plain (arsenic, cadmium), and the sewage farm *Reuden* (arsenic, cadmium, ammonium, nitrate, phosphate, and AOX).

Generally, all observed substance groups of the Bitterfeld-Wolfen groundwater contamination are harmful concerning their high toxic potential, their persistence, and mobility. The metabolism process has to be taken into account due to the origin of substances such as vinyl chloride, which is much more humanly toxic than its initial substance tetrachloroethylene (PCE).

Due to the fact that a full decontamination of the Bitterfeld-Wolfen region is impossible from an economical point of view, the actual remediation concept focuses on an efficient combination of remediation and securing strategies (LANDESANSTALT FÜR ALTLASTENFREISTELLUNG, 2010). The applied remediation concept includes three parts:

(1) Hydraulic barriers had been installed to suppress a further contaminant spreading into non-contaminated waters, surface water bodies and uncontaminated surface zones;

(2) Downstream securing and local source remediation;

(3) Source decontamination;

The current forensic transport modelling approach for source identification problems supports the local remediation management, since source areas are particularly unknown or not attributable.

2.5   Chapter summary

The case study area Bitterfeld-Wolfen had been affected by extensive impacts of lignite mining and chemical industry for more than a century.

The naturally complex geological setup of Quaternary and Tertiary sediments was destroyed and reshaped in consequence of wide ranging open-pit lignite mining. Mining related groundwater abstraction disrupted the natural groundwater regime at a regional scale.

Moreover, intensive industrial production left chemical substances in almost all environmental compartments. Chemical residuals from the local industry were dumped arbitrarily in abandoned open-cast mines without having any securing measures for groundwater protection.

Long-term pollutant discharge from former industrial complexes and local dump-sites caused a multi-source groundwater contamination at a regional scale. The contaminant distribution patterns comprise a high diversity in horizontal and vertical scale and are mainly characterised by aromatic hydrocarbons and chlorinated aliphatics. Long-term contaminant spreading was overlaid significantly by the mining induced groundwater withdrawal. Changes concerning groundwater flow directions and intensity varied greatly in time and caused complex contaminant patterns which cannot be compared to usual single source plumes. Pollutant source areas cannot be clearly attributed, which complicates the implementation of a more efficient remediation concept.

3 Forensic modelling − numerical approaches

Forensic solute transport modelling, in forward or backward mode, is based on a previously simulated groundwater flow velocity field as its basic input. Thus, the computational results of transport models are highly sensitive in regards to the involved transport mechanisms as well as to local occurring variations of the groundwater flow velocity field.

However, groundwater flow modelling as well as theory on conventional transport modelling constitutes the essential basis of the presented modelling concept. Therefore, it is considered absolutely crucial to introduce the relevant flow and transport processes and their numerical approximation (sections 3.1 and 3.2). Based upon this, theory and methodological aspects of reverse particle tracking and backward-in-time modelling for source identification problems are given in section 3.2 and 3.3.

In the following, both backward-in-time modelling approaches are applied to an experimental, transient 2-D model scenario (chapter 4.2) as well as to the complex real world application of the Bitterfeld-Wolfen megasite (chapter 4.3). Based on virtual contaminant scenarios, both techniques are analysed and compared concerning methodological aspects, numerical stability, and accuracy.

3.1 Groundwater flow modelling

Being generally a fundamental part of numerical transport modelling, the application of groundwater flow modelling meanwhile constitutes the standard instrument when being faced with geohydraulic questions. Predominantly, the flow modelling procedure targets the prediction of consequences of a proposed action by following either an interpretative (system analysis) or a generic approach (hypothetical phenomena). Beside its main application such as hydrogeological exploration and water supply (KUMAR 2005), predictions on the dimension of groundwater withdrawal (JACKSON *et al.* 2008), the designation of groundwater protection zones (FRIND *et al.* 2006) or the reproduction of historical velocity fields (GOSSEL *et al.* 2009), groundwater flow modelling forms the major basis of any groundwater transport problem.

When simulating groundwater flow in the subsurface, the aquifer matrix is treated as a porous medium. With respect to the dominating aquifer settings, the system is characterised as a confined-, semi-confined- or unconfined (phreatic) model. Finally, the numerical groundwater model provides a spatial and temporal discretised water balance of an arbitrary model area which involves the participating groundwater recharge, external inflows/outflows, injection or extraction by groundwater wells, and the water storage.

3.1.1 Fundamentals on groundwater modelling

The fundamental equation for modelling subsurface groundwater flow involves Darcy's Law and the continuity principle. While the continuity formulation is demanding the water mass conservation along discretised model elements, the validity of Darcy's law requires a dominating laminar flow within the porous medium. In general, the groundwater flow is driven by gravity and a hydraulic head gradient (pressure head) of the groundwater. Thus, differences between several hydraulic heads initiate the motion of water (convection). Solving a groundwater flow problem by using finite element analysis, the in- and outflows are balanced along involved element boundaries. Total mass is subsequently quantified with respect to its temporal variation by following the continuity principle. The participating fluxes are mathematically described by Darcy's law. DARCY (1856) formulated the following empirical relations for the linear dimension:

$$v = \frac{Q}{A} = k_f \frac{\Delta h}{L} \qquad \qquad Eq.\ 0\text{-}1$$

where the specific discharge v [L/T] is related to a specific volume of water Q [L³/T] passing per unit in time through an area A [L²] of a porous medium cross section. Moreover, the specific discharge is a function of the k_f value [L/T], representing the hydraulic conductivity of the porous medium and the hydraulic gradient defined as the quotient of Δh [L] and L [L]. A generalisation of Darcy's law for an isotropic porous medium in non-linear dimensions leads to the following equation:

$$\vec{v} = -k_f \nabla h \qquad \qquad Eq.\ 0\text{-}2$$

where the specific discharge $\vec{v}$ [L/T] is proportional to the product of the negative hydraulic gradient ∇h [-] and the hydraulic conductivity k_f [L/T]. For the anisotropic media, the hydraulic conductivity differs for the respective dimensions and is therefore replaced by a conductivity tensor K_F [L/T] for describing the material constant:

$$\vec{v} = -K_F \nabla h = -\begin{pmatrix} k_{xx} & k_{xy} & k_{xz} \\ k_{yx} & k_{yy} & k_{yz} \\ k_{zx} & k_{zy} & k_{zz} \end{pmatrix} \begin{pmatrix} \partial h/\partial x \\ \partial h/\partial y \\ \partial h/\partial z \end{pmatrix} \qquad \qquad Eq.\ 0\text{-}3$$

this tensor matrix is symmetric, where the tensor element k_{ij} adds a specific discharge component in the i-direction caused by the hydraulic gradient of the j-direction.

Fundamentals on the numerical description of groundwater flow processes are given in BEAR (1972), BEAR (1979), and MATTHEß & UBELL (1983).

3.1.2 3-D groundwater flow model

The differential equation for the 3-D groundwater flow is derived from the water balance of specified model elements or rather volumes. The balance of inflows and outflows along element boundaries over a temporal variation Δt [T] is related to the increment of water within the considered element. Balance compartments are horizontal in- and outflows as well as water addition/removal over the top and bottom side. Here, the specific storage S_0 [L^{-1}] is introduced which characterises the capacity of an aquifer to release or store groundwater in response to a decline of the hydraulic head/movement of the groundwater table. Moreover, additional sinks and sources are included. By combining Darcy's law and the continuity principle, the following equation applies:

$$\nabla \vec{v} = \nabla (K_F \nabla h) = S_0 \frac{\partial h}{\partial t} \qquad \text{Eq. 0-4}$$

Then, for the heterogeneous and isotropic media the 3-D groundwater flow model is:

$$\nabla (k_f \nabla h) = \frac{\partial}{\partial x}\left(k_f \frac{\partial h}{\partial x}\right) + \frac{\partial}{\partial y}\left(k_f \frac{\partial h}{\partial y}\right) + \frac{\partial}{\partial z}\left(k_f \frac{\partial h}{\partial z}\right) = S_0 \frac{\partial h}{\partial t} \qquad \text{Eq. 0-5}$$

For the heterogeneous, anisotropic media:

$$\nabla (K_F \nabla h) = \frac{\partial}{\partial x}\left(k_x \frac{\partial h}{\partial x}\right) + \frac{\partial}{\partial y}\left(k_y \frac{\partial h}{\partial y}\right) + \frac{\partial}{\partial z}\left(k_z \frac{\partial h}{\partial z}\right) = S_0 \frac{\partial h}{\partial t} \qquad \text{Eq. 0-6}$$

The three-dimensional flow equation of the unknown hydraulic head $h(x, y, z, t)$ is a second order partial differential equation (PDE) which requires numerical boundary- and initial conditions for its numerical solution. Conceptually, in terms of groundwater flow modelling, the boundary and initial conditions characterise the observed system in regards to its dominating flow characteristics. This includes the definition of the global groundwater table elevation, water levels along river courses, model inflows and outflows (fluxes), groundwater recharge, and the injection/extraction due to, for example, pumping wells.

Initial Conditions

The initial conditions specify the flow model concerning its hydraulic head (h) [L] distribution, at all computational nodes of the entire numerical model domain at some initial time, normally taken as $t = 0$. Here the initial condition can be expressed by:

$$h = f\ (x, y, z, 0)$$

Eq. 0-7

Boundary Conditions

In general, three kinds of boundary conditions (BC) exist for solving the PDE of the motion of water in terms of the piezometric head (h). A distinction is made between the boundary of a prescribed piezometric head (1st kind BC, Dirichlet Boundary Condition), a prescribed water flux (2nd kind BC, Neumann Boundary Condition), and a semi-pervious/leakage boundary (3rd kind BC, Cauchy Boundary Condition). These conditions can vary in time (transient) or stay constant (steady).

The *Dirichlet condition* or the boundary of prescribing a pressure or hydraulic head is the most profound boundary that restricts the numerical model solution the most. Here it is assumed that the elevation of the surface water is equal to the elevation of the water table, which is reasonable when a lake or a stream is losslessly penetrating the aquifer.

$$h = f\ (x, y, z, t)$$

Eq. 0-8

This prescribed boundary of (h) is a function of space at any time.

The *Neumann condition* defines a water flux (positive or negative) which is entering/exiting the model domain through its boundary. The often used no-flow boundary is a special form of this prescribed flux boundary. This is the case when streamlines are identical to the no-flow boundary, the dominating flow terminates against an almost entirely impermeable material and no further flow dynamic occurs or a typical watershed situation is assigned. This specified water flux v_n [L³/T] is defined as the normal $\vec{n}$ [L²] of the material surface at the boundary segment and the specific discharge $\vec{v}$:

$$v_n = \vec{v} \cdot \vec{n} = f\ (x, y, z, t)$$

Eq. 0-9

Thus, the condition of the prescribed flux provides no explicit information about, for example, hydraulic head values (h) at this boundary location. The located head values adjust themselves by receiving a specified flow rate with respect to the set boundary condition.

The 3rd kind boundary condition represents the so-called *Cauchy condition*, which is generally used for representing a semi-pervious boundary such as a leakage of a surface water body due to clogging effects. In consequence, the surface water is imperfectly connected to the aquifer and its boundary potential affects the aquifer only in a restricted way. The exchange of water depends on the specific head difference between the surface water and the groundwater influenced by a leakage factor c:

$$c = \frac{k_f}{d} \qquad\qquad\qquad \textit{Eq. 0-10}$$

where k_f [L/T] represents the hydraulic conductivity of the river bed and the parameter d [L] its thickness. The semipervious boundary is a linear combination of the groundwater head and the resulting groundwater flux which is derived from the head difference over the leakage of the river bed:

$$v_n = (h_{sw} - h) \cdot c \qquad\qquad\qquad \textit{Eq. 0-11}$$

where h_{sw} [L] is the head of the surface water body and h [L] is the hydraulic head of the aquifer. Thus, this type of boundary is able to reproduce influent and effluent condition in relation to the head differences between the aquifer and a lake, river or reservoir.

The often-called well boundary (4th kind BC) is a special type of boundary condition to describe the water injection/extraction rate set from groundwater wells. SUDICKY *et al.* (1995) provides a non-iterative technique for its direct implementation in three-dimensional heterogeneous formations. A water flux is defined for the extraction/injection rate, and the hydraulic head values at the computational node are adjusted by receiving/losing this specified flow rate.

The finite element model FEFLOW (DIERSCH 2009a) was used to solve the 3-D partial differential equation of groundwater flow in consideration of transient flow boundaries for the experimental 2-D simulation and the real world scenario of the Bitterfeld-Wolfen case study area.

With respect to the case study area, mining related groundwater extraction was implemented by the usage of the 4th kind BC which reproduces the spatio-temporal mining operations of the study region illustrated in section 2.2. The dominating surface waters (chapter 2.1.2) were represented by transient 1st kind and 3rd kind boundary conditions. Detailed information about their practical implementation in FEFLOW is given in the respective sections of chapter 4.

3.2   Transport modelling (forward-in-time)

The knowledge about the migration of solutes in groundwater is highly important with respect to groundwater protection, environmental protection, and health care of humans. Since the 1970s (OGATA 1970, BEAR 1972, KINZELBACH 1992 etc.), numerous transport models have been established for analysing and managing groundwater harms. In an accustomed manner, the focus is on a quantitative system comprehension, followed by predictions about potential impacts of groundwater harms (BORDELEAU *et al.* 2008), finding and analysing remediation strategies (THIESSEN *et al.* 2009, PROMMER 2000) or giving hints for future fate (MIRBAGHERI & MONFARED 2009). Once a substance has migrated from its origin into the groundwater, its macroscopic spreading is an interaction of conservative transport and groundwater flow, interference effects, adsorption and reaction processes. The movement of groundwater solutes through a porous medium is a complex mechanism of multiple fundamental physicochemical processes. Diffusion is the transport of molecular species dissolved in groundwater by concentration gradients from high concentration areas to areas of lower concentration. The advection mechanism describes the substance transport in regards to a fluid being in motion. The dispersion mechanism raises the transport distance and lowers the solute concentration at the same time. Physicochemical processes lead to retardation effects, such as sorption, which limit the solute transport referred to the ideal advection rate, while chemical and biochemical mechanisms of biodegradation and decay affect the mass balance of the solvent directly.

3.2.1 Solute transport mechanisms

Advection

The advective part of the transport mechanism describes the motion of a solute with the groundwater flow, characterised by the flow velocity and the corresponding flow direction. This advective form is the dominating transport process which represents an averaged transport movement (without dispersion, sorption, or degradation). Besides, when the groundwater movement is initiated by density- or temperature gradients, this process is often denoted as convection. The rate of a solute that is being transported is a function of its concentration in the groundwater and the quantity of the flowing groundwater. Initiated by a hydraulic gradient, the resulting Darcy flow of the groundwater depends on a material parameter (hydraulic conductivity or kf-value) of the porous medium. In addition, only the effective porosity takes part in the groundwater flow and transport mechanism and needs to be considered. The theoretical background of the groundwater flow is illustrated in section 3.1.

The one-dimensional advective mass flux F_{adv} can be expressed by:

$$F_{adv} = v_x \cdot n_e \cdot C$$

<div align="right">Eq. 0-12</div>

where v_x is the averaged Darcy flow of the groundwater [L/T], n_e the effective porosity of the porous medium [-] , and C the concentration of the dissolved solid [M/L³]. In a differential form the advective concentration change per unit in time is a function of the flow velocity and the concentration gradient:

$$\frac{\partial C}{\partial t} = -v_x \frac{\partial C}{\partial x}$$

<div align="right">Eq. 0-13</div>

This idealistic solute transport with respect to the averaged flow velocity in natural systems is overlaid by material characteristics of the porous media. Material heterogeneities affect the averaged velocity field regarding the flow direction and intensity and lead finally to a spreading of the concentration front. This phenomenon is treated as the mechanical dispersion effect and needs to be distinguished at a micro and macroscopic scale.

Hydrodynamic dispersion

When groundwater transports any solvents, it is almost impossible to separate quantitatively the diffusive from the dispersive part. SCHEIDEGGER (1961) introduced the hydrodynamic dispersion coefficient in longitudinal and transversal dimension, which mathematically includes the mechanical dispersion and the molecular diffusion:

$$D_L = \alpha_L \cdot v_x + D_d \ \ \text{and} \ \ D_T = \alpha_T \cdot v_x + D_d$$

<div align="right">Eq. 0-14</div>

where the hydrodynamic dispersion coefficients include the dispersion length α [L], the flow velocity v_x [L/T], and the effective diffusion coefficient D_d [L²/T].

In general, *molecular diffusion* describes a transport mechanism, driven by concentration gradients, where a solute moves from a point of a specified concentration level towards a point which is less concentrated. This process is based on the Brownian (molecular) movement. Running towards all sides of the system, the mechanism occurs as long as the concentration gradient is present, even if the fluid is not moving! Fick's laws describe the mass flux caused by the diffusion process.

$$F_{diff} = -D_d \frac{\partial C}{\partial x}$$
Eq. 0-15

Fick's first law (Eq. 0-15) expresses that the diffusive part of the solute transport mechanism depends on a diffusion coefficient D_d [L²/T] and a present concentration gradient $\partial C / \partial x$. Within an aquifer system, only the effective pore volume is available for the the diffusion processes. Therefore the resulting mass flux needs to be multiplied by the effective porosity n_e:

$$F_{diff} = -n_e \cdot D_d \frac{\partial C}{\partial x}$$
Eq. 0-16

If mass concentrations are changing over time, Fick's second law applies. Molecular diffusion coefficient values range from $1*10^{-9}$ to $2*10^{-9}$ m²/s (at 25 °C) and do not vary significantly with the concentration level but are sensitive to temperature. ROBINSON & STOKES (1965) stated additionally, that diffusion coefficients are about 50% less at 5 °C. Thus, the total diffusive proportion of contaminant transport at larger scales is negligibly small. According to KINZELBACH (1992), the diffusive amount can be ignored if the groundwater flow velocity is bigger than 0.1 m/d. But under stagnating flow conditions, such as in less conductive clay layers, the diffusion mechanism often is the only and dominating solute transport process, since the advective transport is more or less non-existent. According to KINZELBACH & STAUFFER (2005), only an effective diffusion coefficient should be used which considers the retardation factor R [-] of the solvent and the tortuosity T [-] of the porous media:

$$D_{eff} = \frac{D_d}{TR}$$
Eq. 0-17

Contaminant spreading and mixing effects which are based on the diffusion mechanism occur in the scale of millimetres to centimetres. This process is significantly overlaid by the outnumbering mechanical dispersion. SCHÄFER (2004) specified the scale of diffusion effects being in the range of decimetres whereas the *mechanical dispersion* mechanism reaches the scale of meters.

Heterogeneities of the aquifer material at microscopic and macroscopic scale cause a variation of the flow velocity profile within the participating pore volumes. Even if the aquifer matrix is relatively homogenous at a microscopic scale, the velocity profile is characterised by non-parallel flow paths initiated by irregular pore matrix configurations, varying pore sizes, and an inhomogeneous intra-pore velocity field due to friction phenomena at the pore edges. Moreover, aquifer heterogeneities in the range of meters or larger significantly affect the

velocity field of the flow system and amplify the solute transport process (GELHAR & AXNESS 1983). In general, due to the dispersion mechanism, the migration distance of a dissolved solute through an aquifer is larger than only the advection based transport rate. Thus, mechanical dispersion causes a gradual dilution effect at the migrating plume and affects the surrounding water volume by its positive dispersive mass flux. Here, the longitudinal dispersion describes the mixing process along the flow path, while the dilution normal to the groundwater flow is named transversal dispersion.

Normally, the longitudinal dispersion is specified to be of one order larger than the transverse dispersion. Since the dispersion mechanism causes a similar spreading effect such as the diffusion mechanism, its mathematical approximation is formulated analogously. The only difference between dispersion and diffusion is the anisotropic character of the longitudinal and transversal distinction. The participating dispersion coefficients are expressed by the product of the groundwater flow velocity and related dispersion lengths:

$$D_L = \alpha_L \cdot v_x \ \text{ and } \ D_T = \alpha_T \cdot v_x \qquad\qquad \textit{Eq. 0-18}$$

where the longitudinal and transverse dispersion coefficients D_L [L²/T] and D_T [L²/T] are the product of the groundwater flow velocity v_x [L/T] and the dispersion lengths α_L [L] and α_T [L].

The conceptual theory of Fick's law is used again to express the dispersion relation of:

$$F_{disp_L} = -n_e \cdot D_L \frac{\partial C}{\partial x_L} \ \text{ and } \ F_{disp_T} = -n_e \cdot D_T \frac{\partial C}{\partial x_T} \qquad\qquad \textit{Eq. 0-19}$$

where n_e is the effective porosity [-], D the dispersion coefficient [-] and $\partial C/\partial x$ the concentration gradient, in longitudinal (L) and transversal direction (T), respectively.

The dimension of the macroscopic dispersion is strongly scale dependent, and dispersion lengths as well as coefficients are increasing directly in regards to the scale of the transport problem. Dispersion lengths obtained from tracer experiments were published by BEIMS (1983) and GELHAR et al. (1992). Moreover, KINZELBACH (1992) and GELHAR & AXNESS (1983) presented approaches to evaluate macroscopic dispersion lengths from empirical relations as well as statistical parameters and autocorrelation functions based on hydraulic conductivity parameters.

Retardation and transformation processes

All the solvents which migrate by advection, diffusion, and mechanical dispersion through the porous medium are additionally subjects of processes which have a limiting effect on the solute transport mechanism. Furthermore, these processes can initiate a solute mass

reduction or even a complete removal. Non-conservative materials are the subject of chemical, biological, or radioactive decay processes.

As a result of sorption, solutes move much more slowly through the porous media than the flowing groundwater might transport them. This process is called retardation. Sorption processes between solutes and the matrix of the porous medium have a delaying and diluting effect onto the solute transport process. In general, the sorption term includes the processes of adsorption and absorption. When the sorption process is reversible (desorption), the previously bound solvent accumulates in the groundwater again. In regards to the assumption that the sorption process takes place rapidly, the solute reaches an equilibrium condition with the sorbed phase.

Then, the sorbed phase C_a [1] is a function of the dissolved phase C [M/L³] of the groundwater:

$$C_a = f(C)$$
<div align="right">*Eq. 0-20*</div>

This function $f(C)$ is called an isotherm and represents an equilibrium state between the sorbed and dissolved substance at a constant temperature. The linear isotherm or K_d-concept (Henry-concept) is the simplest form of an equilibrium state:

$$C_a = K_d \cdot C$$
<div align="right">*Eq. 0-21*</div>

where C_a is the sorbed concentration at the matrix material [1], C the dissolved concentration in water [L³/M], and K_d the distribution coefficient [L³/M], which can be derived from the octanol-water partition coefficient and the available amount of organic carbon within the aquifer matrix. In addition to the linear concept, non-linear sorption concepts such as the Freundlich isotherm and the Langmuir isotherm exist. As a consequence of all individual sorption mechanisms, the solute migrates with a smaller rate than the groundwater. For numerical implementation, a retardation factor is introduced. The retardation factor R [-] for the linear Henry-concept evolves from:

$$R = 1 + \frac{\rho_s \cdot K_d}{n_e}$$
<div align="right">*Eq. 0-22*</div>

where R is the retardation factor [-], K_d the Henry distribution coefficient [L³/m], n_e the effective porosity [-], and ρ_s the density of dry matrix material [M/L³]. For the case to consider non-linear Langmuir and Freundlich isotherms, the concentration relation $\partial C_a / \partial C$ is added:

$$R = 1 + \frac{1}{n_e} \cdot \rho_s \cdot \frac{dC_a}{dC}$$

Eq. 0-23

Finally, the retardation factor limits the advective, dispersive, diffusive transport mechanism by reducing the flow velocity of the groundwater v_x [L/T] to an apparent flow velocity v_c [L/T] which is considered to estimate sorption characterised solute transport process:

$$v_c = \frac{v_x}{R}$$

Eq. 0-24

The Henry-concept is often used to test model sensitivity with respect to the retardation process. Again, this concept causes only a retardation of the migration processes and does not fix any solvent onto the matrix material. Advection, hydrodynamic dispersion, and sorption do not affect the mass concentration of the solvent, whereas chemical and biochemical reactions can influence significantly the total mass balance by degradation mechanisms. Chemical transformation, biodegradation processes as well as radioactive decay are running quite slowly in comparison to the previous described sorption process. Therefore, these processes are expressed by reaction kinetics.

The simplest form of expressing some degradation of an organic compound is the first-order reaction kinetic, which follows the principle that the concentration change over time is proportional to the initial concentration. Its rate law is expressed by:

$$C_t = C_0 e^{-kt}$$

Eq. 0-25

where C_t [M/L³] characterises the concentration of a solute after some reaction time t [T]. Besides the initial concentration C_0 [M/L³] at $t = 0$ [T], a reaction rate constant k [1/T] is involved. This rate coefficient and the general proof of the existence of a first-order reaction need to be determined experimentally. Radioactive decay is also described by this first-order rate law, since an arbitrary amount of radio-nuclides is halved constantly after its specific radioactive half-life.

A general more complex representation of degrading organic compounds where bacteria are involved is given by Michaelis-Menten kinetics, which is often termed Monod kinetics without microbiological growth (BLUM *et al.* 2009), as the model involves the assumption of a constant microbiological population. This kinetic characterises a zero-order reaction at large concentration values, implying that the concentration change is not related to the initial concentration. Here, the decay rate is characterised by constant maximum decay rate. In

contrast, at low concentration values, this kinetic specifies a first-order reaction where the decay rate depends on the contaminant concentration. This kinetic can be expressed by:

$$\frac{\partial C}{\partial t} = -k_{max} \frac{C}{C + K_c}$$

<div align="right">*Eq. 0-26*</div>

where k_{max} [M/L³ T] characterises the maximum decay rate and K_c [M/L³] the Michaelis-Menten constant.

In general, the degradation of groundwater contaminants which are being transformed by chemical or biochemical reactions is a function of the contaminant concentration as well as the concentration of some other species involved in the reaction. Therefore, multi-reaction models have also become state of the art, where the decay rate of a contaminant has to be represented by more complex functions. Examples are given e.g. in RAUSCH *et al.* (2005). Different reaction kinetics are compared generically in a virtual aquifer by SCHÄFER *et al.* (2007).

All those transformation/biodegradation models which directly affect the mass concentration of groundwater contaminants are of particular interest regarding, for example, the planning and testing of appropriate remediation strategies and technologies.

3.2.2 3-D transport model

Principally, the structure of a 3-D transport model is similar to the form of the 3-D flow model. The transported quantity of a flow model is the mass of the fluid phase (water), whereas in a transport model the transported quantity is the mass of a solute (contaminant) carried by this fluid phase. The different mechanisms of solute transport and their physical descriptions have been introduced in the previous chapter 3.2.1. The 3-D transport model includes the governed concentration mass fluxes of the involved transport mechanisms. The considered mass concentration describes the mass of a chemical species per unit volume of the fluid phase [M/L³]. The transport equation is based on the mass conversation principle. The mass balance of inflows/outflows along all element boundaries of the discretised model element over a temporal variation Δt [T] is related to a change in the solute mass concentration. The classical form of the advection-dispersion-equation (ADE) for a conservative contaminant migration within a one-dimensional system is expressed after BEAR 1972 as follows:

$$\frac{\partial C}{\partial t} = D_x \frac{\partial^2 C}{\partial x^2} - v_x \frac{\partial C}{\partial x}$$

<div align="right">*Eq. 0-27*</div>

where C is the solute concentration [M/L³], D_x the hydrodynamic dispersion coefficient [L²/T], and v_x the averaged pore water velocity [L/T]. For the three-dimensional transport equation,

the mass transport is separated into three components, parallel to all axes of the Cartesian coordinate system:

$$\frac{\partial C}{\partial t} = D_x \frac{\partial^2 C}{\partial x^2} + D_y \frac{\partial^2 C}{\partial y^2} + D_z \frac{\partial^2 C}{\partial z^2} - v_x \frac{\partial C}{\partial x} - v_y \frac{\partial C}{\partial y} - v_z \frac{\partial C}{\partial z} \qquad \text{Eq. 0-28}$$

In addition to the classical 3-D form of the advection-dispersion-equation, source/sink terms can be added optionally and further terms can be included to represent biodegradation or chemical transformations. Due to their complexity, see detailed transport model descriptions given in BEAR & CHENG (2010), FETTER (1992) and KINZELBACH (1992).

The three-dimensional transport equation of the unknown mass concentration $C(x, y, z, t)$ can be of parabolic or hyperbolic form with respect to a dominating dispersive or advective character, derived from the Peclet number (HAEFNER *et al.* 1996 and KARAMOUZIS 1990).

Similar to the groundwater flow model, initial and boundary conditions are needed for an approximate numerical solution of the transport equation.

Initial conditions

The initial condition specifies the transport model concerning its mass concentration C [M/L³] at some initial time, normally taken as $t = 0$.

$$C = f(x, y, z, 0) \qquad \text{Eq. 0-29}$$

If a transport model scenario targets the solute/pollutant discharge from a known mass source, the initial condition is set normally equal to zero at the beginning of the simulation period, except at the source location itself. In contrast, if the model focuses on a continuous transport process of an already detected solute distribution, the initial condition represents the observed distribution pattern.

For the case that several sub-models are involved to represent a global transport scenario, simulation results of a particular model stage serve as initials in the next model stage, etc., to ensure a fluent model transition.

Boundary conditions

Mass transport boundary conditions are required to specify the model domain concerning relevant transport characteristics which are finally affect the mass concentration value (C). Equivalent to the existing flow boundary conditions (section 3.1.2), four different kinds of

boundary conditions (BC) are defined for the mass transport, too. Again, these conditions can be either time-stable (steady) or transient.

The 1st kind BC or *Dirichlet* Boundary Condition defines a fixed solute concentration [M/L³] at the selected model element. This boundary codition is used to describe an existing background concentration, e.g. to assign a contaminant source or to represent a temporal pulse loading characterised by a fixed concentration value.

$$C = f\ (x, y, z, t)$$

<div align="right">*Eq. 0-30*</div>

It is important to state that the 1st kind BC represents only an advective flux of a known concentration as an inflow/outflow and does not incorporate any dispersive mass transport.

If the focus is on prescribing a concentration flux, the 2nd kind of transport BC or *Neumann* Boundary Condition comes into account. This prescribed mass flux boundary or fixed gradient boundary is expressed by:

$$\frac{\partial C}{\partial x} = f\ (t)$$

<div align="right">*Eq. 0-31*</div>

Its most common application is the no-gradient boundary (flux is set equal to zero) which is applied at impervious flow boundaries or at outflow boundaries where the mass concentration is zero. Another important application of a prescribed mass flux is a solute concentration of the groundwater recharge which enters the model domain at the top layer.

The linear combination of the 3rd kind boundary condition or *Cauchy* Boundary Condition is used to characterise a transport setup based on an advective and a dispersive component. The variable-flux boundary is given as:

$$-D\frac{\partial C}{\partial x} +\ vC = vC\ (t)$$

<div align="right">*Eq. 0-32*</div>

where a specific flux vC [M/L³] as a function of t [T] enters the model domain. This describes, for example, a pollutant leaking from a high contaminated source.

The quantity of all incorporated transport processes depends significantly on the applied groundwater flow velocity field which forms the major basis of any transport modelling problem. If a representative flow model of the study area is available, the application of transport related processes (advection, diffusion, dispersion, sorption, decay and reaction kinetics) can be combined individually, whereas the advection-dispersion equation (ADE) is the basic model for describing solute transport problems in groundwater. The incorporated transport mechanisms should be selected and parameterised carefully with respect to the

quality of input data. Once a numerical model setup has been chosen, the model needs to be characterised by transport boundary conditions (e.g. contaminant fluxes along the model boundary, point sources, temporal pollutant loads, hypothetical input areas, sinks, etc.). Subsequently, a transport simulation is run for the specified model setup. Achieved results describe the likely future position of the respective solute as it travelled through the model system. In addition, received model results are usually compared to recorded field data (e.g. breakthrough curves of groundwater observation wells) to verify and calibrate the model configuration. If the so-called "history matching" between measured and simulated datasets is insufficient, the numerical model has to be further specified by adjusting its boundary conditions (e.g. the location of mass sources, mass fluxes or respective material transport parameters). In contrast, if the model provides acceptable results within the range of the observed field data which indicates a calibrated model status, the model is utilised to give future fate predictions of the substance transport over a predefined simulation period.

3.3 Forensic transport modelling (backward-in-time)

As pointed out previously, the classic source-based advection-dispersion equation (ADE) can be used to determine the probable future position and travel time of a solute by forward-in-time modelling. In contrast, forensic modelling aims at the identification of the initial position (source area) and release time estimation of a solvent at injection. Due to this, either a suspected source area is confirmed or even a completely unknown source location is identified. In addition, probabilities on travel and arrival times of the solute transport process can be estimated.

The forensic identification of prior locations and travel times can be performed by using the classical forward-in-time modelling by following the heuristic principle. Therefore, probable source locations are assigned within the model domain, and an individual forward-in-time transport simulation is run for each of the pre-defined source location(s). This initial source location is then adjusted iteratively until the simulation results sufficiently match the observed field data. Even if the source area(s) is unknown and the considered system is complex and of regional scale, as it is the case for real-world scenarios, this direct approach is highly inefficient or will fail as a consequence of the large simulation effort and the required time extent for the numerical solution.

Reverse particle tracking as well as backward-in-time transport modelling are effective receptor-based alternatives for the estimation of location and travel time probabilities, since only a few simulations are needed. Both approaches are based on the reversal of the dominating groundwater flow velocity field and are capable of modeling solute transport mechanisms backward-in-time. While backward particle tracking is the classic approach for capture zone delineation of groundwater observation wells, backward-in-time transport modelling is a relatively new and more accurate method to obtain forensic probabilities.

In the particle tracking procedure, imaginary solute particles are tracked advective-based through the considered system at the basis of the flow simulation. As particle tracking is representative for conservative contaminant transport, the approach does not include the dispersion transport mechanism which is normally present due to aquifer heterogeneities at the microscopic and macroscopic scale. The particle tracking technique is applicable for steady-state and transient flow fields and is characterised by a general low computational effort.

Backward-in-time transport modelling is a more accurate approach than the particle tracking technique, since it is based on the classic ADE of solute transport, which incorporates the advective transport mechanism and an additional dispersive term. Here the receptor-based backward-in-time ADE transport model is the adjoint of the classical source-based forward-in-time ADE transport model. Its numerical implementation is non-trivial, since numerous configurations in space and time concerning the flow field reversal and boundary conditions need to be made. The approach was implemented first-time for realistic 3-D world scenarios under steady-state flow conditions by NEUPAUER & WILSON (2005) and FRIND et al. (2006). Within the presented thesis, the steady-state backward-time-transport method was modified for transient non-uniform flow fields and provides an innovative enhancement for source identification problems.

The conventional flow and contaminant transport code of FEFLOW (DIERSCH 2009a) was used to apply and analyse both retrospective modelling techniques - reverse particle tracking and backward-in-time transport modelling. As both techniques are based on classical theory of groundwater flow and transport modelling, the following sections (3.3.1 and 3.3.2) contain their respective theoretical background, mathematical formulation and required modifications.

3.3.1 Reverse particle tracking

Advective particle tracking is usually used to analyse and visualise the groundwater velocity field by tracking the movement of an imaginary particle with respect to the velocity distribution of the groundwater flow field. As a result, the motion is described by a constructed pathline which signifies its course through the considered model system. While providing information about the groundwater velocity field in a visual form, practical applications are the calculation of arrival- or travel times (VISSER et al. 2009, CRANDALL et al. 2009), the delineation of groundwater protection areas (KONSTADINOS et al. 2008) or the design of hydraulic measures in regards to groundwater remediation/management subjects (BAYER et al. 2004). With respect to the assumption that pollutant transport is basically driven by the advection mechanism, small-scale dispersion is negligible and large-scale dispersion does not exists, pathline analysis are applicable to represent an averaged contaminant transport. Following this, the contaminant movement is represented only by the advective movement of the particles released by some source. According to BEAR & CHENG (2010), each of these particles can additionally carry a certain quantity such as a solute mass concentration or temperature. Thus, the particle tracking method describes a dispersion-free

approximation of contaminant transport. Particle tracking is performed commonly in forward direction, downstream to the normal oriented flow velocity field, to assess the future position of particles. In the current study, reverse particle tracking was applied to create probability estimates on prior source locations and travel times of an already observed groundwater contamination. Therefore, imaginary particles are induced at locations where a contamination was observed. Those particles are tracked advectively in backward direction, upstream oriented to the negative flow velocity field. In regards to this, the considered flow field needs to be reversed in space and time. This negative flow velocity field is derived from a previous simulated and normal oriented groundwater flow model. Forward particle tracking as well as reverse particle tracking can be performed in steady-state or transient flow velocity fields. In both cases, the numerical pathline computation is based on an available groundwater flow velocity field.

The major advantage of reverse particle tracking against conventional heuristic transport modelling is that only one particle tracking simulation is needed to obtain location and travel time probability estimates for the areas/objects of interest. Moreover, the calculation time is significantly lower than of classical forward-in-time transport simulations. In contrast, due to the fact that the dispersive transport mechanism is not incorporated in the advective based particle technique, the method involves some inaccuracy regarding the representation of the solute transport process in time and space.

The tracking scheme

A continuous groundwater flow velocity field of the entire model area is the basic input for the creation of particle tracks. Particles are placed in the flow field which move according to the amplitude of the given flow velocity through the model system. A retarded transport process, caused by adsorption mechanisms, can be considered additionally by a retardation factor. The accuracy of the 3-D pathline computation is linked directly to the accuracy of the previously processed flow simulation. A non-representative hydraulic head distribution and associated flow velocities will lead automatically to inaccurate pathline constructions.

In more detail, for tracking particles in 3-D groundwater flow fields, the flow velocity $\vec{v_a}$ [L/T] of a random location (x, y, z) at the initial point in time t_0 is required. The vector sum of the partial velocities (v_{ax}, v_{ay}, v_{az}) is the basis for the pathline computation over a specific period of time (t).

$$v_{ax} = \frac{\partial x}{\partial t} \quad ; \quad v_{ay} = \frac{\partial y}{\partial t} \quad ; \quad v_{az} = \frac{\partial z}{\partial t} \qquad\qquad \textit{Eq. 0-33}$$

If retardation is considered as a limiting factor of the particle movement, the partial flow velocities of all three dimensions are reduced as follows:

$$\frac{\partial x}{\partial t} = \frac{v_{ax}}{R} \quad ; \quad \frac{\partial y}{\partial t} = \frac{v_{ay}}{R} \quad ; \quad \frac{\partial z}{\partial t} = \frac{v_{az}}{R}$$

Eq. 0-34

where R [-] represents the considered retardation mechanism. For the case that no limiting factors are considered, the retardation factor is simply neglected. The integration of the flow velocity over a specified time period yields for the future position (forward particle tracking) of the particle, considering its initial location (x_0, y_0, z_0) at a specific point in time t_0.

$$x(t) = x_0 + \int_{t_0}^{t} \frac{1}{R} \, v_{ax} \, (x\,(\text{T}), y(\,\text{T}), z\,(\text{T}), T) \Delta \text{T}$$

$$y(t) = y_0 + \int_{t_0}^{t} \frac{1}{R} \, v_{ay} \, (x\,(\text{T}), y\,(\text{T}), z\,(\text{T}), T) \Delta \text{T}$$

Eq. 0-35

$$z(t) = z_0 + \int_{t_0}^{t} \frac{1}{R} \, v_{az} \, (x\,(\text{T}), y\,(\text{T}), z\,(\text{T}), T) \Delta \text{T}$$

The inversion of the underlying velocity field enables the possibility to track the particle reversely, backward-in-time, to identify its prior position (x, y, z) at an arbitrary point in time (t).

$$x_0 = x - \int_{t}^{t_0} \frac{1}{R} \, v_{ax} \, (x\,(\text{T}), y(\,\text{T}), z\,(\text{T}), T) \Delta \text{T}$$

$$y_0 = y - \int_{t}^{t_0} \frac{1}{R} \, v_{ay} \, (x\,(\text{T}), y(\,\text{T}), z\,(\text{T}), T) \Delta \text{T}$$

Eq. 0-36

$$z_0 = z - \int_{t}^{t_0} \frac{1}{R} \, v_{az} \, (x\,(\text{T}), y(\,\text{T}), z\,(\text{T}), T) \Delta \text{T}$$

The presented integrals need to be solved numerically. Several methods such as the *Euler* method, *Euler predictor-corrector* technique (Runge-Kutta second order), *Heun* or higher-order *Runge-Kutta* methods are applicable. According to the statements of BENSABAT *et al.* (1998) and CHENG *et al.* (1996), the *Euler predictor-corrector* technique is superior to the *Euler* technique, whereby high-order *Runge-Kutta* methods provide excellent accuracy. According to this, the fourth-order Runge-Kutta method is used to create location and travel time probability estimates by reverse particle tracking.

Fourth-order Runge-Kutta method

In addition to CHENG *et al.* (1996) and BENSABAT *et al.* (1998), the accuracy and functionality of (high-order) Runge-Kutta methods is also confirmed by POKRAJAC & LAZIC (2002). In general, the accuracy of a tracking code depends on (I) the internal interpolation scheme which is required to make the nodal flow velocities continuous available in the entire model domain and (II) the technique to track the particles through the model domain based on the previous interpolated velocity distribution.

The flow velocities are calculated at the basis of the hydraulic head values which are only accessible at the computational nodes of the groundwater flow model. Against this, when a particle migrates through the model domain, the flow velocity needs to be accessible not only at the computational nodes, but also at every location within the model domain. Furthermore, in unsteady flows, the flow field changes in space as well as in time. With respect to this, these flow velocities need to be interpolated in space for respective time stages by an appropriate algorithm. The often used interpolation methods range from linear, bilinear to quadratic interpolation techniques (CORDES & KINZELBACH, 1992). Therefore, computational grid elements are divided into sub-domains and the corresponding flow velocities are derived from stored hydraulic head values and the applied interpolation scheme.

For the pathline generation, several intermediate 3-D pathline coordinates (XYZ) are combined and connected which were previously calculated by the tracking algorithm. When the groundwater flow is non-uniform and varies often in time, more intermediate positions of the particle are used for the pathline generation than for tracking a particle in a steady-state flow field. The tracking procedure or the calculation of intermediate pathline coordinates is ended when the total simulation time is completed. Already implemented in the finite element system FEFLOW (DIERSCH 2009a), the positive mentioned fourth-order Runge-Kutta method was chosen for 3-D reverse particle tracking analyses in transient flow fields.

In more detail, an intermediate triple of coordinates (XYZ), characterising an intermediate tracking point location, is estimated by the fourth-order Runge-Kutta scheme based on an internal weighting procedure. This weighting procedure includes four individual travel distance calculations for each of the Cartesian axes. Finally, the intermediate coordinates describe a weighted particle movement.

The numerical tracking scheme considers the three Cartesian axes components $x(t), y(t), z(t)$ in combination with their initial conditions $x(t_0) = x_0$, $y(t_0) = y_0$, $z(t_0) = z_0$ where x_0, y_0, z_o define the particle starting coordinates. In consideration of the particle initial position, the final coordinates are calculated for the time step $t + \Delta t$.

The final coordinates $x(t + \Delta t), y(t + \Delta t), z(t + \Delta t)$ are derived from a weighting procedure which uses a subset of four temporal travel distances (k_{1-4}, l_{1-4}, m_{1-4}), one subset for each Cartesian dimension (XYZ). The fourth-order Runge-Kutta method has the form of:

$$x(t + \Delta t) = x_0 + \frac{1}{6}(k_1 + 2k_2 + 2k_3 + k_4)$$

$$y(t + \Delta t) = y_0 + \frac{1}{6}(l_1 + 2l_2 + 2l_3 + l_4)$$

$$z(t + \Delta t) = z_0 + \frac{1}{6}(m_1 + 2m_2 + 2m_3 + m_4)$$

Eq. 0-37

Subset parameters (k_{1-4}, l_{1-4}, m_{1-4}) also result particularly from some internal distance weighting procedure, except for (k_1, l_1, m_1). The subset parameters are determined in accordance to:

$$k_1 = \Delta t \cdot v_{ax}(x_0, y_0, z_0)$$
$$l_1 = \Delta t \cdot v_{ay}(x_0, y_0, z_0)$$
$$m_1 = \Delta t \cdot v_{az}(x_0, y_0, z_0)$$

$$k_2 = \Delta t \cdot v_{ax}\left(x_0 + \frac{k_1}{2}, y_0 + \frac{l_1}{2}, z_0 + \frac{m_1}{2}\right)$$
$$l_2 = \Delta t \cdot v_{ay}\left(x_0 + \frac{k_1}{2}, y_0 + \frac{l_1}{2}, z_0 + \frac{m_1}{2}\right)$$
$$m_2 = \Delta t \cdot v_{az}\left(x_0 + \frac{k_1}{2}, y_0 + \frac{l_1}{2}, z_0 + \frac{m_1}{2}\right)$$

Eq. 0-38

$$k_3 = \Delta t \cdot v_{ax}\left(x_0 + \frac{k_2}{2}, y_0 + \frac{l_2}{2}, z_0 + \frac{m_2}{2}\right)$$
$$l_3 = \Delta t \cdot v_{ay}\left(x_0 + \frac{k_2}{2}, y_0 + \frac{l_2}{2}, z_0 + \frac{m_2}{2}\right)$$
$$m_3 = \Delta t \cdot v_{az}\left(x_0 + \frac{k_2}{2}, y_0 + \frac{l_2}{2}, z_0 + \frac{m_2}{2}\right)$$

$$k_4 = \Delta t \cdot v_{ax}(x_0 + k_3, y_0 + l_3, z_0 + m_3)$$
$$l_4 = \Delta t \cdot v_{ay}(x_0 + k_3, y_0 + l_3, z_0 + m_3)$$
$$m_4 = \Delta t \cdot v_{az}(x_0 + k_3, y_0 + l_3, z_0 + m_3)$$

Transient particle tracking simulations enclose a significant uncertainty in regards to the variability of the advective flow velocity field and the time step lengths used for the calculation of particle coordinates. Here, the more the non-uniform flow field varies, the smaller the simulation time step length should be to avoid inaccuracy, such as underestimated/overestimated pathline lengths. At the same time, small time step lengths

increase the simulation time, whereas larger steps reduce the total simulation time significantly.

Therefore, an automatic time step adjustment is used, which is controlled by a pre-defined error criterion. The optimisation routine is based on the calculation of three travel distances for three individual time step lengths. If the discrepancy between the travel distances exceeds the internal error criterion (longitudinal value), the maximum time step length used is reduced and the tracking procedure is repeated. In contrast, if the error criterion is not fulfilled, the time step length is increased to speed up the computation.

3.3.2 Backward-in-time transport modelling

Conceptually similar to the advective particle tracking which can be applied in a forward or backward mode, an advective-dispersive transport model can be utilised in forward and backward direction, too. Thus, the backward-in-time advective-dispersive transport approach also solves the problem of a probable initial position (source) of a solute being part of a current observed contamination. Formally, backward-time-transport modelling is the adjoint solution of the forward-in-time transport modelling (WILSON & LIU 1994, 1997 and NEUPAUER & WILSON 1999, 2001, 2004), which can be used to solve for location and travel time probabilities backward in time. With the current state of knowledge, the approach has been implemented successfully for steady-state three-dimensional problems. The method was used by NEUPAUER & WILSON (2005) for capturing zone delineation of a pump-and-treat remediation system at the Massachusetts Military Reservation and by FRIND *et al.* (2002, 2006) for capturing zone delineation of the Greenbook Wellfield, Waterloo. For the current study, the steady-state backward-in-time transport modelling was modified and implemented successfully to be applicable also for transient backward-in-time transport problems.

While the result of forward transport modelling is interpreted physically in terms of a solute concentration, no physical analogue for the backward probability exists. In regards to this, the backward-in-time transport model focuses on a location probability $p = p\,(x, y, z)$, which expresses the probability that a solvent has originated/entered the aquifer at some position (x, y, z). This additionally involves the probability estimation of the travel time (T), which indicates that a solvent has originated at some location and at some specific point in time $\leq (T)$. Received probability distributions represent probable prior locations or travel times of the considered solute but give no information about its prior concentration or, for example, the source mass!

The backward-in-time transport model can be derived from the standard advection-dispersion equation (Eq. 0-27) as introduced by BEAR (1972). The physical principles of the advection and dispersion transport mechanism in conventional forward mode are described in detail in section 3.2.1.

Formally, since no physical analogue for the concentration $C = C\,(x, y, z, t)$ exists in the backward approach, the concentration term is replaced by the location probability $P = $

$P\,(x, y, z, T)$, with (T) being the backward time. For modelling the adjoint advective-dispersion equation, the flow velocity $v\,(x, y, z)$ is inverted by $-\,v\,(x, y, z)$, similar as for the reverse particle tracking approach. For the one-dimensional case, the reversed advective-dispersion equation is:

$$\frac{\partial P}{\partial T} = D_x \frac{\partial^2 P}{\partial x^2} + v_x \frac{\partial P}{\partial x}$$

Eq. 0-39

In three-dimensional form, the advective-dispersion equation is adapted to:

$$\frac{\partial P}{\partial T} = D_x \frac{\partial^2 P}{\partial x^2} + D_y \frac{\partial^2 P}{\partial y^2} + D_z \frac{\partial^2 P}{\partial z^2} + v_x \frac{\partial P}{\partial x} + y \frac{\partial P}{\partial y} + v_z \frac{\partial P}{\partial z}$$

Eq. 0-40

The considered dispersion mechanism of the adjoint transport equation serves the same purposes as in the forward-in-time equation. According to the theory of macro-dispersion by GELHAR & AXNESS (1983), the dispersion coefficient expresses the uncertainty of the heterogeneous structure of the porous media and its effect on solute transport. Although the velocity term in the backward mode is reversed, the direction of the dispersion term does not change, since the uncertainty due to heterogeneity depends on the magnitude of velocity, not its direction (NEUPAUER & WILSON 1999).

To avoid any misconception concerning the adjoint ADE model and the incorporated dispersion term, it is of particular importance to state that the included dispersion term does not represent a temporally inverted dispersion mechanism! In fact, the dispersion term in the backward mode fulfils the same function as in the forward mode, leading finally to an increased spreading rate of the transported solute, based on material heterogeneities at the microscopic and macroscopic scale.

In theory, since a contaminant had been released by a source location, its discharge is detected at a monitoring well as function of the solute concentration C and the time (t). The recorded breakthrough curve can provide quantitative characteristics such as the exceedance of a threshold concentration or a concentration maximum of the solute as well as temporal characteristics about the time taken to reach the threshold or maximum. For the source zone allocation, a mass signal is induced at the affected observation well location at an arbitrary point in time which is subsequently tracked backward based on the adjoint solution of the classic ADE model. The received probability distribution $P = P\,(x, y, z, T)$ represents prior locations and travel times.

Temporal information derived from breakthrough curves, such as the point in time when a maximum solute concentration was reached or a threshold was exceeded, constitute favourable time markers for the injection of the mass load impulse. Here the simulation time

for the backward-in-time transport modelling can be characterised location specific, which limits the uncertainty of the resulting backward probability estimates. In contrast to this, when no information about the arrival time from monitoring data is available, the mass impulse is injected at the time stage when the contamination was detected, and the simulation is performed for an arbitrary simulation period backward in time. This can lead to an overestimated backward simulation time, which automatically increases the uncertainty of the received backward probability estimates as they are overestimated, too.

As the spatial flow field reversal of the adjoint ADE model is capable of creating backward probability estimates in steady state flow fields, additional modifications are required to make the approach working for transient flow/transport problems. In forward oriented transient transport problems, the advective mass flux is linked to the temporal variations of the groundwater flow velocity field. In backward mode, these temporal variations of the groundwater flow velocity field need to be provided reversed in time to solve a transient characterised system by the adjoint ADE model.

In more detail, in forward mode, the transient system is specified by time-dependent functions (time series data) which define transient flow model boundary conditions, for example, along river courses, the groundwater recharge at the top model layer, positive or negative well fluxes as well as model inflows/outflows. In the backward mode, descriptive functions of related time variant parameters (hydraulic head, extraction rate, inflow/outflow etc.) are reversed in time. Therefore, the last time stage of the forward model function represents the first time stage of the backward model function. Thus, it is warranted that the transient model can be solved reversed in time, based on inverted functions specifying the model boundary conditions. Moreover, the backward model needs to be modified additionally concerning its initial conditions. Since the backward model simulation starts at the last time stage of the forward model, the final solution of the forward model (e.g. hydraulic head distribution) serves as the initial condition in the backward model.

Here the transient backward-in-time transport approach is based on the spatial flow field reversal implemented by the adjoint ADE model (a), a temporal reversed velocity field which is enforced by inverted time series data for the characterisation of model boundary conditions (b), and the modified initial conditions (c). By following this, transient backward location and travel time probabilities are received for the reference data point where the mass signal was induced. By considering a predefined simulation time, the generated location specific capture zone provides probable prior source locations at some specific point in time.

For the source identification procedure, transient backward location and travel time probability estimates are created individually for the involved observation point locations where a contamination was observed. In the final analysis, these backward probabilities of multiple reference points are intersected by each other to identify primarily common source zones which represent model-indicated contamination origins. The intersection process is done in a GIS environment. Thus, probable source zones are confirmed and emphasised by

individual backward probabilities from multiple observation points, which finally reduces the model uncertainty of the transient source location problem.

3.4   Chapter summary

As described in section 3.1 and 3.2, numerical models of groundwater flow and solute transport can be utilised to generate a predictive model assumption or system analysis about the future fate of a solute being transported in groundwater. If the focus is on groundwater contamination problems, future predictions about the plume development can serve for finding optimal remediation strategies and providing an essential basis for environmental risk assessment studies.

Simultaneously, the contaminant source location and its release history are often unknown or only suspected, which hinders significantly the assignment of responsibility and complicates the implementation of an effective remediation concept. The classical advection-dispersion transport concept can be applied for forensic source identification problems by heuristic modelling. In this form, the heuristic approach is highly inefficient in terms of the required simulation effort because numerous iterative model runs are needed to obtain practicable results.

Reverse particle tracking (3.3.1) is an effective alternative to describe advective based transport processes. Based on a reversed groundwater flow velocity field, an imaginary particle is tracked backward in time and provides information about location and travel time probabilities in respect to its initial position. However, reverse modelling is significantly more efficient than conventional forward-in-time (heuristic) modelling, since only one single backward model run is necessary to obtain source location and travel time probabilities instead of many forward model runs. The particle tracking technique includes generally the disadvantage that the transport process is described only by the advective transport mechanism and neglects the uncertainty of aquifer heterogeneities which is normally represented by the dispersion term. Nevertheless, reverse particle tracking is the classical standard method for capture zone delineation of groundwater wells and is available for steady-state and transient model environments.

Due to the conceptual limitation of particle tracking, backward-in-time transport modelling is introduced (section 3.3.2), which is derived from the classic advection-dispersion equation (forward-in-time) to describe solute transport processes retrospectively. Since the dispersive transport mechanism is considered, this approach is more accurate in regards to obtained source and travel time probability estimates than those received from the particle tracking scheme. With respect to this, it is stated that the included dispersion term of the adjoint ADE model does not represent a temporal inverted dispersion mechanism! Due to its mathematical formulation of the classic ADE concept, this mechanism is based on some initial concentration of the solute and some location-specific hydraulic gradient at the location of mass input to a specific point in time which are generally unknown in the case of source

identification problems. Therefore, there is no reliable procedure to solve a complete inverted dispersion mechanism yet! The spatial inverted dispersion mechanism of the adjoint ADE model fulfils the same function as in the forward mode, which leads finally to an increased spreading rate of the transported solute. Therefore, received backward location and travel time probabilities for source identification involve the effects of aquifer heterogeneities onto the retrospective solute transport process, which is a major advantage against the advective based reverse particle tracking. Thus, the presented adjoint ADE model constitutes a favourable technique for contaminant source identification problems, since it is based on the classic formulation (ADE concept) of solute transport mechanisms in groundwater.

So far, the method is rarely used, because several model modifications are required to apply this technique. With the current state of knowledge, backward transport modelling was established successfully for 3-D steady-state problems. For the presented study, the approach was further developed to also be applicable in 3-D transient model environments. Transient backward-in-time transport modelling includes (1) an advective velocity field reversal within the adjoint ADE model, (2) the temporal inversion of the transient velocity field by modifying involved boundary conditions, and (3) the consideration of appropriate initial conditions.

4 Numerical application and simulation

4.1 Finite element method (FEM)

Partial differential equations abstract groundwater flow and solute transport mechanisms are solved (approximated) by numerical methods. For the current study the finite element code FEFLOW (Diersch 2009) is used. In contrast to the often used and popular finite difference method (FDM), the FEM has the following major advantages:

- High flexibility for designing the computational mesh of the model domain
- Local mesh refinement(s)
- Adjustment of mesh orientation to reduce numerical dispersion

Generally, the model domain Ω is subdivided into a number of irregular shaped elements in horizontal and vertical scale. These elements provide a computational mesh while the computational nodes of the irregular grid are located at the element vertices:
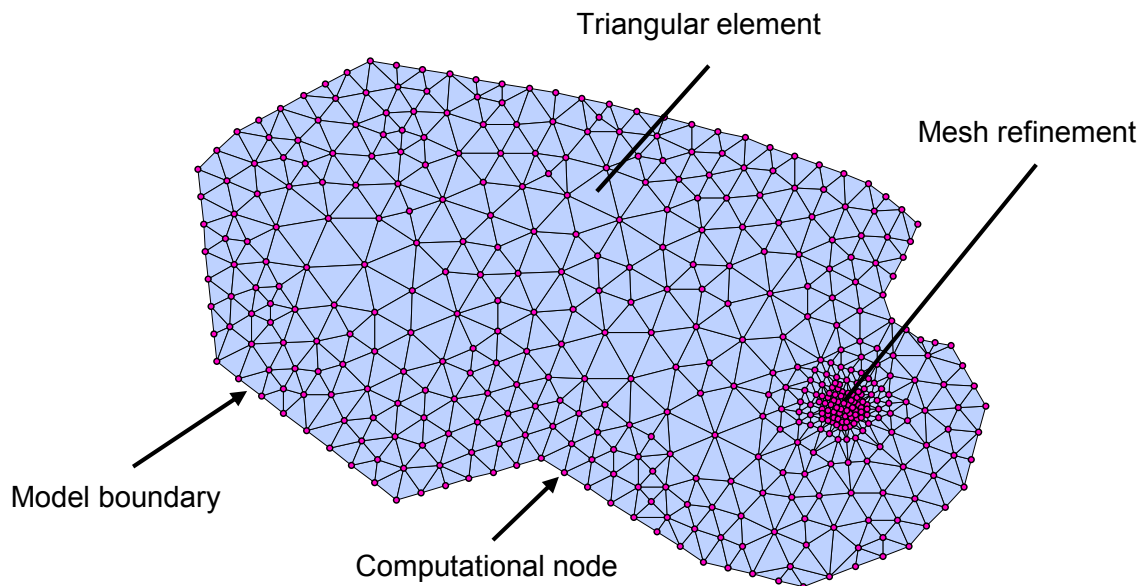
Figure 4-1: The finite element mesh discretises the model domain Ω into triangular sub-elements. The numerical approximation of groundwater flow and transport is realised at the element participating vertices.

A single computational node represents element vertexes of multiple elements. Globally, a complex model domain is represented by various and simplified model elements. In the

following, the basic operation principle of the FE method for a groundwater flow modelling problem is introduced. The conceptual implementation of a solute transport model is applied similarly with respect to the governing mathematical formulations of section 3.2. For a deeper understanding of the complex mathematical background of FEM, see available literature such as PINDER & GRAY (1979) or KAZDA (1990).

The FE-method describes a piezometric head at an arbitrary location (x, y, z) within a model element by the means of an interpolation function. The unknown head value is approximated by linear, bilinear or quadratic interpolation techniques (CORDES & KINZELBACH, 1992) based on values at the computational nodes. Thus, the interpolation function provides a hydraulic head value at any point inside the element as a function of known nodal head values.

In addition, the averaged Darcy velocity vectors of a single element are derived for each Cartesian axis from the three associated nodal head values, related hydraulic conductivities, and the lateral element area. From neighbouring elements, the velocity vectors are projected as surface normals to the triangle sides of the particular element. The entering flow rate $(Qs1, Qs2, Qs3)$ [L³/T] is estimated in consideration to the flow velocity [L/T] of the adjacent element and the penetrated side element area [L²].
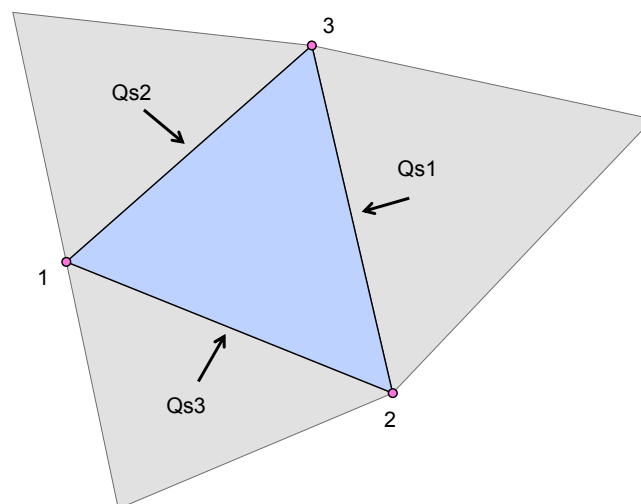
Figure 4-2: External inflows $(Qs1, Qs2, Qs3)$ from adjacent model elements are used to represent the piezometric head change at the particular element nodes (1,2,3).

Finally, the piezometric head adjustment at the element nodes $(1, 2, 3)$ is applied by assigning a nodal-specific flow rate (W_1, W_2, W_3) to the particular element vertices in regards to Eq. 4-1, which leads finally to a change of the node specific hydraulic head value.

The nodal flow rate (W_1) of node (1) is estimated by using the half of the outer inflows $(Qs2, Qs3)$ which enter the model element along the two adjacent element sides of the grid node:

$$W_1 = 0.5\ Qs2 + 0.5\ Qs3 = -0.5\ Qs1$$

$$W_2 = 0.5\ Qs3 + 0.5\ Qs1 = -0.5\ Qs2 \qquad\qquad \textit{Eq. 4-2}$$

$$W_3 = 0.5\ Qs1 + 0.5\ Qs2 = -0.5\ Qs3$$

The nodal specific flow rates (W_1, W_2, W_3) are calculated according to Eq. 4-2.

This means that the nodal flows are used to define elemental inflows/outflows to adjust the unknown hydraulic head values at the element nodes by linear functions. This principle formulation is representative for an individual model element. To involve all remaining model elements of the entire model domain of Figure 4-1, the linear functionality for the unknown hydraulic heads from the local scale is transformed into a global "element-consistent" formulation. Therefore, in FE-methods, the elemental linear functions of a single triangular element (e) which are based on local coordinates or indices are translated into global coordinates. This is realised by an incidence matrix. It defines a global number (k) for each node, as a function of an element number (e), and a local node number (i). In addition, nodes which represent an element vertex of more than one element are characterised by more than one global coordinate. Further details on coordinate transformation are given in KINZELBACH (1987). Here all elemental equations are transformed into a global equation system for determining the unknown hydraulic head values of the model system.

Since numerical boundary conditions are required for solving the global system of linear functions, these BC are assigned to the global element nodes of the system. For using a 1st kind BC, the constant and prescribed head value is set directly at the node location. When a second-type boundary is used, the flux-boundary can represent a zero flux boundary or a non-zero flux boundary. For impermeable boundaries, the external flux (Qs) is simply set to zero and a zero flow rate enters the model domain with respect to Figure 4-2. For the case of a non-zero boundary flux, the external flux (Qs) is assigned to both nodes related to the respective element side. The 3rd kind boundary condition is treated equivalently. With a distributed recharge at some top element, such as the process of groundwater recharge at the top surface of the global model, the flux rate is split up either homogenously to all three element nodes or is distributed area-related based on previous constructed Thiessen polygons.

Finally, the system of linear equations for the approximation of the unknown piezometric heads is solved by using numerical solver techniques such as the Gauss-Seidel method, preconditioned conjugate gradient (PCG) technique, post-conditioned bi-conjugate gradient stable method (BiCGSTABP), or the algebraic multigrid technique (SAMG). The latter three equation solver techniques are implemented in the FEFLOW system used.

4.2   Generic simulations in 2-D transient flow fields

Synthetic box models have been applied in FEFLOW to test the numerical implementation of the previous introduced forensic modelling approaches (chapter 0). This includes conventional forward-in-time transport modelling as well as reverse particle tracking and backward-in-time transport modelling in a transient model environment. Finally, it is intended to analyse the functionality as well as the accuracy of the chosen approaches for source identification problems.

4.2.1 Problem definition

Initially, the numerical model is characterised by a confined 2-D model setup under transient flow and transport conditions. The created transport scenario represents a single-source scenario. The transport simulations include advective, dispersive, and retarded transport mechanisms. During the transport simulation, the resulting mass discharge is registered at several reference data points to specify the considered transport mechanisms. All the datasets which had been used for the model setup/input have a completely fictitious origin. For the following simulations, the classic mode of FEFLOW version 6.0 (build 6.0.6004) was used.

Spatial and temporal discretisation

The box model has the dimension of 3000 [m] by 1000 [m], has a virtual area of $3 \cdot 10^6$ [m²], is discretised by 49024 triangular elements and contains 24781 computational nodes.
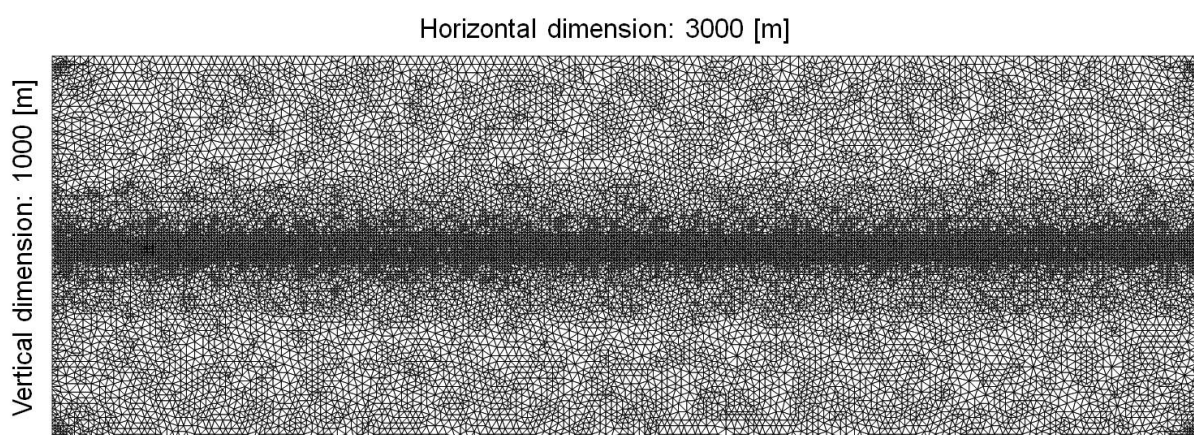
Figure 4-3: The horizontal model discretisation comprises 49024 triangular elements and covers a spatial model dimension of 3000 [m] by 1000 [m].

A higher discretisation level was chosen along the horizontal centre line (Figure 4-3) to enhance the numerical stability during the following transport simulation runs. The element sizes range from 3.0 [m²] to 115.0 [m²], the averaged element area is approximately 61.1 [m²].

The total simulation time of the generic 2-D transport scenario was set to 5475 [d]. To optimise the total computational time and to enhance the quality of results, an automatic time step control and a maximum time step limit of 10 [d] was used.

4.2.2 Transient flow simulation (forward-in-time)

Flow material properties, initial and flow boundary conditions

The two-dimensional flow model was parameterised globally with a transmissivity of $5 \cdot 10^{-3}$ [m²/s], which is related to an aquifer thickness of 50.0 [m] and a hydraulic conductivity of $1 \cdot 10^{-4}$ [m/s]. Those material properties or any parameters can be defined either globally or for each node individually by a manual node-wise selection, via selection rectangle, or predefined database. Especially the database option provides a high functionality, since file formats such as ASCII (*.dat), Dbase (*.dbf), and ESRI shapefiles (*.shp) are supported.

Numerical flow boundary conditions have been specified to characterise the transient flow system. A time-constant 1st kind prescribed head boundary of +50.0 [m] was defined at the western model side element (Figure 4-4). In addition, at the eastern model boundary, a non-constant (transient) 1st kind BC was used, which prescribes an initial head value of +35.0 [m] at the beginning of the simulation and drops slightly to +29.0 [m] at the end of the simulation time after 5475 [d]. A transient boundary condition in FEFLOW is defined by a function of the piezometric head (h) with respect to time (t). Moreover, the southern and northern model boundary is consistently characterised by a 2nd kind no flux boundary condition. Based on the chosen boundary condition setup, a dominating groundwater flow direction from the west to the east is expected.

Moreover, an initial piezometric head distribution specifies the initial flow condition for the transient simulation. This initial head distribution was created from a previous run steady-state flow model, which considered a constant 1st kind BC (+50.0 m) at the eastern model side and a constant 1st kind BC (h= +35.0 m) at the western model boundary. The final results of the steady-state flow model serve as the initial condition of the transient model. The data transfer was managed by the previously mentioned database feature.
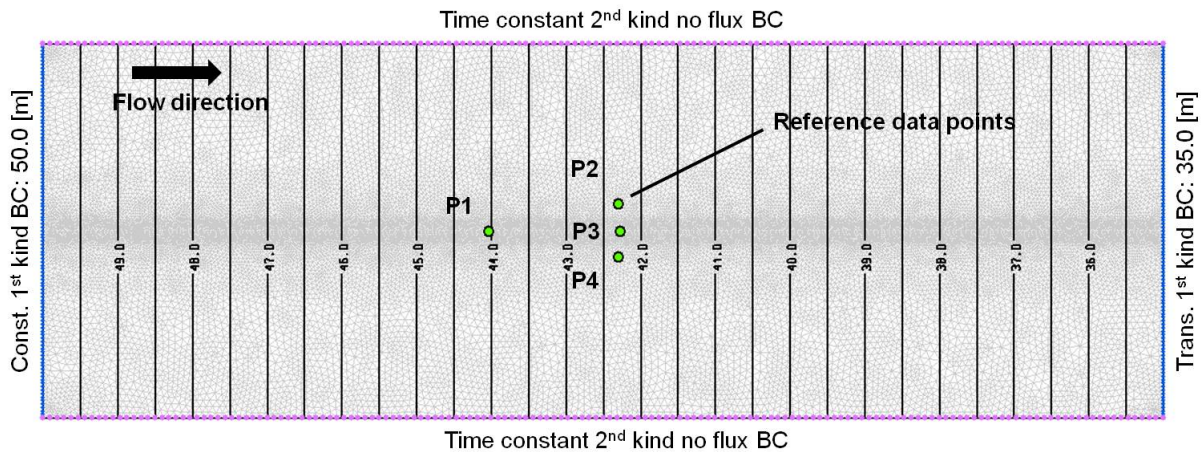
Figure 4-4: The flow model is characterised by several flow boundary conditions. Constant prescribed piezometric heads (1st kind BC) were used at the western model side, whereas a transient 1st kind BC was assigned at the eastern boundary. The groundwater flow direction is from west to east. An initial hydraulic head distribution configures the initial BC at the beginning of the simulation. Reference data points (P1-P4) are used to observe changes in the hydraulic head in regards to the transient system.

To observe respective hydraulic variations during the simulation, so called observation points had been added to the model (Figure 4-4) which constitute imaginary reference data points and represent, for example, observation well locations. Therefore, existing element nodes of the irregular mesh are used. The observation point location can be either set manually or can be imported and assigned based on a supported data file format as, for example, the (*.shp) file format. An appropriate import file contains the observation point locations in form of spatial XY coordinates.

Groundwater flow simulation

When the groundwater flow model is configured regarding its material parameters to characterise the porous media, its initial flow conditions and the characteristic flow boundary conditions, the numerical model is ready to run. For solving the numerical equation system, the BiCGSTABP solver was used. During the total simulation period of 5475 [d], the transient variations of the piezometric head had been recorded at the predefined observation well locations of Figure 4-4. The received observation point data is similar to time series data, as it comprises location specific hydraulic head values at appropriate simulation time stages. Based on this, the hydraulic variations can be visualised in form of location specific hydrographs. Post-processed in Excel, Figure 4-5 contains the hydrographs of the considered reference data points P1-P4.
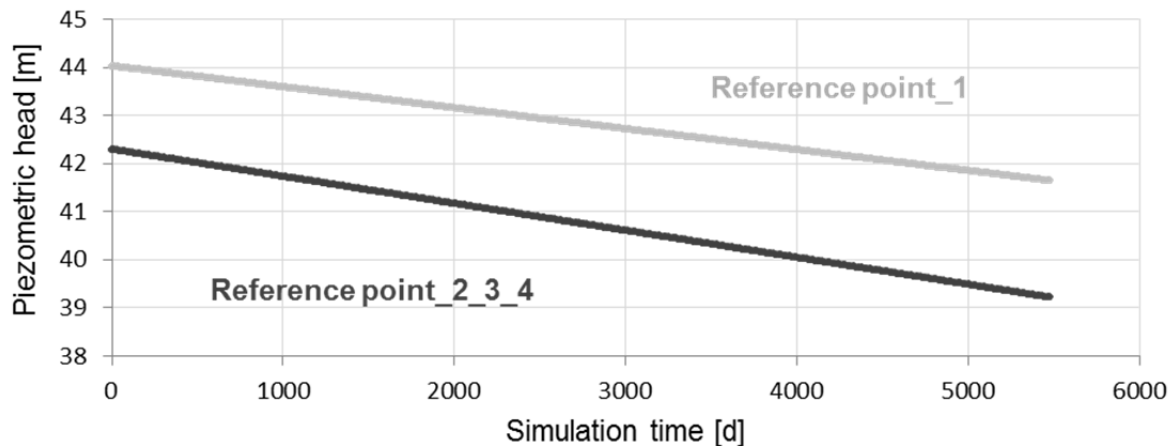
Figure 4-5: Transient 2-D flow simulation: The hydrographs of the reference points P1-P4 illustrate the transient character of the model setup by a general decrease of the hydraulic head values at those observation point locations. Based on simulation results, the observation points P2-P3-P4 showed equivalent hydraulic characteristics.

After the simulation is started, model specific data is saved to a result file. In general, the results are saved either to a reduced file format (*.dar), a standard ASCII format which comprises only time series data of assigned reference data points, or in form of a binary file format (*.dac) that includes a complete dataset of the entire model domain. Here the (*.dac) file format includes data for each node of the computational model mesh. Model relevant data can be saved at pre-defined time stages. This might be of advantage if the modelled system needs to be monitored in specific intervals or at selected time stages. Pre-defined time steps are specified by (*.txt) or (*.csv) file formats. During the transient 2-D flow simulation, data was saved in 100 [d] intervals.

Conclusion

A simplified 2-D FEFLOW box model was used to reproduce a transient groundwater flow velocity field controlled by a time varying 1st kind boundary condition. Virtual reference data points were assigned in the model domain (Figure 4-4) to observe the temporal variation of the flow velocity field over a total simulation time of 5475 [d]. Simulation results were saved to a FEFLOW internal result file format (*.dac). The resulting hydrographs (Figure 4-5) of the reference points attest the transient character. This non-steady flow model provides the basis for the following 2-D transient transport simulation.

4.2.3 Transient transport simulation (forward-in-time)

The following transport simulations include the combination of individual solute transport mechanisms which had been introduced by their theory and numerical approximation in section 3.2.1. The FEFLOW code is used to reproduce advective, dispersive, and retarded transport processes which serve in a conventional way for future fate predictions on solute transport in groundwater systems. Therefore, a 2-D transient transport scenario within a transient flow environment was simulated to obtain the effects of advection, dispersion, and retardation onto the solute mass distribution. Related simulation results are presented in form of breakthrough curves at the previously used reference data points of the transient 2-D flow model.

Transport material properties, initial and transport boundary conditions

Similar to the flow model, the transport model must be configured concerning its transport parameters as well as transport boundary and initial conditions.
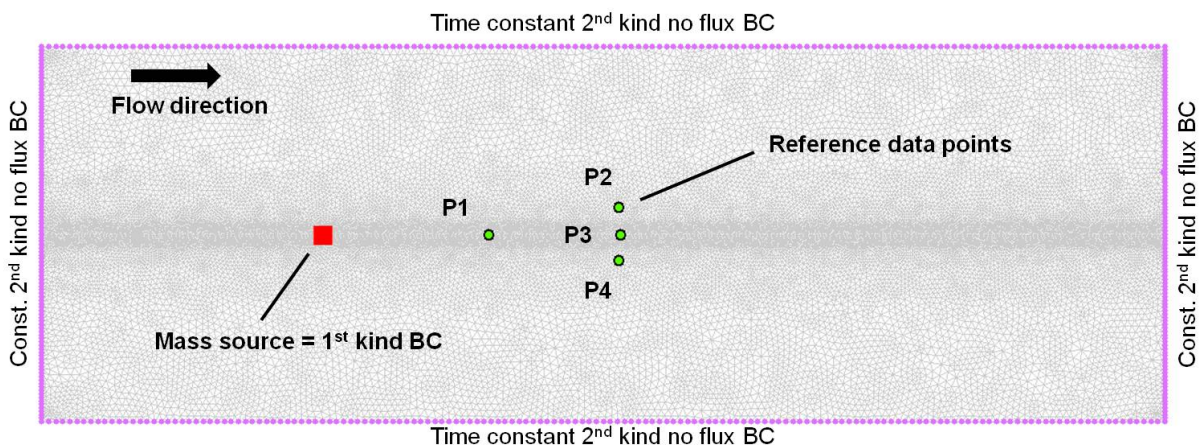
Figure 4-6: A temporal load impulse of 100 000 [mg/l] was defined as a mass source by using a nodal 1st kind transport BC. The model periphery has been characterised consistently by a no flux boundary (2nd kind BC). Observation point locations were adopted from the transient 2-D flow model. Since the groundwater flow direction is from west to east, the mass transport follows this direction simultaneously.

First, a temporal mass impulse was defined in the transport model by using a transient 1st kind BC which describes a temporal pollutant load or mass source (Figure 4-6). For this purpose, a prescribed mass concentration of 100 000 [mg/l] is induced at the source location for a period of one day, at the beginning of the total simulation time of 5475 [d]. Similar to transient flow BC, transient transport BC are implemented as time series data or power functions (*.pow). In addition, a time-constant 2nd kind no flux BC was used to specify the transport model periphery. Moreover, a mass concentration of 100 000 [mg/l] is set at the

source location as an initial BC which defines an already existing mass pool at the beginning of simulation. All remaining mesh nodes are assigned with an initial condition of 0 [mg/l]. The transport model was run for three different scenarios, describing three individual transport processes: (I) advective transport, (II) advective-dispersive transport, (III) advective-dispersive-retarded transport.

Until no specifications are set concerning diffusion coefficients, longitudinal/transversal dispersion lengths, sorption (retardation) parameters, the mass transport is based only on the advective transport mechanism (I). Probable existing default values have to be considered and removed! For the advective-dispersive transport scenario (II), a longitudinal dispersivity of 2.5 [m] and a transversal dispersivity of 0.25 [m] was used globally. Conditions for hydrodynamic dispersion are fulfilled by adding a diffusion coefficient of $1 \cdot 10^{-9}$ [m²/s]. The previously created advection-dispersion configuration was extended by a sorption mechanism, following the Henry concept, to represent a retarded solute transport process (III). The Henry concept/coefficient used in FEFLOW is implemented by the Kd-value multiplied by the solid density! With respect to this, a Henry coefficient of 0.1 [-] was used for the retarded transport simulation. Since only the effective porosity is available for the selected solute transport process, an aquifer porosity of 30% was parameterised.

Mass transport simulation

Generic transient transport simulations were run to simulate the differentiated transport mechanisms (I), (II), and (III). Therefore, a steady-flow environment was created which is primarily based on the flow boundary condition setup of Figure 4-4, except for the transient flow boundary condition in the east. This steady-state 1st kind boundary condition was defined by a constant head value of 35.0 [m]. The total simulation time of each individual simulation was set to 5475 [d]. A predefined mass was induced at the source location of Figure 4-6, and resulting concentration breakthrough curves were recorded only for the reference data point 1, individually for the considered solute transport mechanisms (1), (2), and (3). Associated concentration time series data was exported and transferred by using the FEFLOW internal *.pow file format. During the modelling procedure, the advective transport simulation tended to oscillations and numerical model instability, caused by an insufficient discretisation in time and space. Therefore, to overcome this problem, an additional mesh refinement and a reduction of the time step limit to 0.1 [d] were applied. Then, advective-dispersive and advective-dispersive-retarded transport was modelled in consideration of these settings. The received time series data of the different solute transport mechanisms were post-processed and are illustrated in Figure 4-7.
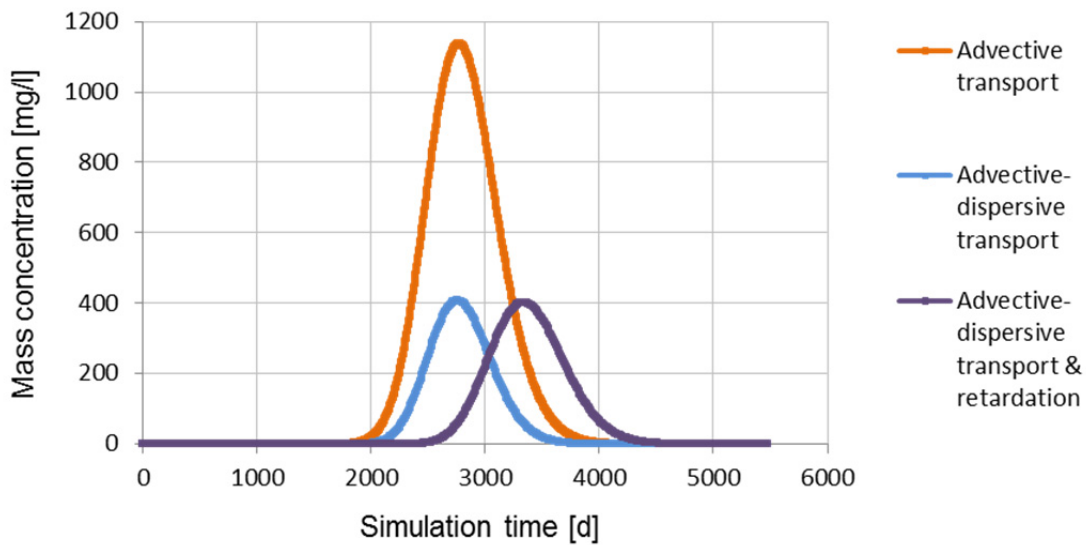
Figure 4-7: 2-D steady-state flow/transient transport simulation: Three breakthrough curves based on differentiated transport mechanisms had been recorded at the single reference data point location P1 of Figure 4-6. The resulting curves differ concerning their concentration maximum due to the dispersive dissolution mechanism and additionally by their arrival times resulting from an incorporated retardation process which reduces the idealistic advective transport rate.

In addition to the previous run steady-state transport simulations, a transient contaminant scenario was created which combines the transient flow boundary condition setup of Figure 4-4 and related BC's of the previous used transient transport scenario of Figure 4-6. In this scenario, a transient advective-dispersive transport configuration was simulated. Again, a temporal mass load impulse of 100 000 [mg/l] was induced at the source location, and the resulting mass plume migrated with respect to the transient velocity field from the western model domain towards the east.

Required transport material parameters were assigned: The hydrodynamic dispersion is parameterised by a diffusion coefficient of $1 \cdot 10^{-9}$ [m²/s], a longitudinal dispersion length of 5.0 [m], and a transversal length of 0.5 [m]. The inclusion of dispersion was chosen deliberately, since the dispersion mechanism accounts for a spreading effect, caused by aquifer heterogeneities, which is the more realistic representation of solute transport processes in groundwater than by neglecting this term entirely. Concentration breakthrough curves were recorded at reference data points. An overview of the parameter settings of the transient transport model are given in Table 4-1. The total simulation time was set again to 5475 [d]. The results of the contaminant scenario are shown in the following Figure 4-8 and Figure 4-9.

Table 4-1: Model properties of the transient 2-D transport simulation. All listed parameters are assigned to the FEFLOW model in the respective menus, such as temporal and control data, reference data, transport materials, transport boundary condition etc.

Parameter	Unit	Transient 2-D flow and transport
Length	[m]	3000
Width	[m]	1000
Number of elements	[-]	49024
Mean element area	[m²]	61.1
Mean side element length	[m]	10.7
Bottom elevation	[m]	0.0
Aquifer thickness	[m]	50
Transmissivity	[m²/s]	$5 \cdot 10^{-3}$
Source location	[m]	(X= 750, Y= 500)
Source mass	[mg/l]	100 000
Reference point_1	[m]	(X= 1193, Y= 500)
Reference point_2	[m]	(X= 1540, Y= 572)
Reference point_3	[m]	(X= 1542, Y= 500)
Reference point_4	[m]	(X= 1541, Y= 430)
Longitudinal dispersivity	[m]	5
Transversal dispersivity	[m]	0.5
Effective diffusion coefficient	[m²/s]	$1 \cdot 10^{-9}$
Porosity	[-]	0.3
Total simulation time	[d]	5475
Maximum simulation time step	[d]	10

The induced mass signal migrated through the model domain based on an advective-dispersive transport mechanism. The moving mass plume was observed in form of breakthrough curves at the respective reference data points P1-P4 of Figure 4-8. Those graphs characterise the solute transport process concerning its travel time and mass quantity (Figure 4-9). During the simulation, the plume reached the reference data point number P1 first and reached subsequently the model area of the observation points P2-P4. At the end of the simulation time of 5475 [d], the mass distribution passed the reference data point number P1 completely, while the remaining observation points were still surrounded by the mass plume (Figure 4-8). This plume development is also reflected by the characteristics of respective breakthrough curves. While the plume front reached the reference data point number P1 at approximately 1800 [d], this location was affected by a maximum mass concentration of about 190.0 [µg/l] after a simulation time of 2675 [d]. The mass distribution passed the location after a simulation period of about 4000 [d]. The remaining observation point locations 2-3-4 had been affected after an arrival time of approximately 3345 [d], whereas related impacts concerning the mass quantity differ significantly. The maximum concentration at reference point number P3 had been observed after about 4640 [d].
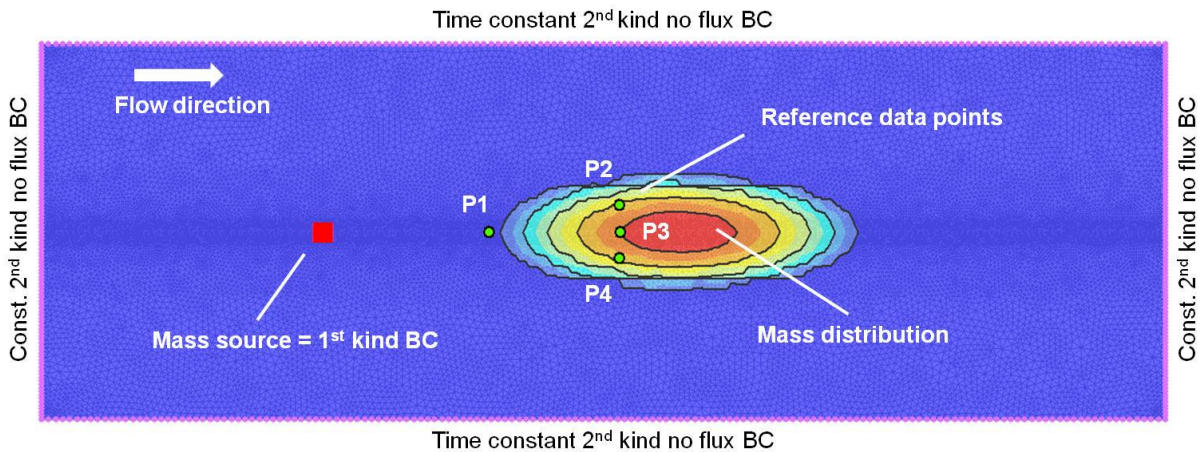
Figure 4-8: The figure illustrates a mass distribution which moved after its source release towards eastern direction based on an advective-dispersive transport mechanism. The red colour indicates high mass concentration levels while blue colours indicate lower levels. At the end of simulation, the plume front passed obs. P1 and is currently situated in the area of obs. points P2-P4.
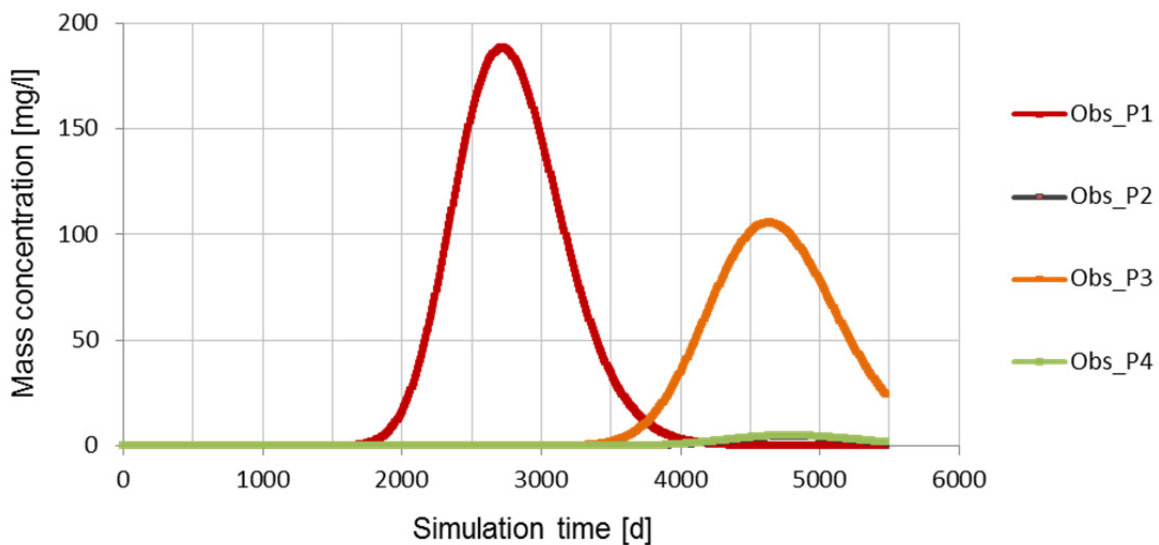
Figure 4-9: Breakthrough curves: The moving mass plume was registered at all four observation points. The mass distribution passed obs. point P1 entirely after app. 4000 [d] and reached subsequently the observation point locations P2-P4. With respect to mass quantity, obs. P3 are characterised by a significant lower concentration than obs. P1, which is caused by an increased dilution effect of the hydrodynamic dispersion.

Reference data point number P3 is characterised by a maximum concentration of about 105 [mg/l] at a simulation time stage of 4640 [d]. In contrast, in a quantitative manner, the reference points P2 and P4 are affected only marginally, since they are situated at the plume edge. Related concentration levels are in the range of a few micrograms per litre.

Moreover, the observation point location P3 is characterised by a significantly lower maximum concentration than reference data point P1, which is caused by an increased dilution effect of the incorporated hydrodynamic dispersion. This effect of mass dilution is directly proportional to the travel time or travel distance. For more details, see Figure 4-9.

The final stage of the transient contaminant scenario (Figure 4-8) represents the initial stage for the methodological application of forensic modelling concepts.

Conclusion

As obtained from Figure 4-7, the advective transport mechanism is characterised by the highest mass distribution, while the dissolution effect which is incorporated in the advective-dispersive scenario, and the advective-dispersive-retarded scenario reduces the detected maximum mass concentration significantly, as it is expected from theory. Moreover, the sorption mechanism, included by using a retardation factor, increased the travel time of the migrating mass plume. Moreover, the curve widths of the advective-dispersive and advective-dispersive-retarded scenario differ from each other. This is caused by a longer travel time of the retarded mass, which automatically increases the dispersive dilution effect. In addition, the dispersive dilution effect causes an expansion of the plume dimension and simultaneously increases its characteristic impact zone. Thus, the implementation of an advective-dispersive-(retarded) transport model leads to more differentiated solute mass distributions than only using advective based transport mechanism.

4.2.4 Reverse particle tracking (backward-in-time)

An advective based solute transport process in steady or transient groundwater systems can be described by advective particle tracking which was introduced in chapter 3.3. In forward mode, it is used to estimate the future position or travel time probabilities of the considered solute. In backward mode, the method is applicable to derive probabilities on its prior position (source location) at a specific former point in time.

Thus, the backward location probability describes the position of an observed groundwater contamination at some time in the past. The backward travel time probability reflects the amount of time prior to observation that the pollution was released from its source or was located at a particular upgradient position.

The 4th-order Runge-Kutta particle tracking method, which is presented in chapter 3.3.1, is already implemented in the finite element code of FEFLOW. For the following experimental simulation, 2-D reverse particle tracking was applied for the forensic source identification problem based on the previous simulated 2-D transient transport problem (section 4.2.3, Figure 4-8). Backward particle tracking was used to estimate the source location of the solute mass impacts which had been observed at the reference data points P1-P4.

Reverse particle tracking for source identification problems

As introduced previously, the particle tracking technique requires for its pathline computation a continuously available flow velocity field. In forward mode, particle tracking can be processed during a running flow simulation, because the required flow velocity field is adjusted and available at every time step for the computation. The pathline is generated stepwise until the full simulation time is reached. In contrast, for reverse particle tracking, an already existing flow velocity field needs to be available, since the last time step of the previous run flow simulation constitutes the first computational stage of the backward pathline generation.

In general, when a flow model is started for simulation, the user can specify time step intervals at which the flow velocity field is saved to the FEFLOW internal result file (*.dac). In principle, every simulated time step could be saved to a corresponding result file. But this would lead to large datasets which probably tend to be difficult to manage. Therefore, it is recommended to save simulation data in reliable time steps which subsequently form the basis for the pathline computation. These time steps are set either manually or by a prepared list in the form of a simple text file format (*.txt). For the current experimental flow/transport simulation, an annual time step interval of 365 [d] was chosen. The data, stored in the FEFLOW result file (*.dac), forms the basis of reverse particle tracking, because the flow field reversal is applied onto the saved velocity field data of the result file (*.dac).

Particle tracking configuration

Reverse particle tracking is performed from an existing (*.dac) in post-processing mode. Settings concerning the model orientation (forward or backward mode), steady or unsteady tracking computation, starting points, pathline type, and the considered time period for the pathline computation needs to be defined. When particle tracking is used for source identification problems, it is necessary to (I) reverse the groundwater flow field, (II) to define particle starting point locations (e.g. the locations of groundwater observation wells), and (III) to specify the simulation time period for the pathline computation.

The flow field reversal in FEFLOW (I) is configured in post-processing mode and causes a spatial reversal of the flow velocity vector at each computational node of the finite element mesh. The theory about the flow field reversal in terms of reverse particle tracking was given in chapter 3.3.1.

The placement of particle starting point locations (II) is organised either by a manual setting of point locations or by using an internal FEFLOW file format, the (*.pnt) file format, which includes starting points in form of their spatial coordinates. This file can be easily created in a GIS-system, Microsoft Excel, or any other type of editor. Subsequently, the pathline computation is initiated. Methodologically, a groundwater observation well could be represented by a single particle that is tracked backward in time to delineate its "prior transport pathway". But the usage of only a single particle has the disadvantage that the

delineated pathway might be spatially limited, which simultaneously reduces its information value. Concerning this, it is of advantage to place additional particles within a predefined radius around these well locations to finally achieve more accurate backward source location probabilities. Those probabilities characterise a "prior source capture zone" that is much more meaningful for particle tracking analyses than only using a single particle. This is especially recommendable for transient heterogeneous hydraulic systems. For the current simulation, seven particles define each of the reference data points P1-P4. A single particle was placed at the reference location itself and six additional particles in a radius of 25 m around this observation point. The used particle coordinates are given in Table 4-2.

Table 4-2: For reverse particle tracking, particles are defined by position coordinates and are subsequently tracked backward-in-time. Each reference point is represented by seven particles, while one starting point is defined at the reference point location itself, and six additional particles were set in a buffer radius of 25 m around the respective reference location.

Location	2-D position coordinates of particle starting points (X,Y)
Reference point_P1	(1193,500); (1193,525); (1215,512); (1215,487); (1193,475); (1172,487); (1172, 512)
Reference point_P2	(1540,572); (1519,584); (1519,559); (1540,547); (1562,559); (1562,589); (1540,597)
Reference point_P3	(1542,500); (1522,512); (1522,487); (1543,475); (1565,487); (1565,512); (1543,525)
Reference point_P4	(1541,430); (1519,443); (1519,418); (1541;406); (1562;418); (1562,443); (1541,455)

Finally, it is required to choose an appropriate simulation time (III) which defines the time period of the tracking procedure. In the forward transport model, the plume migration was simulated for a total time period of 5475 [d]. After analysing the related breakthrough curves of observations P1-P4, the reference point location P1 was affected by the advective-dispersive plume front in maximum after app. 2675 [d], the reference points P2-P3-P4 after app. 4640 [d]. Reverse particle tracking was performed by using observation well specific travel times, at which the maximum mass concentration was reached, as their location specific backward simulation times. In addition, a further tracking routine was run for comparison purposes by using a full simulation time of 5475 [d].

Transient 2-D backward particle tracking

Backward particle tracking in transient flow fields was applied in the post processing mode based on the previous created FEFLOW result file (*.dac). According to Figure 4-11, pathlines were created backward in time for a total simulation time of 5475 [d]. Seven particles served as starting points for each of the reference point locations P1-P4. The import

of particle starting points was done by using the FEFLOW internal text file format (*.pnt). In total, 28 pathlines were created (Figure 4-10). Received particle tracks symbolise prior transport pathways of each individual particle. The model area which is covered by generated pathline tracks forms the source capture zone of all respective observation points. Here this capture zone includes all probable source locations of the respective observation point locations, within a travel time period of 5475 [d] and under the given velocity field characteristics.

It is noted that the received source zone comprises an increased uncertainty regarding the localisation of the predefined mass source of the forward transport scenario (section 4.2.3), since the pathline lengths are significantly overestimated. This is related to the chosen simulation time of 5475 [d], which is larger than the location specific arrival times of the forward oriented advective-dispersive transport simulation.
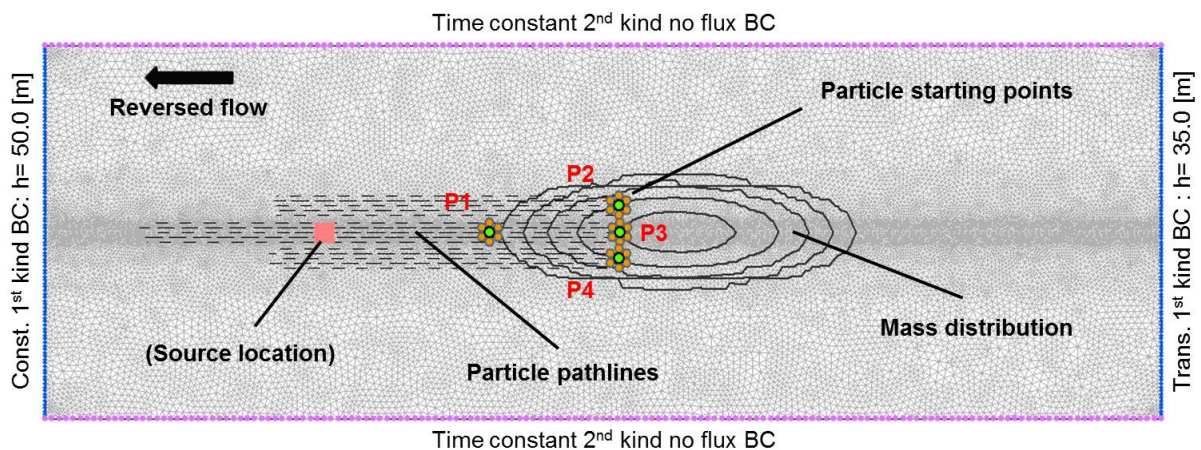
Figure 4-10: Particles were induced in a radius of 25 m around each of the reference locations P1-P4. Reverse particle tracking was performed for a total simulation time of 5475 [d]. The resulting pathline configuration represents backward source location probabilities (source capture zone) of the initial starting point locations. The figure illustrates additionally the mass source as well as the final mass distribution pattern of the 2-D transient transport model.

In a second backward particle tracking simulation (Figure 4-11), observation point specific arrival times of the forward transport simulation were used as related particle simulation times for the reverse particle tracking procedure. These time lengths were estimated from related breakthrough curves (Figure 4-9). A simulation time of 2675 [d] was used for the observation point number P1 while for the pathline computation of the reference points P2-P4 a simulation period of 4640 [d] was defined.

Again, seven particles were assigned for each of the reference data points P1-P4. Based on individual particle simulation times, 28 transient 2-D pathlines were created, seven pathlines for each reference data point. The simulation results are visualised in simple form within the FEFLOW model environment. Data export features enable the usage in other visualisation

systems. Several file formats which are compatible to GIS systems and databases such as (*.shp), (*.grd), (*.dat), (*.dxf), and (*.trp) file formats are supported for the data exchange.
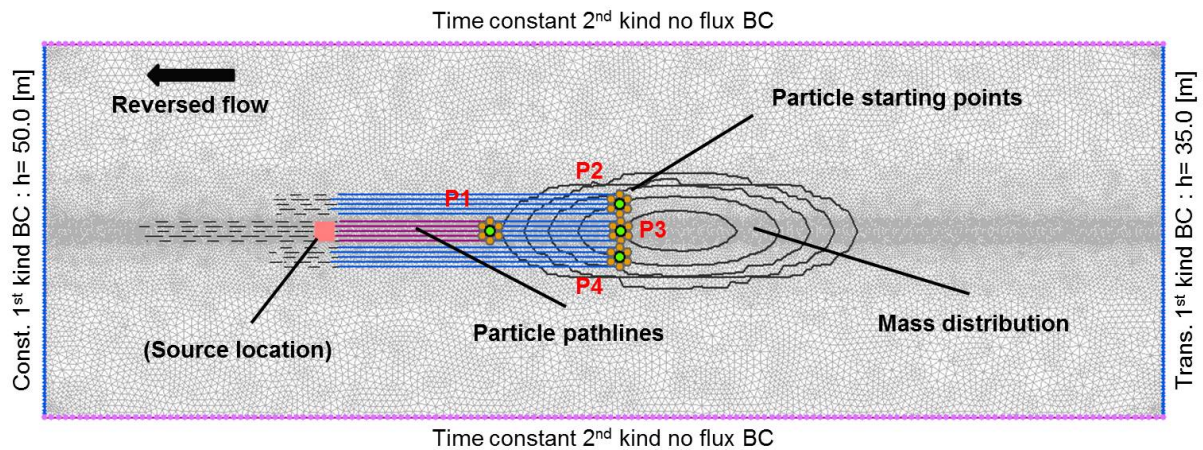
Figure 4-11: 28 pathlines were created for the reference data points P1-P4 by using optimised particle travel times. The blue tracks were simulated for a time range of 4640 [d], the purple pathlines for a time range of 2675 [d]. The dashed pathlines specify the results after a simulation time of 5475 [d]. In respect to the predefined mass source, the received source capture zone is more accurate than those obtained from Figure 4-10 but still involves some discrepancy for an exact spatial localisation.

At this point it can be stated clearly that the usage of an inverted advective transport model for the description of an advective-dispersive solute transport process tends to be entirely underestimated! This is generally caused by the fact that the dispersive transport mechanism is not included in the advective based particle tracking approach, which increases the uncertainty for the delineation of source locations as well as travel time probabilities!

While created particle tracks of Figure 4-10 (dashed lines) are overestimated significantly regarding an accurate localisation of the predefined mass source, the pathline lengths of Figure 4-11 (blue and purple lines) tend to be underestimated for an accurate source area localisation of the forward oriented advective-dispersive transport simulation. Moreover, the received particle front is strongly widened, which increases the uncertainty for a clear delineation of points sources.

Based on the received simulation results, it is stated that only the major direction of the solute transport process could be reproduced reasonably by the backward particle tracking approach, whereas the localisation of the assigned mass source comprises a significant uncertainty.

Conclusion

Reverse particle tracking was used with FFELOW by having the aim of identifying the mass source location of the transient forward oriented advective-dispersive transport simulation of

section 4.2.3. Multiple particles were induced within a predefined radius of 25m around the reference data points P1-P4. For the transient tracking procedure, an individual simulation time for each reference point was derived from the corresponding breakthrough curves representing the accurate arrival times of the forward transport problem.

Since the received particle tracks are significantly underestimated to in clearly attributing the mass source as the source location, the pathlines merely provide some information about the major solute transport direction. This underestimation is caused by the fact that particle tracking scheme only reflects advective transport and does not include the dispersive flux. Therefore, the reproduced advective transport process is under-dimensioned in regards to the idealistic rate of the advective-dispersive transport scenario. Moreover, the configuration of received particle endpoints comprises a wide particle front, which characterises probable source locations of the corresponding particle starting points. As the mass source of the forward transport scenario had been a nodal point source, the significant wider particle front involves a spatial uncertainty concerning its point localisation.

The simulation time used for the reversed tracking procedure additionally affects the accuracy of the source identification problem. While the full simulation time of 5475 [d] led to an overestimated source capture zone, reference point specific simulation times, estimated from corresponding breakthrough curves, optimise the source allocation procedure in terms of a more accurate source capture zone.

Since the reverse particle tracking method entails multiple sources of uncertainty for source identification problems, this technique is suitable for an initial screening procedure to estimate the direction of prior solute transport in transient hydraulic systems. Its low computational time is therefore a major advantage.

4.2.5 Backward-in-time transport modelling

In contrast to reverse particle tracking, the backward-in-time transport modelling includes the missing dispersive transport mechanism and provides a more accurate concept for the estimation of source and travel time probabilities than the advective based particle tracking method. Since the backward ADE is the adjoint model of the classic forward ADE, the model is applicable to represent a reversed transport mechanism. Classical transport models are interpreted in terms of a solute concentration as the state variable and the related simulation time as the time variable. The interpretation of the adjoint probability model is different and not consistent with the interpretation in terms of solute mass. In the backward-in-time transport model the location probability is the state variable and the time variable is represented by the backward time. Thus, backward location probabilities describe the position of a particle or contamination at a prior point in time. In addition, backward travel time probabilities describe the amount of time, prior to observation, that a contamination was released from an upgradient located origin.

Numerical implementation of the adjoint ADE in FEFLOW

As it was stated from theory in chapter 3.3.2, the numerical implementation of the adjoint ADE model requires modifications concerning the reversal of the transport direction. Moreover, to also be applicable for transient systems, this approach additionally requires the temporal inversion of boundary conditions. The following experimental simulation is again based on the previous used transient flow model of section 4.2.2.

In contrast to the reverse particle tracking technique, the backward-in-time transport model is solved iteratively during a running transport model simulation. Thus, the estimation of backward location and travel time estimates is not based on any previously solved velocity fields as it was the case for backward particle tracking.

The general flow field reversal is organised manually in FEFLOW by using a specified setting and leads to the sign reversal of the advective part of the classic ADE equation as described in 3.3.2.

When the considered system is characterised by a steady-state flow field, no further specifications of the flow model are necessary for running a backward transport model. For the transient case, the non-steady flow velocity field needs to be reversed in time. Therefore, the numerical flow boundary conditions are temporally inverted, which is accomplished by an inversion of related time series functions. Thus the last time stage of the forward model BC represents the first time stage of the backward model.

The western transient boundary condition of the 2-D flow model (section 4.2.2) is used for an illustration: During the total simulation time of 5475 [d], the western prescribed head boundary drops evenly from an initial hydraulic head value of +35.0 m down to a prescribed head of +29.0 m at the end of the simulation. In the backward model, the initial time stage of the BC is specified to +29.0 m and increases during the simulation run to a hydraulic head value of +35.0 m at the end of the simulation (Figure 4-12).

In addition to the modifications of flow boundary conditions, configurations concerning the initial conditions are necessary, too. Here, the hydraulic head distribution of the last time stage of the forward model describes the initial head distribution at the beginning of the backward transport model. This is managed by accessing the result file (*.dac) of the forward model to export the hydraulic head distribution at the last simulation stage of the forward model simulation. Subsequently, in the backward model, the exported dataset is assigned as the initial hydraulic head distribution. For data transfer the commonly used GIS shape format (*.shp) is suggested.

The mentioned settings are required to reproduce a classic transient flow field backward-in-time, which forms the basis of the backward-in-time transport modelling approach. All modifications focus on an accurate inversion of the velocity field in space and time. For justification, Figure 4-13 and Figure 4-12 contain function graphs which illustrate the hydraulic head distribution of two reference data points in forward mode and backward

mode. The illustrated, non-steady flow field reversal enables a backward-in-time transport modelling based on the adjoint ADE model.
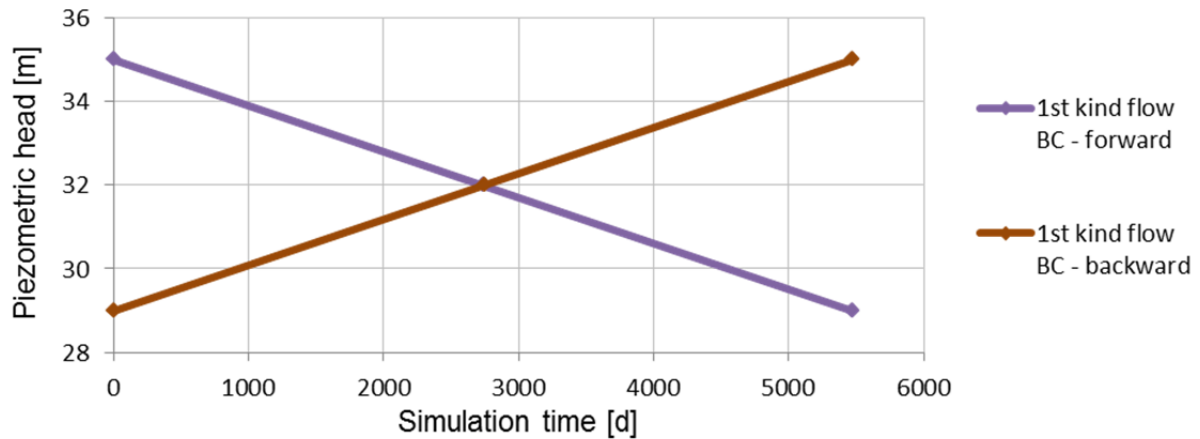
Figure 4-12: Transient flow BC in forward & backward mode: The purple graph specifies a transient flow boundary condition which is dropping evenly from + 35.0 m at the beginning of the simulation down to + 29.0 m at the end of the model run. In backward mode, the function graph is reversed in time and the simulation starts with the last hydraulic head definition of the forward run. Here during the backward run, the hydraulic head value (brown curve) is increasing slightly from +29.0 m upwards to +35.0 m.
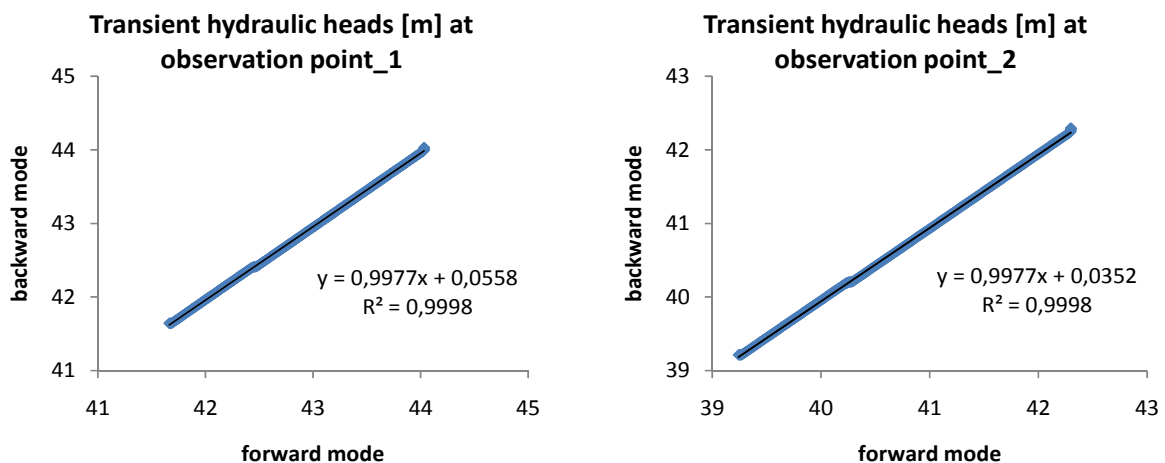
Figure 4-13: The diagrams contain piezometric head variations of the transient forward and backward flow simulation (simulation time 5475 [d]), exemplarily for the reference data points P1 & P2. The high linearity between results from forward and backward model, expressed by R² = 0.9998 (n=561), prove a successful flow field reversal of the transient flow model environment.

As it was stated in the theoretical chapter, the dispersion mechanism does not need any further adaptation, since its effect is related to the magnitude of the flow velocity which is already reversed in space and time by the previous modifications.

Backward-in-time transport modelling for source identification problems

Basically this concept requires an injection of a temporal or constant mass load which is implemented by using a numerical transport BC. The inserted mass signal migrates subsequently through the model domain based on a reversed ADE transport mechanism backward-in-time within a steady-state or transient flow velocity field. The resulting location and travel time probabilities are finally interpreted with respect to probable source locations and temporal release history.

Numerical transport BC's are assigned to specify the backward transport model. In the following, a transient transport 1st type boundary condition was set at the reference point location number P3 (Figure 4-14). The mass input can be defined either as a temporal mass impulse or as a constant mass load that stays active for the whole simulation time.
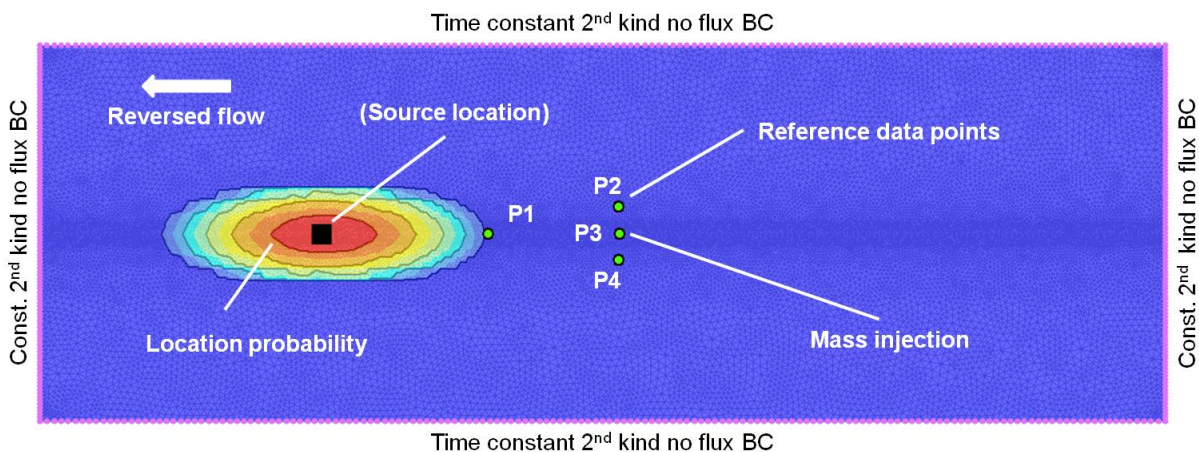
Figure 4-14: Backward location probability distribution for source identification of the observation point P3; a single mass impulse was induced at the reference point P3 which migrated for a travel time of 4640 [d] through the aquifer backward in time. As a result, the prior source area is located in the inner centre of the backward location probability distribution with the highest probability density.

The initial time stage at which the mass impulse is inserted at the reference point P3 is derived from its corresponding breakthrough curve (Figure 4-9) of the forward model. Here, the mass distribution reached the reference data point after a travel time of 3345 [d] and formed a maximum after app. 4640 [d]; see Figure 4-15. With respect to the total simulation time of 5475 [d], the mass injection is implemented initially in the backward model after 835 [d], at the time of the maximum concentration of the forward model. With respect to the total

backward simulation time of 5475 [d], a simulation period of 4640 [d] remained for the migration of the mass signal through the model domain.

The Figure 4-14 illustrates the corresponding backward location probability distribution for the observation data point number P3. A single temporal mass impulse of 100 000 [mg/l] was injected at the reference data point P3 at an initial time stage of 835 [d] for only 1 day. The mass injection is configured by a transient 1st kind boundary condition. Based on the adjoint ADE model, the mass signal migrated through the model domain for a travel time of 4640 [d] based on an advective-dispersive transport mechanism. Material parameters of the transport model were specified according to Table 4-1.

For comparison, Figure 4-15 contains respective breakthrough curves of observation points of the forward transport model (section 4.2.3; Figure 4-8) and the backward transport model (Figure 4-14) and illustrates a successful reversal of the advective-dispersive transport mechanism. The mass signal was induced in the forward model at the mass source location and migrated subsequently through the transient model domain, where a solute mass maximum was registered at the observation point location P3 after a travel time of 4640 [d]. In the backward mode, the mass signal was induced at the observation point P3, migrated through the transient model domain for a travel time 4640 [d], and a backward location probability high was registered at mass source location.
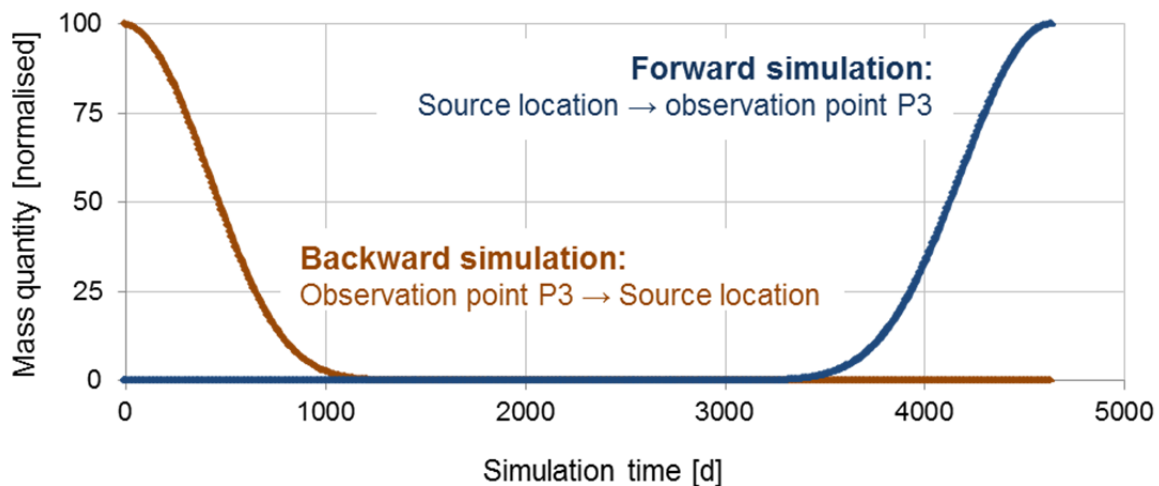
Figure 4-15: ADE model & adjoint ADE model under transient model conditions: The maximum solute mass impact was registered at the observation point P3 of the forward model run after 4640 [d]; the maximum probability distribution was registered at the mass source location of the backward model run after 4640 [d]. Since the adjoint ADE model is not mass consistent to the forward model, results of both models were normalised for visualisation purposes.

As it was stated from theory, backward location probability is not mass consistent to the forward model and is therefore not comparable to received mass concentration values! For

visual comparison in the following Figure 4-15, both "mass quantities" were normalised to 100% and were plotted against the simulation time.

In the backward model, the previously used mass source location of the forward model is located in the inner centre of the backward location probability distribution (Figure 4-14) which is characterised by a maximum probability density level (Figure 4-15). This implies that the source location constitutes the most probable contamination source of observation point P3 prior to a solute travel time of 4640 [d]. Therefore, the source identification process is successfully implemented for an advective-dispersive transport mechanism in a transient simulation environment.

Backward-in-time transport modelling for travel time and source capture zone probabilities

In addition to location probability distributions, backward-in-time transport modelling also provides the possibility to create continuous time-related source capture zones, which additionally provides a temporal model feedback. These backward travel time probability zones describe the amount of time prior to detection that a mass load was distributed from a particular upgradient position within this source capture area. Thus, beside the temporal information, the backward probability estimates additionally include location specific information that is comparable to classical capture zone delineation approaches.

To achieve time and location related probability estimates, the mass injection is constantly assigned time which finally leads to a consistent probability plume or capture zone, as it is illustrated in Figure 4-16. Therefore, the mass injection was realised at the reference data point P3 by a transient 1st type BC, which is characterised by a constant mass load of 100 000 [mg/l] for the simulation period 835 – 5475 [d]. Thus, the mass source had been active for 4640 [d], which is consistent with the arrival time of reference point number P3 in the forward model.

The simulated backward probability distribution was logged globally for the entire model domain at predefined time steps. Mass distribution data was recorded for the time intervals (3 yrs., 6 yrs., 9 yrs., and 12 yrs.) after the beginning of mass injection (835 [d]) and at the final simulation time step of 5475 [d]. An individual dataset of the respective mass distribution was exported by using the internal (*.shp) data interface of FEFLOW. Related capture zones were created for the individual time slices (Figure 4-16). For the visualisation purpose, each single backward probability plume was normalised to 100 % with respect to its probability quantity. Then, the 1% contour level was used as the outline of the respective source capture zone for visualisation.
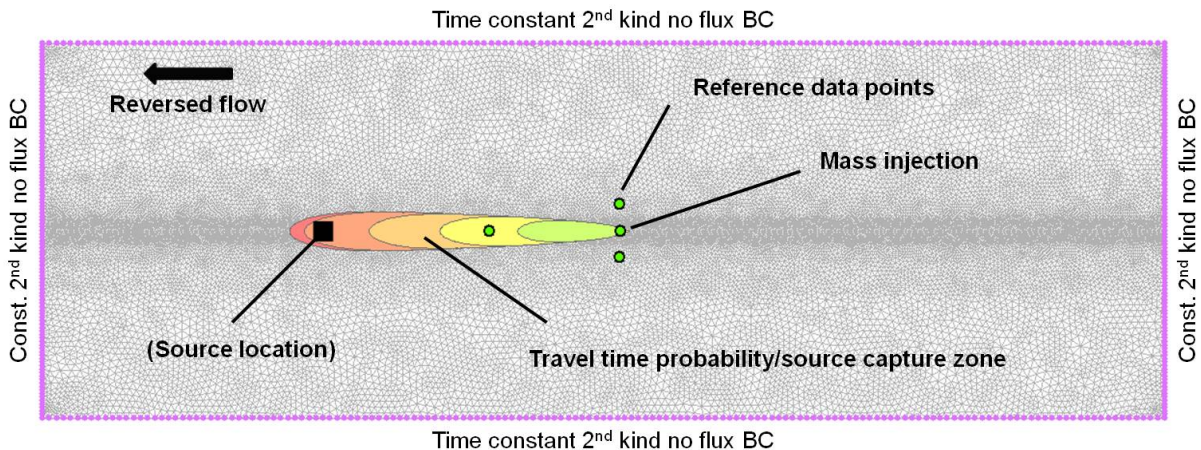
Figure 4-16: A constant mass injection was simulated backward in time, and the resulting backward probability estimates were post-processed representing time related source capture zones for the time intervals 3 yrs. (green), 6 yrs. (yellow), 9 yrs. (orange), 12 yrs. (brown), and the final simulation time of 5475 [d] (red). These backward travel time probability zones describe the amount of time prior to detection that mass was distributed from an upgradient position within this particular capture zone.

Figure 4-16 illustrates time related source capture zones of the reference data point number P3, which contain probable source locations for a respective time prior to detection. These backward travel time probability zones describe the amount of time prior to detection that mass was distributed from a particular upgradient position within this capture area. The dimension of modelled capture zones increases in time that is quite logical, since the distance of advective-dispersive transport increases, too. Moreover, the width of the backward plume also becomes larger with time, which is caused by the involved dispersive dilution effect. In contrast to the underestimated pathlines from advective particle tracking (Figure 4-11), the backward plume contains the assigned mass source of the forward oriented transient transport simulation (section 4.2.3). The defined mass source of the forward model is finally enclosed by the 12 yrs. time capture zone, which indicates that a probable mass load took about < 3540 [d] to arrive at the observation well number P3. This result fits quite well with the information available from the corresponding breakthrough curve of the forward transport model (Figure 4-9). Here, the mass signal was first detected after 3345 [d]! While the mass source is spatially enclosed by the backward plume, a more accurate estimation of travel time could be derived by a higher time interval resolution.

The delineation of time related source capture zones derived from backward-in-time transport modelling finds practical application for, for example, capture zone delineation of groundwater observation or monitoring wells which had been affected by some pollution.

Multiple-observation backward probability for source zone identification

In the previous section, a single backward location and travel time probability distribution was applied for source zone identification and release time recovery. When multiple observations

points are available, each individual record provides additional information for the source zone identification problem. This approach follows the assumption that a probable source location is determined more significant when it is confirmed by backward location probabilities of multiple reference data points.

The two reference data points P2 and P4 were chosen to demonstrate this multi-observation backward location probability approach. Both observations points had been influenced only marginally by the mass distribution of the transient forward transport model caused by their spatial locations with respect to the solute mass distribution. Located at the plume edge (Figure 4-8), their mass impact was mainly caused by the dispersive spreading effect, which makes it even more interesting to involve these observation points for the multiple-observation backward probability procedure.

Backward location probabilities were simulated for both reference data points. The simulation procedure is analogous to the scenario which was applied for the creation of backward location probabilities at the reference data point P3. A temporal mass impulse of 100 000 [mg/l] is injected for a period of 1 [d] by a transient 1st type BC at an initial time stage of 835 [d]. An individual simulation run of 5475 [d] was performed for each reference data point.

After the simulation, backward location probability data was exported and post-processed in ArcGIS for visualisation purpose (Figure 4-17). Two individual and continuous backward location plumes were created from nodal simulation data by spatial interpolation. Again, the mass quantity was normalised to 100%, and the 1% contour level represents the visualised plume margins. Subsequently, both backward probability plumes were used for the source zone characterisation by GIS-based spatial intersection.
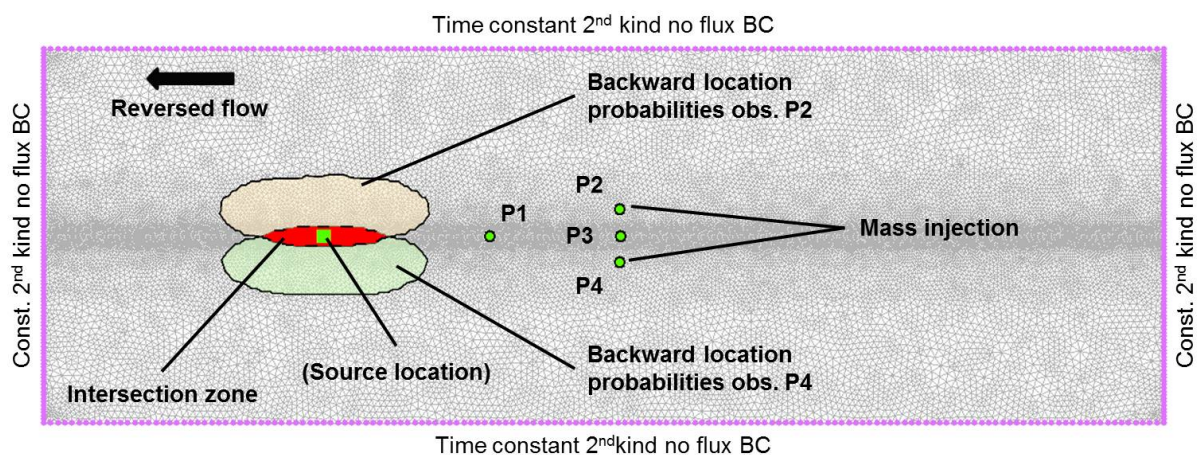
Figure 4-17: Multiple backward location probabilities were simulated for the observation points P2 & P4 (green/orange). Received probability estimates overlay each other in an intersection area (red) of the prior source location. The intersection of backward probabilities of multiple reference data points increase significantly the location probability density used for the source identification procedure.

While the previously assigned mass source is principally enclosed in the both individual backward source capture zones of P2 and P4, their spatial dimension comprise a significant uncertainty for the general source location procedure. Therefore, the intersection of backward source capture geometries from multiple observation leads to a more accurate source capture zone for the identification process than using only a single geometry of P2 or P4. Here, this methodology significantly reduces the uncertainty, since information from multiple reference data points is involved and combined for the identification process.

According to Figure 4-17, both probability zones (observation P2 – orange; observation P4 – green) were intersected and led to an intersection area (red) which encloses the assigned mass source location of the transient forward model. This intersection zone characterises a much smaller and more accurate probable capture source zone than one which would have been derived from an individual single backward probability plume!

The assumption that the utilisation of backward location probability estimates of multiple observation points increases the overall location probability density for the source identification procedure is additionally proven by respective breakthrough data.
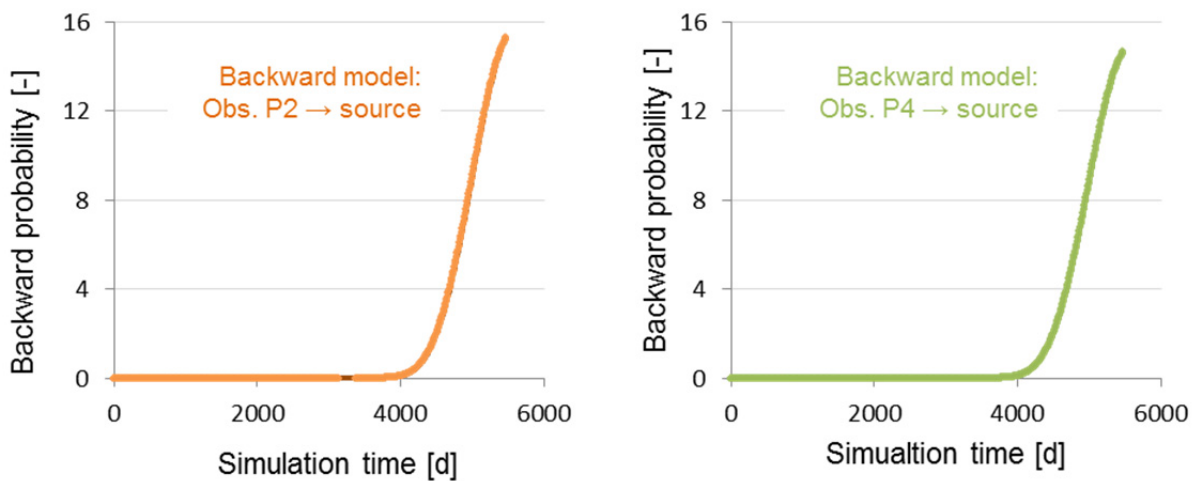
Figure 4-18: Backward location probability was registered at the prior mass source location for the source identification procedure of observation point P2 (orange) and P4 (green). After a travel time of 4640 [d], individual backward probability peaks were registered at the prior source location.

Therefore, backward location probability data was registered at the prior mass source location. After a travel time of 4640 [d], individual backward probability peaks of the respective observation points P2 and P4 were registered (Figure 4-18).
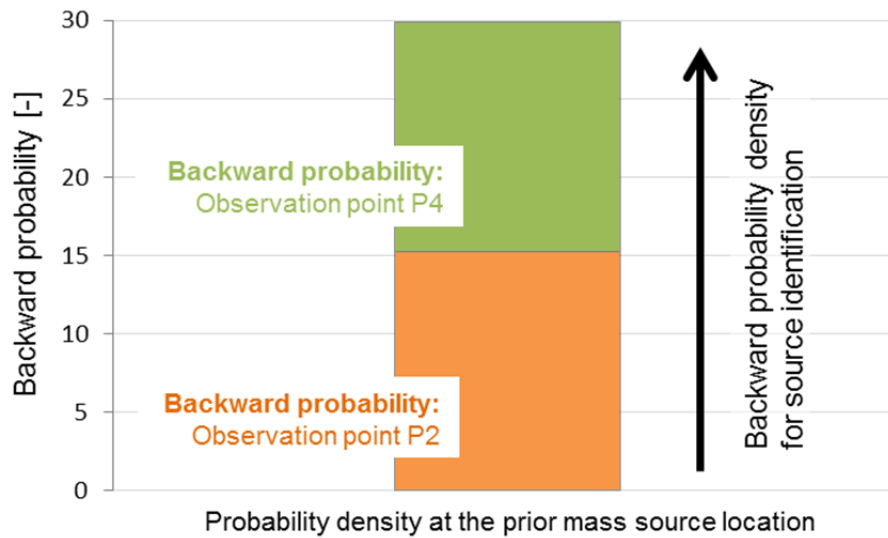
Figure 4-19: Backward location probability estimates of multiple reference data points lead to a significant higher probability density for the source identification process than probabilities which had been generated from only a single reference data point. Here, the combination of backward probabilities of the observation points P2 and P4, registered at the prior mass location of the transient transport scenario, increase the overall probability that this location was the primary mass source prior to a travel time of about 4640 [d].

The combination of multiple probability distributions (observation points P2 and P4) increases the overall probability that this location was the primary mass source of the generic contaminant scenario. This is supported by information given in Figure 4-19, since the backward location probability density for the source identification process was almost doubled by the combination of the individual probability estimates received from the reference data points P2 or P4.

Conclusion

Backward-in-time transport modelling was implemented successfully by using the finite element code FEFLOW. Existent for steady-state scenarios, this approach was extended to also be applicable in transient model environments. Required numerical configurations or modifications are presented in detail. Backward-in-time transport modelling was applied to a transient 2-D problem. The approach provides probability distributions which can be interpreted in terms of prior locations and travel time. It is noted that the approach does not create concentration levels of prior time stages!

Backward location and travel time probabilities were created for single and multiple observation points. At these reference points, either a single or a consistent mass signal is induced. In principle, backward probabilities created from a consistent mass signal lead to a source capture zone that provides the largest informational content concerning a probable mass origin and related travel times (Figure 4-16). Moreover, the multiple-observation

backward probability approach increases the overall probability density (Figure 4-19) and decreases the spatial uncertainty (Figure 4-17) for the source identification procedure.

Simultaneously, from a theoretical point of view, advective-dispersive backward-in-time transport modelling is much more accurate for source identification problems than advective particle tracking, since a dispersive transport mechanism is incorporated.

Finally, the prior mass source location of the forward model run could be identified quite well by backward-in-time transport modelling (Figure 4-17 and Figure 4-19), whereas reverse particle tracking indicated a broader, more inaccurate source area and only suggested the direction of prior solute transport (Figure 4-10 and Figure 4-11).

4.2.6 Model accuracy and numerical stability

In numerical modelling, several error types or sources exist which influence the general model stability and accuracy of numerical results. In general, when a numerical model is proven to describe representatively the process of groundwater flow and/or solute transport by a system of partial differential equations, the model is potentially applicable to reproduce the considered state variable (simulated hydraulic head and/or solute concentration) with respect to the obtained field phenomena (measured hydraulic head and/or solute concentration). Numerical model stability is given when the difference between the magnitude of the field value and its numerical solution tends to be zero, which indirectly implies a high model accuracy. This crucially indicates that the reflected process is well approximated by the numerical model.

With respect to the numerical model used for reversed flow and transport mechanisms, it can be clearly stated that the flow field reversal is unrestrictedly possible and is simultaneously characterised by a high model accuracy that is illustrated in Figure 4-13. In contrast, an involved transport mechanism such as dispersion and diffusion cannot be reversed physically, due to their mathematical formulation and/or completely unknown parameters such as the concentration gradient, which is implemented fundamentally in their concepts. This involves significant limitations regarding their information value. In the current study, diffusion and dispersion mechanisms were reversed spatially and temporally in a transient model environment by their adjoint model descriptions. This enables representative spatial and temporal implementations, but is completely inconsistent in terms of the physical interpretation of the state variable – the solute mass concentration. In relation, by using the adjoint models, transport processes can be implemented reversely in space and time to generate representative transport directions, distances and travel times, but it is not possible to reproduce representative concentration levels of prior time stages!

During a numerical simulation, several problems can arise which will lead to numerical instability and affect finally the accuracy of achieved results. These effects are caused to a great extent by numerical oscillations, often based on an insufficient model discretisation in time and space. A typical example for numerical oscillations is the overshoot/undershoot of a

solute concentration caused by an inadequate resolution of discretisation. In addition to this, high variable concentration fields often paired with sharp concentration fronts are reasons for numerical oscillation.

Additional sources of numerical errors are given in the following by simplified "cause and error" relationships:

- Coarse spacing → numerical dispersion
- Large time steps → oscillations
- Abrupt changes in time and space (in terms of defining boundary conditions) → model instability
- Initial sharp concentration fronts → "overshoot"
- Coarse spatial discretisation in areas of heterogeneous parameter settings → numerical dispersion

Moreover, an iteration residual error can provoke a further inaccuracy onto model results. If present, this error originates from the internal iteration solution process. Here, a predefined convergence criterion leads to an abrupt abortion of the numerical solution when the maximum iteration steps are exceeded, even if the numerical solution for the state variable is incomplete. This type of error is denoted as the "iteration residual error".

In the past, several control functions were introduced to manage these error sources that affect the model stability and accuracy of numerical results. This includes the control function of the Courant criterion, Peclet criterion, and Neumann criterion. While the Courant criterion focuses on optimal time step lengths, the Peclet and Neumann quantity aims at the spatial discretisation of the model to suppress numerical dispersion. Therefore, the approaches are based on parameters such as the flow velocity, the dimension of spatial discretisation, and dispersion coefficients for their quantification procedure of numerical model stability. For more details, see BEAR & CHENG (2010), HUYSMANS & DASSARGUES (2005) and KINZELBACH (1992).

Several recommendations can be given to avoid or reduce the magnitude of numerical errors, oscillations, and model instability:

- Gradual variation of temporal and spatial discretisation
- Ensure moderate cell aspect ratios
- Keep values as small as possible → rounding error
- Decrease time step lengths to increase model stability
- Mesh enrichment in areas of changing parameters
- Use 3rd type BC instead of 1st type BC

These recommendations can be helpful if probable model instabilities occur which affect finally the results of the numerical model.

Numerical models of the experimental modelling were discretised sufficiently in time and space to achieve stable and plausible model solutions. If some model instability occurs which cannot be controlled by the given recommendation, the so called upwind techniques provide further possibilities for stabilising the model. If numerical oscillations or model instability arise due to, for example, high gradients at sharp concentration fronts, upwind techniques create numerical dispersion to smooth this concentration front and thus avoid related oscillations. This may ultimately help to stabilise the numerical solution process. As additional mass is induced to the model domain by these upwind techniques, the total mass quantity is distorted. This distortion phenomenon is denoted as "smearing effect".

Different types of upwind techniques were established and are implemented in the FEFLOW modelling system: shock capturing, streamline upwinding, least-square upwinding, and full upwinding. All these different methods vary concerning their operation principle and magnitude of intervention. For more details, see DIERSCH (2002), COLLIS & HEINKENSCHLOSS (2002).

4.2.7 Chapter summary

2-D generic model scenarios of groundwater flow and solute transport were simulated by using the numerical code of FEFLOW (section 4.2.1). In principle, those simulations reproduce the methodology and numerical approximation of conventional and forensic transport modelling in transient model environments, which is presented in chapter 0.

Initially, a transient 2-D groundwater flow box model serves as the fundamental basis of the following transport modelling (section 4.2.2). Based on the characterisation of a single source contamination problem, advective, advective-dispersive, and advective-dispersive-retarded 2-D solute transport was simulated based on a previously created groundwater flow model. Breakthrough curves of assigned reference data points were registered with respect to incorporated solute transport mechanisms (section 4.2.3). Those reference data points can be treated as potential groundwater observation wells that had been affected by pollutant discharge which originated from the assigned pollutant source.

The advective-dispersive transport scenario was chosen as the central transport scenario to investigate two forensic modelling approaches for source identification problems. The technique of reverse particle tracking and the method of backward-in-time transport modelling was tested and analysed concerning the accuracy and uncertainty for the identification process. Several modifications were necessary in FEFLOW to implement the backward-in-time transport approach which was additionally extended for additional validity in transient model environments.

With respect to the identification of the previous assigned mass source of the forward transport model, backward-in-time transport modelling is more accurate than reverse particle tracking. As particle tracking only accounts for advective transport, backward-in-time transport modelling is based on the adjoint model of the classical ADE, which includes an additional dispersive transport mechanism.

Related to the findings, reverse particle tracking was evaluated to be suitable as an initial screening tool for the characterisation of prior exposure routes of solute transport. Its accuracy for the identification of the assigned mass source was limited. Its low computational time is a major advantage. In contrast, reverse transport modelling was capable of reproducing the mass source location by generating backward location probabilities significantly more accurate. Therefore, the utilisation of multiple reference data points increased the probability density for the identification procedure and simultaneously reduced the uncertainty of the model. Solute transport distances and related travel times were reproduced representatively and enabled a coherent identification of the previous assigned mass source. At the same time, since the state variable of the adjoint ADE model is interpreted physically in terms of location and travel time probabilities, the model does not generate any comparable concentration levels of the forward model!

4.3 The Bitterfeld-Wolfen megasite: a 3-D case study scenario under real-world conditions

The Bitterfeld-Wolfen Megasite had been influenced by extensive impacts of lignite mining and the chemical industry for more than a century (chapter 2.2 and 2.3). Today the region is characterised by a multi-source groundwater contamination at a regional scale (chapter 2.4).

Multiple groundwater contaminants are present within a complex geological system specified by sediments of the Tertiary and Quaternary period (chapter 2.1.4). With respect to the dominant hydrogeological characteristics (chapter 2.1.5), the region comprises a lower Tertiary and an upper Quaternary aquifer system. Due to extensive mining activities, the natural settings of the subsurface were sustainably destroyed (chapter 2.4). Contaminant source origins are unknown or even only suspected, which hinders the implementation of efficient site remediation strategies.

Both forensic modelling approaches for source identification problems, presented in the experimental modelling section 4.2, are applied to the test scenario Bitterfeld-Wolfen to evaluate their model uncertainty and accuracy under complex and realistic model conditions.

4.3.1 Problem definition

(I) A three-dimensional groundwater flow model of the Bitterfeld-Wolfen region reproduces the effects of mining related groundwater lowering onto the regional aquifer system for the time period 1955 to 2005.

(II) Information about temporal and spatial variations of the 3-D flow velocity fields enables the characterisation of prior contaminant transport processes and is applied to forensic modelling techniques for source identification problems. While reverse particle tracking can be performed based on an already existing flow model data, backward-in-time transport modelling requires numerical model configurations.

(III) Both techniques were studied at a virtual contaminant scenario, which is related to the local hexachlorocyclohexane (HCH) groundwater pollution; a chemical residual of the former Lindane production in Bitterfeld-Wolfen.

An already existing 3-D groundwater flow model of the region, established by Gossel et al. (2009), was modified and extended concerning the mesh discretisation, flow and transport boundary conditions, and relevant transport model parameters. Implemented model verifications led to a more accurate reflection of the mining affected 3-D flow velocity field, since the groundwater abstraction is approximated in more detail in space and time.

4.3.2 Spatial and temporal model discretisation

Since the local mining activities in the Bitterfeld-Wolfen region had been of regional scale, the model domain needed to be chosen sufficiently large to reflect the spatio-temporal impacts of

groundwater drawdown onto the hydraulic system. In principle, the model domain is aligned on regional hydrologic characteristics of the study area. Therefore, the shape of the model boundary replicates the river courses of the regional surface water system (Figure 4-20, section 2.1.2). Running waters limit the model area in the west, north, and east; a watershed forms the southern boundary. The overall area covers about 330 km² and stretches about 19 km in south-north direction and has a length of about 18 km from the east towards west.

Spatial discretisation

The entire model area is laterally discretised by a finite element mesh consisting of 159,536 triangle elements connected by 80,433 nodes.
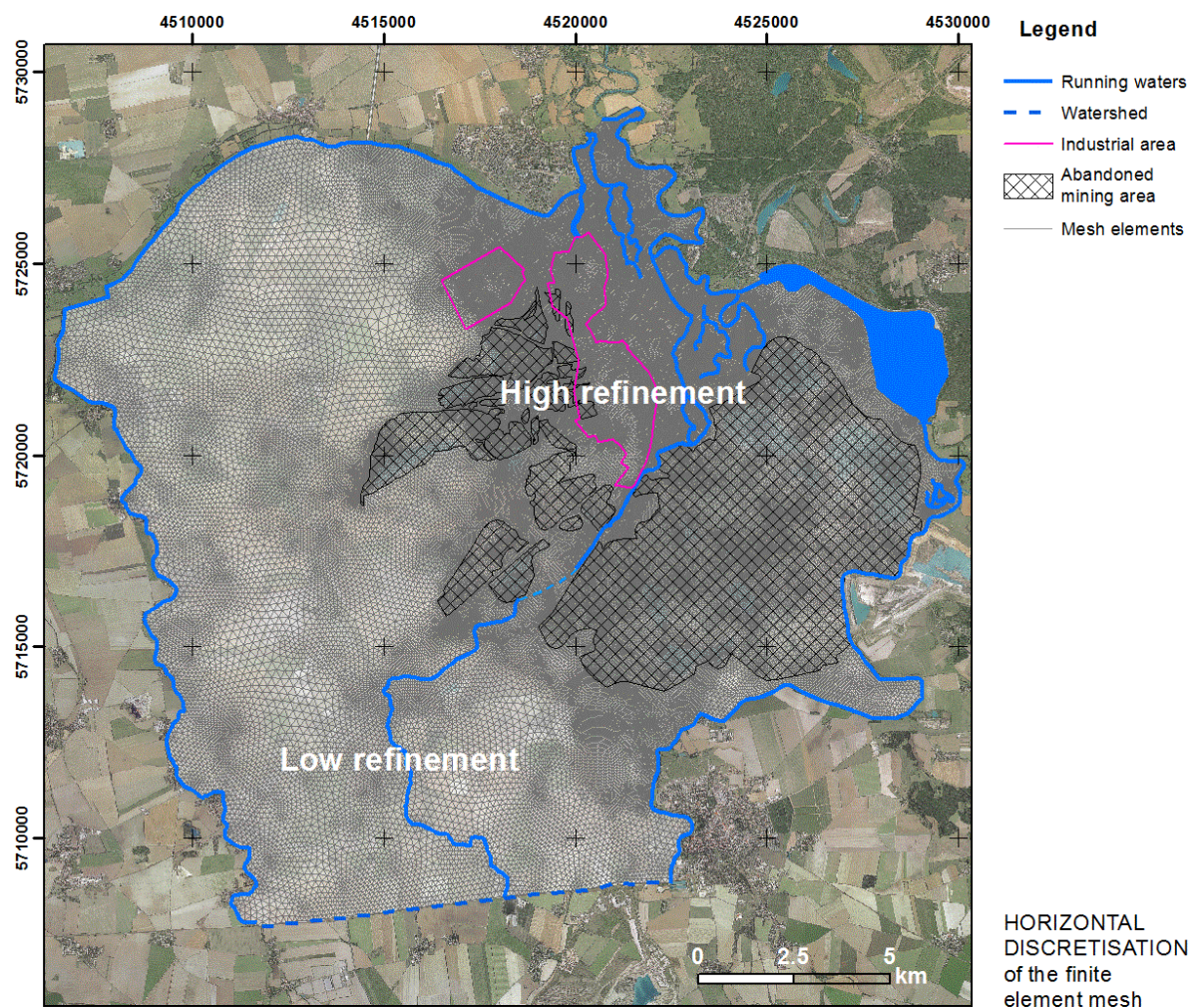
Figure 4-20: The model boundary is aligned on river courses of the regional surface water system. The inner domain is discretised by a finite element mesh of variable resolution. Areas of interest are characterised by a higher mesh density, whereas outer areas are of lower mesh resolution.

The edge lengths range from 10.0 m to 300 m and the statistical median is about 49.0 m.

The mesh was spatially refined in areas of the open-cast fields, the industrial production complexes of Bitterfeld and Wolfen, along "areas of interest" such as landfill sites, and at potential inner and outer boundary conditions (Figure 4-20). When using finite element models, individual levels of refinement can be implemented locally without being forced to use a specified scale of resolution globally. In the FEFLOW system, modifications concerning the mesh configuration can be inserted at any time.

The upright model discretisation is based on the regional geological and hydrogeological settings which had been introduced in chapter 2.1.4 and 2.1.5. The vertical model structure follows the local geological stratification profile of the Bitterfeld area, presented in detail by Wollmann (2004) and Hubert (2005). Several geological horizons of different stratigraphic age form an individual hydrogeological unit due to similar hydraulic sediment characteristics. The hydrogeological model classification is given in the following Table 4-3:

Table 4-3: The vertical model structure is classified into 13 hydrogeological model units (HGMU) which are represented in the FE model by 37 numerical layers. Detailed descriptions about the geological and hydrogeological characteristics of the model domain are given in chapter 2.1.4 and 2.1.5.

				Hydrogeological Units	HGMU	Numerical Layer
Cainozoic	*Quaternary*		Holocene	Anthropogenic made ground	1	1/2
				Anthropogenic landfill		
				Flood plain loam		
				River gravel terrace		
		Pleistocene	Weichselian	Loess or loess loam	2	3/4/5
				Glacial cover sands		
				Weichselian river gravel (upper part)		
				Periglacial horizon	3	6/7/8
			Saalian	Weichselian river gravel (lower part)	4	9/10/11
				Fluvial to glaciofluvial outwash sediments		
				Saalian till complex	5	12/13/14
			Elsterian	Saalian Main Terrace	6	15/16/17
				Galciofluvial outwash sediments		
				Galciolimnic sediments		
				Elsterian till complex	7	18/19/29
	Tertiary	*Miocene*	Bitterfeld Complex — Clay Cover Complex	Bitterfeld clay cover	8	21/22/23
				Roitzsch Sands		
				Bitterfeld clay cover		
				Bitterfeld seam complex	9	24/25/26
			Bitterfeld Complex — Mica Sand Complex	Bitterfeld sands	10	27/28/29
		Oligocene		Breitenfeld horizon	11	30/31/32
				Zöckeritz sands	12	33/34/35
				Glauconite sands		
				Glauconite silts	13	36/37
			Rupelian	Rupelian clay		

The lowest vertical boundary of the hydrogeological model is characterised by the impermeable Tertiary Rupelian clay horizon which constitutes a regional and consistent aquitard of northern Germany. The lower Tertiary Mica Sand formation forms the Tertiary aquifer system which is overlaid by the Bitterfeld lignite seam complex and accompanying less conductive sediments. The Quaternary formation is characterised by various glacial sediments of the Elsterian, Saalian, and Weichselian epoch. The model classification ends with anthropogenic units and landfills at the terrain surface.

While the hydrogeological model is structured into 13 individual hydrogeological units, the numerical flow model is defined by 37 numerical layers. Several geological units can be merged to one hydrogeological unit (HGMU) of the numerical model. Each of the hydrogeological units is represented by three numerical layers, except the first and the last unit, which only consist of two slices. This is necessary for an adequate representation of hydraulic conductivity in vertical scale, due to numerical model specifications of the FEFLOW system. Moreover, each numerical model layer is characterised by a reproduction of the horizontal reference mesh, illustrated in Figure 4-20, which varies by the layer specific elevation.

In total, the entire 3-D model domain contains 2,976,021 computational nodes and 5,902,832 triangle elements.

Temporal discretisation

The total simulation time of the numerical flow model of Gossel *et al.* (2009) covers the time period 1840 to 2005. This period includes the full era of active lignite mining and the following phase of groundwater rebound. The current study on forensic modelling covers only the prior time stage from 1955 to 2005. This time stage is related to the period of local Lindane production which forms the basis of the presented case study scenario. Lindane, a hexachlorocyclohexane isomer, was synthesised at the Bitterfeld site from 1952 to 1982.

In general, the total simulation period was not organised within one single model file, since required input data, the assignment of numerical boundary conditions, and the size of output files tended to be extremely complex. Therefore, the total simulation time was split up into several sub-model time stages while each time stage is represented by an individual numerical sub-model:

Stage_1: 1955 – 1963; stage_2: 1964 – 1975; stage_3: 1976 – 1992; stage_4: 1992 – 2002; stage_5: 2002 – 2005.

Due to this organisation, the model configuration as well as the output data management was easier to control but complicated the internal data transfer (between these sub-models) at the same time.

4.3.3 The structural model

The numerical model approximates the lithostratigraphic units of Table 4-3 regarding their geometries and dimensions in a three-dimensional scale. FABRITIUS (2002), WOLLMANN (2004) and HUBERT (2005) created detailed high-resolution 3-D spatial models for the central part of the industrial region Bitterfeld-Wolfen. Geological borehole information served as the major data input. The geological 3-D models provided the basis for the structural finite-element model. The different used structural modelling approaches as well as local features, constraints and dimensions are discussed in WYCISK *et al.* (2002), WYCISK *et al.* (2006), WYCISK *et al.* (2009), and HUBERT (2011).
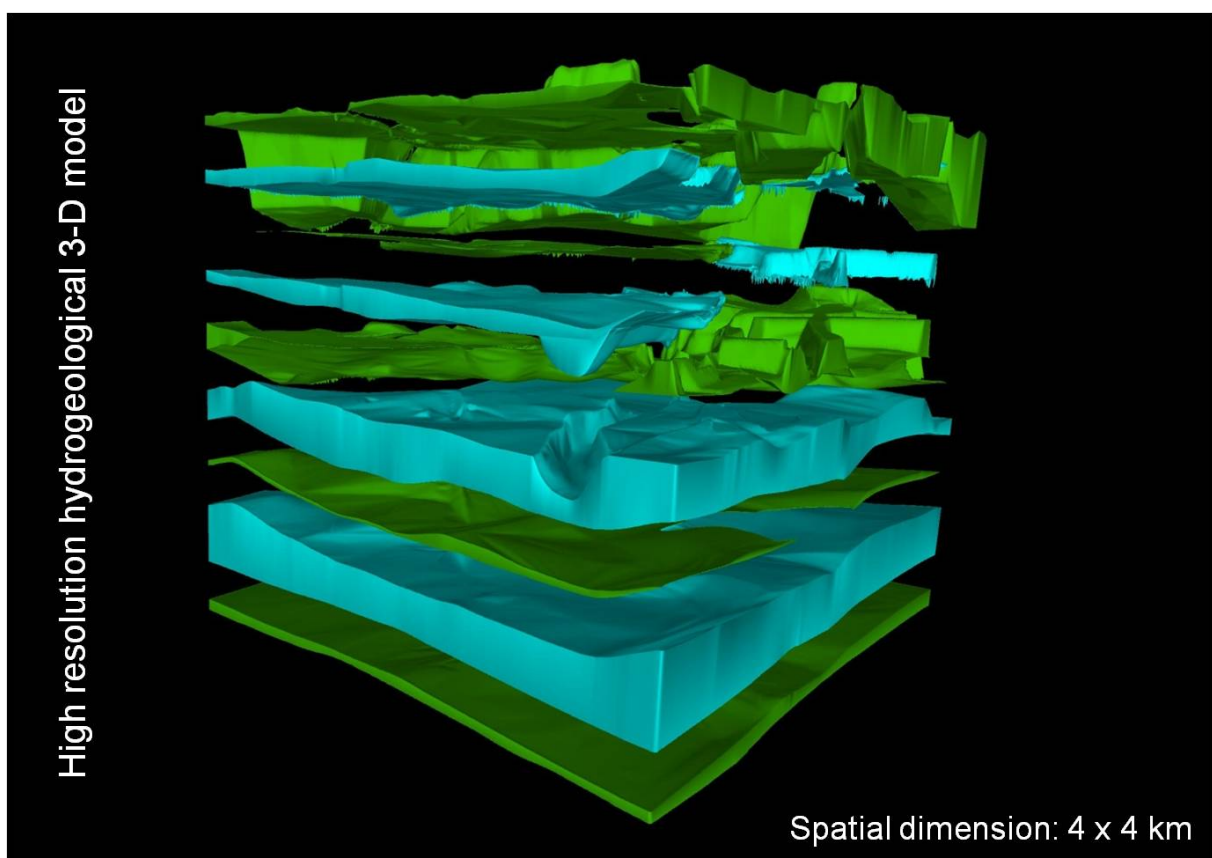
Figure 4-21: Geometries of high resolution (hydro-)geological 3-D models served as data input for the structural numerical model process. The figure illustrates exemplarily a 4 x 4 km section of the Bitterfeld-Wolfen area. Aquifer horizons are blue-coloured; aquitard units are green-coloured. Details about the model creation can be obtained from FABRITIUS (2002).

Model areas outside the dimension of the geological 3-D models were characterised by GOSSEL (2009) based on geological and hydrogeological information derived from available maps published by HELMERT (1984), GROTE & KRÜGER (1984), MARCINOWSKI & MÜLLER (1980), and EISSMANN & MÜLLER (1978).

Three-dimensional spatial information of the structural model was transferred from geological structural modelling systems to ArcGIS. An individual XYZ dataset was pre-processed for each of the numerical layers listed in Table 4-3. Those datasets served for the characterisation of numerical model slices. Data transfer from ArcGIS to FEFLOW and the following internal interpolation is managed by the GIS file format (*.shp).
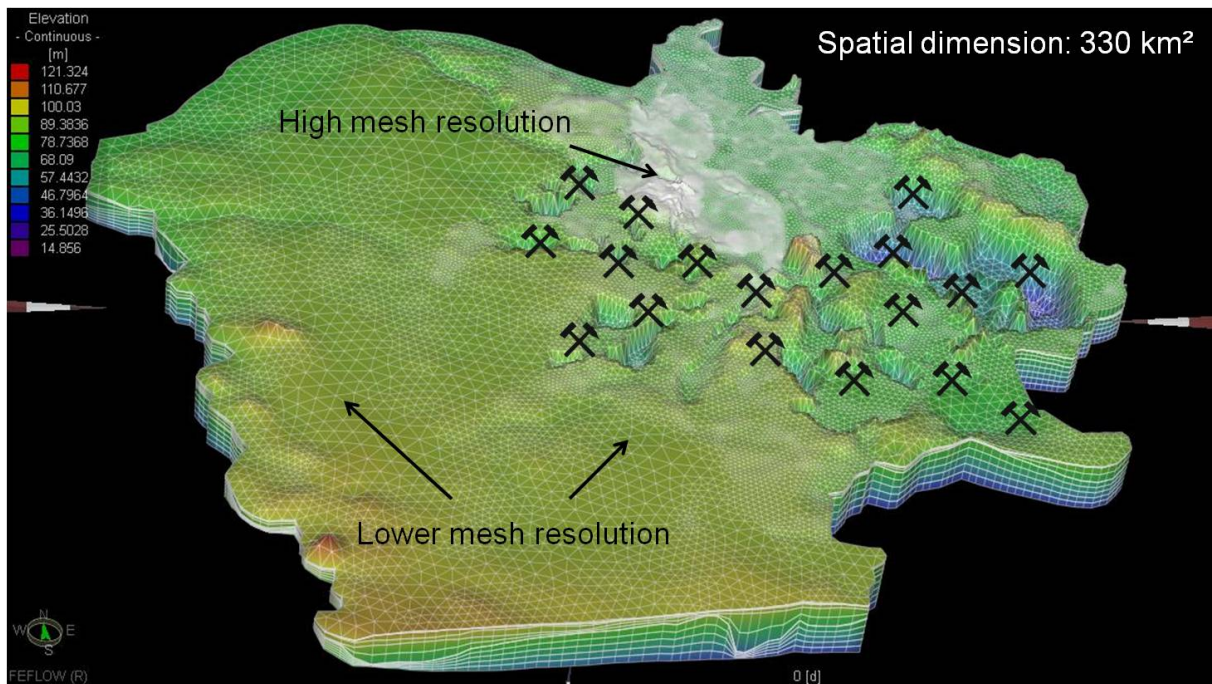
Figure 4-22: The structural FE model covers an area of 330 km² and is discretised by almost three million triangle elements. Terrain elevations range from > 120.0 m in landfill areas down to < 50.0 m in abandoned mining areas. Local mesh refinements were implemented in areas of interest such as e.g. the industrial centre of Bitterfeld-Wolfen.

4.3.4 Regional groundwater flow model

Numerical groundwater flow modelling was applied to reproduce effects of mining related groundwater withdrawal onto the hydraulic system of the Bitterfeld-Wolfen region for the time period 1955 to 2005. The transient 3-D groundwater flow model includes the hydrogeological settings of the model area, involves the hydrological characteristics (surface waters and groundwater recharge) and reproduces the spatio-temporal groundwater abstraction of active lignite mining areas.

General assumptions and model specifications

The regional 3-D flow model is specified by transient and steady-state 1st kind and 3rd kind flow boundary conditions to characterise the regional surface water system which had been introduced previously in chapter 2.1.2.

Mining related groundwater withdrawal was implemented by assigning a transient 4th type boundary condition which was specified by a pre-calibrated extraction rate to fulfil the target levels of groundwater lowering in respective mining areas. The time dependent configuration controls the temporal characteristics (operation time) of local lignite mines during the simulation time period 1955 to 2005.

Unconfined aquifer conditions can be characterised in FEFLOW as a "phreatic model" which treats the simulated water table as a free and moveable surface. This mode ensures the representation of a sinking water surface in times of active groundwater drawdown as well as the possibility to represent a process of groundwater rebound after the stop of respective dewatering measures. This phreatic mode includes a simplified physical representation of the unsaturated zone. Therefore, unsaturated model elements are controlled by a linear approach between the predefined hydraulic conductivities and the residual water depths of the model elements. When the residual water depth decreases, due to, for example, groundwater lowering, the related hydraulic conductivity is reduced linearly. For further details, see DIERSCH (2009b).

The groundwater recharge is characterised by a transient fluid flux (2nd kind BC) which is assigned to the top surface of the numerical model.

Flow boundary setup

Flow model boundary conditions characterise the present model concerning the hydrologic specifications such as the groundwater recharge as well as the regional surface water system and controlling the implementation of mining related groundwater withdrawal. Assigned time series data for the specification of respective boundary conditions were pre-processed by GOSSEL *et al.* (2009) and GOSSEL (2008). As no consistent long-term time series data (surface water levels, climate data etc.) of ancient time periods were available for the model characterisation, differentiated data processing techniques have been applied: (I) time-invariant parameters were determined from temporal measurements, (II) steady time series were prolonged deductively and (III) transient data was correlated with exterior data.

The regional surface water system (chapter 2.1.2) is characterised by 1st kind and 3rd kind BC's which can be specified either steady-state or transient. Illustrated in the following Figure 4-23, the western and north-western model margin is assigned by a steady-state 1st kind boundary condition. The Strengbach water level dips slightly from +102 m in the south to app. +75 m in the northern part, which is characterised by the Fuhne river course. The Mulde River in the east and northeast, as the major receiving stream of the model domain, is characterised by a transient 1st kind boundary condition. The original river course (see Figure 4-23; dashed orange line) was rearranged in consequence of the lignite mining activities of the Goitzsche mining field started in 1975. The riverbed arrangement is considered due to individual sub-models which contain either the original or the modified river course. In both sub-stages the river course is specified by a transient 1st kind boundary condition.
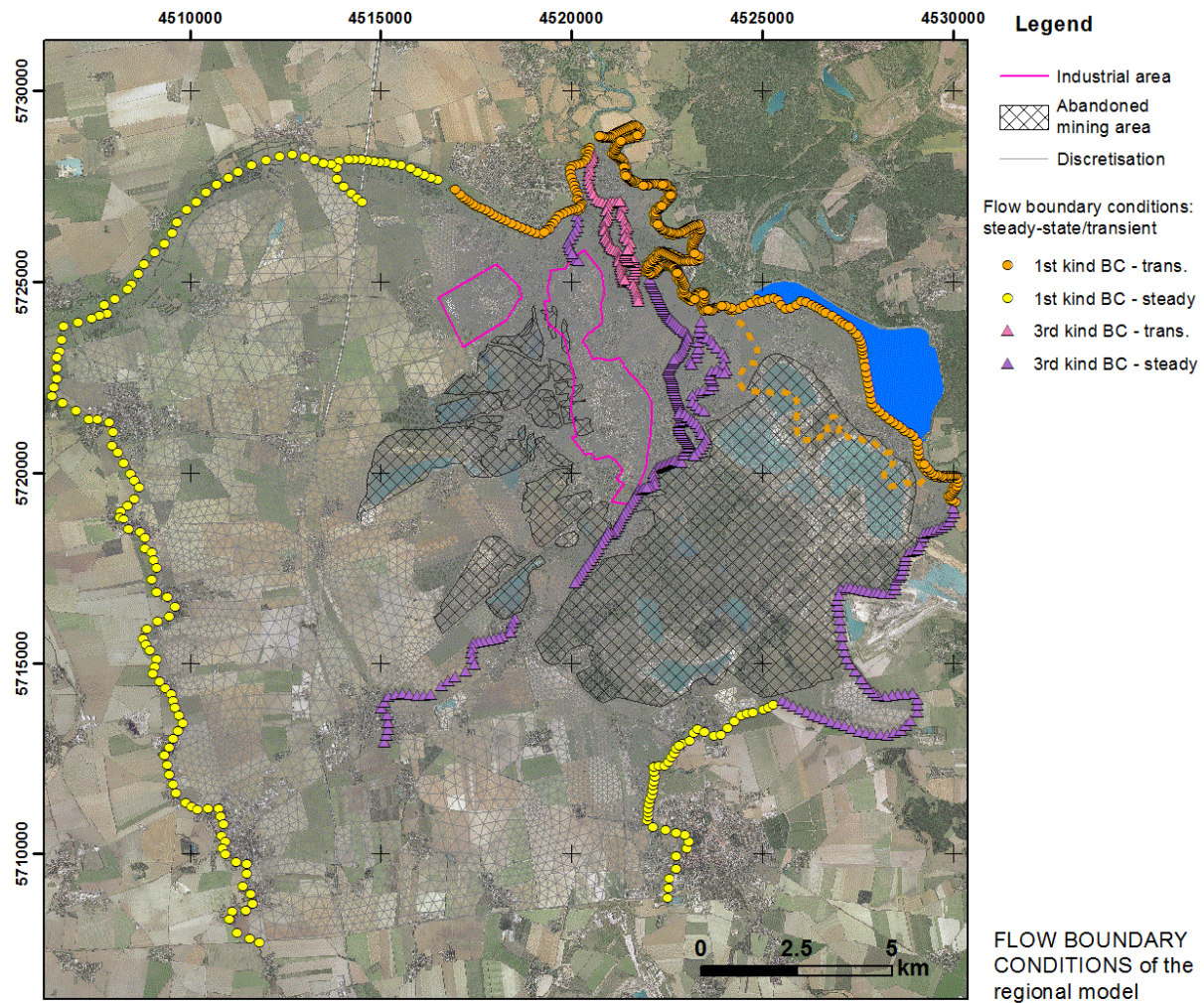
Figure 4-23: Running waters are characterised by numerical steady-state/transient 1st or 3rd kind boundary conditions. The model boundary follows the orientation of river courses. The natural Mulde river course (dashed lined) was rearranged in consequence of active lignite mining.

The inner model domain is traversed by the Strengbach-Lober-Leine system, which is characterised by a steady-state 3rd kind boundary condition. This waterway system drains the model domain from the south (+92.0 masl) to the north (+74.0 masl) by following the general run-off characteristics towards the north. The Lobber-Schlangengraben-Spittelwasser waters are assigned by a transient 3rd kind boundary condition.

Outer flow boundary conditions were primarily assigned over the whole vertical model discretisation involving the numerical model layers 1 to 37. The inner river systems are only assigned from the first to the fifth model layer, which follows the assumption that those surface waters are linked hydraulically only to the upper Quaternary aquifer units (see Table 4-3).

Since input data for assigning boundary conditions of rivers are often only available as nodal information from local measurements such as river water levels, the nodal input data was

100

interpolated linearly along the river course geometries. The linear interpolation requires the usage of a GIS polyline file (*.shp). This polyline represents the river course geometry, along which the 1-D interpolation is performed. Moreover, when BC's are assigned to be transient instead of being steady-state characterised, a time function of the hydraulic head is defined by using the FEFLOW internal *.pow file format. Subsequently, a 1-D linear interpolation between the individual time series data is performed, too.

The representation of mining related groundwater drawdown was approximated by the usage of the 4th kind well boundary condition, which is controlled by a pre-defined extraction rate. While in the Bitterfeld-Wolfen area the drainage was mainly installed in the upper Tertiary aquifer system, below the mining relevant seam complex, the 4th kind boundary condition was assigned in the numerical model layer 31. Since no data was available about extracted water volumes for the characterisation of the boundary condition, it was assumed to lower respective groundwater levels at least down to the base of the lignite seam complex. Information about the base elevation was derived from available lignite exploratory boreholes and available 3-D geological models (section 4.3.3). Those target base levels varied for individual mining fields. The following Table 4-4 contains the achieved water level elevations for modelling the mining related groundwater abstraction.

Table 4-4: Since no information about extracted water volumes was available for the simulation of the groundwater drawdown, target elevations were specified from borehole data and geological 3-D models which characterise the base of mined lignite seams. Those target levels varied for specific mining areas.

Mining field	Operation time	Target level for groundwater abstraction [m asl]
Holzweißig West	1958 – 1980	55.0
Holzweißig Ost	1931 – 1961	55.0
Goitzsche field I	1951 – 1960	55.0
Goitzsche field IIa	1959 – 1976	55.0
Goitzsche field IIb	1963 – 1967	55.0
Goitzsche field IIc	1965 – 1977	50.0
Goitzsche field IIIa	1971 – 1976	40.0
Goitzsche field IIIb	1976 – 1991	45.0
Goitzsche field "Niemegk"	1978 – 1994	45.0
Köckern	1984 – 1992	65.0
Freiheit II *	1907 – 1951	62.0 – 67.0
Freiheit III *	1888 – 1954	62.0 – 73.5

* Some groundwater lowering for the regional groundwater management is still in progress.
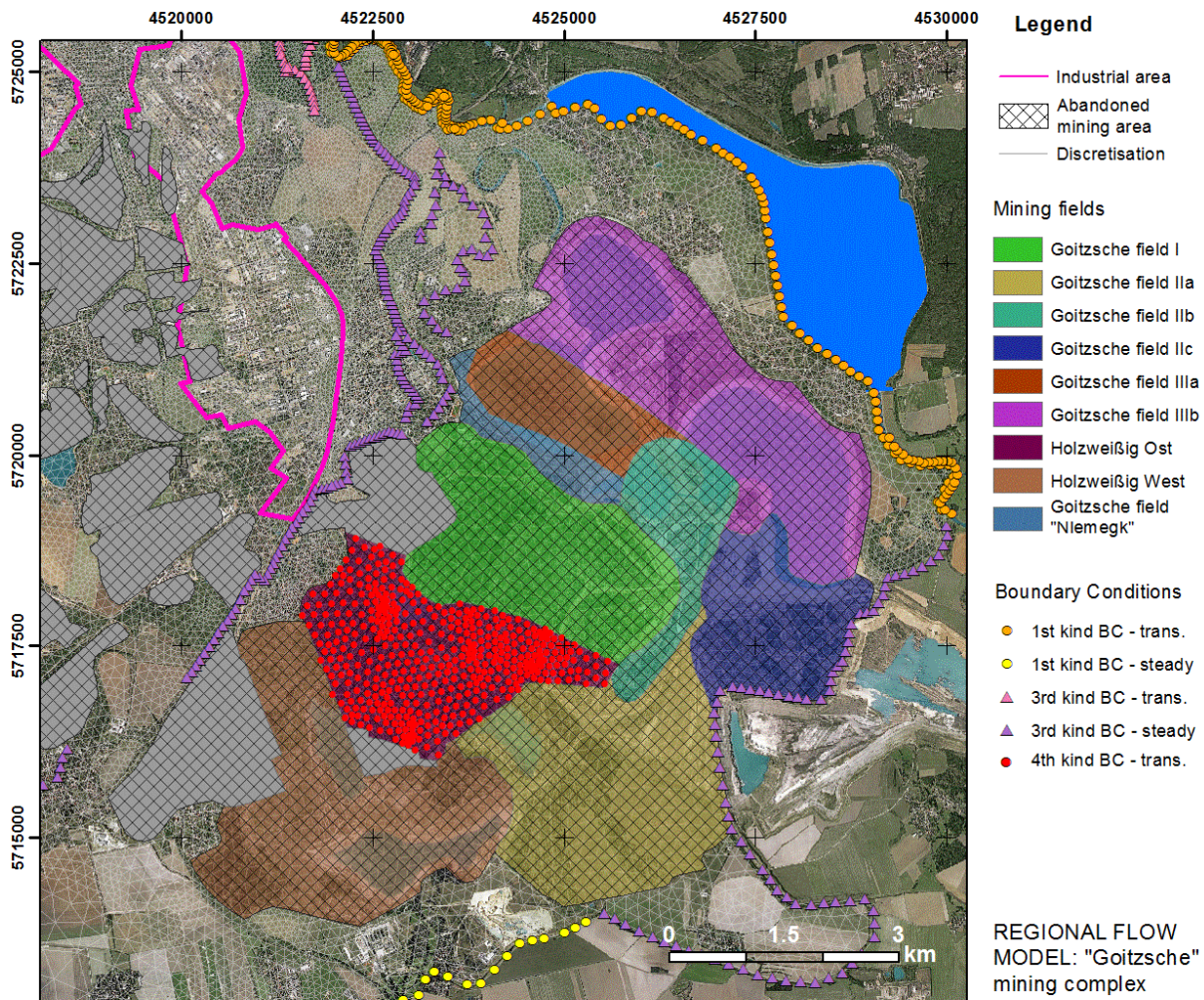
Figure 4-24: Mining related groundwater abstraction is approximated by a transient 4th kind BC which is assigned to the element nodes of respective mining areas. Boundary conditions are only implemented in times of active mining. Individual extraction rates were derived from model calibration to fulfil predefined groundwater target levels (Table 4-4).

Since multiple open-cast mines operated during variable time stages, related groundwater extractions were implemented in the flow model by using a transient 4th kind boundary condition. This well BC was assigned at each element node which is located within the spatial dimension of a particular open-cast mine. As illustrated in Figure 4-24, the element nodes within the polygon of the mining area *"Holzweißig Ost"* are characterised by a 4th kind BC. Within the FEFLOW system, these transient BC locations are linked to an internal model ID which is assigned by a time-dependent power function (*.pow) or time series with respect to an assigned extraction rate. By using this time-dependent function, a temporal activation of the well boundary is considered to reflect the operation time of the particular mining field. The specified extraction rate was derived iteratively from a calibration process which fulfils predefined groundwater target levels (Table 4-4).

The initial BC (hydraulic head distribution) of the first flow model stage was used from the model version of GOSSEL *et al.* (2009). As several sub-model stages are involved to reproduce the mining related groundwater abstraction for the simulation time 1955 to 2005, the final hydraulic head distribution of one sub-model serves as the initial condition for the next model stage. Here individual model stages were simulated successively until the complete simulation period was completed.

Groundwater recharge

Since transient BCs were used for the characterisation of the regional surface water system as well as the process of the spatio-temporal groundwater drawdown, the process of groundwater recharge is also implemented time-dependently. Transient recharge rates were calculated by WYCISK & GOSSEL (2006) using the TUB-BGR approach described by WESSOLEK *et al.* (2004). The approach includes the estimation of the evapotranspiration and corresponding recharge fluxes with respect to the rate of precipitation. Moreover, information about the depth to groundwater, soil classification, and land-use were included for the estimation of groundwater recharge which was managed by using a GIS system. For more details concerning the applied methodology, see GOSSEL (2008). Thus, spatio-temporal variable flux rates are defined at the top slice of the numerical flow model. The groundwater recharge is implemented as spatially variable and is specified temporally with a monthly resolution.

Parameterisation of flow materials: hydraulic conductivity, storativity, and leakage

The characterisation of the flow model concerning the hydraulic conductivity and storativity (drainable/fillable porosity) were taken over from the model calibration status of GOSSEL *et al.* (2009). The storativity was included globally with a value of 20%, which is compliant with the order of magnitude published by WEIß *et al.* (2004), GROßMANN *et al.* (2003), and WEIß *et al.* (1997). The model characterisation with respect to the hydraulic conductivity distribution was derived from lithological borehole data which was sorted into several kf-value classes. Those scattered hydraulic conductivity values were regionalised by geostatistical interpolation within a GIS system. For spatial interpolation, kf-values were processed in a logarithmised form to achieve reliable, smooth and continuous parameter fields. The FEFLOW internal assignment was easily managed by using the shape file (*.shp) data interface. An individual kf-value dataset was created for each of the 13 hydrogeological model units. In particular, the parameter distribution within the upper Quaternary horizons is highly variable since complex sediment structures are linked to variable material settings.

Table 4-5: The flow model is characterised by complex spatial distributions of hydraulic conductivity which had been derived from lithological borehole data and were regionalised by geostatistical interpolation. The lateral kf-values can vary within an individual hydrogeological model unit (HGMU) based on locally occurring material changes. Chosen parameter distributions were verified and validated by a successful model calibration.

				Hydrogeological Units	HGMU	Conductivity [m/s]	
Cainozoic	Quaternary			Holocene		Anthropogenic made ground	1	$5 \cdot 10^{-4}$	$7 \cdot 10^{-4}$
				Anthropogenic landfill		$1 \cdot 10^{-7}$	$7 \cdot 10^{-4}$
				Flood plain loam		$5 \cdot 10^{-6}$	$7 \cdot 10^{-5}$
				River gravel terrace		$3 \cdot 10^{-3}$	
		Pleistocene	Weichselian	Loess or loess loam		$2 \cdot 10^{-7}$	
				Glacial cover sands		$9 \cdot 10^{-4}$	$2 \cdot 10^{-4}$
				Weichselian river gravel (upper part)	2	$3 \cdot 10^{-3}$	$2 \cdot 10^{-3}$
				Periglacial horizon	3	$1 \cdot 10^{-6}$	$2 \cdot 10^{-5}$
				Weichselian river gravel (lower part)	4	$4 \cdot 10^{-4}$	$1 \cdot 10^{-3}$
			Saalian	Fluvial to glaciofluvial outwash sediments		$3 \cdot 10^{-5}$	$2 \cdot 10^{-3}$
				Saalian till complex	5	$5 \cdot 10^{-10}$	$1 \cdot 10^{-8}$
				Saalian Main Terrace		$5 \cdot 10^{-4}$	$2 \cdot 10^{-3}$
			Elsterian	Galciofluvial outwash sediments	6	$2 \cdot 10^{-4}$	$1 \cdot 10^{-4}$
				Galciolimnic sediments		$1 \cdot 10^{-5}$	
				Elsterian till complex	7	$1 \cdot 10^{-8}$	$8 \cdot 10^{-5}$
	Tertiary	Miocene	Bitterfeld Complex	Clay Cover Complex	Bitterfeld clay cover	8	$1 \cdot 10^{-8}$	$8 \cdot 10^{-7}$
					Roitzsch Sands		$8 \cdot 10^{-4}$	$3 \cdot 10^{-3}$
					Bitterfeld clay cover		$1 \cdot 10^{-8}$	$8 \cdot 10^{-7}$
				Mica Sand Complex	Bitterfeld seam complex	9	$2 \cdot 10^{-7}$	
					Bitterfeld sands	10	$5 \cdot 10^{-5}$	
		Oligocene			Breitenfeld horizon	11	$1 \cdot 10^{-7}$	
					Zöckeritz sands	12	$2 \cdot 10^{-5}$	
					Glauconite sands		$2 \cdot 10^{-5}$	
					Glauconite silts	13	$1 \cdot 10^{-10}$	
			Rupelian		Rupelian clay			

FEFLOW offers the possibility to consider a separate kf-value for each Cartesian coordinate (x, y, and z-direction) for incorporating the effects of anisotropy, to provide the principle of a kf-tensor. The regionalised hydraulic conductivity fields were assigned equally to the x-axis and y-axis of respective element nodes. Parameters in z-direction were characterised by a kf-values of one magnitude smaller than the previous used kf-value in lateral dimension. Table 4-5 lists the used parameter ranges of hydraulic conductivity for each hydrogeological unit.

The previously evaluated conductivity classes were adjusted and validated by a following calibration process with respect to measured field data (hydraulic head). A successful model calibration confirms the chosen model setup, parameter setting and qualifies the model to evolve and reproduce reliable model scenarios.

Model calibration

The calibration process of regional long-term (groundwater) models tends to be mostly difficult, since the required and available field database for the model verification is

insufficient in time and space. Therefore, GOSSEL *et al.* (2009) applied a gradual calibration procedure to achieve a best known and verified model status.

The calibration is based on individual datasets which vary concerning their temporal and spatial dimension. For the considered time period of 1955 to 2005, the available dataset consists of groundwater contours of the years 1955 and 1980, water levels of the river Mulde from 1994 to 2002, data of the regional groundwater monitoring (1992 to 2002), as well as climatic data of a local station which is covering the total simulation time.

Since the regional flow settings in the Bitterfeld-Wolfen area have been assumed to be characterised by steady-state conditions after the regional flood event in August 2002, the calibration of the time invariant hydraulic conductivity parameters (Table 4-5) was performed based on a short-term groundwater measuring campaign in autumn 2002. A quite good calibration status was achieved between observed and predicted hydraulic head values for the sub-model stage 2002 to 2005 as illustrated in the following Figure 4-25.
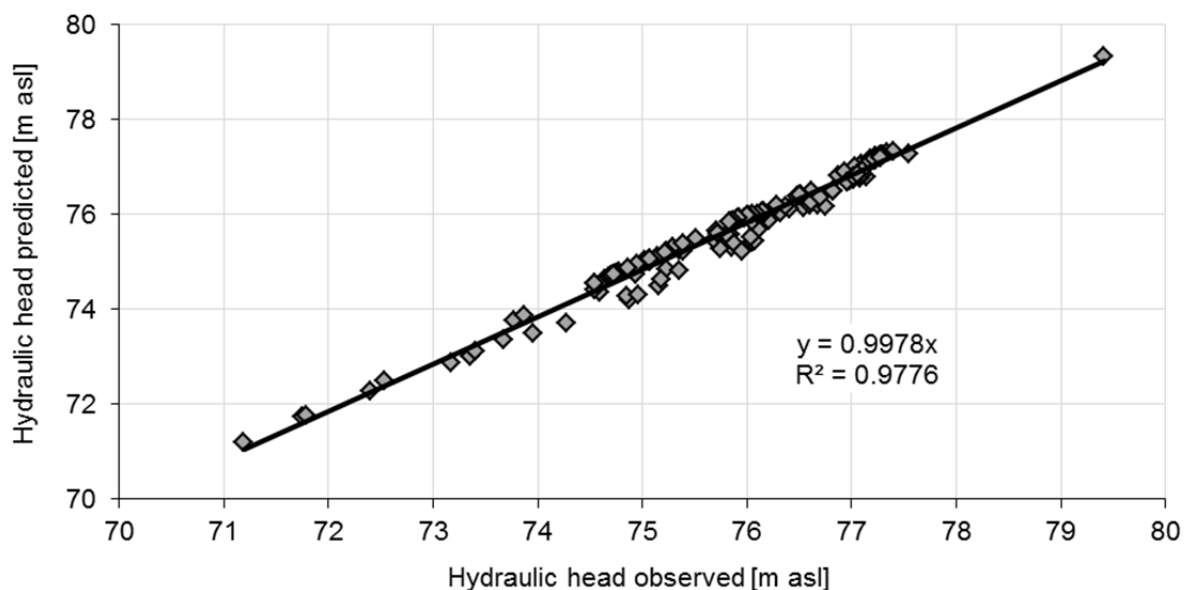
Figure 4-25: Steady-state flow model calibration (model stage 2002-2005): Data of a short-term groundwater measuring campaign in autumn 2002 was used to calibrate the hydraulic conductivity fields of the regional flow model as a steady-state flow scenario after the flooding event in August 2002. A strong correlation between observed and predicted data could be achieved by calibration (R²= 0.9776). (According to GOSSEL 2008)

Moreover, the calibration of time-dependent flow parameters such as porosity or groundwater recharge was performed by using time variant field data. Therefore, time-dependent data of the regional groundwater monitoring from 1992 to 2002 was considered for the calibration procedure. The dataset consists of transient hydraulic head values (time series data) of multiple observation points. Since the data quality was limited in terms of incomplete and

short-term time series as well as by a limited distribution of data sampling locations, the results of the transient model calibration could only be verified on a selection of available groundwater monitoring measurements. Results of the transient calibration are given in the following Figure 4-26.
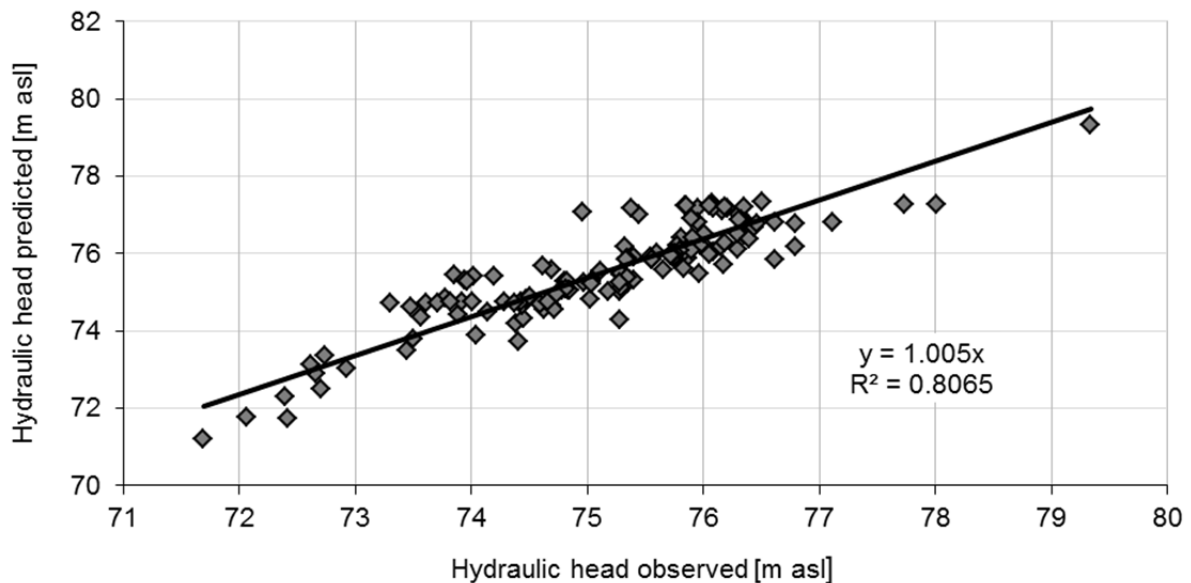
Figure 4-26: Transient flow model calibration (model stage 1992-2002): Time variant parameters such as groundwater recharge and porosity were calibrated on transient groundwater monitoring data of the time period 1992 to 2002. A high correlation of R²= 0.8065 could be achieved model calibration. (According to GOSSEL 2008)

For further details on the gradual calibration procedure of flow parameters, see GOSSEL (2008) and GOSSEL *et al.* (2009).

In a third stage, the flow model was additionally specified to incorporate mining related groundwater withdrawal. In consequence, this information about extracted water volumes was available only marginally; a groundwater drawdown target level was defined based on analysis of available borehole data. By following the assumption that the dewatering activities reached at least the base of mined lignite seams, target elevation levels were derived for the individual mining areas as listed in Table 4-4. Used extraction rates for the 4th kind BC were adjusted and calibrated as long as it was required to fulfil the predefined groundwater elevation level. Since four sub-models are used to represent transient groundwater flow velocity fields of the time period 1955 to 2002, the extraction rates needed to be recalibrated for each individual mining field and sub-model stage. This was required, since the number of active mining areas varied from model stage to model stage, and neighboured groundwater drawdowns influenced each other with respect to local defined target elevations. While an increased assignment of groundwater extraction tended to a rapid undershoot of the target elevations, an inactivation of specified boundary conditions led to significant overshoots.

In addition, local dewatering measures had been held active for longer time periods or are still active to control the groundwater rebound in abandoned mining areas. Those areas were identified from available groundwater contour maps. Appendix A provides information about calibrated extraction rates as well as target-actual comparisons of preselected calibration targets for individual mining areas and model stages.

Model sensitivity

Several numerical problems occurred during the first simulation runs which were related to model instabilities caused by numerical oscillations and affected finally the simulation time and the quality of model results.

In general, the spatial dimension of the 3-D flow model as well as the complex model setup including a free and moveable groundwater surface as well as numerous assigned steady-state and transient flow boundary conditions (surface water system and mining related groundwater abstraction) imply a high simulation effort to solve this numerical model. Therefore, it becomes even more bothering if model interruptions or crashes induced by numerical oscillations occur after a certain simulation time.

In more detail, the 3-D flow model reacted quite sensitively to extracted water volumes, which led to oscillation in local model elements and directly affected the convergence of the numerical model solution. In consequence, simulation time step lengths are reduced to suppress those occurring oscillations and to achieve stable model solutions again. But this time step reduction increased the total simulation time significantly. These local occurring oscillations were caused by too small element volumes which were incapable of providing the assigned extraction rates implemented by the 4th kind well boundary condition.

As a countermeasure, affected model elements were identified manually and the assigned BC was removed. This manual localisation was done visually by analysing related hydrographs of assigned model elements. When an oscillation was registered, the corresponding BC was removed from the flow model by using its unique model ID. Simultaneously, it was ensured that the aimed target elevation level of the local groundwater abstraction was fulfilled by adjusting the extraction rates of neighboured model elements!

Moreover, the model stability was increased by a limitation of the maximum simulation time step length which was set to two days. In general, the limitation or control of the used time step length is aligned to the principle of the Courant criterion for model stability (see chapter 4.2.6).

Moreover, as a free and moveable groundwater surface is simulated for the model domain and the groundwater table might decrease significantly by groundwater extraction, model elements near the terrain surface can fall dry. In a rapid groundwater rebound, these dry model elements can cause oscillations which again lead to model instabilities or a complete model crash. This is due to the fact that the hydraulic conductivity at the element node is linearly decreased with the decline of the corresponding hydraulic head for representing a

simplified unsaturated zone approach. In consequence of the linear decrease, the element node or the model element becomes increasingly impermeable. In terms of a rapid groundwater rebound, the impermeable cell is not capable of becoming "rewetted" that fast, which in turn causes numerical oscillations and model instability.

The suppression of "falling dry" can be implemented by defining a residual water depth for appropriate model elements. Numerically, this can be done by implementing a residual water depth in form of a constant 1st kind boundary condition which, keeps a specified hydraulic head value in the model element. In that case, hydraulic head relates to the bottom elevation of the model element and some specified minimum water height.

The second option follows a different approach which is based on a general increment of the model transmissivity. Here, element transmissivity is increased by multiplying the predefined kf-value with some assigned water height which is set manually.

Both approaches will distort the parameterised flow model in its original settings. The constrained option induces additional water into the flow model but is the more efficient method to stabilise the model with respect to dry cells. The unconstrained mode changes the original hydraulic conductivity field, is less model-invasive but is mostly not that effective as the constrained option. The unconstrained mode was used for the current flow model, and the residual water depth was increased from its default value of 0.01 m to 0.10 m.

Model stability was gained due to these modifications, and the total simulation time could be reduced from about two weeks to approximately six to seven days per simulation run. A maximum simulation time step of two days was implemented. By using these configurations, stable model solutions of the 3-D transient flow model were obtained.

Data analysis and results

A regional 3-D groundwater flow model was created for Bitterfeld-Wolfen. The numerical model includes a complex structural setup and characterises the hydrogeological settings of the model domain. Thirteen different hydrogeological units of the Cainozoic age are differentiated within the model domain. In addition, due to its long-term character, the 3-D flow model is capable of reproducing the mining induced changes of the regional groundwater flow velocity fields in the Lower Tertiary and the Upper Quaternary aquifer for the prior time period 1955 to 2005. The total simulation time of 50 years is internally split into several sub-time stages, represented by individual numerical sub-models.

During the simulation, intermediate results of the 3-D hydraulic head distribution were recorded to the FEFLOW result file (*.dac) in monthly intervals. Subsequently, generated result files can be analysed regarding variations of the hydraulic head, velocity field, and pressure head by using, for example, contour lines, fringes or particle tracking. Each previously saved time step can be selected separately to analyse data individually and time-dependently.
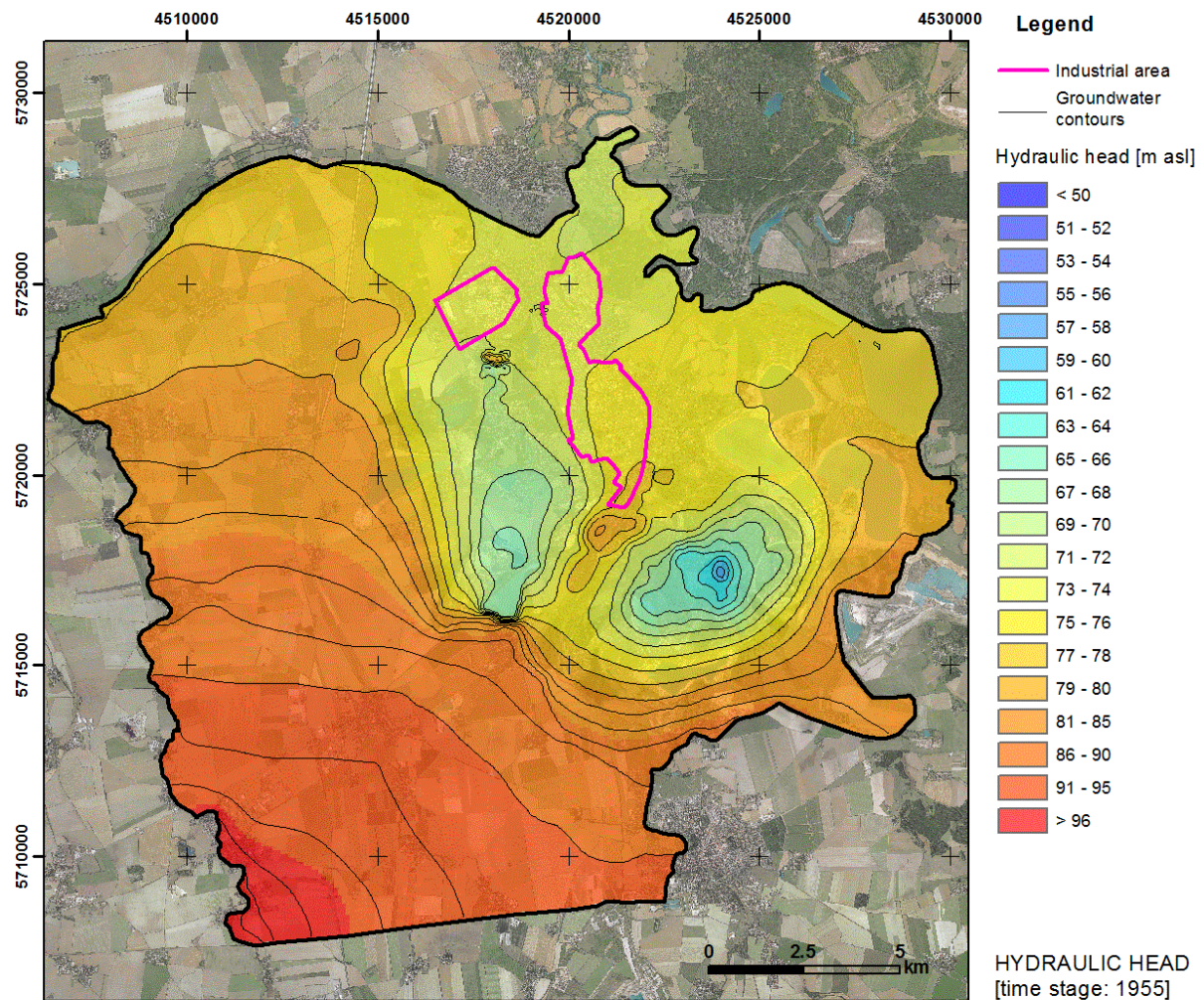
Figure 4-27: Post-processed from flow modelling data, the graphic illustrates the hydraulic head distribution of the regional aquifer system of year 1955. Two large drawdown areas are present in the central and south-eastern model domain. With respect to the industrial area, predominant groundwater flow directions were oriented towards the west, southwest and southeast.

For analysing the simulated groundwater flow data, regional hydraulic head distributions were exported for selected time slices by using the GIS file format (*.shp). Exemplarily, this was done here for the upper part of the Quaternary aquifer (numerical layer no. four). Data was post-processed and visualised in ArcMap. Exported nodal quantities were regionalised by using an Inverse Distance Weighted interpolation algorithm. Subsequently, the regionalised data was transferred into a grid file format having a resolution of 25x25 m. The GRID dataset was colour classified concerning its hydraulic head value. Moreover, the grid data was analysed with respect to surface contours (2 m intervals) which had been added to the illustration to highlight areas of high gradients. This form of visualisation can be applied to all numerical model layers of Table 4-5.

According to Figure 4-27, the hydraulic head distribution is visualised colour classified for the initial time stage of the year 1955. Equivalent visualisations are attached in Appendix B giving a chronological development of the groundwater flow velocity field within the Quaternary aquifer for the time period 1955 to 2002.
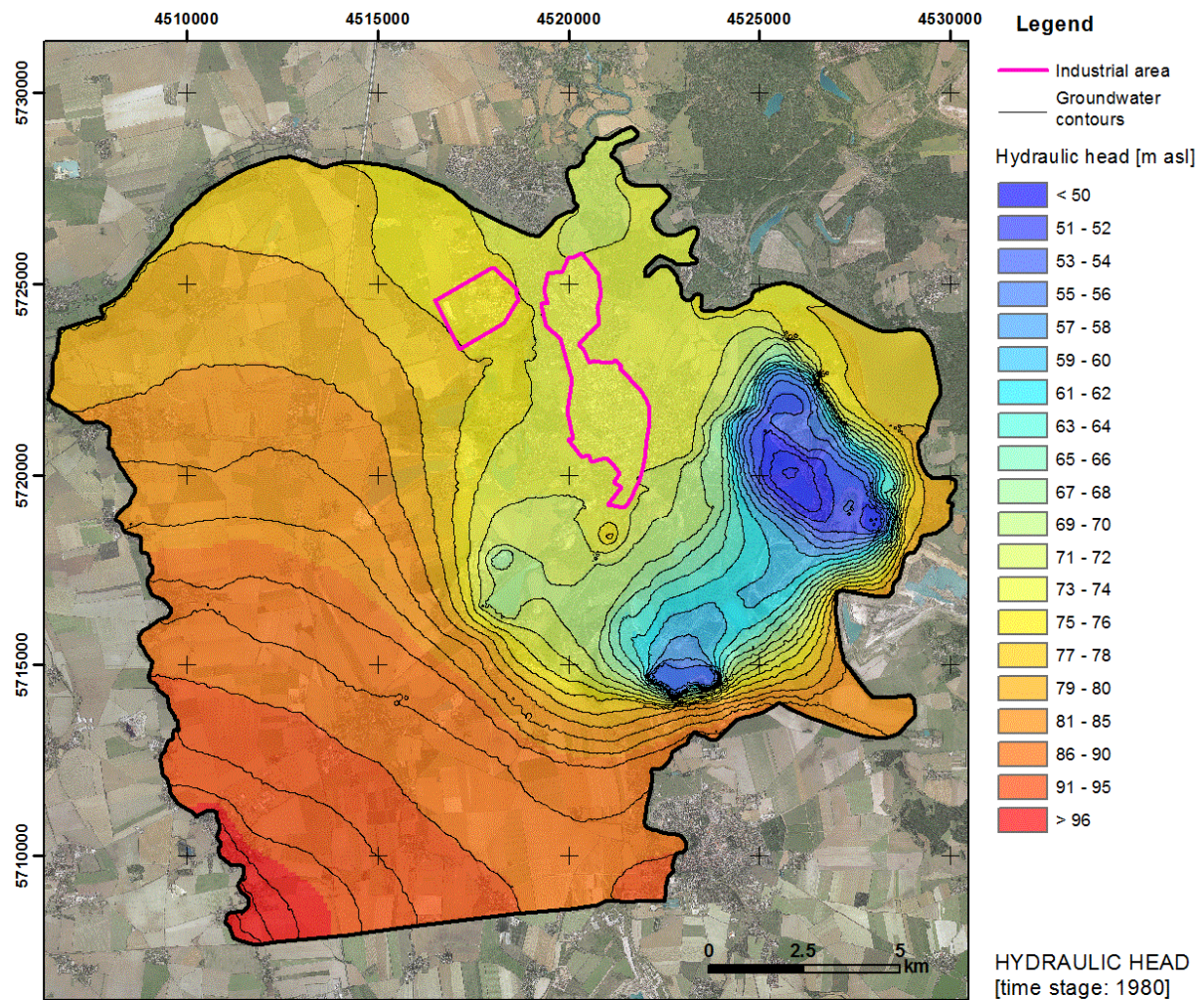
Figure 4-28: In consequence of the Goitzsche mining field opening and related groundwater withdrawal, the dominating groundwater flow direction from the industrial area Bitterfeld-Wolfen was oriented predominantly towards the south and southwest.

In general, the groundwater characteristics of the Bitterfeld-Wolfen area have been widely affected by the lignite related groundwater extraction. The groundwater flow direction and gradients were oriented primarily towards the resulting drawdown areas. In consequence of the Goitzsche mining field being open since the early 1950s, groundwater withdrawal was mainly installed in the southeast of the industrial area (e.g. Figure 4-28).

The spatio-temporal development of lignite mining activities consistently affected the flow system in regards to its characteristics such as groundwater flow velocities and directions. During 1955 and 1992, mining related groundwater extraction moved from the southwest to the south, southeast, and east, which is illustrated by separate time slices in Appendix B.

With the end of active lignite mining in 1992, mining related groundwater extraction was not necessary anymore and stopped. Only some local areas and drainage for groundwater management issues still exist.

A general and natural phase of groundwater rebound followed after 1992 (Appendix 7-7). The natural groundwater rise was overlaid by the Goitzsche flood event in 2002. The mining field was flooded within a few days (Appendix 7-8).

As the focus of the current study is not on the analysis of the transient flow velocity fields at a local scale, reproduced long-term 3-D flow velocity fields are applied to forensic source identification problems of groundwater contaminants. For further details about the spatio-temporal effects of mining related groundwater extraction onto the Bitterfeld-Wolfen aquifer systems, see GOSSEL *et al.* (2009).

Conclusion

A transient 3-D flow model of the Bitterfeld-Wolfen megasite was established by Gossel et al. (2009). In the presented study, the flow model was additionally verified concerning its flow boundary conditions for the time period 1955 to 2002. Therefore, mining related groundwater extraction and related variations of groundwater flow directions and gradients are described more accurately.

Moreover, the regional and long-term 3-D flow model was optimised concerning its simulation time. The removal of occurring numerical oscillations caused by unfitting assignments of flow boundary conditions (groundwater extraction) as well as by dry falling model elements led to a drastic reduction of the total computational time and led to more accurate simulation results.

Finally, a reproduced long-term 3-D groundwater flow velocity field is available for testing the forensic modelling approaches for source identification problems within complex model settings at a regional scale.

4.3.5 Regional transport model

The regional 3-D flow model was extended in FEFLOW to also be applicable for simulating transient solute transport processes in groundwater. As the aim is to test the functionality and accuracy of appropriate forensic modelling approaches for source identification problems, the Bitterfeld-Wolfen transport model is used to generate a virtual multi-source contaminant scenario. In principle, this scenario is based on site investigation data of the local hexachlorocyclohexane (HCH) contamination. HCH is a chemical residual of the local

Lindane production which was synthesised from 1952 to 1982. An overview of available site investigation data is given in Appendix C. Multiple contaminant loads were assigned, which are related to local HCH site investigation data. To generate a virtual multi-source contaminant scenario, the classic advective-dispersive solute transport mechanism was chosen for the following transport simulation. This implies that the solute is treated as a conservative tracer, and retarded as well as reactive mechanisms are not included. Moreover, groundwater observation points of the local monitoring network were added to the model domain to document the solute discharge.

Virtual contaminant scenario and model specifications

A multi-source contaminant impact scenario imitates local HCH releases from former production facilities and various deposits. The solvent is treated as a non-reactive solute which only underlies advective and dispersive transport. The FEFLOW system was investigated on how to implement a complex multi-source contaminant setup. The following scenarios were placed: (I) consistent mass loads ($\rightarrow$ leaching from a deposit), (II) single mass impulses ($\rightarrow$ short-term spilling incidents at e.g. production sites), and (III) time varying mass inputs.

The virtual scenario comprises a constant surface discharge at a former production site (II), five mass releases from local depositions (I & III), and a single mass impulse which represents a large scale pollutant loss at a prior production site (III). Therefore, transient 3rd kind and 4th kind transport boundary conditions were used to assign the aspired mass sources.

Finally, the virtual contaminant scenario forms a virtual case study of forensic modelling for source identification problems (reverse particle tracking and backward-in-time transport modelling) underlying ambitious and realistic real world conditions.

Computational mesh and transport model boundary conditions

When assigning transport BCs to represent mass sources such as deposits or prior production facilities, it is of particular importance to implement those sources by their characteristic spatial geometry in horizontal and vertical scale. Since BCs can be only assigned to the nodes of existing computational mesh, the implementation is limited to the given mesh configuration. For the case that the available mesh discretisation is insufficient for creating a representative approximation of the source location geometry, a local mesh refinement is required and additional nodes are added to the existing computational mesh. In the following, the BCs of potential source locations need to be specified concerning their temporal characteristics.

The numerical solution of solute transport processes in groundwater is much more sensitive to numerical instabilities than simulating only flow processes and therefore requires a generally higher discretisation.

The used mesh configuration of the flow model (Figure 4-20) was refined in the surrounding area of the Bitterfeld-Wolfen industrial centre, since this is the model region where pollutant sources are located and solute migration is expected. In addition to this, a higher mesh resolution was incorporate in areas of assigned pollutant sources. Mesh refinements in FEFLOW can be implemented by using polygons or lines (*.shp) along model areas for which a higher mesh discretisation is aspired. The adjusted mesh configuration of the regional transport model is illustrated in Figure 4-29.

Finally, a virtual multi-source contaminant input scenario was specified in accordance with the local HCH site investigation data (Appendix C). The scenario consists of a permanent mass load from a leaching prior production facility, a temporal mass injection by an additional industrial site, and pollutant discharges of five local deposits. The following Table 4-6 lists the involved source areas and their temporal model specifications.

Table 4-6: Multiple source areas were assigned to the transport model. Individual scenarios represent characteristic situations. The source areas vary regarding their temporal and spatial implementation. Spatial locations of the assigned mass source 1-7 are illustrated in Figure 4-29.

No.	Scenario	Characterisation	Model implementation	Numerical layers
S1	Production facility	Surface leaching	1955 – 2002	L1
S2	Production facility	Temporal mass load	1968 [10 days]	L1 – L4
S3	Disposal	Consistent mass load	1963 – 2002	L1 – L25
S4	Disposal	Consistent mass load	1963 – 2002	L1 – L22
S5	Disposal	Consistent mass load	1963 – 2002	L1 – L22
S6	Disposal	Consistent mass load	1963 – 2002	L1 - L22
S7	Disposal	Consistent mass load	1963 – 1992	L1 – L4

According to Table 4-6, all scenarios are implemented by a constant 3rd kind boundary condition, except for number S2, which is defined by a transient 4th kind boundary condition. The source areas 1-7 are added for different characteristic time periods. Different synthetic mass concentrations were assigned to the listed source zone numbers: 100 mg/l = no. S1, S4, S5, S6, S7; 1000 mg/l = no. S3; 100 000 mg/l = no. S2. The usage of different concentration levels had the intension to create a complex contaminant distribution pattern.
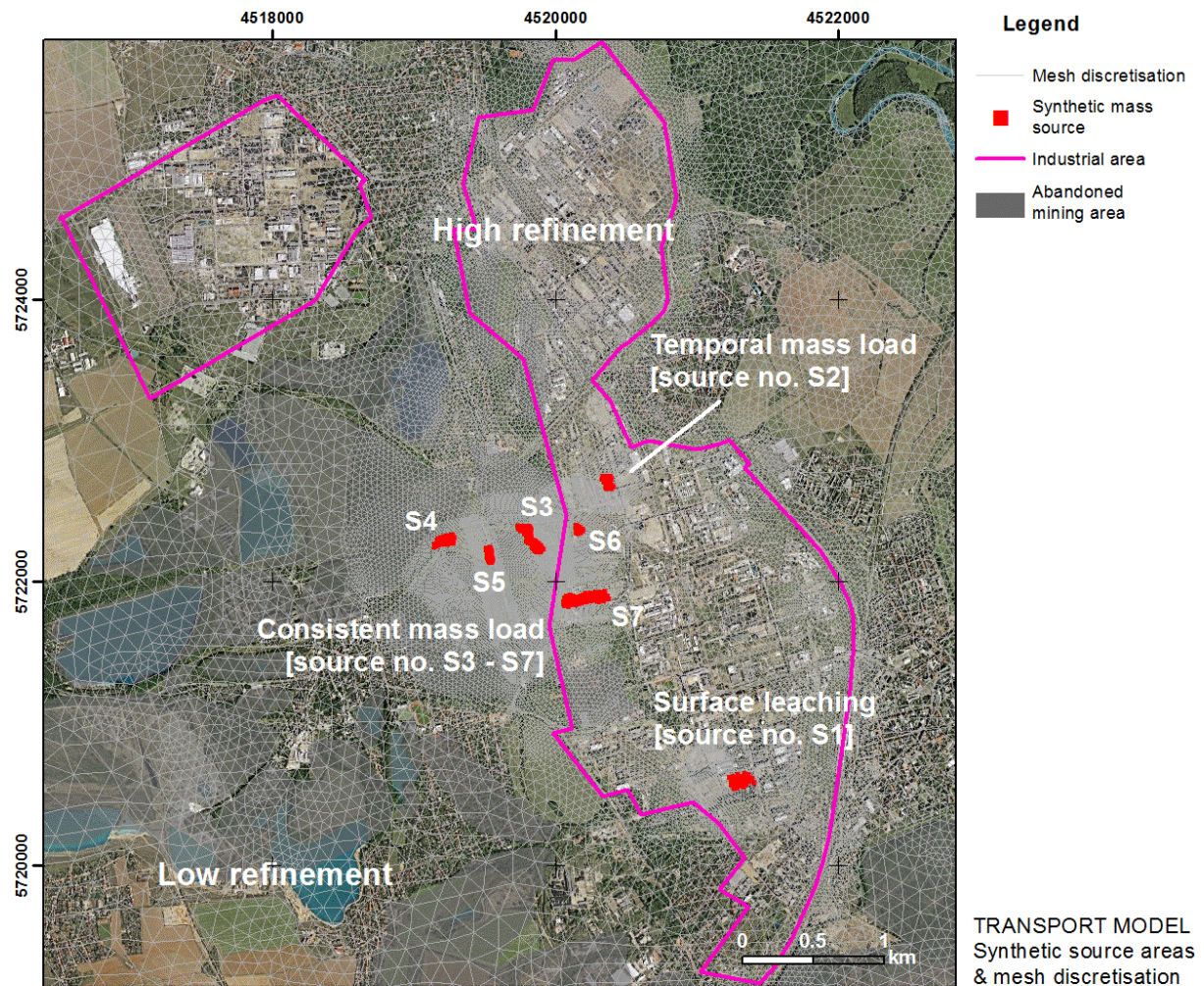
Figure 4-29: Seven mass source locations were assigned to the regional 3-D transport model which represent different types of contaminant source scenarios such as consistent leaching disposals as well as temporal and constant mass impulses from prior production facilities. In addition, mesh resolution was increased in the Bitterfeld-Wolfen industrial area and around specified source areas.

Respective BC's were assigned differentiated in vertical scale to simulate variable source geometries which are retrieved from available site investigation data. For example, location no. S3 characterises a source zone which is represented by a 3rd kind BC from model layer 1 to model layer 25. As the numerical layer 1 specifies the terrain elevation, layer 25 specifies the basis of the Bitterfeld lignite seam complex. Here, this location reflects a local disposal which had been created at an abandoned open pit mine being characteristic for the Bitterfeld-Wolfen region.

The procedure of assigning constant or transient transport boundary conditions is equivalent to the configuration of respective flow boundary conditions. The temporal aspect of transient boundary conditions is organised by a function of time which can be inserted by the FEFLOW internal (*.pow) file format. Again, it is suggested to assign the boundary conditions

of mass sources based on a predefined GIS based point file format (*.shp) which can be easily imported. This is additionally of advantage, since complex geometries can be simply transferred from GIS map data to the modelling system.

Parameterisation of transport materials: diffusion and dispersion

As the transport simulation is based on the advective-dispersive mass transport principle, additional parameters for the characterisation of the hydrodynamic dispersion are required. This includes values for longitudinal and transversal dispersion lengths as well as for diffusion. Qualitatively, transport simulations are highly sensitive with respect to the dimension of chosen transport parameters (e.g. dispersion lengths). The determination of reliable dispersion parameters is a challenging aspect which is often realised during the calibration process for fitting simulation results onto measured field data.

For the current study, related dispersion lengths were assumed synthetically with respect to the dimension of the regional scaled transport problem. As for the current study, the focus was on the creation of a virtual multi-source contamination scenario at a regional scale, which involves specific local site characteristics; the chosen transport parameters such as dispersion lengths had not been adjusted by calibration. For simulation, the longitudinal dispersion length was set globally to 50.0 m and the transversal dispersion length is 5.0 m which seems to be reliable with respect to the considered simulation time and spatial model scale. Dispersion parameters have been chosen according to BEIMS (1983), who collected longitudinal dispersion length data in relation to the scale dependency of the transport problem.

For representing a diffusive transport mechanism, a coefficient of $7.34 \cdot 10^{-9}$ [m²/s] was defined. According to EPA (1996), this diffusion coefficient is characteristic for the HCH isomer spectrum.

Finally, an advective-dispersive solute transport is simulated for the Bitterfeld-Wolfen area at the basis of an effective porosity of 20%.

A model based groundwater monitoring network

Reference data points in FEFLOW represent groundwater observation points at which variations of the hydraulic head [m] and the solute concentration [mg/l] are registered in form of time series data. These observation points are assigned three-dimensionally to the computational nodes of the finite element mesh.

As a regional groundwater monitoring network is installed in the Bitterfeld-Wolfen region for the observation of the hydrochemistry in the Quaternary and Tertiary aquifer, selected monitoring locations were added to the transport model as reference data points by considering their spatial characteristics. Horizontally, these locations are characterised by their spatial coordinates. In vertical scale, the reference data points are implemented with

respect to their screen level elevations. Therefore, 24 observation points of the local monitoring network were added to the transport model for tracing the spatio-temporal development of the virtual contaminant discharge. Basically, these observation points are installed in the Quaternary aquifer but can also tap the transition zone towards the lower Tertiary aquifer unit. An overview of the spatial locations is given in Figure 4-30. Corresponding data, such as spatial coordinates, labels, screen level elevations, and the assigned model layers is attached in Appendix D.
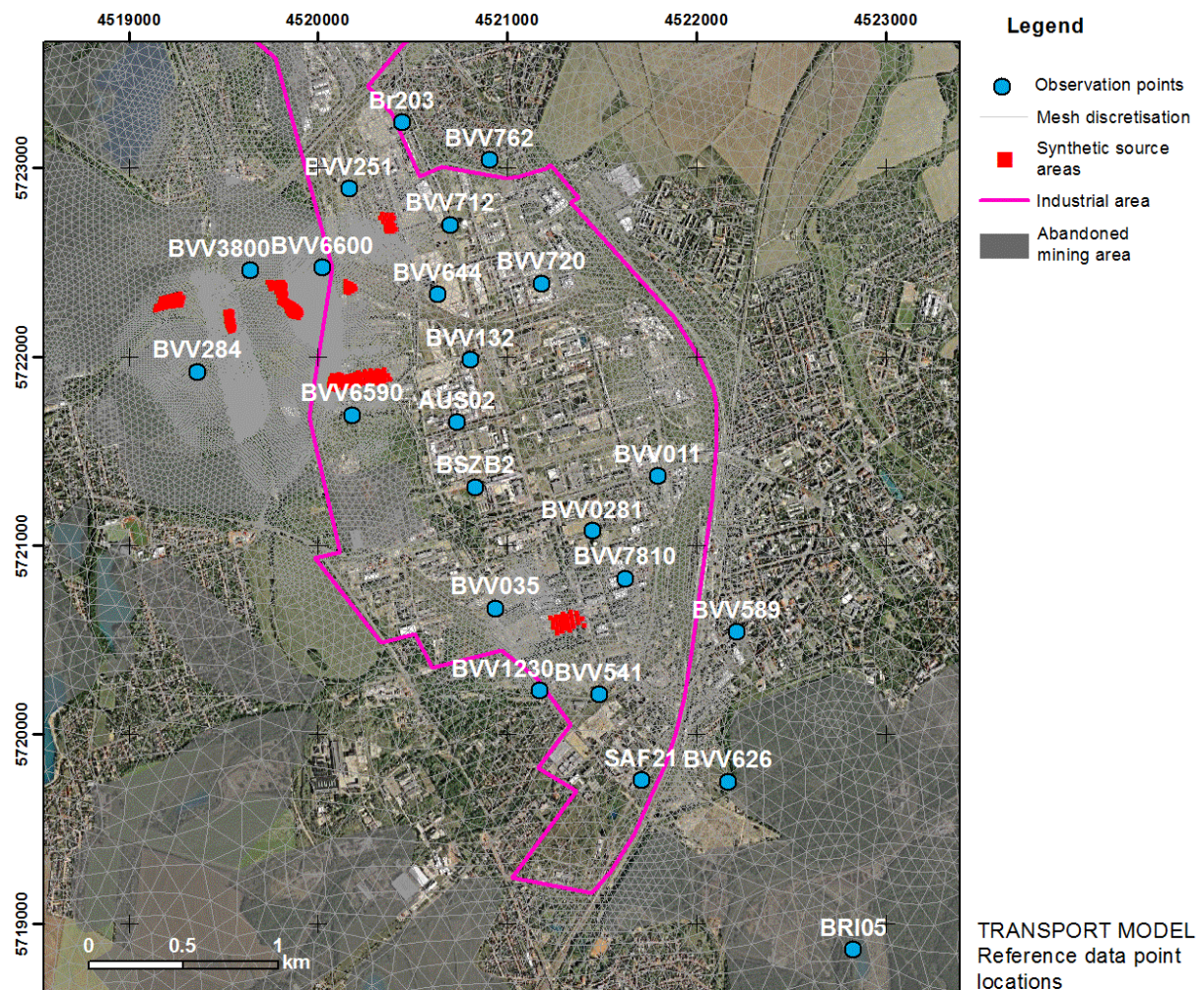
Figure 4-30: Locations of the Bitterfeld-Wolfen groundwater monitoring were added to the numerical model as reference data points. Observation points are assigned to the nodes of the finite element mesh and enable the collection of time series data concerning, for example, the solute concentration.

Reference data points are assigned to the numerical model either manually or by importing a GIS based point file format (*.shp), which contains respective XYZ locations. Assigned nodes

are labelled FEFLOW internally by unique IDs. Those ID's are used to organise location specific time series data such as the solute mass concentration.

Transport model stability

In general, the advective-dispersive transport simulation is based on the previously run flow simulation. Thus, transport modelling is sensitive to probable occurring model instabilities of the flow modelling process. As reasons for oscillations of the current flow model (dry falling elements or unfitting boundary conditions) were eliminated, the numerical simulation of solute transport processes also tends to numerical instability due to several reasons.

In most cases, errors are caused by oscillating mass distributions or numerical dispersion, which is in turn based on an insufficient discretisation in time and space. Therefore, local mesh enrichments as well as the reduction of the simulation time step can resolve this problem. The effect of numerical dispersion often occurs in the presence of sharp concentration fronts, which can take place when a high mass impulse is induced by some boundary condition. With respect to insufficient (coarse) mesh spacing, the transported solute mass cannot be quantified adequately at the element nodes. Therefore, the mass assignment is overlaid by some extrapolation effect, which induces "additional mass" into the model domain. Moreover, the migration of sharp concentration fronts often tends to numerical oscillations (concentration overshoot/undershoot) when the corresponding simulation time step is chosen to large and the transport process is not depicted accurately enough. Finally, insufficient discretisation in time and space will lead to mass balance errors which often end up with numerical oscillations, model instabilities or a model crash. The virtual contaminant scenario of about 50 years was simulated by using a limited time step interval of 0.5 days. This time step interval was evaluated iteratively by the trial-and-error method. To overcome insufficient discretisation in space, the mesh resolution was increased in the area of the Bitterfeld-Wolfen industrial centre. In addition, further mesh refinements were applied in the surroundings of the synthetic mass sources no. 1-7 of Figure 4-29.

Often the so called Peclet criterion is used to control the spatial discretisation of the computational mesh to avoid mass balance errors and numerical instability. The Peclet criterion is represented by a quantitative value, which is ideally smaller than one. Its determination needs to be performed for each Cartesian axis of the numerical model as the flow velocity differs in space. For more details, see BEAR & CHENG (2010), HUYSMANS & DASSARGUES (2005) and KINZELBACH (1992). Since this calculation is complex for transient flow velocity fields in combination with 3-D model dimensions, the model discretisation was also adjusted by the trial-and-error method until stable simulation results were achieved.

In addition to previous suggestions, the right choice of transport boundary conditions, the handling of dry falling elements and the usage of damping upwind techniques increased the general model stability. Using the advective-dispersive 3rd kind BC instead of the advective based 1st kind BC for describing local mass loads has the advantage of smoothing the resulting sharp concentration front additionally by including the dispersive flux in the 3rd kind

boundary condition. This stabilises the model solution in terms of numerical oscillations caused by sharp concentration fronts.

Upwinding schemes provide some additional potential to stabilise oscillating model solutions. These techniques induce an additional solute mass into the model, which reduces the effects of an insufficient discretisation, but simultaneously distort the overall mass balance. Different types of upwinding methods are implemented in FEFLOW which differ concerning their working mechanisms and impact levels onto the affected mass balance. For the current model, the streamline upwinding was used, which constitutes a smooth technique to suppress numerical oscillations. Here, numerical dispersion is only added in the major direction of the groundwater flow velocity. Besides the general smearing effects of upwind techniques, these approaches suppress numerical oscillations gently and lead to a stable model solution during the simulation. Their implementation has to be decided situation-based.

Since the groundwater flow simulation reacted sensitively concerning dry falling elements, the transport model showed a similar behaviour. The utilisation of a predefined residual water depth in affected elements helped to handle respective oscillations. Therefore, this strategy was also taken over for the transport model. A residual water depth of 0.15 m was defined for dry model elements in the transient transport model.

General model stability often constitutes a balance act between a sufficient spatio-temporal model discretisation for obtaining stable and accurate model results and the numerical simulation effort with respect to the computational time! Stability criterions such as the Peclet number to control the spatial model discretisation and the Courant number to control the temporal discretisation can serve as initial test procedures to discover corresponding deficiencies. As their estimation is very complex in transient 3-D model environments, they are difficult to implement. Thus, the current model setup was adjusted iteratively by the conventional trail-and-error approach.

Data analysis and results

A virtual transient 3-D contaminant scenario was simulated at the basis of the regional Bitterfeld-Wolfen groundwater flow model. The transient flow velocity field is highly variable due to excessive mining related groundwater extraction, which also affected the regional contaminant discharge by variable groundwater flow directions and gradients. Covering the time period 1955 to 2002, this scenario represents a multi-source groundwater contamination scenario which is representative for the local site history. Different forms of pollution origins are implemented by 3rd kind and 4th kind boundary conditions, which reproduce pollutant discharge from waste deposits or, for example, contaminant surface leaching at a prior production facility. For simulation, solute mass is treated as a conservative tracer which underlies only the advective and dispersive transport mechanism and does not include retardation or reactive mechanisms. The simulated pollutant discharge was observed at selected reference data points. At those locations the contaminant impact was registered in

form of breakthrough curves. These reference data point locations were adopted from observation well locations of the local groundwater monitoring in Bitterfeld-Wolfen.

Since the natural downstream is directed towards the northern located surface waters, respective solute transport processes are expected in this direction analogously. In contrast, wide ranging groundwater extractions of multiple open cast mines changed the natural groundwater regime and led to significant changes of natural flow conditions which also affected the regional contaminant discharge.
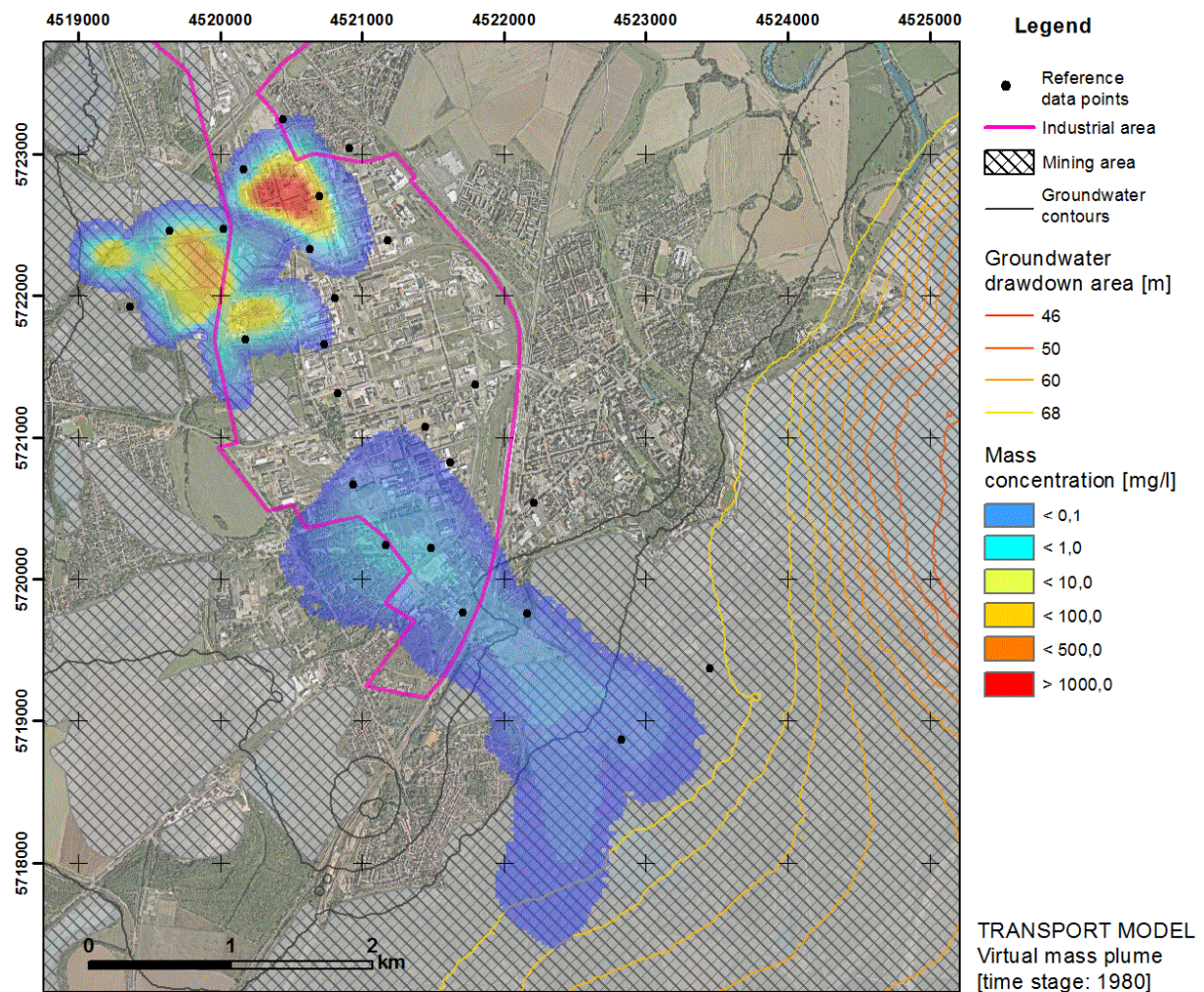
Figure 4-31: After simulation period of 25 years, several mass plumes emerged from assigned mass sources. The regional contaminant discharge is overlaid and oriented towards the mining related drawdown areas of the Goitzsche mining complex in the south, southeast and east.

During the simulation time of almost 50 years, mass loads at assigned source locations (Figure 4-29) were discharged towards the south, southeast and east, in the direction of drained Goitzsche mining fields. In the course of time, individual mass plumes merged and

followed the prevailing groundwater flow direction. Results of the simulated multi-source contaminant spreading are documented in form of mass distribution maps in ten year-intervals, attached in Appendix E.

According to Figure 4-31, after a simulation time of 25 years, individual mass plumes of varying dimension and quantity emerged from several contaminant sources (Figure 4-29 and Table 4-6) at the time stage 1980. The southern contaminant pattern covers a larger area than the northern grouped plumes. However, all plume geometries already indicate a south-eastern oriented transport direction which was primarily initiated by active groundwater extraction in the south-eastern located open-cast mines of the Goitzsche complex.
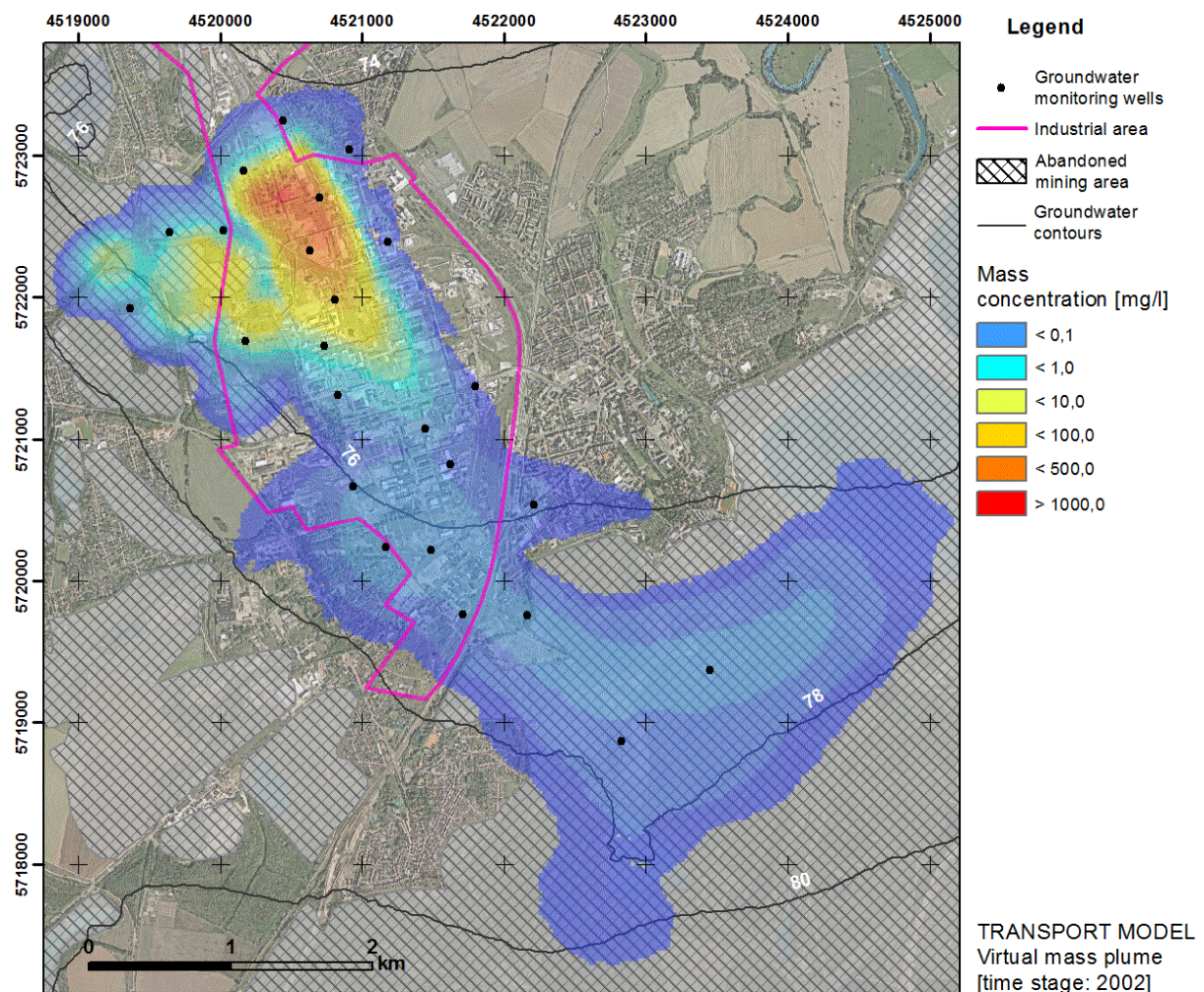
Figure 4-32: After a simulation of 50 years, the mass distribution pattern implies a predominant transport direction towards the south and southeast. Individual mass plumes joined and the tracer was dragged deeply into prior mining related drawdown areas. After the flood event in August 2002, the groundwater flow situation changed to almost pre-mining conditions. A general transport direction towards the north is expected.

As already mentioned, the individual plumes differ concerning their characteristic mass concentration levels caused by specifications of pollutant load at assigned mass sources. With an increasing simulation time, contaminant discharge continued and led to larger plume extensions and diffused contamination patterns. Figure 4-32 illustrates the mass distribution at the time stage 2002. It is noted that the individual mass plumes of 1980 (Figure 4-31) merged and a prevalent downstream direction towards the south, southeast and east is indicated by the plume shape. This predominant southeast/northwest aligned transport direction is additionally reinforced by a north/south oriented sub-glacial channel structures, which constitutes high hydraulic conductivity contrasts and provides preferential solute transport pathways.

While the regional pollutant transport was primarily oriented towards the south/southeast, smaller parts of the mass plume additionally indicate an eastern oriented transport component. The lower tail of the mass plume is clearly situated in the area of the prior Goitzsche mining area, which is directly related to the excessive groundwater extraction after 1976. During the mining history, southern located open cast mines were closed while mining activities were drastically increased in the east of Bitterfeld-Wolfen (Figure 4-28). In consequence, the regional groundwater flow direction well as the regional mass transport was diverted towards the drawdown area in the east.

Multiple reference data points were added to the model which, characterise observation points of the local groundwater monitoring network at the Bitterfeld-Wolfen site. Dynamics of regional mass transport were registered in form of breakthrough curves at those implemented reference data point locations. Observation points were defined primarily in the Quaternary as well as in the transition zone of Tertiary aquifer unit (Figure 4-30).

Breakthrough curves provide essential information about the chronological and quantitative development of the contaminant impact. Figure 4-33 and Figure 4-34 contain registered breakthrough curves of the observation points BVV644 and BVV3800, which are installed in the upper Quaternary aquifer.
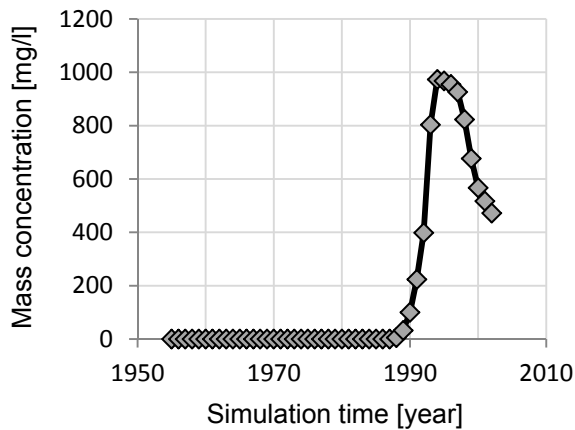
Figure 4-33: Breakthrough curve of the observation point BVV644. The reference point was affected the first time after a simulation time of about 33 years (year: 1988), representing the arrival time. After the arrival, mass concentration increased rapidly to a maximum of about 1000 mg/l in year 1994 followed by concentration drop.
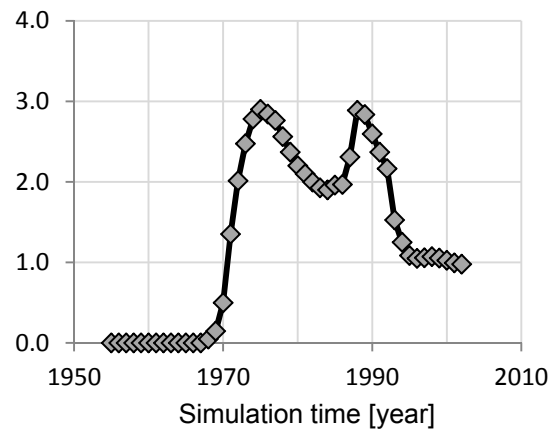
Figure 4-34: Breakthrough curve of the observation point BVV3800. After year 1970, the reference location is affected permanently by a solute mass concentration levels in the range of 1.0 to 3.0 mg/l with temporal fluctuations. A general decline of the concentration mass is observed after 1989.

Breakthrough curves were modelled for 24 individual observation wells. Those graphs include information about the arrival time when a threshold was exceeded as well as information about the course of mass concentration and concentration maximums. Characteristics of individual breakthrough curves differ from reference location to reference location due to a complex aquifer setting, variable distances to source areas, fluctuating transport dynamics and so on. All the registered breakthrough curves and related interpretation concerning the arrival time and concentration maximums are attached in Appendix F.

The form of a breakthrough curve already reveals some information about the proximity between its reference location and the potential source area. If the reference location is affected by a consistent mass load also at an early time stage or short arrival time, source location and observation point might be closely related. In turn, this implies that breakthrough curves of observation points at a greater distance to the source area are characterised by longer arrival times and likely lower concentration levels. This presumption is only valid for steady-state systems. In transient systems, contaminant transport is much more complex, and those presumptions might be invalid, since transport conditions can vary in space and time.

Thus, simplified source-receptor relations in transient systems that are based on the interpretation of breakthrough curves do not lead compulsorily to suppositions about the distance or location of contaminant sources. In addition, consistent time series data from groundwater monitoring is often not available at all and exclude this strategy anyway. Forensic modelling techniques provide a promising approach for the identification of unknown or suspected pollutant sources. Data of the synthetic contaminant scenario (monitoring data) is used to test two individual modelling approaches concerning their accuracy and model uncertainty for source identification issues of an observed groundwater contamination in transient environments.

Conclusion

A virtual 3-D multi-source contamination scenario was simulated for the abandoned Bitterfeld-Wolfen mining area based on characteristic long-term contaminant transport. The regionally scaled transport scenario covers the historical time period 1955 to 2002. It was figured out how different types of mass sources can be implemented characteristically in FEFLOW by their spatial dimensions in horizontal and vertical scale.

Instabilities of the numerical transport model provoked by insufficient spatio-temporal discretisation as well as by problems due to dry model elements had been solved successfully. Therefore, effective techniques such as subsequent mesh refinement and the adjustment of time discretisation were applied. Problems, induced by dry model elements, were solved by the assignment of a predefined residual water depth. This kept affected model cells to a certain extent more permeable and suppressed model instabilities due to numerical oscillations.

Seven individual mass sources were defined by 3rd kind and 4th kind transport boundary conditions representing different types of contaminant input areas. This scenario involves pollutant discharge from industrial disposals, surface entries at, for example, production facilities or temporal mass loads for representing, for example, a case of accident. The induced mass was treated as a non-reactive solute which does not underlie any form of reactive processes affecting the mass quantity. Solute mass transport was simulated by using the classic advective-dispersive transport mechanism.

Local mass transport of the Bitterfeld-Wolfen site was overlaid significantly by mining induced changes of the groundwater flow regime. Excessive groundwater abstraction at prior open cast lignite mines led to varying groundwater flow directions and gradients. Solute transport was mainly oriented towards mining related drawdown areas in the south, southeast and east. While the existence of isolated mass plumes characterised early simulation stages, a merged global mass distribution evolved over time (Figure 4-32). The solute migrated deeply into the areas of prior mining activities. The chronological plume development is documented in form of mass distribution maps for individual time slices (Appendix E). Moreover, reference data points of the local groundwater monitoring network of Bitterfeld-Wolfen were assigned to

the model and enable local analysis about spatio-temporal contaminant impacts based on breakthrough curve data (Appendix F).

4.3.6 Forensic modelling for source identification problems

Results of the virtual transport scenario are used to analyse two forensic modelling approaches for contaminant source identification problems. These techniques differ concerning their mathematical description and methodological approach. Both have in common the capability for backward-in-time modelling in common.

Advective reverse particle tracking and advective-dispersive backward-in-time transport modelling are tested concerning their functionality and accuracy for source identification issues in transient model environments. In the best case, methods should be applicable to reproduce the assigned mass source of the virtual Bitterfeld-Wolfen contamination scenario.

The testing procedure involves a signal injection at affected model observation points (Figure 4-30) where mass quantities were registered during the transport model forward run. In forensic mode, the induced signal is analysed backward in time by considering spatio-temporal reversed advective velocity fields of the forward model.

For forensic backward modelling, a location specific simulation time is used for each of the reference data points, which is derived from the corresponding breakthrough curve of the forward model run. The point in time when a significant mass signal was observed serves as the initial time stage for signal injection of the backward model. Thus, location specific backward simulation times are characterised by the corresponding arrival time of reference data points and the beginning of mass discharge by assigned sources.

The testing routine was applied on 24 reference locations (Figure 4-30). Related breakthrough curves and associated analyses (arrival time and total backward simulation time) are attached in Appendix F. The following Table 4-7 lists the location specific backward simulation times used for the test scenario.

Table 4-7: Location specific backward simulation times are used for applying the two forensic modelling approaches. Backward simulation times are derived from breakthrough curves of the virtual transport scenario (forward run). A specified backward simulation time characterises the period between the detection of a mass signal and the beginning of the virtual transport scenario in year 1955.

No.	Location	Mass peak at [year]	Simulation period	Simulation time [d]
1	AUS02	1996	1996 – 1955	14965
2	Br203	1995	1995 – 1955	14600
3	BRI05	1994	1994 – 1955	14235
4	BSZB2	1996	1996 – 1955	14965

5	BVV011	2002	2002 – 1955	17155
6	BVV0281	2001	2001 – 1955	16790
7	BVV035	1963	1963 – 1955	2920
8	BVV1230	1966	1966 – 1955	2555
9	BVV132	1997	1997 – 1955	15330
10	BVV251	1998	1998 – 1955	15695
11	BVV284	2002	2002 – 1955	17155
12	BVV3800	1964	1964 – 1955	3285
13	BVV541	1964	1964 – 1955	3285
14	BVV589	2001	2001 – 1955	16790
15	BVV626	2000	2000 – 1955	16425
16	BVV644	1997	1997 – 1955	15330
17	BVV6590	1996	1996 – 1955	14965
18	BVV6600	1988	1988 – 1955	11680
19	BVV712	1986	1986 – 1955	11315
20	BVV720	2001	2001 – 1955	16790
21	BVV762	1999	1999 – 1955	16060
22	BVV7810	2002	2002 – 1955	17155
23	LK350	1995	1995 – 1955	14600
24	SAF21	1980	1980 - 1955	8395

For backward simulation, the signal is induced at the reference locations of the forward model and is tracked backward-in-time based on the applied approach. Finally, the signal is spatially distributed in the model domain, which represents related backward location probability estimates (source capture zone) of the respective reference point. Backward source capture zones of multiple reference points can reduce the uncertainty and increase the accuracy onto the source identification process significantly.

4.3.7 Reverse particle tracking

Advective based particle tracking was used in reverse mode for identification of assigned mass source of multi-source contaminant scenario (chapter 4.3.5). Simulated backward-in-time, reversed particle tracks indicate visually prior transport pathways and probable source locations. The approach was applied onto the reproduced transient groundwater flow velocity field of the Bitterfeld-Wolfen region. During the groundwater flow simulation, the 3-D flow velocity field was recorded to the corresponding result file (*.dac). This data was saved in

monthly time intervals. Achieved particle movements were analysed by a transient (unsteady) reversed 3-D particle tracking method. The tracking scheme is based on the 3-D Fourth-order Runge-Kutta method that is described in detail in chapter 3.3.1.

For the tracking analysis, multiple particle starting points are defined three-dimensionally at the reference point locations (Table 4-7). In lateral dimension, nine particles are assigned for each reference data point. A particle at the observation point itself and eight additional particles within a buffer of about 50 m around the reference data point (Figure 4-35). In vertical scale, the distance between the ground surface and the screen bottom is included. Therefore, lateral particles are duplicated vertically in two meter intervals (Figure 4-35). Since screen specifications (level/length/bottom) can differ from observation well to observation well, the amount of particles differs vertically, too.
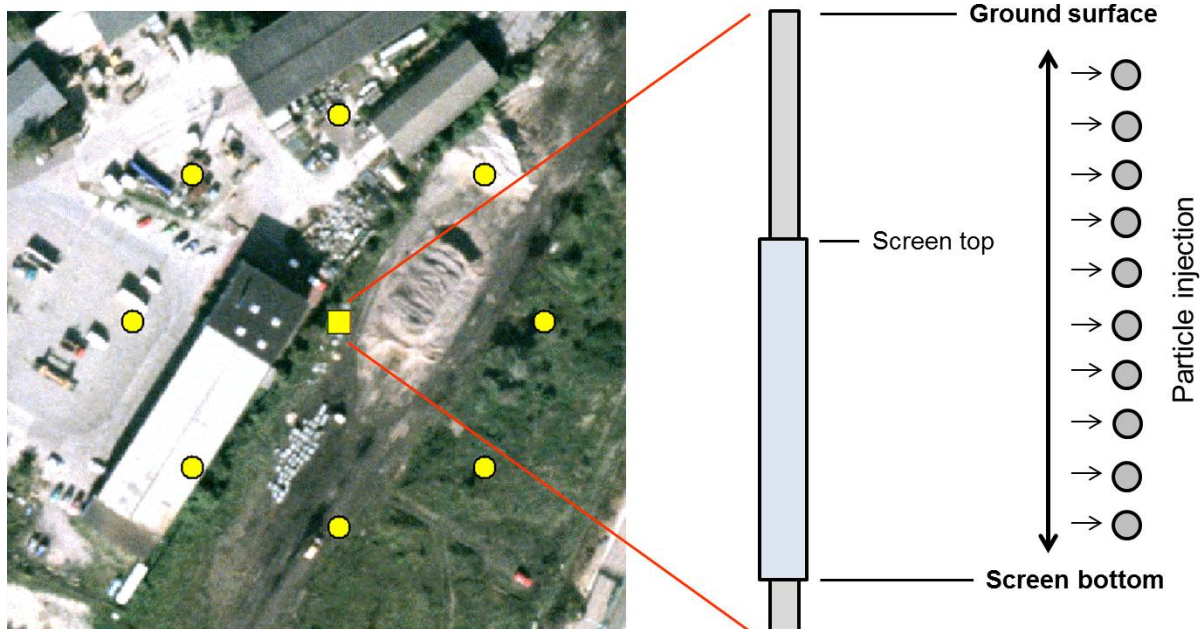
Figure 4-35: Particles for 3-D reverse tracking analyses are induced laterally at the observation point location (red square) and eight additional locations (red dots) within a buffer of 50 meters. In vertical scale, particles are assigned along the depth of the ground surface and screen bottom elevation in two meter intervals and at all nine (lateral) reference locations.

In FEFLOW, particle starting points are handled and imported by an internal triple point file format (*.trp) which is based on the classical *.txt or *.csv file format. Each particle starting point is described by its X-coordinate, Y-coordinate, and Z-value which need to be separated by a blank. All included 3-D coordinates are listed below each other. An individual *.trp file format is required for each of the 24 observation point locations and was imported for the transient reverse particle tracking analysis.

As four sub-models were involved in creating the synthetic multi-source reference transport scenario (1955-2002); all four flow sub-models need to be incorporated for the tracking procedure to reproduce assigned mass sources. Therefore, tracking results (particle end points) of a respective sub-model stage serve as starting points for the previous sub-model stage. In backward mode, the youngest sub-model stage is simulated first (2002 to 1992), while the oldest sub-model stage (1963-1955) is simulated last. When the tracking routine of a sub-model stage was completed, resulting particle points were exported by using the GIS based file format (*.shp). The corresponding dBase database file was filtered in regards to the last time step of the particle point computation, and final 3-D coordinates were selected. Those selected coordinates were converted again to the FEFLOW internal *.trp file format and served as new particle starting point locations for the next sub-model stage.

Final results of the transient reverse particle tracking are either available as a point file, enclosing all intermediate 3-D coordinates of the computation, or as a polyline file that includes 2-D pathlines of particles. Since multiple sub-models were involved, multiple intermediate results appeared which first needed to be merged for subsequent data interpretation. By using ArcGIS, pathline fragments were merged into a continuous pathline representative for the considered observation point location and the complete location specific backward simulation period. 3-D point files were handled analogously. In the following, pathlines from reversed 3-D particle tracking of all 24 reference data points are illustrated in plane views, post-processed in ArcGIS.

Data analysis & results

For testing the accuracy and uncertainty of reverse particle tracking for source identification issues, reversed pathlines were calculated for the 24 reference point locations in Table 4-7. In the following, pathlines of eight reference data points (37%) were attributed clearly to source areas of the virtual contaminant scenario. In addition to this, pathlines of seven observation points (29%) failed any clear source assignment completely. Pathlines of remaining reference locations (34%) at least indicate some source location, but are underestimated in regards to related pathline lengths.

In general, it is noted that constellations of received pathlines tend to be highly diffuse in space, which is related to the extreme variety of the transient 3-D velocity field in horizontal and vertical scale. Furthermore, it is stated that the accuracy of reverse particle tracking for source identification issues does not necessarily depend on the distance between reference locations and source areas.

Achieved particle tracks of the five reference point locations BVV035, BVV1230, BVV541, SAF21 and LK350 indicate the assigned source area S1of the virtual contaminant scenario.
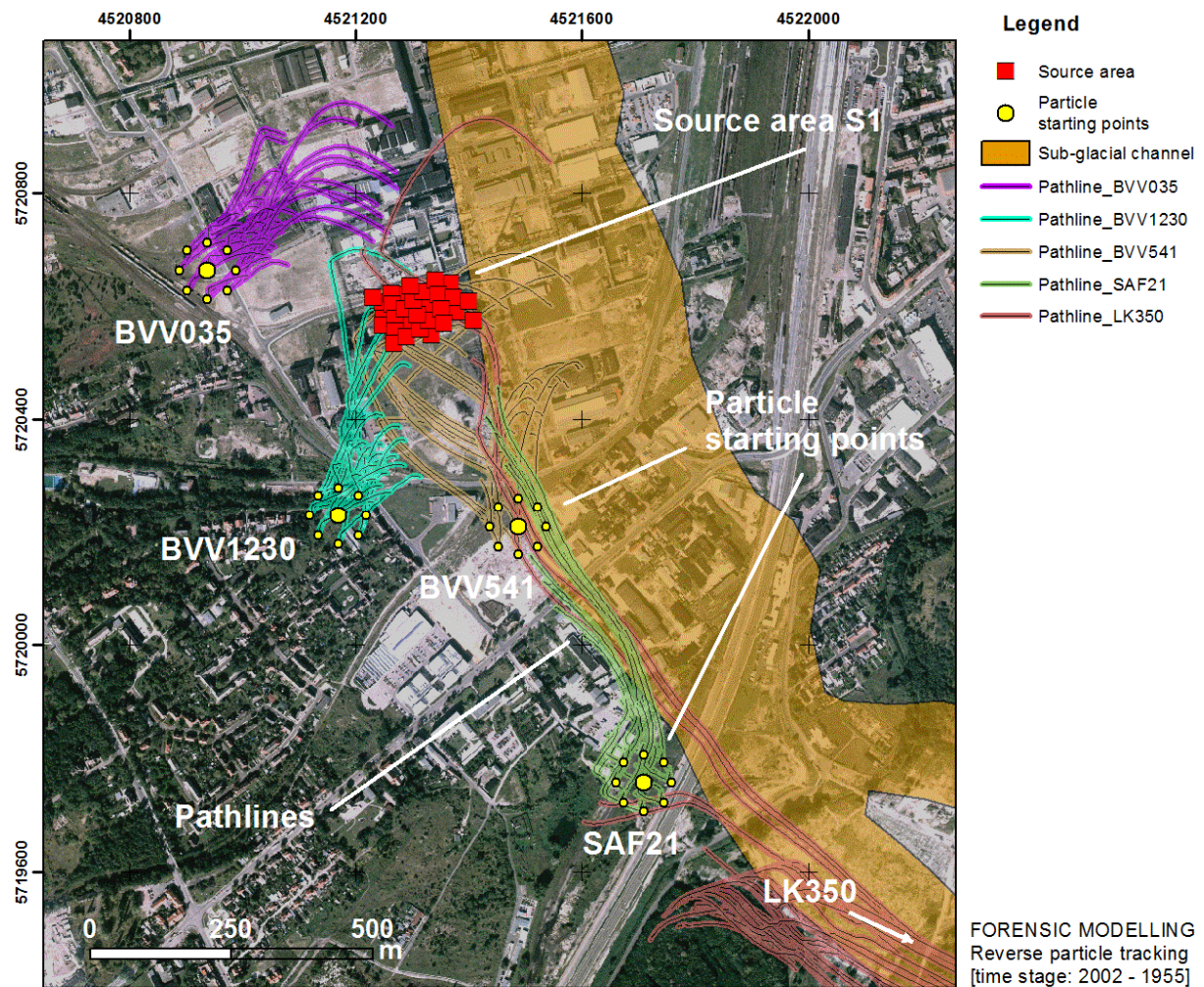
Figure 4-36: Particle tracks of five observation point locations were calculated backward in time to the reference state of year 1955. Pathlines symbolise reversed exposure routes of assigned particle starting points. Moreover, those pathlines indicate the mass source S1 as a probable mass origin.

Received pathline constellations cross the source area directly; the direction is inevitably oriented towards the source zone, or related particle ends are located in the immediate vicinity of the mass source S1.

According to Figure 4-36, pathlines of the observations BVV1230, BVV541, as well as pathline elements of LK350 enter and cross the source zone directly. Particle tracks of SAF21 and BVV035 are oriented inevitably towards the source zone but do not reach the outskirt source area directly. Those tracks seem somehow underestimated with respect to their travel distances.

Particular pathlines (e.g. BVV541 and BVV1230) appear spatially diffused and do not follow a common direction that is related to high variable hydrogeological setting of the aquifer sequence characterised by differentiated hydraulic properties. This heterogeneity is finally reflected three dimensionally by the particle tracking technique.

Additional pathline computations of the reference points BSZB2, BVV0281, BVV7810, BVV589, and BVV626 (Figure 4-37), situated towards the east of the indicated source zone S1, could not be clearly attributed to the source location of the virtual contaminant scenario. While particle tracks of BVV7810 and BVV626 are tangent to the source zone, particle tracks of BSZB2, BVV0281 and BVV589 imply reversed exposure routes from northern, southern and eastern upstream locations.

A certain number of particle tracks (BVV626, BVV589 and BVV0281) are clearly oriented towards the river Strengbach of the local surface water system in the south and the east. This indicates a significant interaction between the local surface waters and the involved aquifer sequence. When including the hydrogeological setting for the assessment of pathline constellations, it is evident that numerous particle tracks follow a sub-glacial channel structure, embedded in the aquifer sequence, which is characterised by an increased hydraulic conductivity contrast. This south-north oriented structural element distracts respective pathlines to southern and northern located upstream locations.

Pathlines of the reference location BSZB2 end up towards the north/northwest, after a transport distance of app. 500 m, without having a relation to any source location of the virtual transport scenario. Source area S7 of is the closest assigned mass source of the multi-source transport scenario, but an indication, based on the respective pathlines, is highly speculative and not proven.

According to Figure 4-37, tracking analyses of the reference points BSZB2, BVV0281 and BVV589 failed a clear source assignment, due to non-relatable pathline constellations. Received pathlines of BVV7810 and BVV626 at least pass the source area S1 in close vicinity.

It is clearly stated that the reverse particle tracking analyses of Figure 4-37 led to ambiguous results that cannot be used for a meaningful assignment of mass origins of the multi-source contaminant scenario.
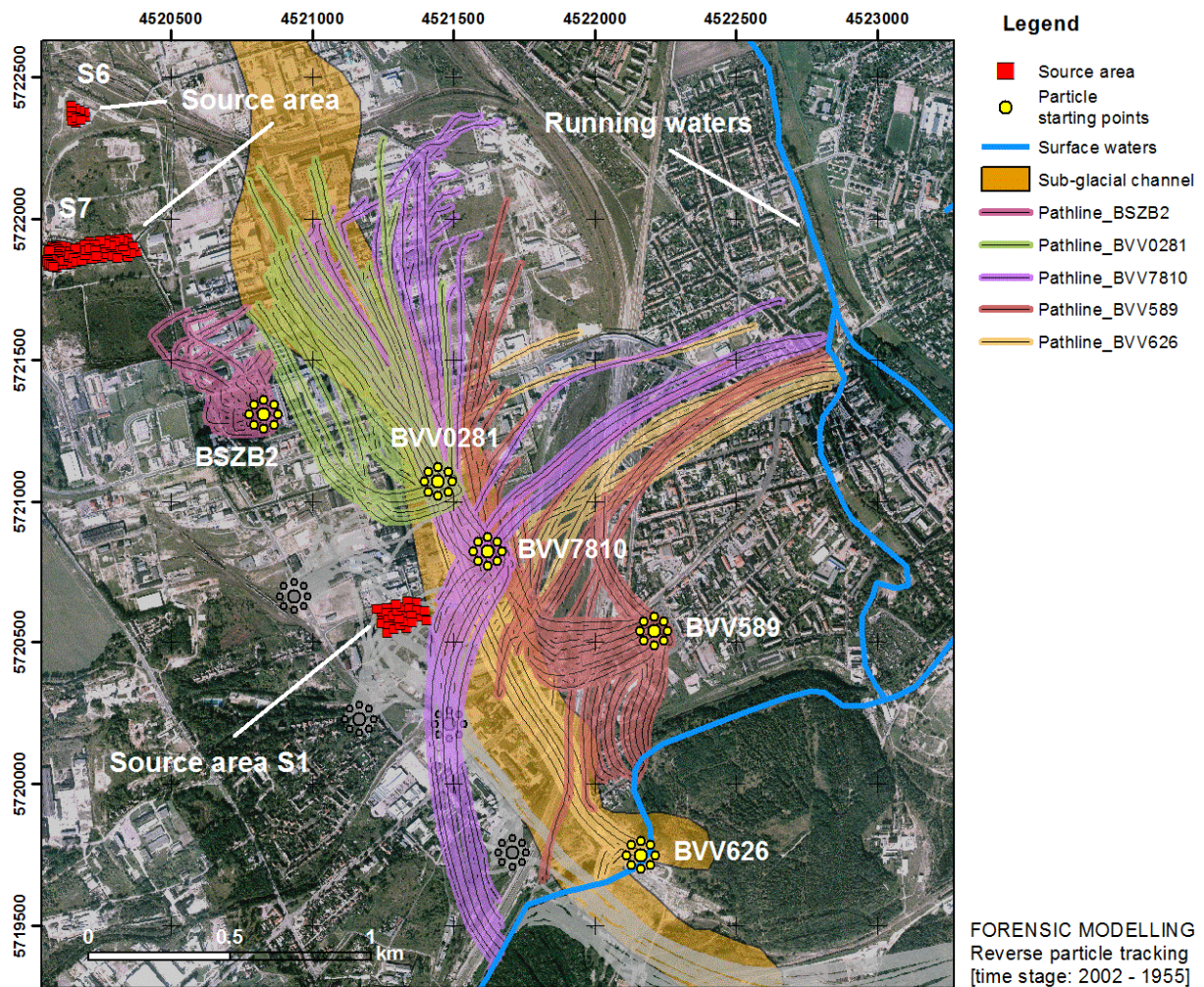
Figure 4-37: Particle tracks of BVV626, BVV589, BVV7810, BVV0281, and BSZB2 cannot be clearly attributed to a source location of the virtual contaminant scenario. While several pathlines of BVV626 and BVV7810 are tangent to the outskirt of the source area S1, numerous pathlines of BVV589 and BVV0281 are oriented towards local surface waters or follow preferential and high conductive flow pathways (sub-glacial channel) within the aquifer sequence.

Figure 4-38 illustrates backward particle tracks of eight more reference data points. While five of eight observation points (BVV712, BVV644, BVV132, BVV6590 and AUS02) pass or indicate related source zones, mass source recovery of three observation points (BVV3800, BVV6600, and BVV251) remain unclear.

Pathline configurations of BVV644, BVV132, and BVV712 show a high variable appearance and a wide particle front that is related again to inhomogeneous flow fields of aquifer units. These constellations indicate multiple probable source locations (S2 and S6) which complicate an explicit source assignment. Nevertheless, it cannot be excluded that individual reference locations had been affected by multiple source areas, as it is the case for BVV644.
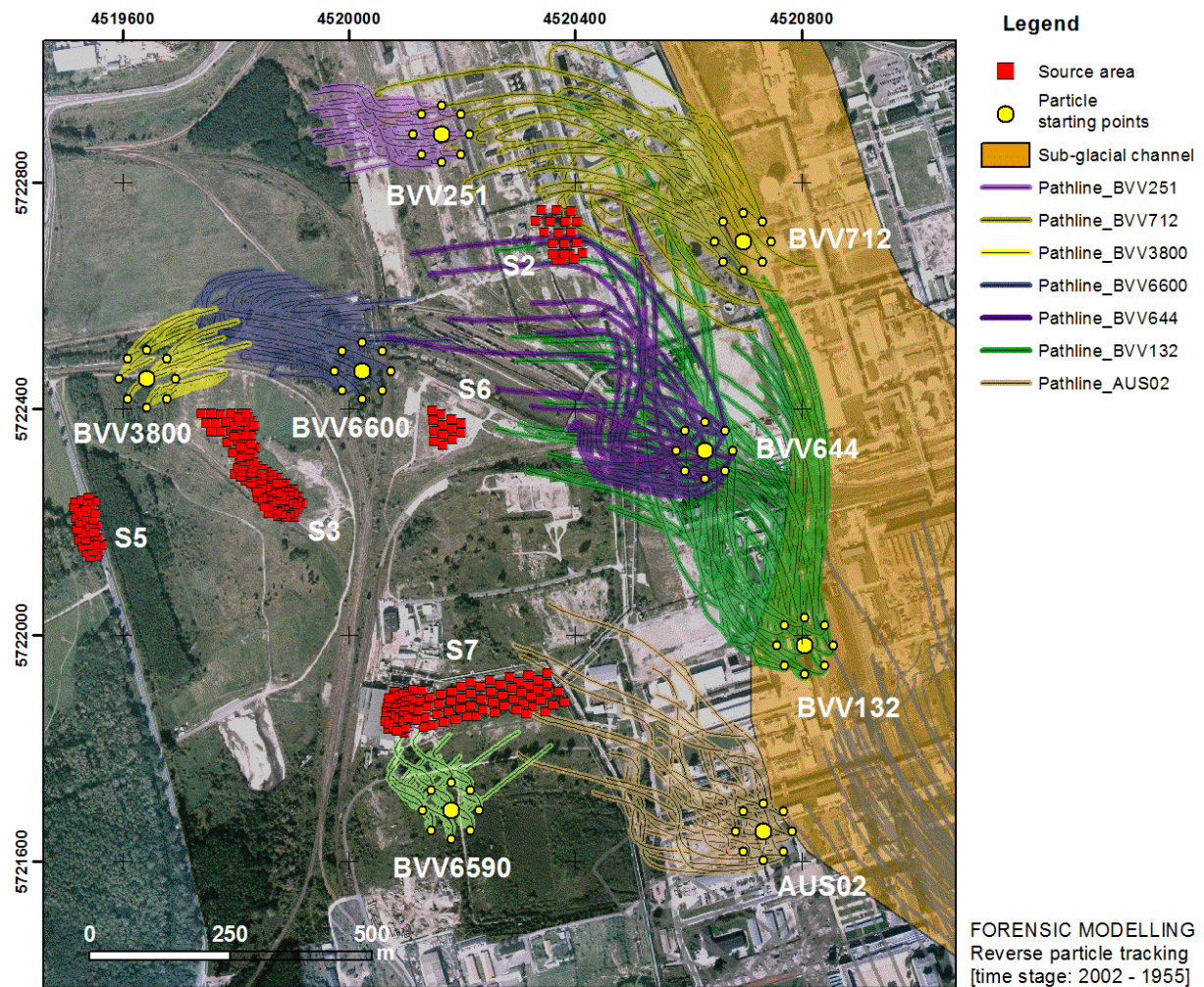
Figure 4-38: With respect to received pathline computations, five of eight reference points (BVV6590, AUS02, BVV132, BVV644 and BVV712) can be attributed to source areas of the contaminant transport scenario by corresponding pathline configurations. Particularly, pathlines seem to be underestimated concerning travel distances and only indicate marginal relations to source areas. Particle tracks of BVV3800, BVV6600 and BVV251 led to non-interpretable results for meaningful source recovery.

Particle tracks of BVV6590 and AUS02 imply marginal relations to the source area S7. With respect to this, pathlines appear particularly underestimated in regards to pathline lengths or travel distances as it was already observed for the reference points BVV035 and SAF21 of Figure 4-36. However, these particle tracks are oriented significantly towards the assigned mass source. Results of BVV251, BVV3800 and BVV6600 do not comprise significant pathline constellations, which enable clear source assignments. At this point, those reverse particle tracks have to be discarded for the source identification procedure.

Conclusion

Reversed particle tracks of 24 reference data points were calculated to evaluate the transient 3-D particle tracking approach in reverse mode for source identification problems. The focus was set on the identification of predefined mass sources of the virtual multi-source contamination scenario (Figure 4-29) by pathline analyses. From theory, reversed pathlines signify an advective solute transport process containing information about the travel time, reversed exposure routes and source location probabilities.

In general, received pathline results did not show the precision for the source zone recovery as it was expected. Oftentimes, pathlines of a single reference data point appear highly scattered and paired with wide pathline fronts that indicate expanded source capture zones and affect the model uncertainty simultaneously. In few cases, clear source assignment based on received particle tracking results was not applicable. In addition, obtained pathline lengths seem to be prevalently underestimated and increase the uncertainty for the source identification process additionally. Nevertheless, more than 60% of considered reference locations could be related to mass source locations by their particle tracks or indicate at least some significant relation to those. Inaccuracy of the applied reverse particle tracking approach can have the following reasons:

(1) Diversified particle tracks are caused by inhomogeneous advective velocity fields in lateral and vertical dimension. As main aquifer units consist of several hydraulic sub units, they include complex hydraulic conductivity patterns. The corresponding advective velocity fields include this complexity too which is indicated by the broad variety of pathline arrangements.

(2) The fact that pathlines often occurred underestimated with respect to the pathline lengths or travel distance is explainable by a constrained mathematical formulation and reproduction of the reversed solute transport process. The advective particle tracking approach does not include the dispersive transport flux that is normally included in solute transport mechanisms due to material heterogeneities of the aquifer. While the dispersive mechanism was included for creating the virtual contaminant scenario of the forward model, dispersive transport is not involved in reverse particle tracking and finally affects the transport distance. Moreover, the long-term simulation time of about 50 years increases this effect of an incomplete solute transport representation significantly.

(3) In addition, non-present hydrodynamic dispersive transport fluxes do not only affect transport distances but do also influence the uncertainty of the pathway recovery for source identification. Reversed particle tracks might be inaccurate, underestimated, or even completely wrong for the case that the solute transport process was mainly based on concentration gradients (e.g. diffusion), where the groundwater flow velocity is close to be zero. This is a general limitation of particle tracking for source identification processes due to its fundamental application.

(4) Another source of errors that can cause underestimated transport distances relates to methodological aspects of the particle tracking computation. Since the pathline computation

is based on stored advective velocity fields of preselected time stages, abrupt changes in the water level height can interrupt a running particle transport calculation. This is the case when the temporal resolution of stored 3-D velocity fields is inadequate to reproduce an abrupt drop of the water level height. Then, the model element that is characterised by a certain hydraulic head value to a given time stage will fall dry at the following time step. Thus, transport velocity (advection) is equal to zero and the particle is not able to "migrate" anymore. If this model element is not reactivated (water level raise) during the following simulation, the tracking procedure will not continue, because the particle remains in the dry model element.

(5) In the presented case study, mining related groundwater abstraction is characteristic for the Bitterfeld-Wolfen region and includes abrupt variations of the groundwater level height. To optimise this methodological limitation, the temporal resolution of preselected time steps for data storage was increased to monthly intervals instead of annual intervals for final computation. In principle, the temporal resolution can be increased infinitely, but then required data space for storage of intermediate data should be taken into account! The chosen time step interval was adjusted iteratively to find an applicable compromise between the required data space and the accuracy of the pathline computation.

Finally, it can be stated that reverse particle tracking did not show the precision for the source recovery of the virtual contaminant scenario as it was expected. The technique is applicable to describe an averaged transport process being capable of indicating the direction of solute transport, but is potentially limited to provide accurate results for transport distances, as it was seen from generated pathlines (e.g. Figure 4-36: SAF21 and BVV035 or Figure 4-38: BVV6590 and AUS02). Only about a half of involved reference locations could be attributed to the source areas being assigned in the virtual multi-source transport problem. In addition to this, the process of source attribution is only possible in visual form and does not provide any qualitative or quantitative feature. Moreover, received pathlines often appeared highly diversified due to inhomogeneous velocity fields of the transient hydraulic system and hampered clear source identification, since the received pathline constellations imply extended source capture zones. Therefore, it is highly recommended to combine reverse particle tracks of multiple reference data points, which may confirm each other for source zone localisation by spatial intersection.

Nevertheless, due to its low computational effort and an easy implementation, particle tracking constitutes an optimal initial screening tool to analyse general transport characteristics in complex model environments. Here, steady-state systems are more suited than transient model systems, since multiple methodological limitations can be neglected which increases simultaneously the model uncertainty.

4.3.8 Backward-in-time transport modelling

Analogously to reverse particle tracking, retrospective transport modelling was applied as a second approach for forensic contaminant source zone identification. Based on 24 reference data points (Table 4-7), backward-in-time transport modelling is analysed concerning its functionality and accuracy for the source zone recovery of the virtual multi-source contaminant scenario of Bitterfeld-Wolfen.

Backward-in-time transport modelling in transient model environments constitutes a new and innovative approach for a retrospective source zone localisation. Its mathematical model is based on the classical advection-dispersion equation (ADE) for describing solute transport processes in groundwater. Thus it provides a fundamental advantage against the previously used and conventional particle tracking technique, as it includes, beside advective transport, hydrodynamic dispersion mechanisms. In consequence, this promises a much more accurate reproduction of prior contaminant discharge leading finally to a reduction of model uncertainty and a more precise source zone identification results.

The numerical implementation of the adjoint ADE model requires modifications on the numerical transport model and simulation procedure. To enable a transient retrospective transport simulation, the transport characteristics need to be reversed in time and space. Therefore, first, a spatial flow field reversal in the classic advection-dispersion equation is required, which is managed in the FEFLOW code by using the corresponding GUI. In a second step, essential for applying the method to transient models, all transient water fluxes which entered or left the numerical model in forward mode, controlled by flow boundary conditions, have to be reversed in time. This includes, for example, the time function for describing the groundwater recharge, time series data for the characterisation of surface waters as well as the mining related groundwater extraction. Those inverted time functions (e.g. time series data of surface waters) start in the backward model with the last function value (prescribed head) of the forward model and end up with its respective first function value (prescribed head). As four sub-models are involved in representing the total simulation time of about 50 years, temporal inversion of boundary conditions were implemented separately for each sub-model stage.

For the implementation of backward-in-time transport modelling, a permanent mass signal is induced at the observation point location. The mass signal is assigned by a 4th kind transport boundary condition. Ideally, the boundary condition is initiated in the backward model at the point in time when a solute was detected first in the forward model ($\rightarrow$ arrival time). If no ideal information is available concerning the arrival time at the observation point from, for example, breakthrough curves, the time at which the solute was registered the first time is chosen. Subsequently, the assigned mass signal is simulated backward in time based on the spatially reversed ADE transport equation and the temporal reversed groundwater flow velocity field. For backward simulation, location specific simulation times are considered for respective reference data points that had been derived from related breakthrough curve data.

Applied backward simulation times are the same as used for reversed particle tracking and are listed in Table 4-7.

After assigning the transient mass signal of 100 mg/l at the reference data point by using a 4th kind transport boundary condition, mass injection is activated at the beginning of the backward simulation time. Subsequently, the mass impulse is discharge backward-in-time based on an advective-dispersive transport mechanism.

Received backward location probabilities at the end of an individual sub-model stage serve as data input of the following model stage until the total simulation time is completed. Received location specific backward probability estimates are applied for the source zone recovery of the virtual contaminant test scenario. For data analysis, simulation results were post-processed in ArcGIS, leading to location specific source capture zones. Outlines of respective source capture zones characterise the 0.1% contour of the simulated mass distribution. These backward capture zones were processed for each of the reference locations listed in Table 4-7 and became involved in the source attribution by spatial superimposing.

As backward-in-time transport modelling additionally provides a qualitative model feedback by its backward probability density, probability density was recorded at the pre-defined mass source locations of the virtual contamination scenario during each simulation.

Data analysis & results

According to Figure 4-39, backward location probability estimates were simulated for BVV035, BVV1230, BVV541, SAF21 and LK350, the same reference data points as used for the reverse particle tracking analysis of Figure 4-36.

Reference point specific source capture zones (coloured) represent the maximum spatial extension of respective backward location probabilities. In principle, all locations enclosed within these source capture zones represent probable pollutant source locations of the reference point at some specific point in time.

In more detail, the visualised source capture zones of Figure 4-39 differ concerning their size and shape, which is related to inhomogeneous flow and transport characteristics within the aquifer system. While the capture zone of BVV035 (purple coloured) is characterised by an expanded backward plume front, probability distributions of BVV1230 (turquoise), BVV541 (orange), and SAF21 (green) show a more stretched appearance. In comparison to these, the backward probability pattern of observation point LK350 (brown) covers a large model area that implies long solute transport distances. However, in regards to the assigned contamination source of the forward transport model (S1, Figure 4-29), all five backward location probability plumes indicate this source zone visually as their potential common origin. While the source area S1 is covered completely by backward location probability estimates of BVV035, BVV1230 and BVV541, backward source capture zones of SAF21 and LK350 only enclose the eastern part of the deposit.
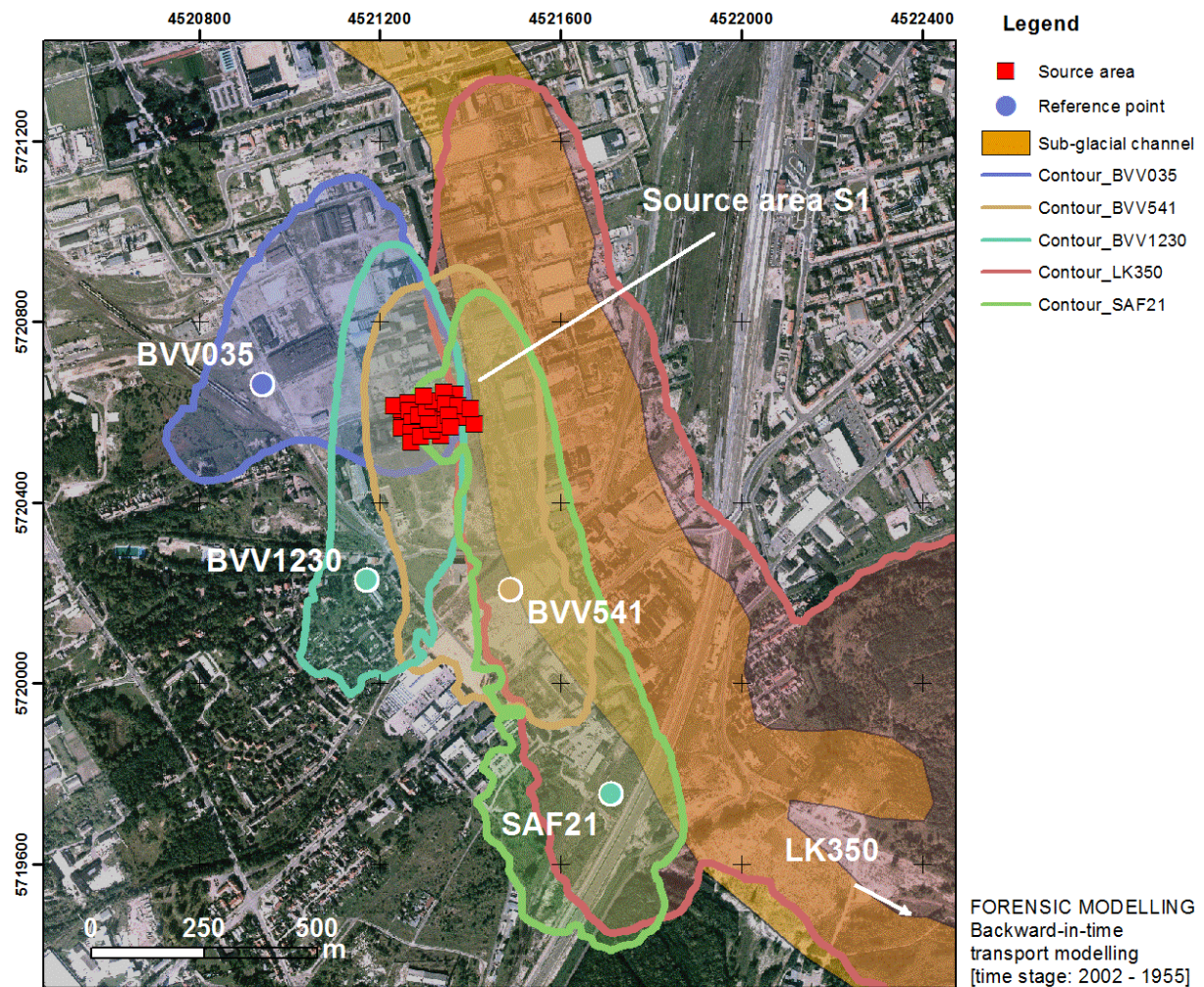
Figure 4-39: Five source capture zones, derived from backward location probability estimates of five reference points, indicate the area S1 as their common contaminant origin. The utilisation of multiple observation points for data interpretation of probable source zones decreases the model uncertainty significantly.

Figure 4-40 contains backward source capture zones of the reference data points BSZB2, BVV0281, BVV7810, BVV589 and BVV626. Spatial dimensions of respective probability distributions are much more expanded than those obtained in Figure 4-39, but indicate a similar spatial diversity as achieved from corresponding pathline analysis of Figure 4-37. Four of five backward location probability plumes (BSZB2, BVV0281, BVV7810 and BVV626) attest a relation to the assigned source zone S1 for being a probable contamination origin. Backward source capture zone of BVV589 does not include the source area and only imply a predominant solute mass load from the west of the reference location.

A significant relation to the large extents of source capture zones is explainable by the sub-glacial channel structure that specifies preferential flow and discharge pathways due to a high hydraulic conductivity contrast and an area of increased groundwater flow velocity.

136
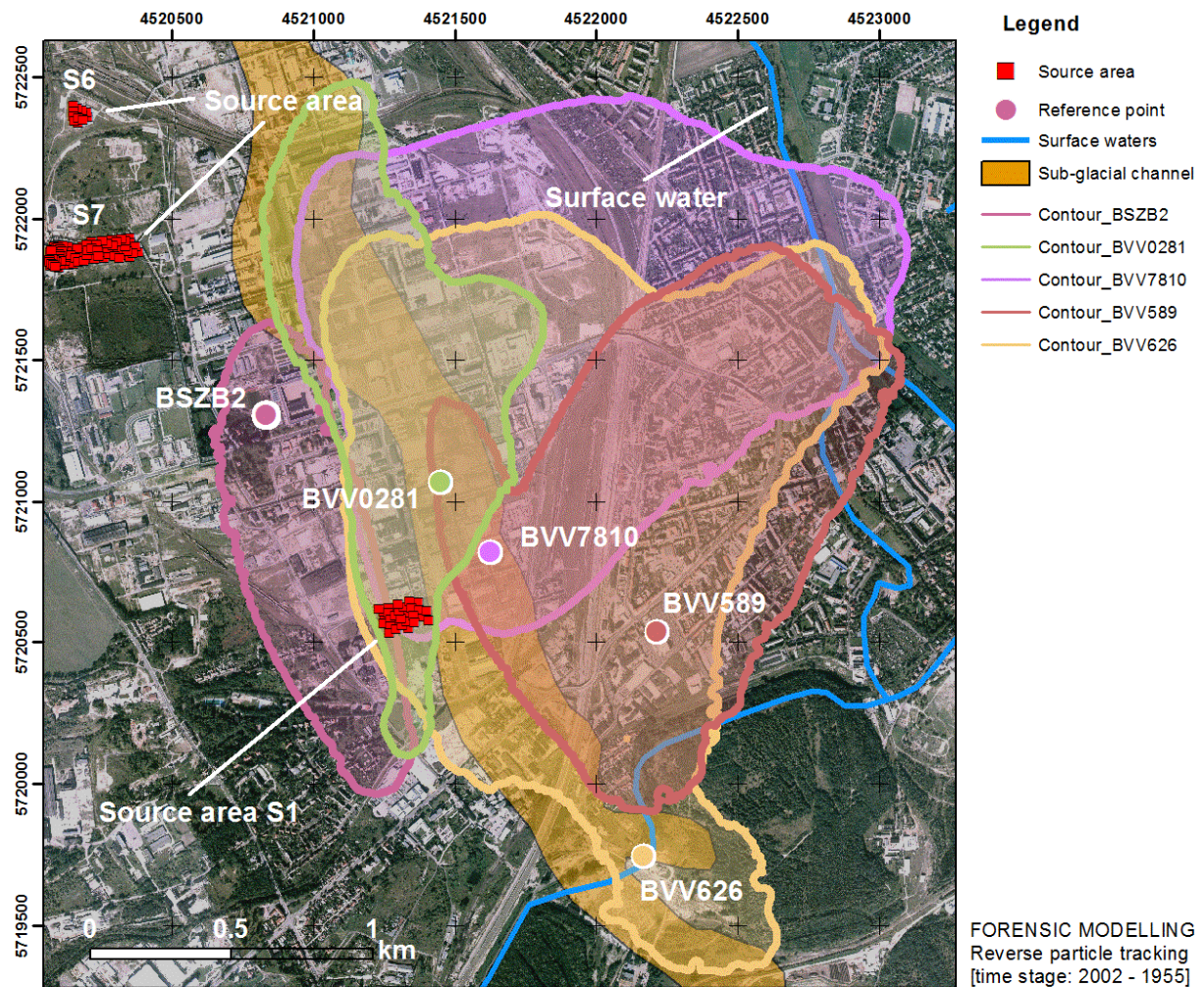
Figure 4-40: Backward location probability estimates of BSZB2, BVV0281, BVV7810, BVV626 and BVV7810 confirm an influence of the previously outlined source area S1 by spatial intersection, except for the backward-in-time probability pattern of reference point BVV589. Extents backward source capture zones show similar spatial diversity as it was observed from reverse particle tracking in Figure 4-37.

It is noted, that received source capture zones do not necessarily include the assigned mass source entirely, but cover at least parts of it. This is reasonable, since a probable contaminant load of some mass source can be spatially limited, which is linked to predominant hydraulic characteristics between the mass source and the flow system. While backward location probability estimates of BVV0281, BVV7810 and BVV626 cover the assigned source S1 completely, the distribution pattern of BSZB2 touches the deposit marginally in the western part. Probability estimates of BVV589 do not indicate any relation to the mass source at all.

Thus, involved reference data points of Figure 4-39 and Figure 4-40 clearly imply the mass source S1 of the forward model as their joint pollutant origin, except for the backward

probability estimates of reference data point BVV589. With respect to received results, it can be stated that transient backward-in-time transport modelling seems to be much more accurate for identifying and confirming source areas of the virtual contaminant scenario than the conventional reverse particle tracking technique. While location specific pathline analyses of Figure 4-36 and Figure 4-37 were characterised by underestimated pathline lengths or even failed the source zone allocation completely, illustrated backward probability patterns attest the virtual contaminant area by spatial intersection.
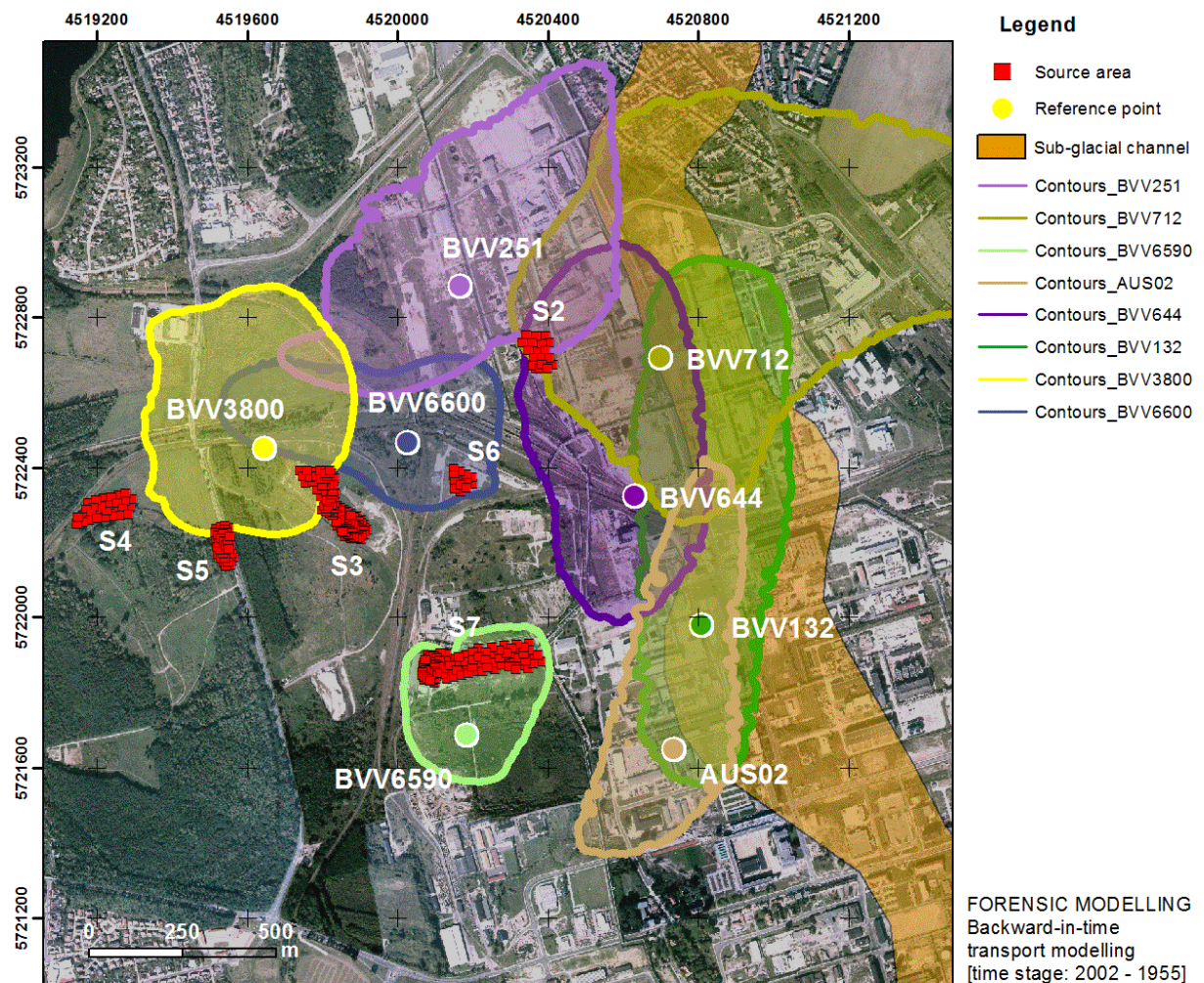
Figure 4-41: Received backward location probability patterns differ significantly concerning the spatial dimensions of source capture zone and geometry, which suggest various transport conditions within a heterogeneous hydraulic system. While backward location probabilities of most reference points illustrate a clear relation to source locations of the virtual contamination scenario, a few reference points, which are situated close to the sub-glacial channel structure, cannot be assigned at all.

The situation illustrated in Figure 4-41 is much more complex than those seen from previous figures, since multiple mass sources are involved, and the reference data points are distributed randomly around the source locations S2-S7.

Figure 4-41 comprises backward location probability estimates of eight reference data points (BVV3800, BVV251, BVV6600, BVV644, BVV712, BVV132, AUS02 and BVV6590). Received source capture zones differ from each other concerning their spatial extension and geometry, which implies inhomogeneous transport conditions caused by hydraulic conductivity contrasts and variable advective velocity patterns.

Based on visualised source capture zones, six of eight reference data points can be related clearly to pre-defined mass source locations of the synthetic multi-source contamination scenario. While four reference data points (BVV6590, BVV251, BVV712 and BVV644) indicate an influence of a single mass source, two observation points (BVV6600 and BVV3800) imply an influence of even two mass origins. The reference point AUS02 and BVV132 could not be assigned to any predefined mass source by backward-in-time transport modelling. It is noted that the locations AUS02 and BVV132 are located very close or within the sub-glacial channel structure, a preferential flow path characterised by high advective velocity fields. Moreover, all backward probability patterns included a general south-north oriented transport component, except for reference point BVV6600. This backward capture zone is oriented predominantly from west to east.

While south-north oriented probability plumes imply the mining-related groundwater in the southern and southeastern mining areas (see Appendix B), the west-east dominated plume contour of BVV6600 is caused predominantly by an increased hydraulic conductivity contrast due to local hydrogeological settings. Moreover, backward probability estimates of AUS02, BVV644, BVV132, and BVV712 comprise spatially a much larger south-north dimension than remaining backward probability patterns and constitute an influence of the well conductive, south-north aligned, sub-glacial channel structure. In addition, the backward capture zone of BVV712 is extended towards the east and indicates an influence of local surface waters (Leine river, see section 2.1.2).

In more detail, backward probability estimates of BVV251, BVV712, and BVV132 are tangent to the source mass location S2. Backward location probabilities of reference point BVV6590 enclose the mass origin S7. The source capture zone of BVV3800 indicates an influence of the source area S3 & S5, whereas backward probability estimates of BVV6600 contains the source location S6 and suggests an additional relation to the source area S3. In contrast, backward location probability estimates of AUS02 and BVV132 indicate a northwards located pollutant origin, but do not address any predefined mass source of the virtual contaminant scenario. No reference location indicated any relation to source area S4.

Conclusion

Backward-in-time transport modelling was implemented successfully for forensic source identification problems in transient model environments. As the approach is based on the classical ADE concept for modelling solute transport processes in groundwater, it constitutes a favourable approach for the localisation of prior contamination sources, besides conventionally used reverse particle tracking. For testing its implementation and accuracy, this technique was applied to reference data points of the synthetic multi-source contamination scenario of the Bitterfeld-Wolfen site. Equivalent to the implementation of backward particle tracked, the application of backward-in-time transport modelling aims at the identification of the assigned mass source locations of the forward model.

Backward location probability estimates were simulated by injecting a consistent mass load at involved reference point locations. The mass load was defined by using a 4th kind transport boundary condition. Subsequently, the mass signal is simulated backward in time, based on the adjoint advection-dispersion transport model. For practical implementation, the adjoint model requires a spatio-temporal inverted groundwater flow velocity field.

As the approach is technically similar to simulate conventional solute transport processes in forward mode, backward-in-time transport modelling involves equivalent requirements for receiving stable simulation results. Here, sufficient spatial mesh discretisation and appropriate simulation time steps are essential to obtain stable results and to suppress numerical oscillations induced by, for example, numerical dispersion.

Moreover, as dry falling model elements affected the model stability significantly in forward transport modelling, an optimised handling of respective model elements in the backward simulation was required, too. For avoiding numerical instabilities caused by dry falling elements, respective cells were handled by increasing related cell transmissivities as it is described in section *transport model stability* of chapter 4.3.5.

In general, backward-in-time transport modelling includes an increased accuracy for the identification of assigned mass source location of the synthetic multi-source contamination scenario. According to Figure 4-39, Figure 4-40 and Figure 4-41, 15 of 18 reference data points could be attributed clearly to respective source areas by simulated backward location probability estimates and delineated source capture zones derived from those. These source capture zones either enclose assigned input areas entirely or attest at least some specific influence, since the source capture zones contain them only partially. In some cases, received backward location probabilities indicate more than one mass source location as their potential origin. In addition, backward-in-time transport modelling failed a clear source identification procedure in three cases: BVV589 (Figure 4-40) and AUS02/BVV132 (Figure 4-41). It is noted that related backward location probabilities of all three reference locations indicate a dominating influence either by (1) the sub-glacial channel structure that constitutes preferential transport pathways by increased advective velocity fields or (2) by some significant hydraulic interactions with local surface waters. In both cases, it seems that high conductivity contrasts and the proximity to assigned flow boundary conditions affect the

sensitivity of forensic advective-dispersive transport modelling by predominant advective velocity fields.

Nevertheless, backward-in-time transport modelling constitutes a favourable approach for source identification problems of groundwater contaminants that are the subject of a dominating advective-dispersive solutes transport process. More than 80% of involved reference locations could be related to the assigned mass source locations of the synthetic Bitterfeld-Wolfen test scenario and represent an acceptable accuracy of the implemented technique.

4.3.9 Chapter summary

A case study scenario of the Bitterfeld-Wolfen area was used to examine the presented backward-in-time modelling approaches for source identification problems under complex real world conditions.

This case study scenario includes the following specifications: 3-D numerical modelling of groundwater flow and solute transport processes at a regional scale (1), transient long-term model characteristics (2), a manifold structural/hydro-geological setting (3), spatio-temporal mining-related groundwater abstraction (4), as well as the multi-source contamination scenario that is based on the local HCH groundwater contamination (5).

The virtual contamination scenario includes seven individual mass sources, which characterise constant mass loads from HCH monofills, leaking production sites, or temporal high concentration mass loads, for specifying, for example, an industrial disaster. Based on reproduced mining-affected groundwater flow velocity fields, transient contaminant discharge was simulated by applying non-conservative solute transport modelling. The simulation period covers more than 50 years. The resulting contaminant discharge was observed at 24 reference locations which had been adopted from the local groundwater monitoring network of the Bitterfeld-Wolfen area. Information received from breakthrough curves, such as mass concentration quantities and travel times, served as data input for evaluating the ability and accuracy of reversed particle tracking and backward-in-time transport modelling for contaminant source identification in 3-D transient model environments.

As similar to the generic contaminant transport model scenario, the focus was set on the identification of respective mass sources of the virtual contamination scenario. The testing routine is based on some signal injection at preselected reference point locations. Subsequently, this signal was tracked backward in time by using an idealised and location specific travel time, which was received previously from the related breakthrough curve (section 4.3.6).

By using the transient 3-D reverse particle tracking approach, the induced signal is represented by imaginary particles which were tracked advectively backward in time (section 4.3.7). In case of backward-in-time transport modelling, an injected mass load was simulated backward by using a transient 3-D advective-dispersive solute transport mechanism (section

4.3.8). While received pathlines of reverse particle tracking often tend to be underestimated concerning their pathline lengths and mostly indicate only the direction of prior contaminant discharge, the new approach of backward-in-time transport modelling was proven to be the more favourable and more accurate technique for the source identification procedure, since assigned mass sources were located more exactly from a quantitatively and qualitatively point of view! While the recall ratio of the reverse particle tracking method was less than 60%, the accuracy of transient backward-in-time transport modelling was about 85% for the source localisation procedure.

The results of the complex 3-D case study scenario confirm principally the major findings previously obtained from the experimental simulations in transient 2-D model environments. Reverse particle tracking is limited concerning its accuracy, while its low computational time is of major advantage. Therefore, it is suited as an initial screening tool, especially in large transient 3-D model environments. In contrast, backward location probabilities of backward-in-time transport modelling have a significantly higher accuracy for the source identification process. The usage of multiple observation points for the identification reduces the uncertainty additionally. At the same time the numerical simulation effort increases drastically.

5 Concluding Remarks and Outlook

For the case that a groundwater contamination in the aquifer is detected at some observation well location or by an appropriate exploration technique, the origin of groundater pollutants is either not necessarily known, mostly unknown or only suspected. With respect to the design and implementation of effective remediation strategies, contaminant source localisation constitutes the essential component for an optimal remediation management. Moreover, by following the "polluter-pays" principle, the assignment of liability constitutes an additional element of the site remediation progress, which requires a clear localisation of the pollution origin.

Numerical groundwater flow and solute transport models are suitable techniques for source identification problems. Conventional flow and transport modelling might be applied heuristically, where a source zone is assigned iteratively and solute transport, in forward mode, is simulated until the model results match the observed values. In any cases, this will require numerous model runs as well as long computational times, especially when dealing with contamination sites of regional or larger scales. Inverse modelling constitutes a further approach for solving the source identification problem. This technique has the major disadvantage that several simplifications have to be accepted, such as strongly idealised aquifer geometries, steady-state conditions or a limited amount of possible contaminant origins. Moreover, this method involves an extensive computational effort, too. Therefore, backward-in-time or reverse modelling constitutes a favourable approach, since the identification procedure is initiated directly at the affected well locations and only a few simulation runs are needed to receive information about probable contaminant source areas. In this context, backward-in-time modelling includes (I) the reverse particle tracking method, as a common used approach for, for example, capture zone delineation of groundwater pumping wells, and (II) backward-in-time transport modelling, which is a promising technique for the source identification objective. Up to today the technique of backward transport modelling has received only little attention for this purpose or has not been published yet!

Due to the fact that realistic contaminant scenarios are subject to complex structural aquifer geometries as well as transient groundwater flow and/or transport conditions, those techniques should be applicable to handle transient systems in a three-dimensional manner.

While reverse particle tracking is already established three-dimensionally and for transient model conditions, the technique of backward-in-time transport modelling was extended to also be valid under transient system conditions.

The tracking procedure describes an advective transport mechanism and requires for the transient implementation a spatio-temporal inverted advective flow velocity field (see section 3.3.1). In contrast to this, backward-in-time transport modelling is based on the adjoint model of the classic advection-dispersion concept. In comparison to the advective tracking technique, backward-in-time transport modelling has the major advantage that the dispersion mechanism is included, which is usually present due to heterogeneities of the aquifer matrix,

which influences the solute transport process significantly. Its technical implementation requires several modifications which are documented in section 3.3.2.

In this study, both approaches were applied to synthetic contaminant scenarios to reveal relative strengths and weaknesses of both approaches for a retrospective source identification procedure. For the qualitative analyses, a generic 2-D transient transport scenario (section 4.2) and a complex, regional scaled 3-D transient transport scenario under real world conditions (section 4.3) were applied.

The testing routine is based on a mass source characterisation simulating non-conservative solute transport, in forward mode, for a predefined simulation time. Solute transport was then registered at specified reference data points in the form of related breakthrough curves. This time series data comprises relevant information about the travel time and the level of impact with respect to the mass concentration. From breakthrough curves, idealised solute travel times were derived for each reference data point. For source identification, a signal was injected at affected reference date points (i), which was subsequently simulated, backward in time, based on the reverse particle tracking approach or backward-in-time transport modelling. These simulations were run individually for each reference date point by using the previously derived and location-specific travel times. Results of both approaches are used for the localisation of the assigned mass source of the initial transport scenario. Results of the reverse particle tracking approach are documented for the generic simulation in section 4.2.4, for the complex case study scenario of the former industrial and abandoned mining area Bitterfeld-Wolfen in section 4.3.7. For related findings concerning the backward-in-time transport modelling approach, see section 4.2.5 and section 4.3.8. Moreover, in comparison, the results allowed the evaluation of both approaches for the source identification procedure by respective pros and cons.

Generated pathlines, from particle tracking, appeared mostly underestimated with respect to the pathline lengths or travel distances, respectively. Therefore, particles reached the area of assigned mass sources only rarely and indicated mostly only the direction of prior solute transport correctly. In some case a clear relation to assigned mass sources failed entirely. In addition to this, particle tracking indicated a general underestimated area of influence of prior solute transport, which increases the uncertainty for the source identification procedure directly. Limitations of this technique, such as underestimated pathline lengths or the underrated area of influence, are caused by the missing dispersion mechanism that is not included in the model conception. Moreover, this approach will fail permanently under system conditions, which are dominated by diffusion and dispersion mechanisms, where the advection tends to be zero. Here the indication by particle tracking can lead to unreliable information. Nevertheless, the easy handling and low computation time is of major advantage and qualifies the approach as an initial screening tool.

Related to the findings, backward-in-time transport modelling comprises a significantly higher accuracy for the source identification problem, since received backward location probabilities could be related more adequately to predefined mass source of the virtual scenarios as they

enclose the source peripherals directly or are in immediate vicinity to them. The usage of multiple backward location estimates, generated from several reference data points individually, reduces the uncertainty for the source area localisation by increasing the accuracy simultaneously. Unfortunately, generated backward location probabilities are not able to reveal any quantitative information concerning the mass concentration at the source zone, since the state variable of the adjoint ADE model cannot be interpreted physically in terms of mass quantity. Thus, the adjoint model does not reflect a physically reversed dispersion mechanism. This is generally impossible, since an unknown mass concentration needs to be added virtually to the system to fulfil a fully reversed dispersive solute transport mechanism. Concerning this matter, the adjoint model only reflects a spatio-temporal reversed dispersion process that accounts seriously for travel distances but is non-sensitive to mass quantities. The implementation of backward-in-time transport modelling necessitates several model modifications such as, for example, the temporal inverting of flow boundary conditions and requires, in comparison to reverse particle tracking, an explicit increased computational simulation time.

The successful implementation of transient 3-D backward-in-time transport modelling enhances the localisation of groundwater contamination sources, which directly supports an efficient site remediation management and can reveal essential information for assigning liability with respect to the established "polluter-pays" policy. Besides the general application to 3-D contaminant source identification problems, the approach was uniquely modified to also be applicable for transient model systems, which enables its application to principally more complex/realistic model scenarios or reduce the necessity of steady-state model simplifications, respectively. In direct comparison to the conventionally used reverse particle tracking technique, reverse transport modelling involves an increased accuracy for describing solute transport processes retrospectively, since a simplified dispersion mechanism is included, which is neglected in the advective based particle tracking. Besides its application to transient 3-D source identification problems, the presented method is also pre-eminently suitable for the delineation of capture zones of groundwater wells, which is commonly realised by reverse particle tracking. Here the general accuracy of potential capture zones is increased similarly, since a dispersive solute transport mechanism is incorporated additionally.

As the presented approaches still comprise limitations and model uncertainty due to incomplete representations of a fully spatio-temporal inverted solute transport process, major attention should be drawn to a reliable parameterisation of the involved input variables that fundamentally influence the outcome of the applied techniques. Both approaches are based on a previously simulated advective flow velocity field, which usually covers longer prior time periods when dealing with source identification problems. Here it is seen as crucial to generate characteristic long-term flow boundary conditions for reproducing representative advective flow velocity patterns, which constitute the basic input for implementation. Therefore, if local time series data for the characterisation of flow boundary conditions is not available, it is recommended to use statistically generated long-term datasets, as those

which found application in the long-term groundwater flow model of the Bitterfeld-Wolfen case study area. An additional sensitive input parameter is the scale-dependent dispersion factor that fundamentally addresses the accuracy of the backward-in-time modelling approach. In general, the dispersion parameter is difficult to estimate and should be quantified ideally by, for example, in situ tracer tests. Since those data are mostly not available or require extensive preparatory site investigation, generally this variable gets roughly estimated from empirical data dependent on the scale of the considered problem. With respect to this, the selection of parameters from empirical data should be done carefully and within a characteristic parameter range of the chosen problem. Moreover, as successful source identification is not only linked to a representative spatio-temporal inverted solute transport process, the structural characterisation of the hydraulic system is of great importance, too. Here, high-resolution geological 3-D modelling comes to the fore.

In summary, this means that the presented approach of transient 3-D backward-in-time transport modelling constitutes a useful model for the retrospective source identification of groundwater contaminants when being applied to a representative model site characterisation. By using this method, model simplification of inverse modelling can be ignored and the reversed modelling approach, initialised from affected reference locations, is much more efficient in terms of computational effort than using a heuristic modelling approach. Finally, backward-in-time transport modelling includes a higher accuracy than the often used reverse particle tracking technique and could also be transferred to other related issues, such as the capture zone delineation of groundwater pumping wells.

6   Bibliography

ALBRECHT, R., KRETSCHMER, K. (1993): Chronik der Industriegeschichte der Bitterfelder Region. Beiträge zur Bitterfelder Industriegeschichte 1, 4-24

ALTERMANN, M., RUSKE, R. (1997): Die Region Leipzig-Halle-Bitterfeld: Geologie und Böden. In: Feldmann, R., Henle, K., Auge, H., Flachowsky, J., Klotz, S., Krönert, R. (Editors): Regeneration und nachhaltige Landnutzung – Konzepte für belastete Regionen. Springer, Berlin, Heidelberg

Barth, J.A.C., Kalbus, E., Schmidt, C., Bayer-Raich, M., Reinstorf, F., Schirmer, M., Thiéry, D., Dubus, I.G., Gutierrez, A., Baran, N., Mouvet, C., Petelet-Giraud, E., Négrel, Ph., Banton, O., Battle Aguilar, J., Brouyère, S., Goderniaux, P., Orban, Ph., Rozemeijer, J.C., Visser, A., Bierkens, M.F.P., Van der Grift, B., Broers, H.P., Marsman, A., Klaver, G., Slobodnick, J., Grathwohl, P. (2007): Selected groundwater studies of EU project AquaTerra leading to large scale basin considerations. *Water Practice & Technology* **2(3)**, doi:10.2166/wpt.2007.0062

BAYER, P., FINKEL, M., TEUTSCH, G. (2004): Kombinierte „Pump-and-treat"-Barrieren-Systeme, Teil I: Minimierung der Grundwasserentnahmeraten durch hydraulische Zusatzmaßnahmen. *Grundwasser* **9**, Bd. 3, 173-180, DOI: 10.1007/s00767-004-0043-x

BEAR, J. (1972): Dynamics of Fluids in Porous Media, American Elsevier, New York, 764

BEAR, J. (1979): Hydraulics of Groundwater, McGraw-Hill Series in Water Resources and Environmental Engineering, New York: McGraw-Hill, 569

BEAR, J. CHENG, A.H.D. (2010): Modeling groundwater flow and contaminant transport – theory and applications of transport in porous media. Springer Dordrecht Heidelberg London New York, 570-573

Becker, D., Minsker, B., Greenwald, R., Zhang, Y., Harre, K., Yager, K., Zheng, C., Peralta, R. (2006): Reducing Long-Term Remedial Costs by Transport Modeling Optimization. *Ground Water* **44**, No. 6, 864-875

BEIMS, U. (1983): Planung, Durchführung und Auswertung von Gütepumpversuchen, Geohydrodynamische Erkundung. *Z. f. angew. Geol.*, 29 (10), 482-490

BENSABAT, J., ZHOU, Q., BEAR, J. (1998): An adaptive path line.based particle tracking algorithm for the Eulerian-Lagrangian method. *Adv Water Resour* **23**, 383-397

BLUM, P., HUNKELER, D., WEEDE, M., BEYER, C, GRATHWOHL, P., MORASCH, B. (2009): Quantification of biodegradation for o-xylene and naphthalene using first order decay models, Michaelis-Menten kinetics and stable carbon isotopes. Journal of Contaminant Hydrology **105**, 118-130

BURCHARDT, I., STROBEL, G. (1992): Ingenieurgeologisch-geotechnische Bewertung des Stadtgebietes Bitterfeld als eine Grundlage für die regionale Raumplanung und städtebauliche Entwicklung. In: Hille, J., Ruske, R., Scholz, J., Walkow, F. (Editors): Bitterfeld: Modellhafte ökologische Bestandsaufnahme einer kontaminierten Industrieregion – Beiträge der 1. Bitterfelder Umweltkonferenz. Schadstoffe und Umwelt Bd. 10, Berlin, Erich Schmidt Verlag, 113-119

BURNETT, R.D., FRIND, E.O. (1987): Simulation of contaminant transport in three dimensions: 1. The alternating direction Galerkin technique. *Water Resources Research* **23**, no. 4, 683-694

CHENG, J.R., CHENG, H.P., YEH, G.T. (1996): A particle tracking technique for the Lagrangian-Euler finite element method in multi-dimensions. *Int J Numer Meth Eng* **39**, 1115-1136

CHIN, D.A., CHITTALURU, P.V.K. (1994): Risk management in wellhead protection. *Journal of water resources planning and management* **120** (3), 294-315

COLLIS, S.S., HEINKENSCHLOSS, M. (2002): Analysis of the streamline upwind/Petrov Galerkin method applied to the solution of optimal control problems. Technical report 02-01, Department of computational and applied mathematics – MS134, Rice University, Houston, Texas, USA, 31

CONSOIL PROCEEDINGS, (2000): Bitterfeld / Spittelwasser Site – Case Study. 7th International FZK/TNO Conference on Contaminated Soil in cooperation with UFZ. CCL Leipzig, Germany, 18-22 September 2000, 163

CORDES, C., KINZELBACH, W. (1992): Continuous groundwater velocity fields and pathlines in linear, bilinear, and trilinear finite elements. *Water resour res* **28** (11): 2903-2911

CRANDALL, C.A., KAUFFMAN, L.J., KATZ, B.G., METZ, P.A., MCBRIDE, W.S., BERND, M.P. (2009): Simulations of groundwater flow and particle tracking analysis in the area contributing recharge to a public-supply well near Tampa, Florida, 2002-05, U.S. Geological Survey Scientific Investigations Report 2008-5231, 53 p.

DARCY, H. (1856): Les Fontaines Publiques de la Ville de Dijon. V. Dalmont, Paris, 647

DIERSCH, H.JG. (2009A): FEFLOW – Finite Element Subsurface Flow & Transport Simulation System. Reference Manual, DHI-WASY GmbH, Berlin, 292

DIERSCH, H.JG. (2009B): Treatment of free surface in 2D and 3D groundwater modeling. White Papers Vol. 1, Chapter 2, WASY Ltd., Berlin, 74-101

DIERSCH, H.JG. (2002): The Petrov-Galerkin least square method (PGLS). White Papers Vol. 1, Chapter 13, WASY Ltd., Berlin, 275-306

EISERLE (1996): Gefährdungsabschätzung der Altablagerung/Althalde Übergabebahnhof Bitterfeld. Ingenieurgesellschaft für Umwelttechnik und Bauwesen mbH, Dresden (unpublished)

EHLING, B.C. (2008): Regionalgeologische Einheiten – Halle-Wittenbergscholle. In: Bachmann, G.H., Ehling, B.C., Eichner, R., Schwab, M. (Editors): Geologie von Sachsen-Anhalt. E. Schweizerbart'sche Verlagsbuchhandlung (Nägele u. Obermiller), Stuttgart, 375-384

EISSMANN, L. (1975): Das Quartär der Leipziger Tieflandsbucht und angrenzender Gebiete um Saale und Elbe. Schriftenr. Geol. Wiss. 2, 263

EISSMANN, L., MÜLLER, A. (1978): Lithofazieskarten Quartär, 1:50000, Blatt 2465 Bitterfeld. 7 Karten; Zentrales Geologisches Institut, Berlin

EISSMANN, L. (1994): Leitfaden der Geologie des Präquartärs im Saale-Elbe-Gebiet. In: Eissmann L & Litt T (eds.): Das Quartär Mitteldeutschlands – Ein Leitfaden und Exkursionsführer mit einer Übersicht über das Präquartär des Saale-Elbe-Gebietes. Altenbg. Nat. wiss. Forsch., Mauritianum 7, Altenburg, 11-46

EISSMANN, L. (2002): Tertiary geology of the Saale-Elbe Region. Quaternary Science Reviews 21, 1245-1274

EPA (1996): Soil Screening Guidance. EPA Document Number: EPA/540/R-95/128, United State Environmental Protection Agency, 138 Retrieved from (date: 17.10.2011): http://www.epa.gov/superfund/health/conmedia/soil/toc.htm

FABRITIUS, H. (2002): Entwicklung eines digitalen geologischen Raummodells im Raum Bitterfeld-Süd. (Diplom-) Thesis, Institute for Geosciences, Department Hydro- & Environmental Geology, Martin Luther University Halle-Wittenberg (unpublished)

FINGER, E. (1996): Wie das Magnetband nach Wolfen kam. Beiträge zur Bitterfeld-Wolfener Industriegeschichte 5, 96-107

FETTER, C.W. (1992): Contaminant Hydrogeology, Macmillan Publishing Company, New York, 458

FRIND, E.O., MOLSON, J.W. (2002): The role of well vulnerability mapping in quantifying the impact of well contamination. Calibration and Reliability in Groundwater Modelling: A Few Steps Closer to Reality (Proceedings of ModelCARE 2002, Prague, Czech Republic, June 2002); IAHS Publ. no. 277

FRIND, E.O., MUHAMMAD, D.S., MOLSON, J.W. (2002): Delineation of Three-Dimensional Well Capture Zones for Complex Multi-Aquifer Systems. *Groundwater* Vol. **40**, No. 6, 586-598

FRIND, E.O., MOLSON, J.W., RUDOLPH, D.L. (2006): Well Vulnerability: A Quantitative Approach for Source Water Protection. *Ground Water* Vol. **44**, No. 5, 732-742

GELHAR, L.W., AXNESS, C.L. (1983): Three-dimensional stochastic analysis of macrodispersion in aquifers. *Water Resources Research*, **19** (1), 161-180

GELHAR, L.W., WELTY, C., REHFELDT, K.R. (1992): A critical review of data on field-scale dispersion in aquifers. *Water Resources Research*, **28** (7), 1955-1974

GLÄSEL, R. (1955): Die geologische Entwicklung Nordwestsachsens. Dt. Verl. D. Wissenschaften, 2. Auflage, 149

GOSSEL, W., WYCISK, P. (2006): Berechnung der monatlichen Sickerwasserrate als Grundlage für die Berechnung der Grundwasserneubildung für ein regionales Grundwassermodell.- In: VOIGT, H.-J., KAUFMANN-KNOKE, R., JAHNKE, C. [Editors]: Indikatoren im Grundwasser Kurzfassungen der Vorträge und Poster der Tagung der Fachsektion Hydrogeologie in der DGG 24.-28. Mai 2006 in Cottbus, Schriftenreihe der Deutschen Geologischen Gesellschaft, 140; Hannover.

GOSSEL, W. (2008): Schnittstellen bei der Kopplung von Modellierungssystemen der Hydrogeologie. Habilitation, Institute for Geosciences, Department Hydro- & Environmental Geology, Martin Luther University Halle-Wittenberg, 150, http://sundoc.bibliothek.uni-halle.de/habil-online/08/08H031/index.htm

GOSSEL, W., STOLLBERG, R., WYCISK, P. (2009): Regionales Langzeitmodell zur Simulation von Grundwasserströmung und Stofftransport im Gebiet der Unteren Mulde/Fuhne. *Grundwasser* **14**, Bd. 1, 47-60. doi: 10.1007/s00767-008-0096-3

BERTHOLD, A., BRITZ, M., MÜLLER-TEVOLDE, A. (1996): Gefährdungsabschätzung Altablagerung/Altlast Titanteiche. Grebner Umwelt GmbH, Mainz, (unpublished)

GRATHWOHL, P. (1998): Diffusion in Natural Porous Media, Contaminant Transport, Sorption/Desorption and Dissolution Kinetics, Kluwer Academic Publishers, Boston, Dordrecht, London, 207

GRIMMER, S. (2006): Sackungsprozesse in natürlichen Lockergesteinsfolgen infolge Grundwasserwiederanstiegs. Dissertation, Institute for Geosciences, Department, Martin Luther University Halle-Wittenberg, 154, http://sundoc.bibliothek.uni-halle.de/diss-online/06/06H152/index.htm

GROßMANN, J., DRANGMEISTER, J., NITSCHKE, F., WILLAND, A. (2003): Inventarisierung von Grundwasserschäden und deren Beurteilung in Großprojekten „Ökologische Altlasten" der neuen Bundesländer. Abschlussbericht, Forschungsbericht 20023250, UBA Text 40/2003, 150

GROTE, K. (1984): Hydrogeologisches Kartenwerk der DDR 1 : 50000, Blatt 1106 3/4. 8 Karten; Zentrales Geologisches Institut, Berlin

HAEFNER, F., BOY, S., WAGNER, S., BEHR, A. (1996): Parameter identification in groundwater flow and transport with the new Front Limitation algorithm. Calibration and Reliability in Groundwater Modelling, Proceedings of the ModelCARE96 Conference, Golden, Colorado, IAHS Publ., no. 237, 1-9

HAFERKORN, B., LUCKNER, L., MÜLLER, M., ZEH, E., BENTHAUS, F.K., PESTER, L., LIETZOW, A., MANSEL, H., WEBER, H. (1999): Schaffung von Tagebaurestseen im mitteldeutschen Braunkohlenrevier. LMBV – Lausitzer Mitteldeutsche Bergbau-Verwaltungsgesellschaft mbH (Editor), Borna, 140

Haferkorn, B., Tienz, B.S., Berkner, A., Guderitz, I., Lehmann, R., Mansel, H., Näther, L., Nitzsche, K., Richter, G., Schlottmann, R., Tropp, P., Zeh, E. (2005): Zum Stand der Integration von Bergbaufolgeseen in den Gebietswasserhaushalt von Westsachsen und Ostthüringen. LMBV – Lausitzer Mitteldeutsche Bergbau-Verwaltungsgesellschaft mbH (Editor), 123

HEIDRICH, S., SCHIRMER, M., WEISS, H., WYCISK, P., GROSSMANN, J., KASCHL, A. (2004): Regionally contaminated aquifers – toxicological relevance and remediation options (Bitterfeld case study). *Toxicology*, **205**, 143-155

HELMERT, (1984): Hydrogeologisches Kartenwerk der Deutschen Demokratischen Republik 1 : 50000, Blatt Bitterfeld 1106 1/2. 8 Karten; Zentrales Geologisches Institut, Berlin

HENTZSCH, E. (1996): Die Geschichte des Kraftwerkes Süd Bitterfeld. Beiträge zur Bitterfeld-Wolfener Industriegeschichte 4, 5-63

HILLE, J., RUSKE, R., SCHOLZ, R.W., WALKOW, F. (1992): Bitterfeld – Modellhafte ökologische Bestandsaufnahme einer kontaminierten Industrieregion – Beiträge der 1. Bitterfelder Umweltkonferenz. Schadstoffe und Umwelt Bd. 10, Berlin, Erich Schmidt Verlag, 326

HILLER, A., LITT, T., EISSMANN, L. (1991): Zur Entwicklung der jungquartären Tieflandstäler im Saale-Elbe-Raum unter besonderer Berücksichtigung von C14-Daten. Eiszeitalter und Gegenwart, 41, Hannover , 26-46. In: Rascher, J., Wimmer, R., Krumbiegel, G., Schmiedel, S. (2008): Bitterfelder Bernstein versus Baltischer Bernstein – Hypothesen, Fakten, Fragen. Exkursionsführer und Veröffentlichungen der Deutschen Gesellschaft für Geowissenschaften, Heft 236, Hannover, 168

HUBERT, T. (2005): Vergleichende 3D-Modellierung eines geologischen Strukturmodells am Beispiel einer industrie- und bergbaugeprägten Region – Bitterfeld. Diploma Thesis, Institute for Geosciences, Department Hydro- & Environmental Geology, Martin Luther University Halle-Wittenberg (unpublished)

HUBERT, T. (2011): Methodische Ansätze zur geologischen 3-D Modellierung oberflächennaher Schichtenfolgen und ihre Auswirkung auf die numerische Grundwassermodellierung. Dissertation, Institute for Geosciences, Department Hydro- & Environmental Geology, Martin Luther University Halle-Wittenberg, 171

HUYSMANS, M., DASSARGUES, A. (2005): Review of the use of Péclet numbers to determine the relative importance of advection and dispersion in low permeability environments. *Hydrogeology Journal*, Vol. **13**, No. 5-6, 895-904

IBGW, (?): Altablagerung "Schadstoffdeponie Heideloh". Ingenieurbüro für Grundwasser GmbH, Leipzig, (unpublished)

INOUE, K., TAKAO, Y., TANAKA, T. (2009): Application of Random Walk Particle Tracking to the Delineation of Capture Zones. Proceedings of the Nineteenth International Offshore and Polar Engineering Conference, Osaka, Japan, June 21-26, 2009.

JACKSON, C.R., MANSOUR, M.M., HUGHES, A.G., HULME, P.J. (2008): Numerical Modelling of Groundwater Abstraction in River Flows. Environment Agency Science Report SC030233/ SR1, British Geological Survey Report OR/08/017, 263

OGATA, A. (1970): Theory of dispersion in a granular medium. U.S. Geological Survey Paper, 411

KALBITZ, K., POPP, P. (1999): Seasonal impacts on ß-hexachlorocyclohexane concentration in soil solution. *Environmental Pollution* **106** (1999), 139-141

KARAMOUZIS, D.N. (1990): A Space Discontinous Galerkin Method for the One-Dimensional Unsteady Convection-Diffusion Equation. *Water Resources Management* **4**, 175-185

KAZDA, I. (1990): Finite Element techniques in groundwater flow studies. Elsevier Science Publishing Company, New York, 310

KINZELBACH, W. (1987): Groundwater modelling: An introduction with sample programs in BASIC. Elsevier Science Publishers B.V., Amsterdam, 332

KINZELBACH, W. (1992): Numerische Methoden zur Modellierung des Transports von Schadstoffen im Grundwasser. 2. Auflage, Schriftenreihe Wasser – Abwasser, Oldenburg Verlag GmbH, München, 339

KNOTH, W. (1995): Sachsen-Anhalt. In: Benda L (eds.): Das Quartär Deutschlands, Borntraeger, Berlin, 148-170

KNOTH, W., KRIEBEL, U., RADZINSKI, K.H., THOMAE, M. (1998): Die geologischen Verhältnisse von Halle und Umgebung. Hallesches Jahrbuch Geowissenschaften, Reihe B, Beiheft 4, 7-34

KRAPP, L., BOLCEK, R., BRAUN, M., DÜLLMANN, H., FISCHER, I.H., GRONINGER, H.G., NEEF, U., SEPPELFRICKE (1992): Sicherung- und Sanierungsvorschläge am Beispiel der Deponie Antonie und Werksgelände der Chemie AG. In: Hille, J., Ruske, R., Scholz, R.W., Walkow, F. (Editors): Bitterfeld: Modellhafte Ökologische Bestandsaufnahme einer kontaminierten Industrieregion. Erich Schmidt Verlag, Berlin, 211-221

KRAPP, L., RUSKE, R. (1992): Geologische Verhältnisse von Bitterfeld und ihre Relevanz zu Kontaminationen des Grundwassers und Bodens. In: Hille, J., Ruske, R., Scholz, R.W., Walkow, F. (Editors): Bitterfeld: Modellhafte Ökologische Bestandsaufnahme einer kontaminierten Industrieregion. Erich Schmidt Verlag, Berlin, 85-92

KRETSCHMER, K. (1993): 1893 – ein historisches Datum für Bitterfeld "Die Chemie kommt zur Kohle". Beiträge zur Bitterfelder Industriegeschichte 1, 37-41

KRIGE, D.G. (1951): A statistical approach to some basic mine valuation problems on the Witwatersrand. *J. of the Chem., Metal. and Mining Soc. of South Africa* **52** (6): 119–139

KUMAR, P. (2005): Evaluation and modeling of groundwater supply in Arbuckle-Simpson aquifer, Oklahoma. Dissertation 1431005, Oklahoma State University, 150

KUNSTMANN, H., KINZELBACH, W. (2000): Computation of stochastic wellhead protection zones by combining the first-order second-moment method and Kolmogorov backward equation analysis. *Journal of Hydrology* **237**, 127-146

LANDESANSTALT FÜR ALTLASTENFREISTELLUNG, (2010): ÖGP Bitterfeld-Wolfen – Projekt im Überblick. Retrieved from (date: 14.12.2010): http://www.sachsen-anhalt.de/LPSA /index.php?id=29280

LANGE, W., RAPPSILBER, I. (2008): Regionalgeologische Entwicklung – Geophysik und Krustenbau. In: Bachmann, G.H., Ehling, B.C., Eichner, R., Schwab, M. (Editors); (2008): Geologie von Sachsen-Anhalt. E. Schweizerbart'sche Verlagsbuchhandlung (Nägele u. Obermiller), Stuttgart, 34-44

LIEHMANN, G. (1993): Der Braunkohlenbergbau im Bitterfelder Revier. Beiträge zur Bitterfelder Industriegeschichte 1, 25-33

LIEHMANN, G. (1996): Braunkohlenrevier Bitterfeld – eine Standortbeschreibung. Beiträge zur Bitterfeld-Wolfen Industriegeschichte 6, 5-51

LIEHMANN, G. (1998A): Entstehung und Entwicklung des Bitterfelder Reviers und seine wirtschaftliche Bedeutung. In: Bitterfelder Bergleute e.V. (eds.): Chronik des Braunkohlenbergbaus im Revier Bitterfeld, Technik und Kulturgeschichte in zwei Jahrhunderten. Bitterfeld, 7-38

LIEHMANN, G. (1998B): Chronik des Braunkohlenbergbaues im Revier Bitterfeld – Technik und Kulturgeschichte in zwei Jahrhunderten. Bitterfelder Bergleute e.V. (ed.), Bd. 1, Druckerei Wieprich, Dessau, 414

LIEHMANN, G. (2003): Chronik des Braunkohlenbergbaues im Revier Bitterfeld. Bitterfelder Bergleute e.V. (ed.), Bd. 2, Druckerei Wieprich, Dessau, 351

LIEHMANN, G. (2004): Chronik des Braunkohlenbergbaues im Bitterfelder Revier. Bitterfelder Bergleute e.V. (ed.), Bd. 3, Druckerei Wieprich, Dessau, 256

LIEHMANN, G. (2006): Chronik des Braunkohlenbergbaues im Bitterfelder Revier – Sanierung und Bergbaufolgelandschaft. Bitterfelder Bergleute e.V. (ed.), Bd. 4, Druckerei Wieprich, Dessau, 304

LIN, H.C.J., RICHARDS, D.A., TALBOT, C.A. (1997): FEMWATER – A Three-Dimensional Finite Element Computer Model for Simulating Density-Dependent Flow and Transport in Variably Saturated Media. US Army Corps of Engineers, Technical Report CHL-97-12, 151

LUCKNER, L., HAFERKORN. B., MANSEL. H., SAMES. D., REHFELDT. F. (1995): Rehabilitierung des Wasserhaushaltes im Braunkohlerevier Mitteldeutschland. Lausitzer und Mitteldeutsche Bergbau-Verwaltungsgesellschaft mbH (LMBV), UniMedia GmbH-Verlag für universelle Medienproduktionen Leipzig und Dresden, 86

MARCINKOWSKI, MÜLLER, (1980): Lithofazieskarten Quartär, 1 : 50 000, Blatt 2365 Dessau. 6 Karten; Zentrales Geologisches Institut, Berlin

MATTHEß, G., UBELL K. (1983): Allgemeine Hydrogeologie – Grundwasserhaushalt. Borntraeger, Berlin-Stuttgart, 438

MIRBAGHERI, S.A., MONFARED, S.A.H. (2009): Pesticide transport and transformation modeling in soil column and groundwater contamination prediction. *Int. J. Environ. Sci. Tech.*, **6** (2), 233-242

MOUTSOPOULOS, K.N., GEMITZI, A., TSIHRINTZIS, V.A. (2008): Delineation of groundwater protection zones by the backward tracking method: theoretical background and GIS-based stochastic analysis. *Environ Geol* **54**, 1081-1090

NEUPAUER, R.M., WILSON, J.L. (1999): Adjoint method for obtaining backward-in-time location and travel time probabilities of a conservative ground-water contaminant. *Water Resources Research*, **35** (11), 3389-3398

NEUPAUER, R.M., WILSON, J.L. (2001): Adjoint derived location and travel time probabilities in a multi-dimensional groundwater flow system. *Water Resources Research* **37** (6), 1657-1668

NEUPAUER, R.M., WILSON, J.L. (2004): Numerical Implementation of a backward probability model of groundwater contamination. *Ground Water*, **42** (2), 175-189

NEUPAUER, R.M., WILSON, J.L. (2005): Backward probability model using multiple observations of contaminant to identify groundwater contamination sources at the Massachusetts Military Reservation. *Water Resources Research* **41**, no. W02015, 1-14

PINDER, G.F., GRAY, W.G. (1977): Finite element simulation in surface and subsurface hydrogeology. Academic Press, New York, 295

PLUMPE, G. (1990): Die I.G.-Farbenindustrie-AG: Wirtschaft, Technik und Politik 1904-1945. Duncker und Humboldt, Berlin, 784

PROMMER, H., BARRY, D.A., DAVIS, G.B. (2000): Numerical modelling for design and evaluation of groundwater remediation schemes. *Ecological Modelling* **128**, 181-195

SHEPARD, D. (1968): A two-dimensional interpolation function for irregularly spaced data. Proceedings of the 1968 ACM (Association for Computing Machinery) National Conference, 517-524

POKRAJAC, D., LAZIC, R. (2002): An efficient algorithm for high accuracy particle tracking in finite elements. *Advances in Water Resources* **25**, 353-369

RAUSCH, R., SCHÄFER, W., THERRIEN, R., WAGNER, C. (2005): Solute Transport Modelling – An Introduction to Models and Solution Strategies, Gebr. Borntraeger Verlagsbuchhandlung Science Publishers, first edition, Berlin, 205

ROBINSON, R.A., STOKES, R.H. (1965): Electrolyte solutions. London: Butterworth Press.

Rock, G., Kupfersberger, H. (2002): Numerical delineation of transient capture zones. *Journal of Hydrology* **269**, 134-149

RUSKE, R., BÖHME, O., FALKE, P. (1999): Ergebnisse der erweiterten geologisch-hydrogeologischen Standorterkundung. In: Weiß H, Daus B, Teutsch G (eds): Safira – 2. Statusbericht – Modellstandort, Mobile Testeinheit, Pilotanlage. UFZ-Bericht 17, UFZ – Umweltforschungszentrum Leipzig-Halle GmbH, 15-23

SCHÄFER, D. (2004): Numerische Modellierung reaktiver Prozesse organischer Kontaminanten in Grundwasserleitern. Postdoctoral thesis, Institute for Geosciences, Christian-Albrechts-University Kiel, 185

SCHÄFER, D., HORNBRUCH, G., SCHLENZ, B., DAHMKE, A. (2007): Schadstoffausbreitung unter Annahme verschiedener kinetischer Ansätze zur Modellierung mikrobiellen Abbaus. *Grundwasser* **12 (1)**, 15-25, doi: 10.1007/s00767-007-0014-0

SCHEIDEGGER, A.E. (1961): General theory of dispersion in porous media. *J Geophy Res Volume* **66**, No. 10

SCHAFMEISTER, M.TH. (1999): Geostatistik für die hydrogeologische Praxis. Berlin; Heidelberg; New York; Barcelona; Hongkong; London; Mailand; Paris; Singapur; Tokio: Springer; 169

SCHWARTZ, R., GERTH, J., NEUMANN-HENSEL, H., BLEY, S., FÖRSTNER, U. (2006): Assessment of Highly Polluted Fluvisol in the Spittelwasser Floodplain – Based on National Guideline Values and MNA-Criteria. *Journal Soils Sediments* **6** (3), 145-155

STANDKE, G. (2004): Geologische Kartierung im Bernsteintagebau Goitsche und regionale stratigraphische Korrelation der tertiären Sedimente. In: Wimmer R, Holz U, Rascher J (eds.): Bitterfelder Bernstein: Lagerstätte, Rohstoff, Folgenutzung. Exkurs.f. u. Veröfftl. 224, GGW, Berlin, 18-22

STEINMETZ, T. (2007): Integration, Analyse und interaktive Visualisierung von Daten für das Risikomanagement großräumig kontaminierter Standorte. Dissertation, Institute for Geosciences, Department Hydro- & Environmental Geology, Martin Luther University Halle-Wittenberg, 169, http://sundoc.bibliothek.uni-halle.de/diss-online/07/08H002/ofindex.htm

SUDICKY, E.A., UNGER, A.J.A., LACOMBE, S. (1995): A non-iterative technique for the direct implementation of well bore boundary conditions in three-dimensional heterogeneous formations. *Water Resources Research* **31**, no. 2, 411-415

SYNNATZSCHKE, K.P. (2010): Historisches aus der Gemeinde Sandersdorf: Braunkohlenindustrie und Infrastruktur. Retrieved from (date: 16.06.2010): http://www.synnatzschke.net/sdfhistbraunkohle.htm

TEUTSCH, G., Rügner, H., Zamfirescu, D., Finkel, M., Bittens M. (2001): Source Remediation vs. Plume Management: Critical factors Affecting Cost-efficiency. *Land Contamination & Reclamation*, Vol. **9**, No. 1, 128-139

THIEKEN, A.H. (2001): Schadstoffmuster in der regionalen Grundwasserkontamination der mitteldeutschen Industrie- und Bergbauregion Bitterfeld-Wolfen. Dissertation, Institute for Geosciences, Department Hydro- & Environmental Geology, Martin Luther University Halle-Wittenberg, 214, http://sundoc.bibliothek.uni-halle.de/diss-online/01/02H175/prom.pdf

Bibliography

Thiessen, K.M., Arkhipov, A., Bantandjieva, B., Charnock, T.W., Gaschak, S., Golikov, V., Hwang, W.T., Tomás, J., Zlobenko, B. (2009): Modelling of large-scale urban contamination situation and remediation alternatives. *Journal of Environmental Radioactivity*, Vol. **100** (5), 413-421

TÜV HANNOVER/SACHSEN-ANHALT E.V., (1996): Sicherungskonzeption der Altablagerung Fasanenkippe – Konzeption zur Gefahrenabwehr. (unpublished)

UFFINK, G.J.M., (1989): Application of Kolmogorov's backward equation in random walk simulations of groundwater contaminant transport. In: Kobus, H.E., Kinzelbach, W. (Editors): Contaminant transport in groundwater. Balkema, Rotterdam

UMWELTBUNDESAMT, (2006): Mulde-Fische weiter mit Hexachlorcyclohexane (HCH) belastet. Hintergrundpapier Oktober 2006, Umweltbundesamt – Für Mensch und Umwelt, 1-5

UMWELTBUNDESAMT, (2009): Schadstoffkonzentrationen in Organismen der Nordsee. Retrieved from (date: 12/14/2010): http://www.umweltbundesamt-daten-zur-umwelt.de/umweltdaten/public/theme.do?nodeIdent=2416

UMWELTBUNDESAMT, (2010): Fische aus Mulde und Elbe kaum noch mit Lindan und seinen Nebenprodukten belastet. Hintergrundpapier Oktober 2010, Umweltbundesamt – Für Mensch und Umwelt, 1-4

VASSOLO, S., KINZELBACH, W., SCHÄFER, W. (1998): Determination of a well head protection zone by stochastic inverse modelling. *Journal of Hydrology* **206**, 268-280

VISSER, A., HEERDINK, R., BROERS, H.P., BIERKENS, M.F.P. (2009): Travel Time Distributions Derived from Particle Tracking in Models Containing Weak Sinks. *Ground Water*, Vol. **47**, No. 2, 237-245

WESSOLEK, G., DUIJNISVELDT, W.H.M., TRINKS, S. (2004): Ein neues Verfahren zur Bestimmung der Sickerwasserrateaus dem Boden: das TUB-BGR-Verfahren. In: Bonstert A., Thieken, A., Merz, B. (Editors): Forum Hydr Wass, 135-145

WALKOW, F. (1996): Umweltreport – Bitterfeld 96. Landkreis Bitterfeld (ed.), 108

WANSA, S., WIMMER, R. (1990): Geologie des Jungpleistozäns der Becken von Gröbern und Grabschütz. Altenburger Naturwissenschaftliche Forschungen, Heft 5, Altenburg. 49-91

WEIß, H., TEUTSCH, G., DAUS, B. (2004): Zusammenfassender Abschlussbericht – Projektverbund SAFIRA. UFZ-Bericht 13/2004. Helmholtz-Zentrum für Umweltforschung UFZ, Leipzig, 366

Weiß, H., Teutsch, G., Fritz, P., Daus, B., Dahmke, A., Grathwohl, P., Trabitzsch, R., Feist, B., Ruske, R., Böhme, O., Schirmer, M. (2002): Sanierungsforschung in regional kontaminierten Aquiferen (SAFIRA) – 1. Information zum Forschungsschwerpunkt am Standort Bitterfeld. *Grundwasser* **7**, Bd. 3, 135-139. doi: 10.1007/s007670200021

WEIß, H., TEUTSCH, G., DAUS, B., (1997): Sanierungsforschung in regional kontaminierten Aquiferen (SAFIRA) – Bericht zur Machbarkeitsstudie für den Modellstandort Bitterfeld. UFZ-Bericht 27/1997. Helmholtz-Zentrum für Umweltforschung UFZ, Leipzig, 233

WESSOLEK, G., DUIJNISVELD, WHM., TRINKS, S., (2004): Ein neues Verfahren zur Berchnung der Sickerwasserrate aus dem Boden: das TUB-BGR Verfahren. In: Bronstert, A., Thieken, A., Merz, B. (Editors): Forum Hydr Wasser, 135-145

WILSON, J.L., LIU, J. (1994): Backward tracking to find the source of pollution. In: Badha, R., Ghassemi, A., Ward, T.J. (Editors): Waste Management: From Risks to Reduction, ECM Press., Albuquerque, New Mexico, 188-199

WILSON, J.L., LIUM J. (1997): Field validation of the backward in time advection dispersion theory. In: Proceedings of the 1996 HSRC/WERC Joint Conference on the Environment, Great Plains-Rocky Mountain Hazardous Substance Center, Manhattan, Kansas, 17

WIMMER, R., STANDKE, G., BLUMENSTENGEL, H., JUNGE, F.W., RASCHER, J. (2004): Altes und Neues zur Geologie der Region Bitterfeld. In: Wimmer, R., Holz, U., Rascher, J. (Editors): Bitterfelder Bernstein: Lagerstätte, Rohstoff, Folgenutzung. Exkurs.f. u. Veröfftl. 224, GGW, Berlin, 12-16

WIMMER, R., PESTER, L., EISSMANN, L. (2006): Das bernsteinführende Tertiär zwischen Leipzig und Bitterfeld. Altenbg. Nat. wiss. Forsch., Mauritianum 19, Altenburg, 11-46

WIMMER, R., RASCHER, J., KRUMBIEGEL, G., RAPPSILBER, I., STANDKE, G. (2009): Bitterfelder Bernstein – ein fossiles Harz und seine geologische Geschichte. Geowissenschaftliche Mitteilungen, GMIT Nr. 38, 15

WOLFIG, C. (2010): Modellierung von Grundwasser- und Wärmehaushalt in einem gut durchlässigen Grundwasserleiter. Master Thesis, Institute for Geosciences, Department Hydro- & Environmental Geology, Martin Luther University Halle-Wittenberg (unpublished)

WOLLMANN, A. (2004): Geologische Bearbeitung einer ehemaligen Bergbau- und Industriefolgelandschaft Bitterfeld/Wolfen. (Diplom-) Thesis, Institute for Geosciences, Department Hydro- & Environmental Geology, Martin Luther University Halle-Wittenberg (unpublished)

WYCISK, P., FABRITIUS, H., RUSKE, R., WEIß, H., (2002): Das digitale geologische Strukturmodell Bitterfeld und seine Bedeutung für die Sanierungsforschung. *Grundwasser*, **3**, Band 7, 165-171

WYCISK, P., GOSSEL, W., WOLLMANN, A., FABRITIUS, H., HUBERT, T. (2006): High resolution digital 3D-models as a base of hydrodynamic calculation in heterogeneous aquifers.- In: Recharge systems for protecting and enhancing groundwater resources – Proceedings of the 5th International Symposium on Management of Aquifer Recharge, ISMAR5, Berlin, Germany, 11–16 June 2005, IHP-VI, Series on Groundwater **13**, 455– 460

WYCISK, P., HUBERT, T., GOSSEL, W., NEUMANN, CH. (2009): High-resolution 3D spatial modelling of complex geological structures for an environmental risk assessment of abundant mining and industrial mega sites. *Computers & Geosciences*, Vol. **35**, 1, 165-182. doi:10.1016/j.cageo.2007.09.001

ZHENG, C., WANG, P.P. (1999): MT3DMS – A Modular Three-Dimensional Multi Species Transport Model. US Army Corps of Engineers, Strategic Environmental Research and Development Program (SERDP), Contract Report SERDP-99, 239

7   Appendix

Appendix A   Target/actual comparison of calibration targets for the model implementation of mining related groundwater abstraction

Appendix 7-1: A transient 4th kind flow boundary condition is used to implement mining related groundwater extraction. Computational nodes are assigned with an associated extraction rate [m³/d] to fulfil the target groundwater elevation [m asl]. Actual values represent the current calibration status.

Model stage	Mining Field	Operation time	Model implementation	Nodes	Rate [Node]	Target	Actual
1955-1963	Holzweißig West	1958-1980	1958-1963	561	35	55	56
	Holzweißig Ost	1931-1961	1955-1963	462	36	55	54
	G_Subfield IIa	1959-1976	1959-1963	325	37	55	55
	G_Subfield I	1951-1960	1955-1961	447	35	55	57
	Freiheit III	1888-1954	1955-1963 [securing]	207	33	62	62
	Freiheit II	1907-1951	1955-1963 [securing]	81	25	62	62
1964-1975	Holzweißig West	1958-1980	1963-1976	626	35	55	56
	G_Subfield IIa	1959-1976	1963-1976	336	37	55	56
	G_Subfield IIb	1963-1967	1963-1968	118	100	55	55
	G_Subfield IIc	1965-1977	1965-1976	203	55	50	50
	G_Subfield IIIa	1971-1976	1970-1976	150	165	40	43
	Freiheit III	1888-1954	1963-1976 [securing]	210	32	62	62
	Freiheit II	1907-1951	1963-1976 [securing]	81	25	62	62
1976-1992	Holzweißig West	1958-1980	1976-1992 [securing]	566	10	53	53
	G_Subfield IIa	1959-1976	1976-1992 [securing]	325	15	65	64
	G_Subfield IIb	1963-1967	1976-1992 [securing]	110	60	50	48
	G_Subfield IIc	1965-1977	1976-1992 [securing]	210	40	55	54
	G_Subfield Niemegk	1978-1994	1978-1992	99	75	45	44
	G_Subfield IIIa	1971-1976	1976-1992 [securing]	108	90	35	36
	G_Subfield IIIb	1976-1991	1976-1992	413	90	45	44
	Freiheit III	1888-1954	1976-1992 [securing]	224	22	67	67
	Freiheit II	1907-1951	1976-1992 [securing]	81	18	73,5	73,5
	Köckern	1984-1992	1982-1992	217	70	65	64
1992-2002	Freiheit III	1888-1954	1992-2002 [securing]	224	22	67	67
	Freiheit II	1907-1951	1992-2002 [securing]	81	15	73,5	73,5

Appendix B   Time slices of reproduced transient groundwater flow velocity field - Quaternary aquifer unit (time period 1955 to 2002)
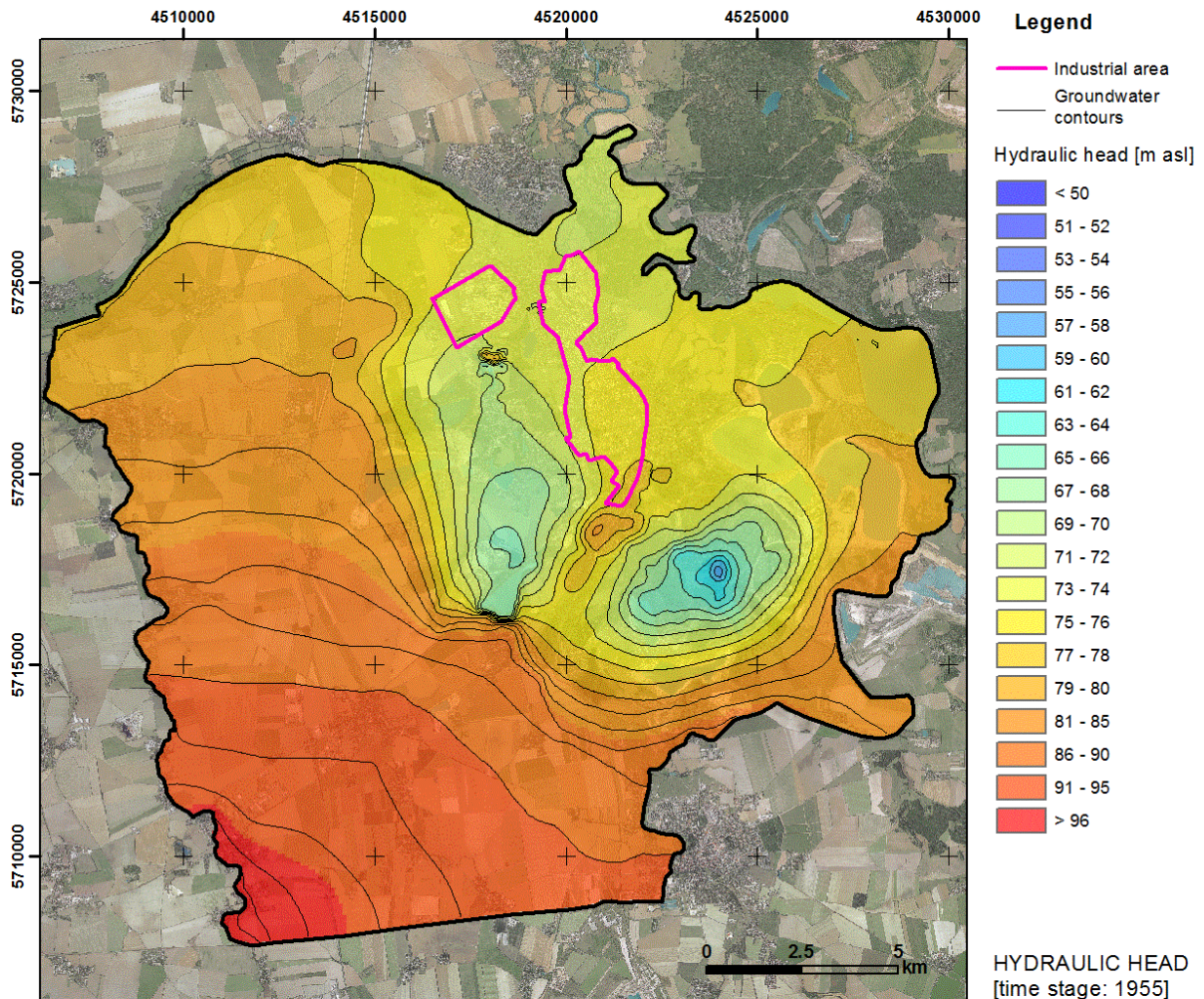
Appendix 7-2: Post-processed from flow modelling data, the graphic illustrates the hydraulic head distribution of the regional aquifer system of year 1955. Two large drawdown areas are present in the central and southeastern model domain. With respect to the industrial area, predominant groundwater flow directions were oriented towards the west, southwest and southeast.
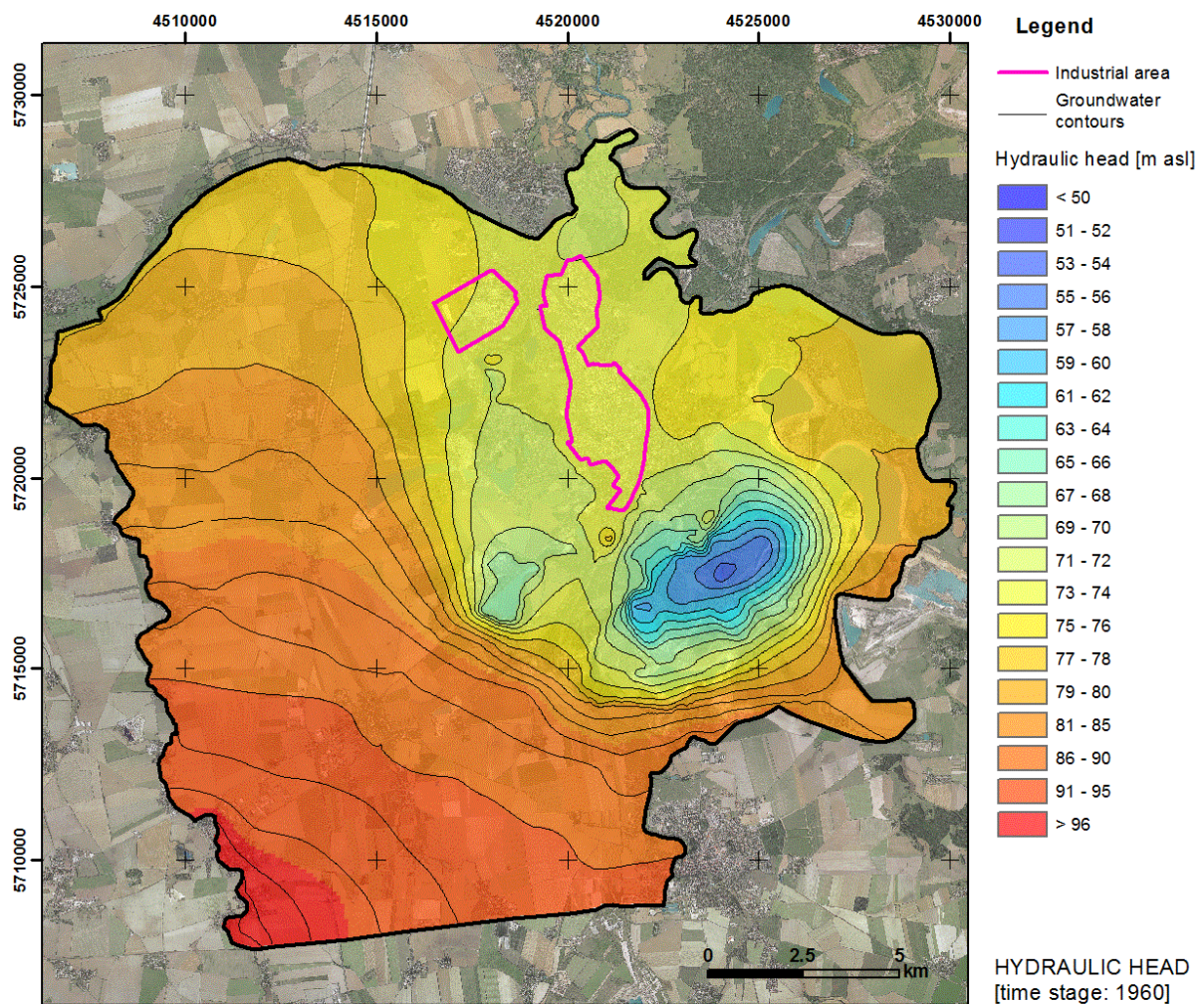
Appendix 7-3: After 1955, further additional open cast lignite mines were opened in the south-eastern located Goitzsche area, which needed to drained by technical dewatering measures. In consequence, with respect to the industrial area, groundwater flow directions were oriented towards the southwest and southeast.
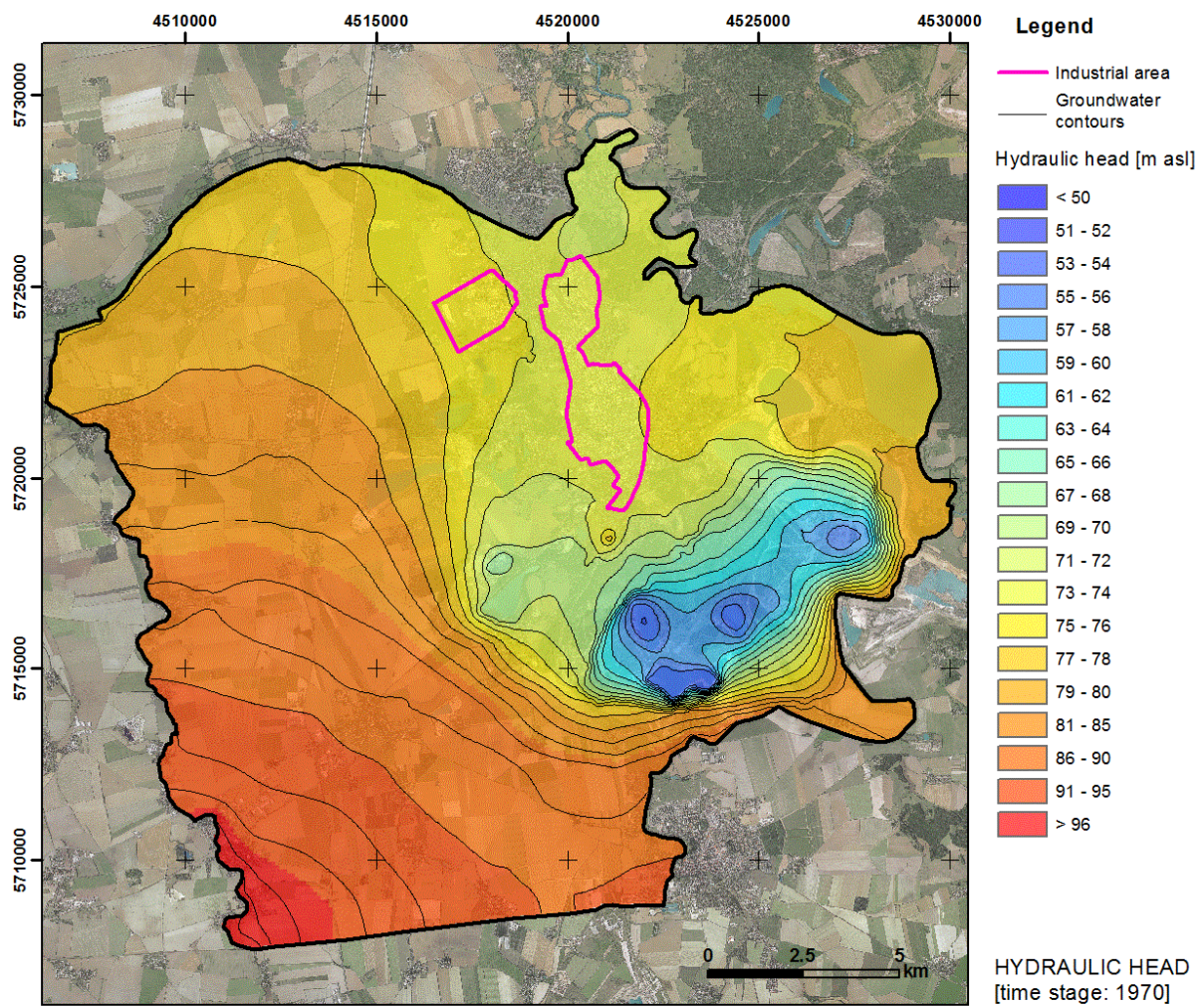
Appendix 7-4: In consequence of extended groundwater lowering in the southeast, major groundwater flow gradients were oriented towards the south and southeast. Local groundwater extraction areas overlaid each other and formed a large drawdown area of regional scale.
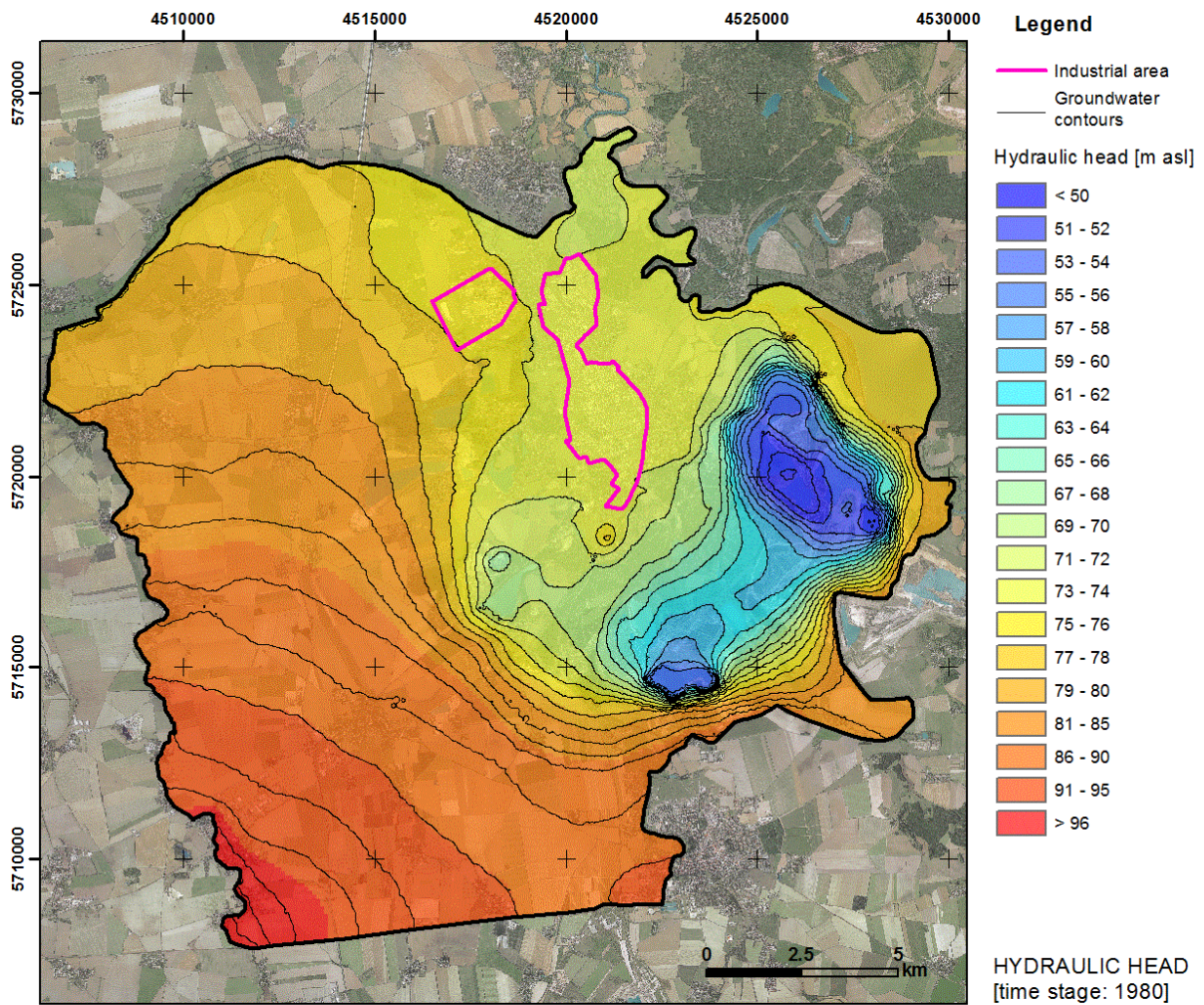
Appendix 7-5: In the 1980s, the lignite mining was characterised by multiple active open cast mines in the east and southeast of Bitterfeld. Extensive groundwater abstraction below levels of +50 m asl led to high groundwater flow gradients towards the south, southeast and east.
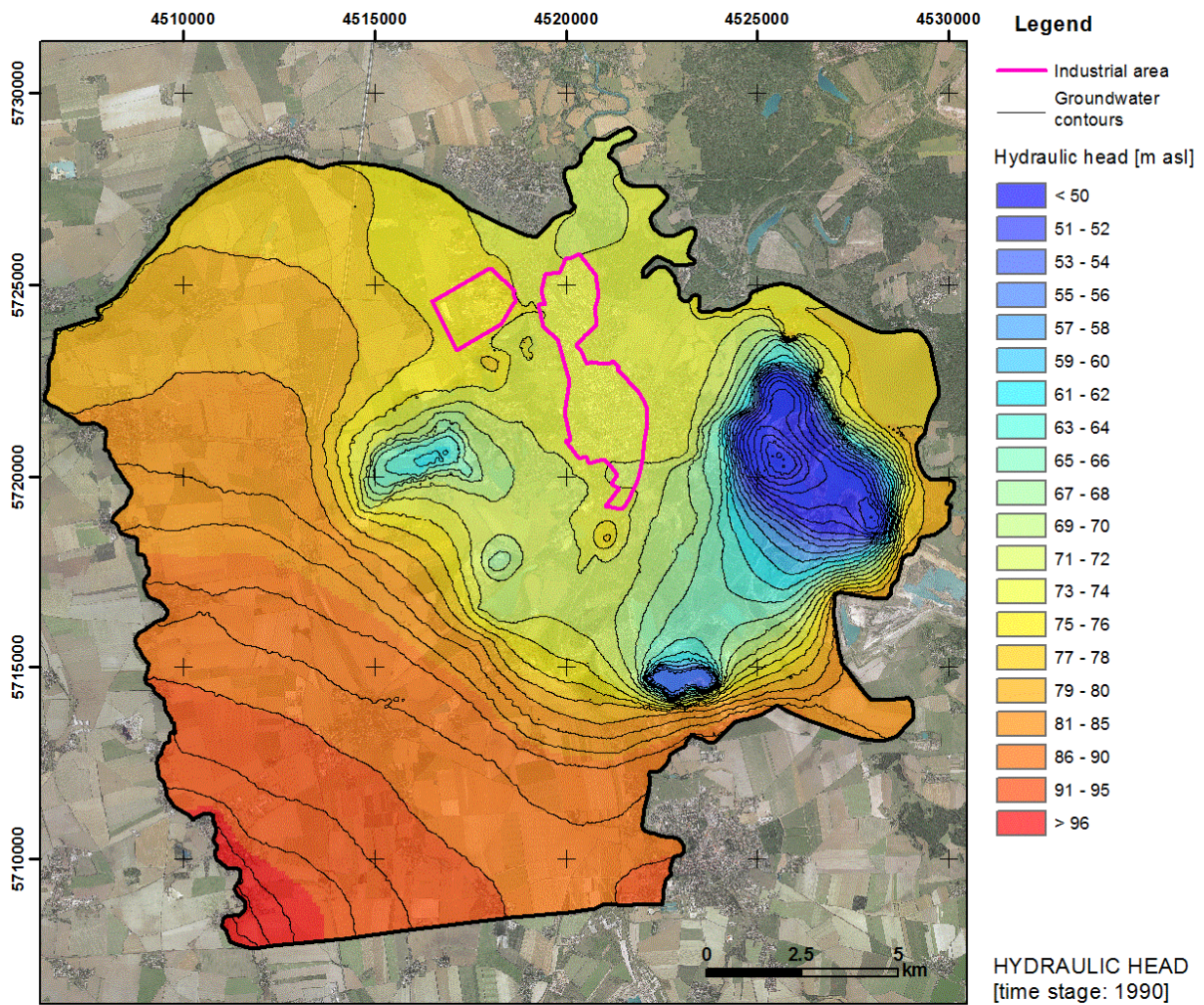
Appendix 7-6: During the 1990s, the mining situation of the Bitterfeld-Wolfen region was similar to the stage of the 1980s. Groundwater extraction in the south was reduced slightly and initiated locally groundwater rebound processes. Groundwater flow mainly oriented towards the large drawdown area in the southeast. A further lignite mine was opened in the east of the industrial area in 1984. This led to additional changes in the regional groundwater flow field.
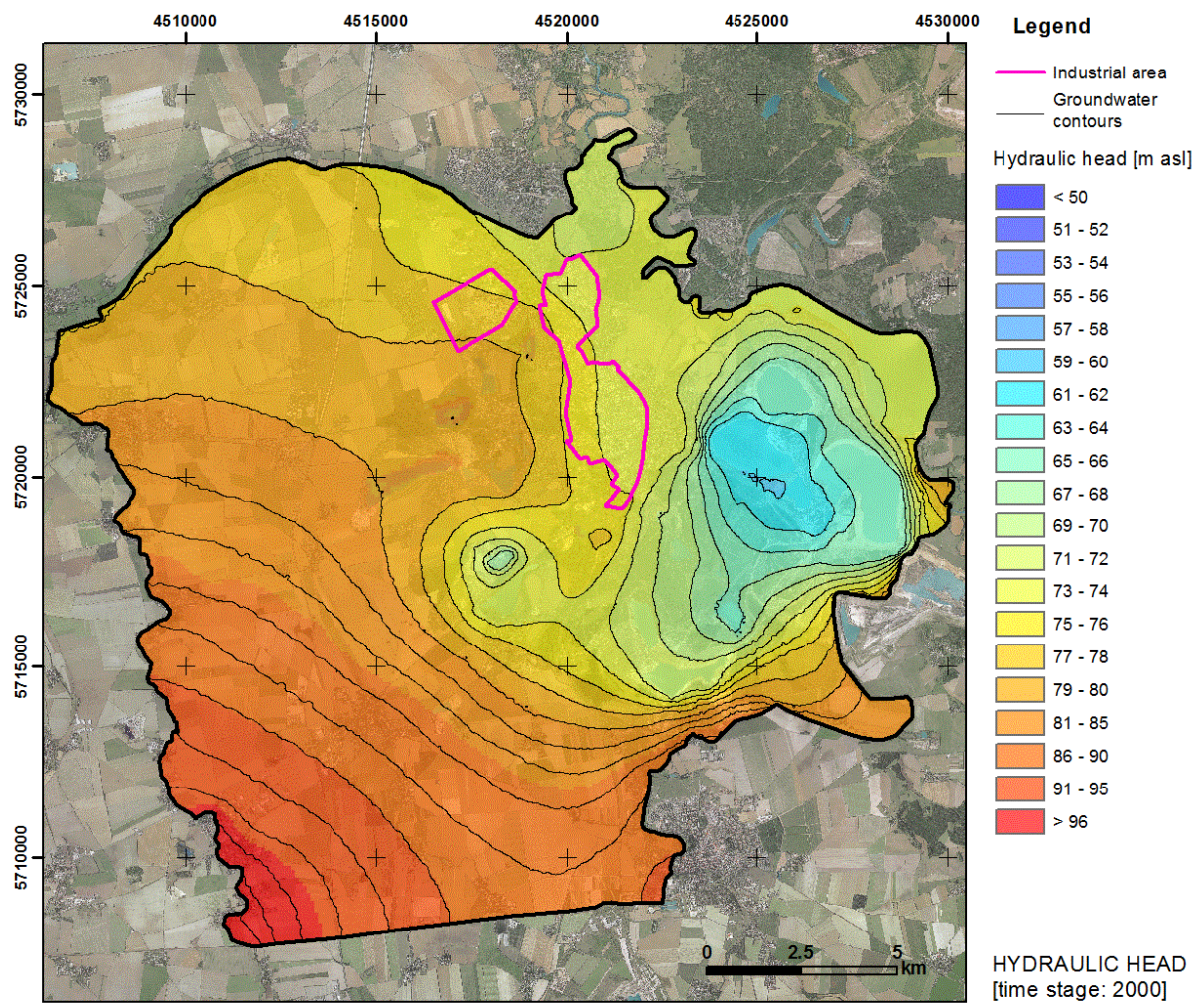
Appendix 7-7: With the end of active lignite mining in year 1992, required groundwater extraction was not necessary anymore. A phase of natural groundwater rebound followed. Local dewatering measures retained for groundwater managing purposes. During the phase of groundwater rebound, dominating groundwater flow towards the southeast and east continued.
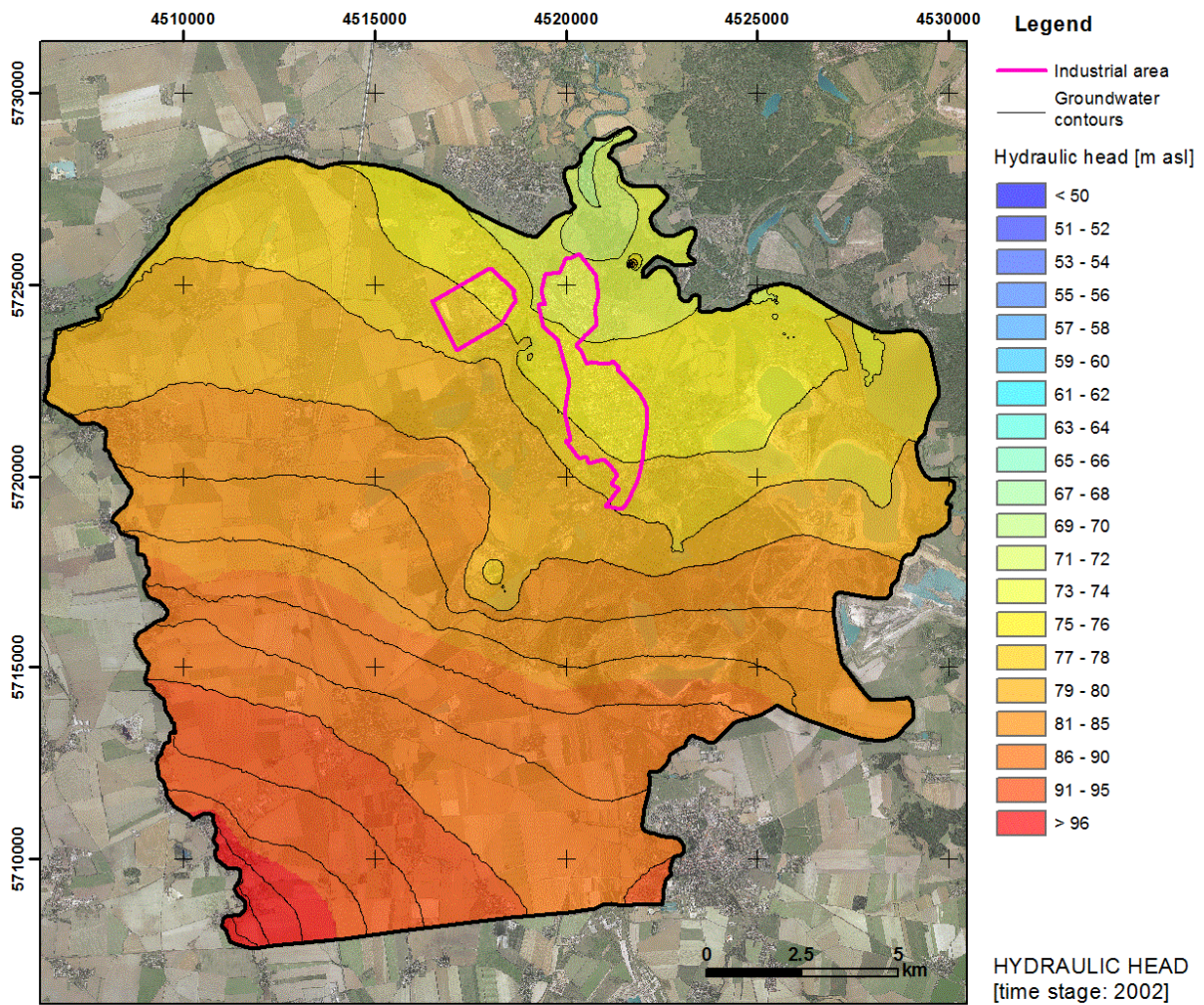
Appendix 7-8: In consequence of the national flood event in August 2002, the mining complex Goitzsche was flooded within a few days. In consequence, prior flow directions towards the southeast and east are not present anymore. Since then, an almost pre-mining groundwater situation has been formed, which is characterised by a regional groundwater flow towards the northern located Mulde river.

Appendix C   Chemical residuals of the local Lindane production

The chemical compound hexachlorocyclohexane (HCH) was synthesised first by Michael Faraday in 1825. Its insecticidal effect was noticed first in 1941/42 and is related to the specific γ-HCH isomer. Later on, according to the Dutch chemist Teunis van der Linden (1884 – 1965), it was named "Lindane". He was the first person who extracted the HCH γ-isomer from synthesised HCH in 1912.

Synthesised from using benzene that is chlorinated under UV light, the production of technical HCH and Lindane was processed in Bitterfeld from 1952 to 1982. Only 9 to 18% of pure Lindane results from the technical HCH synthesis (Appendix 7-9). By-products of the Lindane production, such as the α-isomer (in average 65%) and up to 16% of other isomers, were dumped in former open cast mines close to the industrial area of Bitterfeld-Wolfen.

Appendix 7-9: Composition of technical synthesised HCH (Thieken, 2001); beside the low outcome of the gamma isomer (Lindane), the alpha isomer resulted in a large amount from the technical HCH synthesis. These residuals were dumped multiply at prior mining areas of the Bitterfeld-Wolfen region.

Isomer	Minimal amount [%]	Maximal amount [%]	Average [%]
Alpha	55	70	65
Beta	5	14	8
Gamma	9	18	14
Delta	2	10	6
Epsilon	1	5	2

Referring to Appendix 7-10, several dump sites were identified as potential contaminant sources from data research. This includes the locations Antonie, Heideloh, Titanteich, Übergabebahnhof and Fasanenkippe. Additional sources of secondary order may exist in form of leaching production sites and large-scale plumes in groundwater.

The contamination by Lindane and related HCH products is caused by the local synthesis, the in situ application, and the deposition of chemical residuals. The upper Quaternary as well as the lower Tertiary aquifer is contaminated widely at an area of about 35 km².

Appendix 7-10: Detailed description of HCH containing deposits in the region Bitterfeld-Wolfen.

Dump site	Location description / chemical inventory
Antonie	Active open cast lignite mine until 1914; since the 1920s and until the end of the Second World War dumping of ashes and inorganic waste; 1945 to 1965 deposition of construction waste and residuals from the chemical production; 1962 to 1982 deposition of about 70.000 t of hexachlorocyclohexanes (HCH). Reference: KRAPP *et al.* (1992)
Fasanenkippe	Active open cast lignite mine from 1871 to 1930; flushing dump for industrial ashes (1930 to 1954) and temporal inlet of phenolic waters; HCH materials are deposited close to the terrain surface, especially in the eastern, northern and western part of the landfill. The dump is covered by cultivatable soil. The α-isomer and β-isomer were proven analytically from soil samples. Reference: TÜV HANNOVER/SACHSEN ANHALT E.V. (1996)
Übergabebahnhof	The contamination is characterised by about 5.500 tons of HCH containing material. From 1920s to 1960s industrial residuals such as power plant ashes (since 1918), phosphor sludge and ash, heavy metal slag, electrolysis sludge, and chloride containing residuals from the CaCl2, KCl and NaCl synthesises were dumped. From 1951 to the 1960s, α-isomers and β-isomers were deposited additionally. Reference: EISERLE (1996)
Heideloh	The landfill was created during the Köckern open-cast opening in 1987/88. The full spectrum of HCH isomers as well as DDT material was identified. The material was dumped during the period 1968 to 1970. Dumped chemicals emerged from an industrial incident at the production location. Reference: IBGW (n.d.)
Titanteich	The disposal was used as a flushing dump from 1953 to 1964. From 1961 to 1964, about 5000 t of HCH containing material were deposited. In addition, the chemical inventory includes rendition salts in liquid form, titanium, heavy metals, construction waste, and calcium-sulphates. The area was remediated in 2005. Reference: BERTHOLD *et al.* (1996)
Spittelwasser creek	Up to 1000 mg/kg had been detected near its riverbank which is caused by an inlet of industrial waters. Water from industrial HCH production has been discharge into the Spittelwasser/Mulde river system until 1982. Thus, the riverbank constitutes a typical secondary order contamination source. Reference: HILLE *et al.* (1992)
Industrial sewage water system	Industrial waters from chemical production had been piped from industrial areas into surrounding running waters. Interactions of the surface water system and the groundwater are most likely.

Appendix D   Header data of reference data points of the local monitoring network Bitterfeld-Wolfen

Appendix 7-11: Selected groundwater observation wells of the local monitoring network Bitterfeld-Wolfen were assigned to the transport model in form of reference data points. Therefore, specific spatial coordinates and related screen level elevation were considered. In vertical scale, the reference point is attributed to a numerical model layer in respect to its screen level.

Name	X-Coordinate	Y-Coordinate	Elevation	Screen [bottom]	Model layer	Aquifer unit
AUS02	4520733.0	5721652.0	77.95	71.45	4	Q
Br203	4520442.0	5723237.0	76.70	68.70	7	Q
BRI05	4522826.0	5718862.0	76.60	71.60	4	Q
BSZB2	4520830.0	5721308.0	79.16	73.01	4	Q
BVV011	4521794.9	5721368.1	78.90	67.44	13	Q
BVV0281	4521447.2	5721070.9	79.40	60.19	19	Q
BVV035	4520937.0	5720663.0	80.50	65.36	19	Q
BVV1230	4521168.2	5720229.3	79.80	68.80	19	Q
BVV132	4520806.0	5721981.0	78.60	63.93	19	Q
BVV251	4520163.0	5722886.0	78.21	70.11	16	Q
BVV284	4519361.8	5721917.6	91.10	73.50	19	Q
BVV3800	4519642.7	5722453.6	87.15	76.15	22	Q
BVV541	4521486.5	5720209.5	79.80	59.80	25	Q
BVV589	4522210.4	5720539.4	79.20	71.20	7	Q
BVV626	4522164.2	5719748.0	78.47	63.44	22	Q
BVV644	4520629.2	5722326.8	78.17	71.77	4	Q
BVV6590	4520179.9	5721689.6	80.64	73.64	22	Q
BVV6600	4520023.3	5722467.8	83.05	72.35	25	Q
BVV712	4520696.3	5722695.8	77.30	60.30	19	Q
BVV720	4521180.1	5722385.9	78.60	65.60	19	Q
BVV762	4520908.4	5723038.3	76.50	70.50	4	Q
BVV7810	4521622.4	5720821.0	80.10	63.10	19	Q
LK350	4523448.9	5719367.1	81.80	75.80	16	Q
SAF21	4521709.0	5719757.0	79.41	64.41	25	Q

Appendix E   Mass distribution patterns of the virtual multi-source contamination scenario Bitterfeld-Wolfen (simulation period 1955–2002)
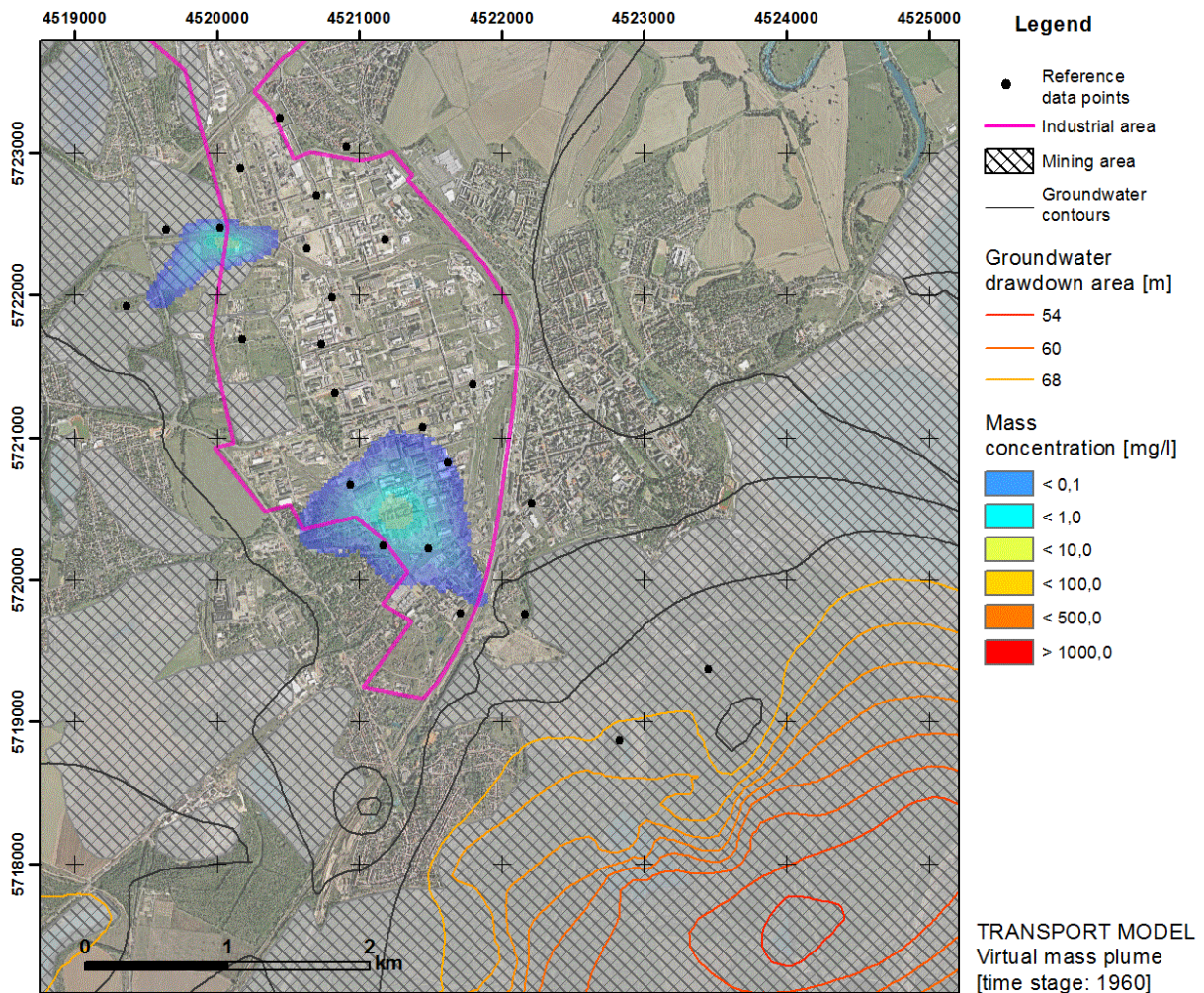
Appendix 7-12: At the beginning of contaminant transport, two mass sources were assigned to the model. The southern input area characterises a surface leaching from a production site, the northern location characterised pollutant discharge from a landfill. Mining related drawdown was situated in the south/southeast of both source areas. In 1960, the plume shape indicates a south-western/south-eastern oriented solute transport direction.
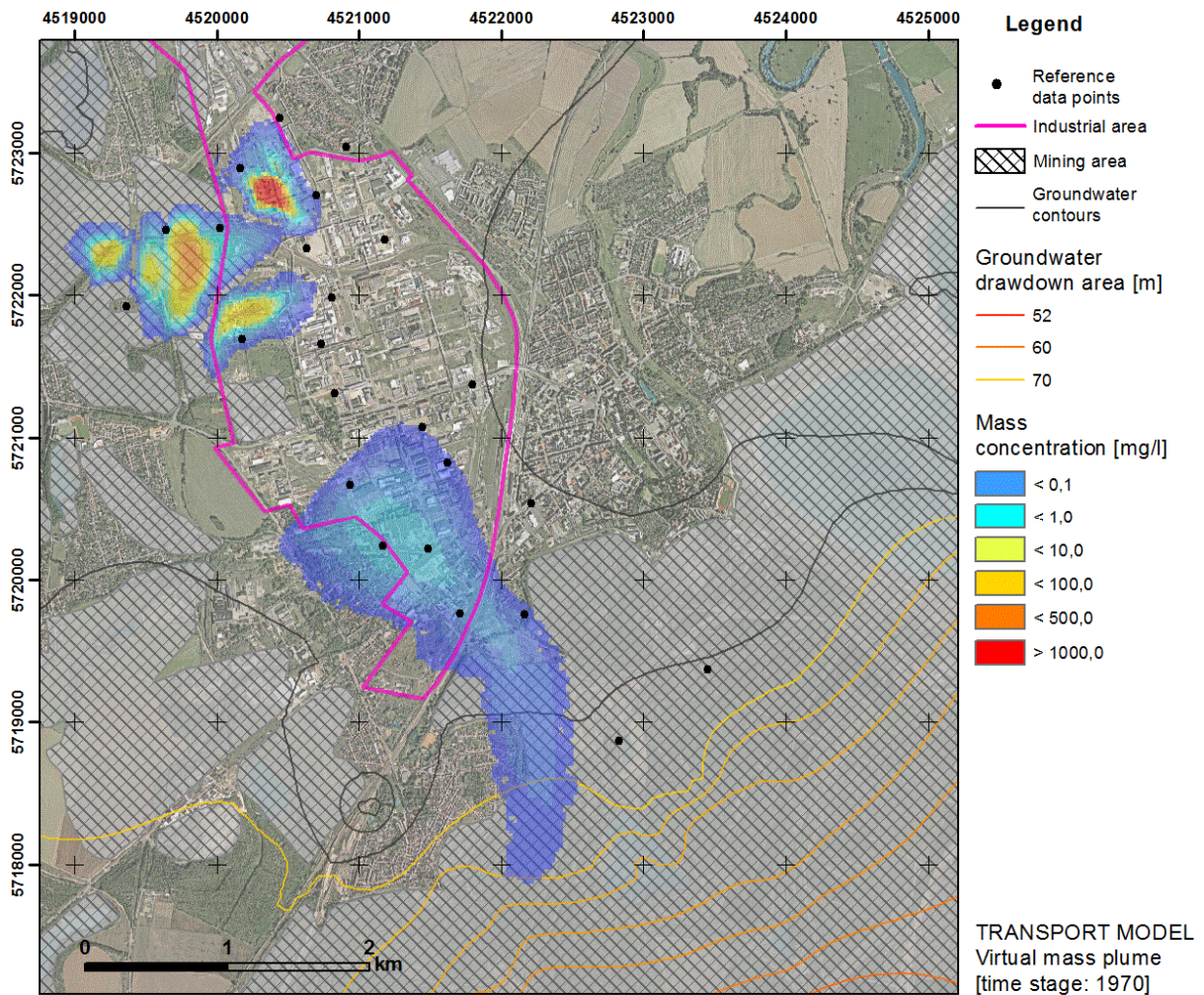
Appendix 7-13: Between 1960 and 1970, further mass sources were added to the transport model in the north. The southern plume spread significantly towards the southern located drawdown area of the mining area "Holzweißig West". Individual plumes emerged from multiple pollution sources in the north.
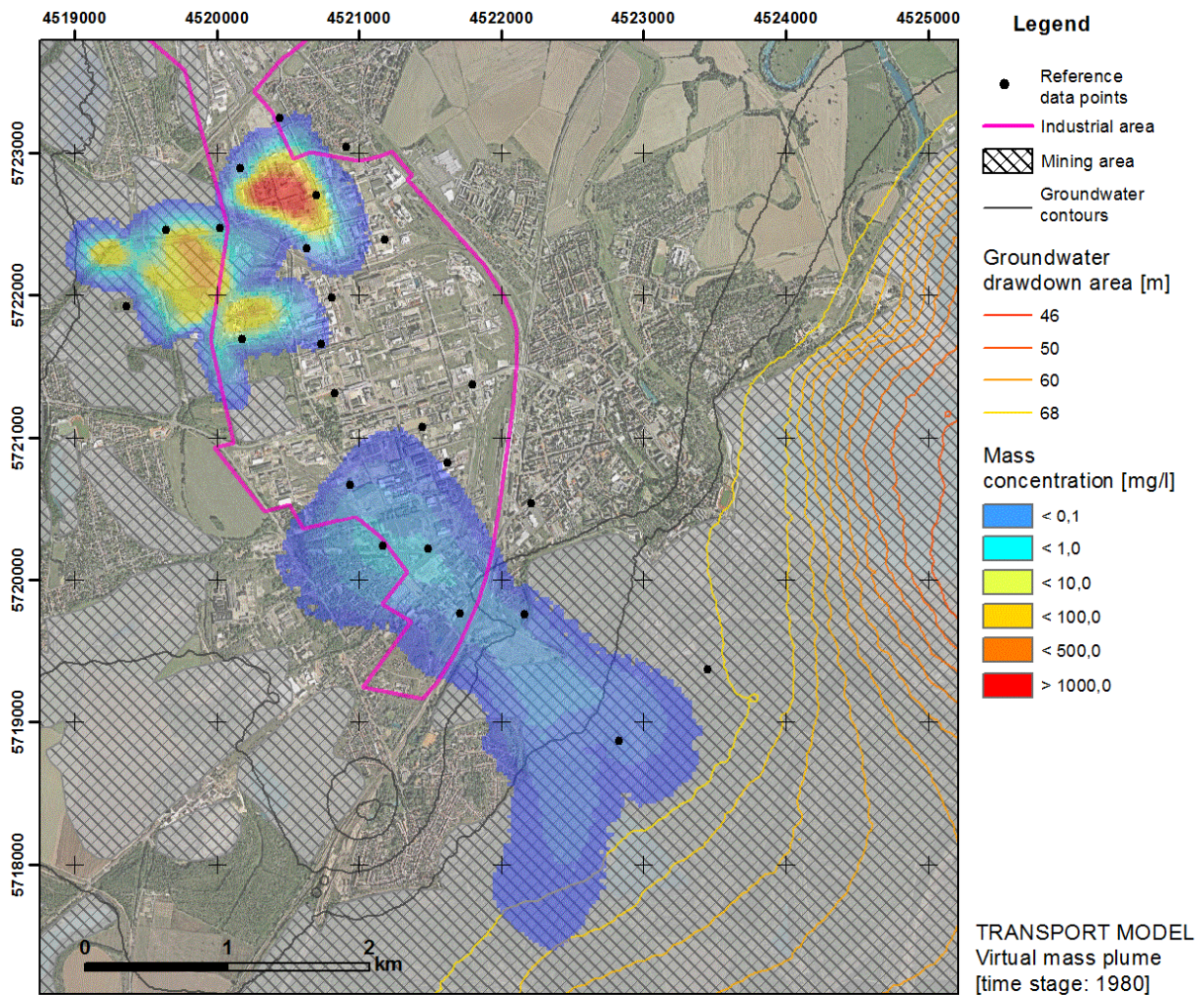
Appendix 7-14: In year 1980, simulated solute transport is characterised by increasing distribution patterns, spreading towards the southeast. The tail of the southern plume indicates an additional transport direction towards the east that is induced by additional groundwater lowering in the open cast mines of the Goitzsche complex.
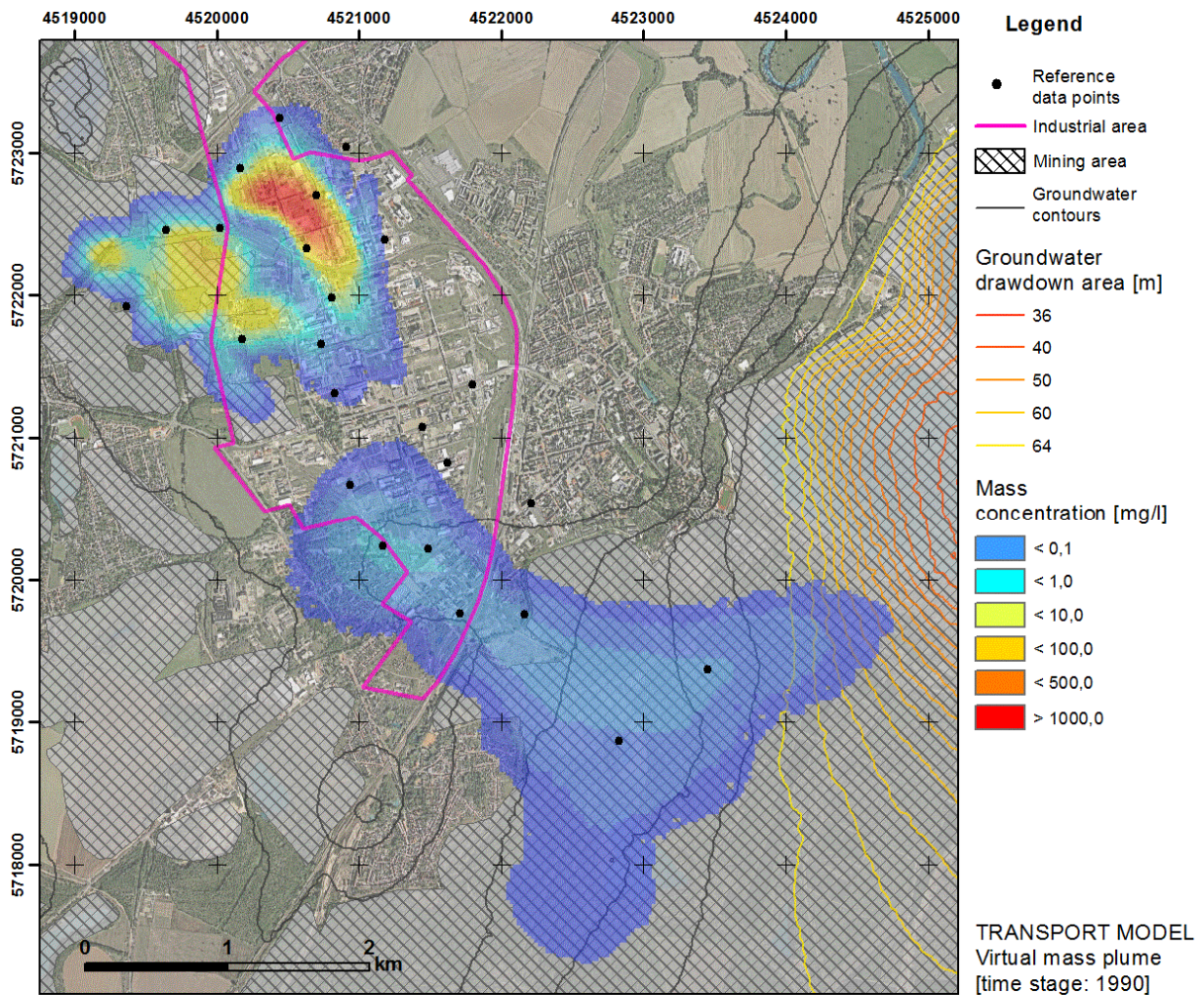
Appendix 7-15: Between 1980 and 1990, northern plumes merged and the predominant contaminant discharge is oriented towards the south/southeast. The southern mass distribution indicates a clear transport pathway in eastern direction. Until 1990, the solute of source location no. 1 exceeded a transport distance of app. 3000 m.
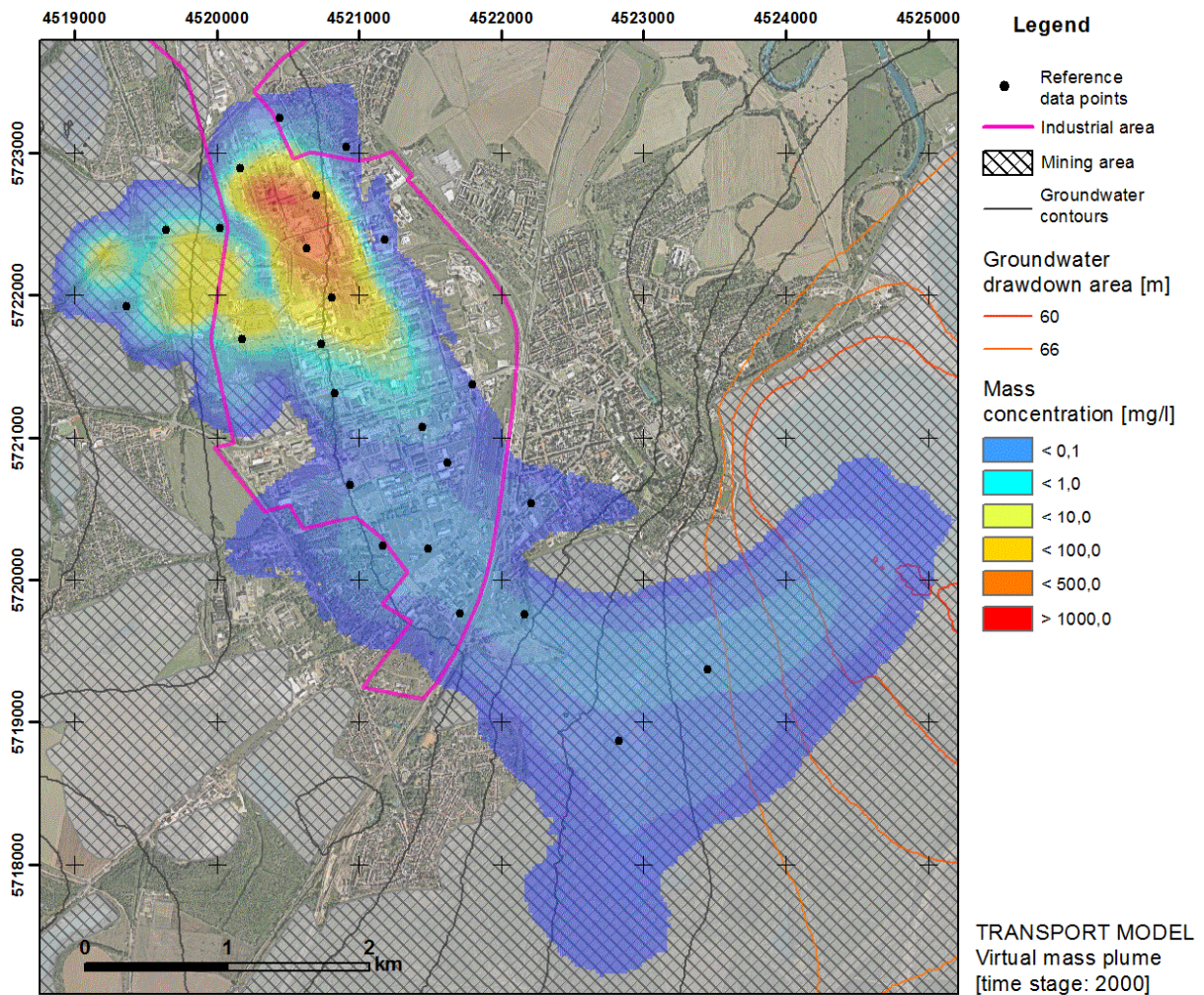
Appendix 7-16: During the total simulation time of about 50 years, mass plumes of multiple source locations merged to a single solute mass distribution pattern. The predominant direction of transport was oriented permanently towards the main drawdown areas in the south, southeast and east. Contaminant discharge reached widely into the Goitzsche mining area.
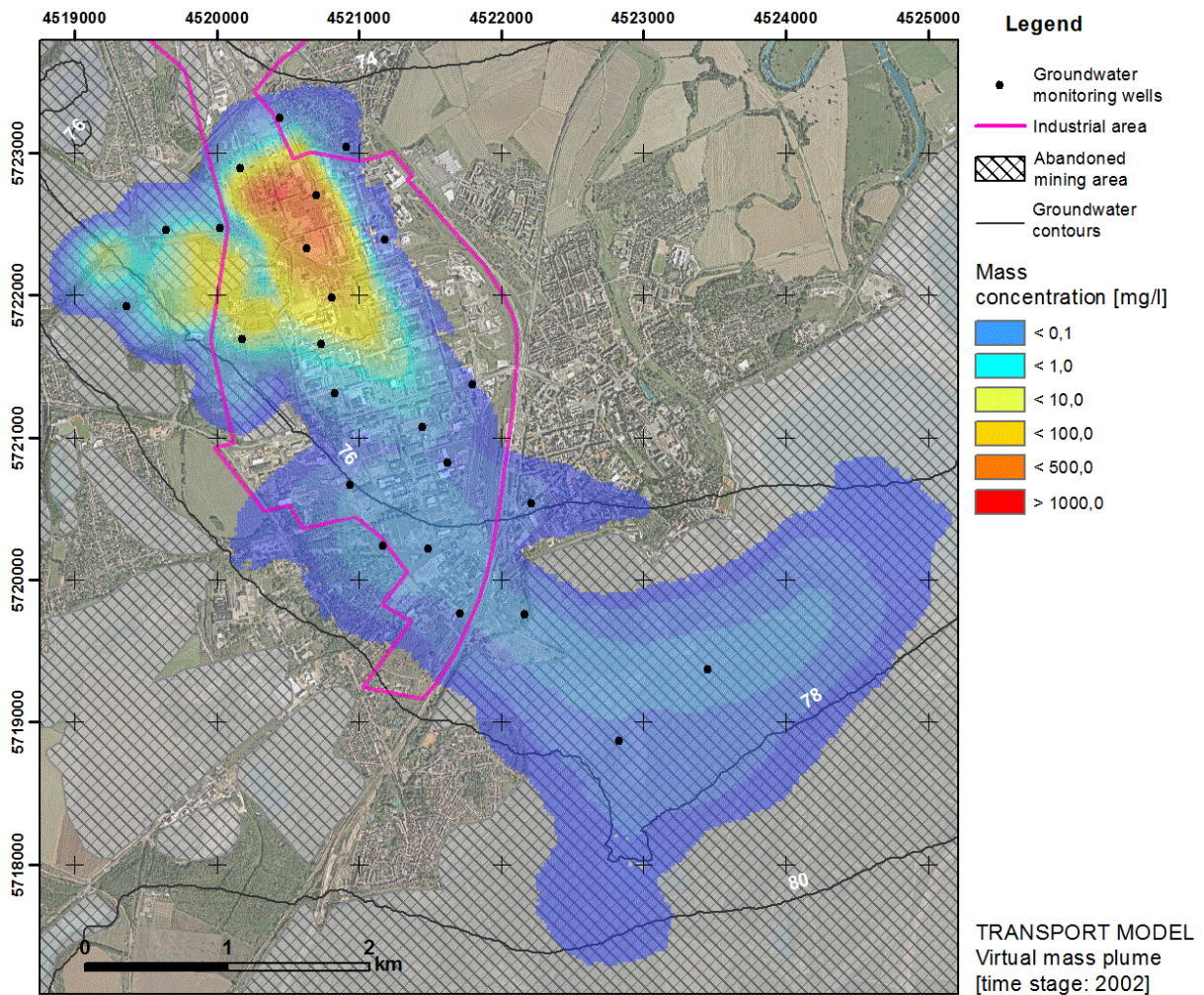
Appendix 7-17: After a simulation of 50 years, the mass distribution pattern implies a predominant transport direction towards the south and southeast. Individual mass plumes joined and the tracer was dragged deeply into prior mining related drawdown areas. After the flood event in August 2002, the groundwater flow situation changed to almost pre-mining conditions. A general transport direction towards the north is expected.

Appendix F   Breakthrough curves of selected reference data points of the local groundwater monitoring network
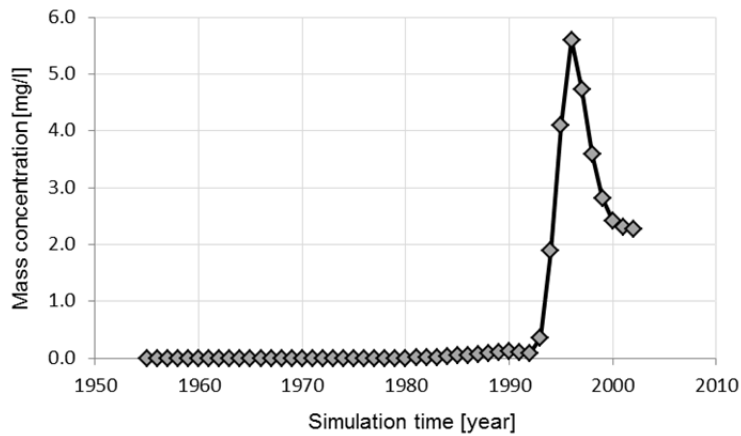
Appendix 7-18: Breakthrough curve of the reference point AUS02.Arrival time: 9125 [d]; maximum mass peak of 5.6 mg/l after 14965 [d].
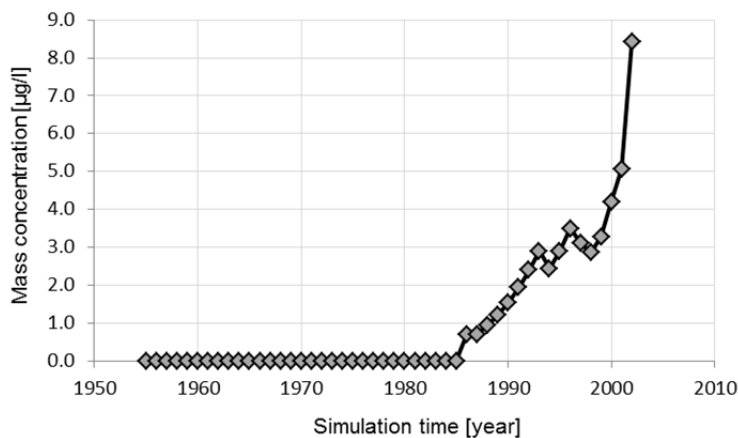
Appendix 7-19: Breakthrough curve of the reference point Br203. Arrival time: 11315 [d]; maximum mass peak of 0.0084 mg/l after 17155 [d].
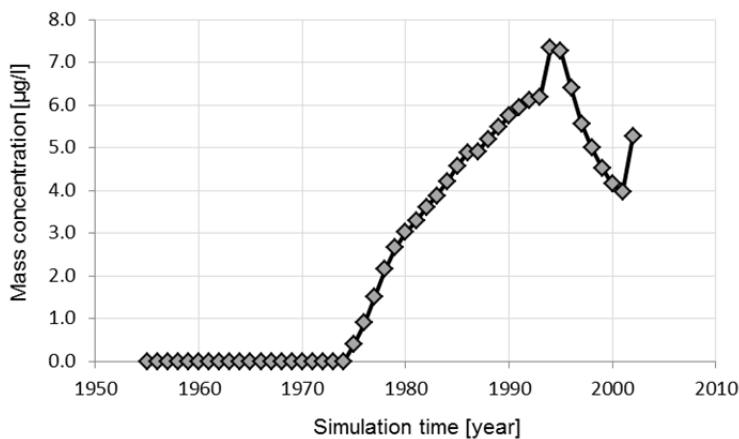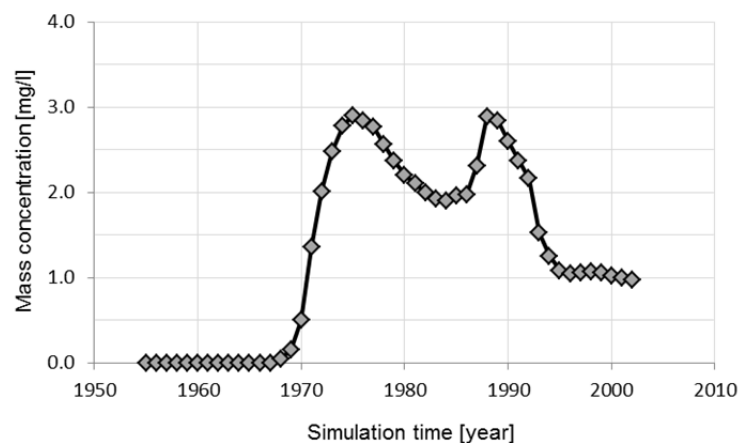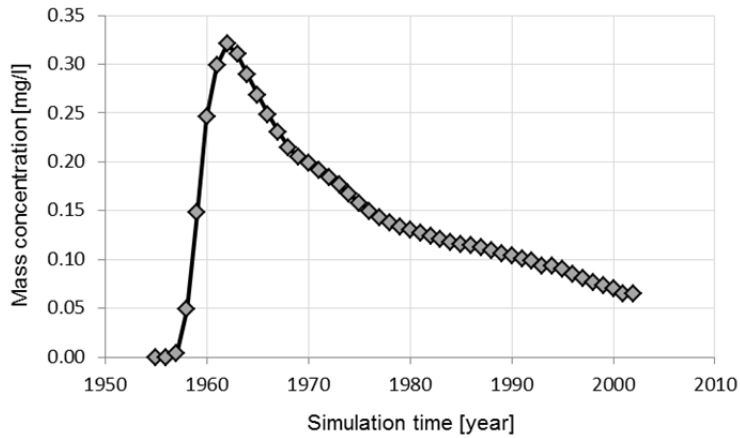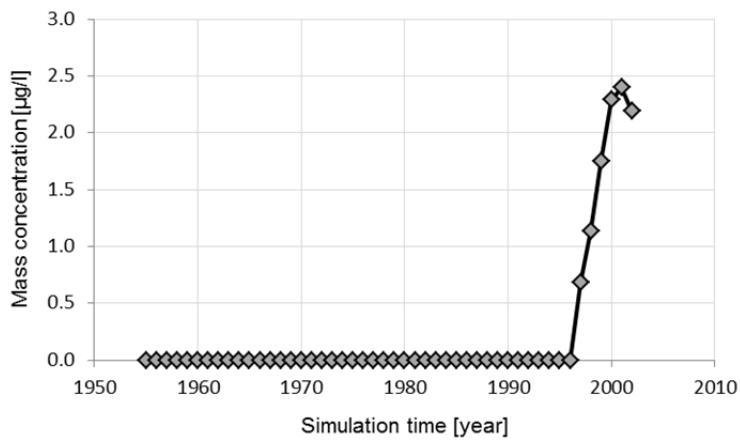

Appendix 7-20: Breakthrough curve of the reference point BRI05. . Arrival time: 7665 [d]; maximum mass peak of 0.0073 mg/l after 14235 [d].
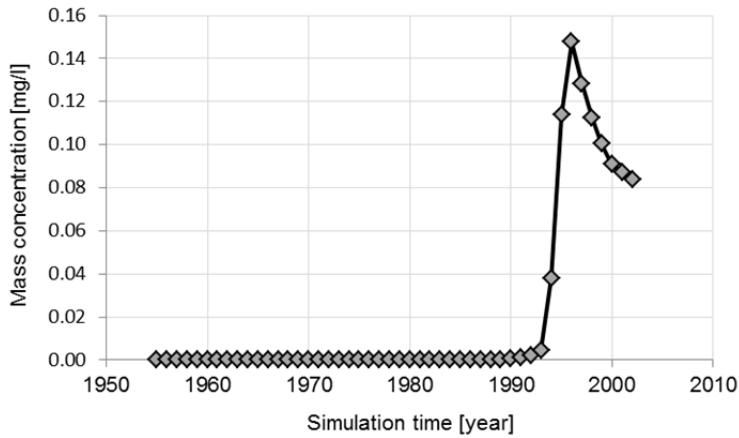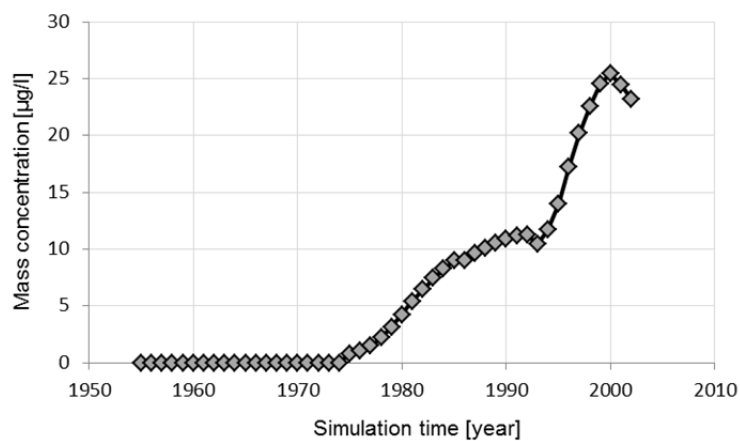
Appendix 7-21: Breakthrough curve of the reference point BZB2. Arrival time: 12775 [d]; maximum mass peak of 0.148 mg/l after 14965 [d].
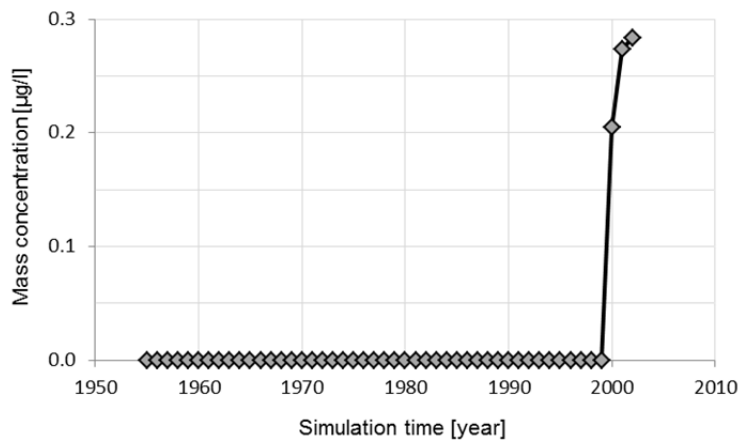
Appendix 7-22: Breakthrough curve of the reference point BVV011. Arrival time: 16425 [d]; maximum mass peak of 0.00028 mg/l after 17155 [d].
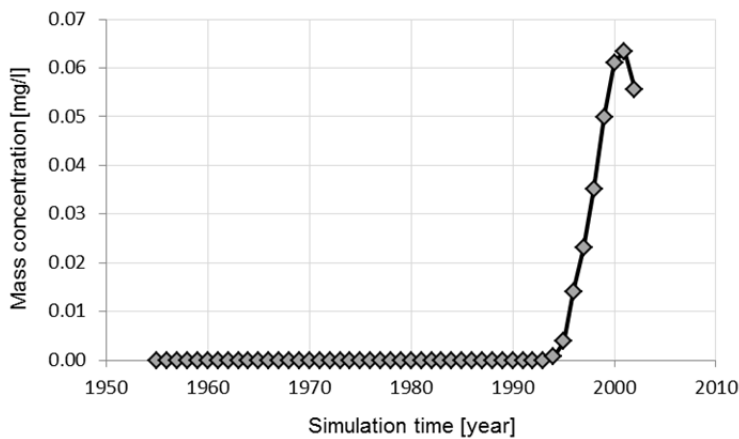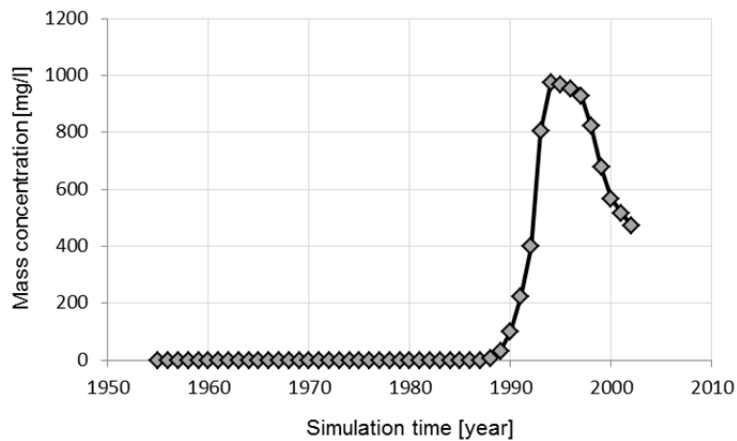

Appendix 7-23: Breakthrough curve of the reference point BVV0281. Arrival time: 14235 [d]; maximum mass peak of 0.063 mg/l after 16790 [d].
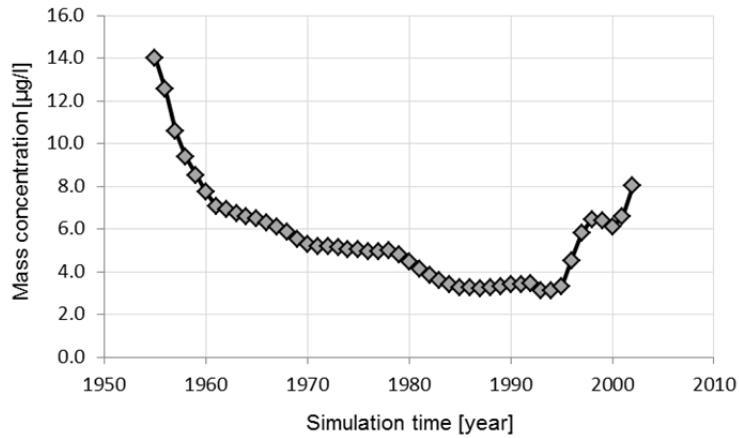
Appendix 7-24: Breakthrough curve of the reference point BVV035. Arrival time: 365 [d]; maximum mass peak of 0.014 mg/l after 730 [d].
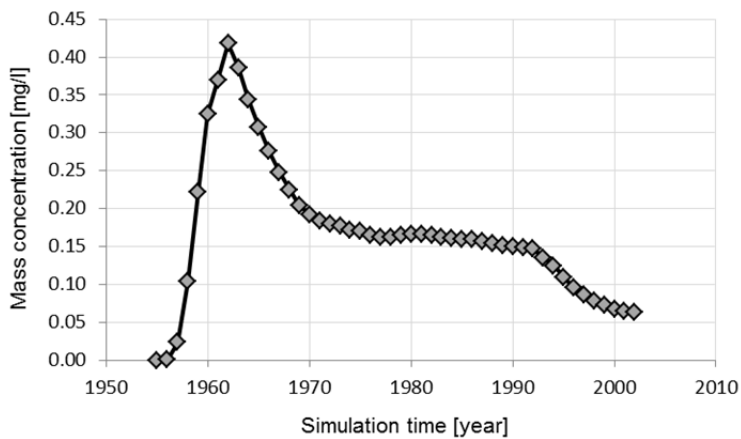
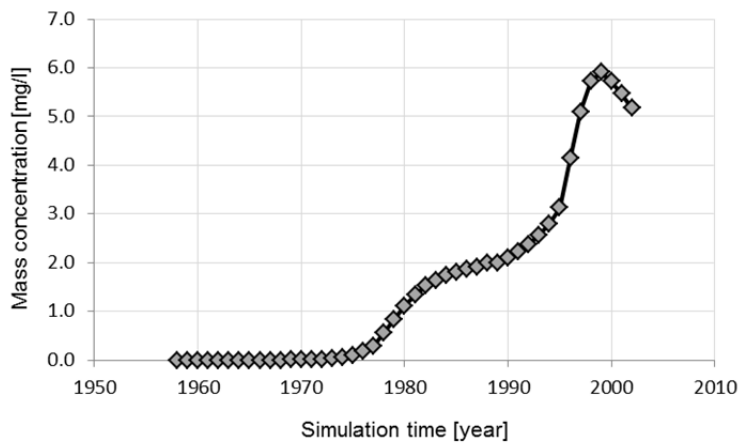*Appendix 7-25: Breakthrough curve of the reference point BVV1230. Arrival time: 730 [d]; maximum mass peak of 0.418 mg/l after 2555 [d].*
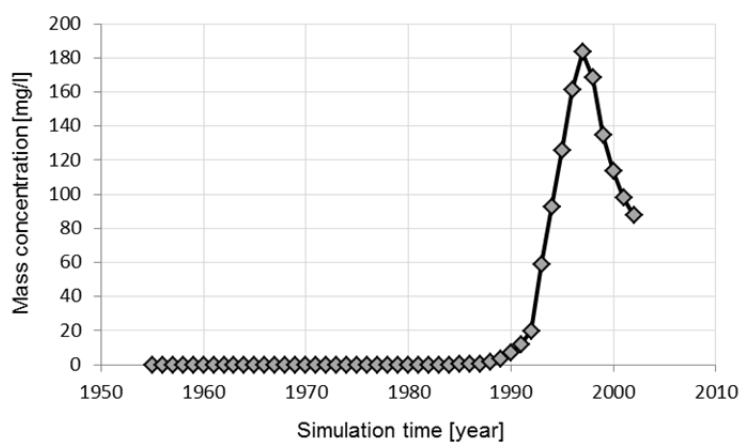
Appendix 7-26: Breakthrough curve of the reference point BVV132. Arrival time: 10585 [d]; maximum mass peak of 183.4 mg/l after 15330 [d].
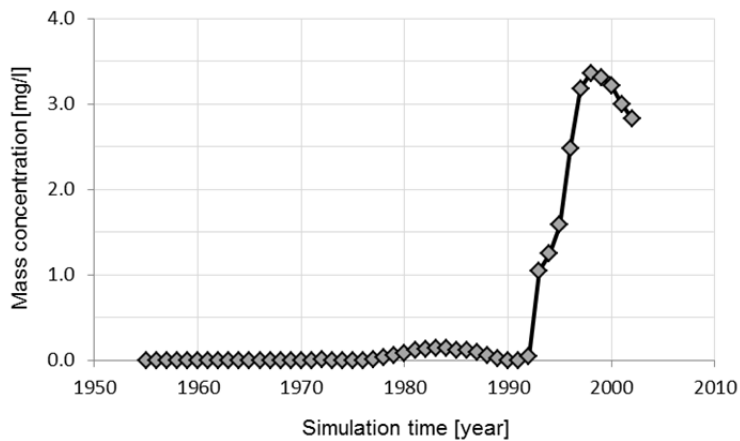
Appendix 7-27: Breakthrough curve of the reference point BVV251. Arrival time: 8030 [d]; maximum mass peak of 3.35 mg/l after 15695 [d].
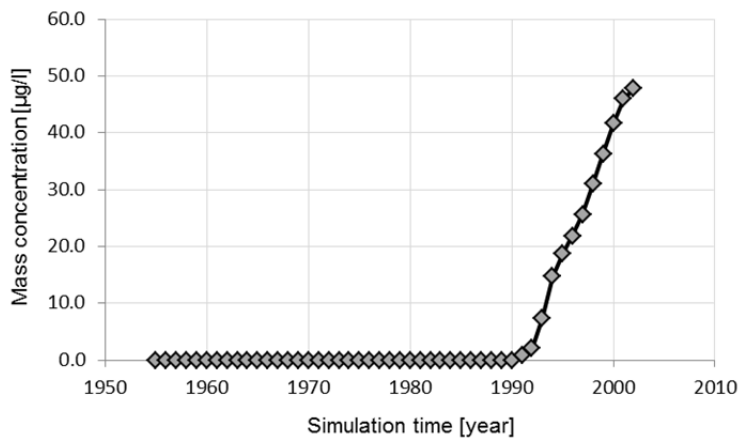
Appendix 7-28: Breakthrough curve of the reference point BVV284. Arrival time: 13140 [d]; maximum mass peak of 0.048 mg/l after 17155 [d].

Appendix 7-29: Breakthrough curve of the reference point BVV3800. Arrival time: 4745 [d]; maximum mass peak of 2.90 mg/l after 7300 [d].

Appendix 7-30: Breakthrough curve of the reference point BVV541. Arrival time: 1095 [d]; maximum mass peak of 0.32 mg/l after 2555 [d].

Appendix 7-31: Breakthrough curve of the reference point BVV589. Arrival time: 15330 [d]; maximum mass peak of 0.024 mg/l after 16790 [d].

Appendix 7-32: Breakthrough curve of the reference point BVV626. Arrival time: 7300 [d]; maximum mass peak of 0.025 mg/l after 16425 [d].
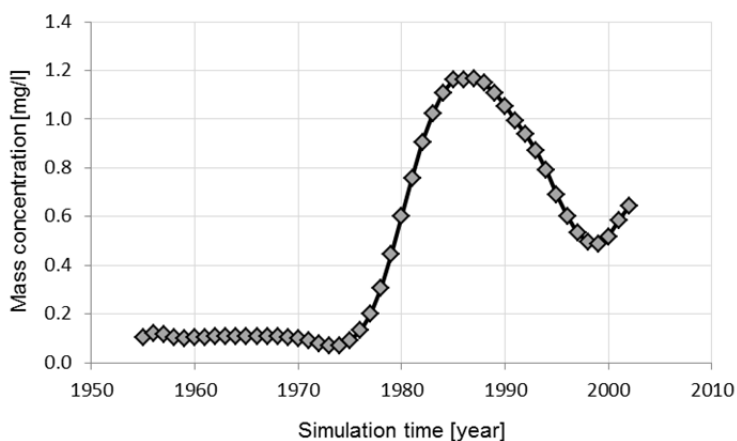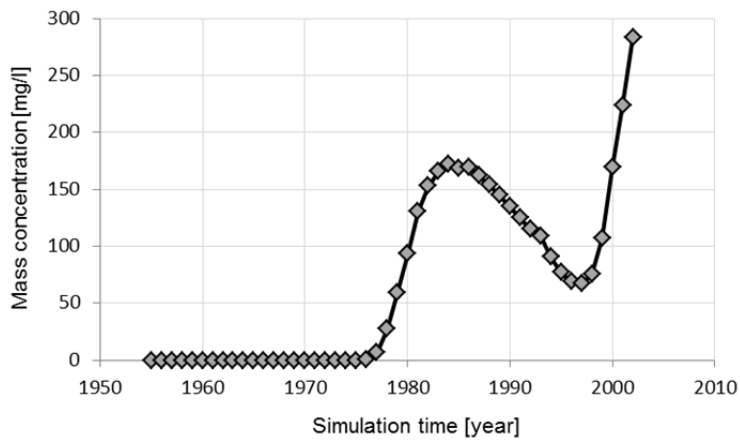
Appendix 7-33: Breakthrough curve of the reference point BVV644. Arrival time: 7300 [d]; maximum mass peak of 972.84 mg/l after 15330 [d].

Appendix 7-34: Breakthrough curve of the reference point BVV6590. Arrival time: 3285 [d]; maximum mass peak of 5.91 mg/l after 14965 [d].
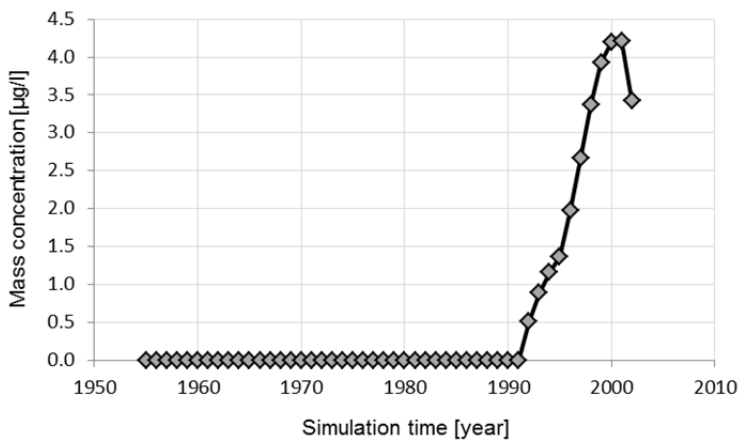

Appendix 7-35: Breakthrough curve of the reference point BVV6600. Arrival time: 365 [d]; maximum mass peak of 1.17 mg/l after 11680 [d].
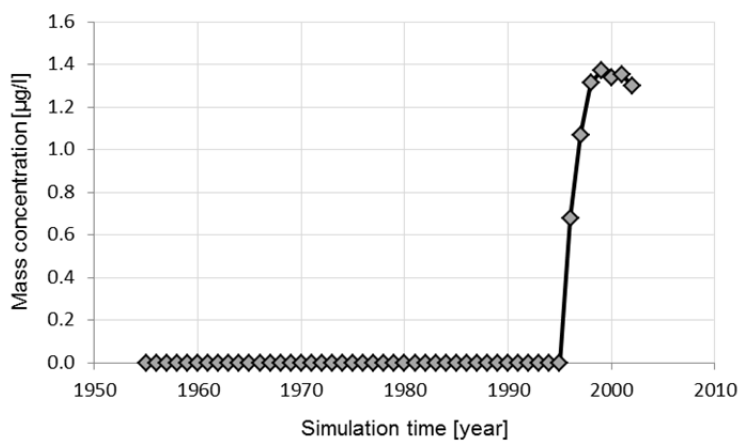
Appendix 7-36: Breakthrough curve of the reference point BVV712. Arrival time: 7665 [d]; maximum mass peak of 283.6 mg/l after 17155 [d].
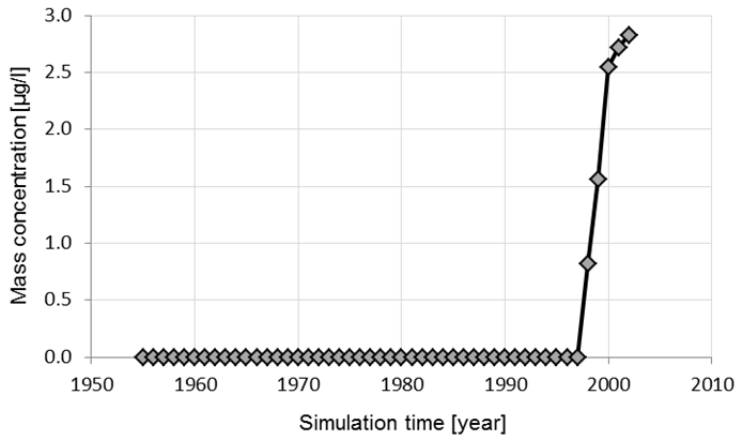

Appendix 7-37: Breakthrough curve of the reference point BVV720. Arrival time: 13505 [d]; maximum mass peak of 0.0042 mg/l after 16790 [d].
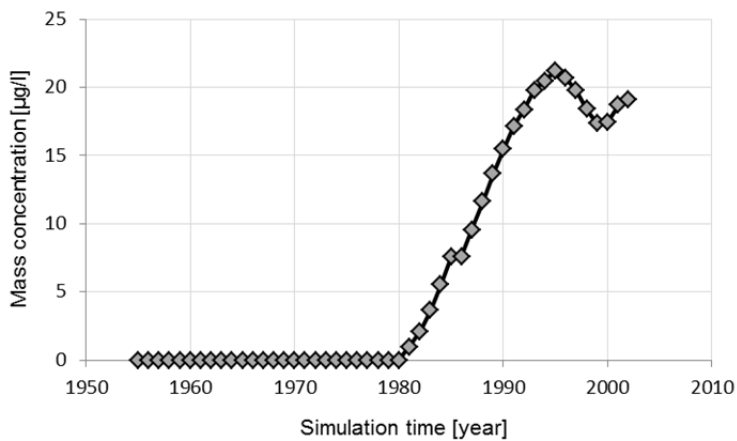

Appendix 7-38: Breakthrough curve of the reference point BVV762. Arrival time: 15695 [d]; maximum mass peak of 0.0014 mg/l after 16060 [d].
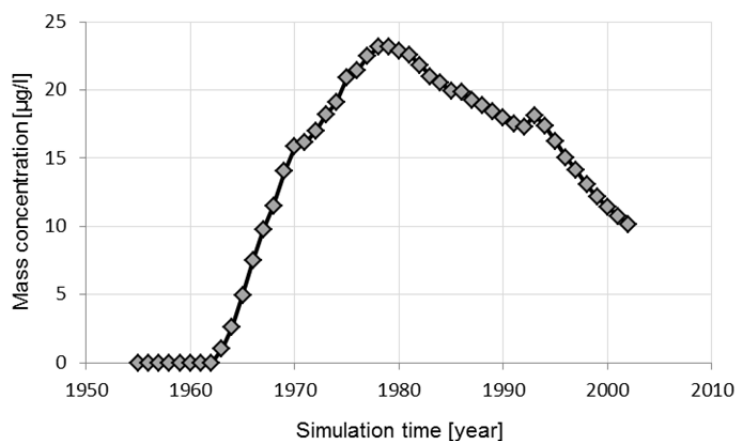
Appendix 7-39: Breakthrough curve of the reference point BVV7810. Arrival time: 15695 [d]; maximum mass peak of 0.0028 mg/l after 17155 [d].

Appendix 7-40: Breakthrough of the reference point LK350. Arrival time: 9490 [d]; maximum mass peak of 0.021 mg/l after 14600 [d].

Appendix 7-41: Breakthrough curve of the reference point SAF21. Arrival time: 2920 [d]; maximum mass peak of 0.023 mg/l after 8395 [d].

Personal Information

Name	Reiner Stollberg
Date of birth	05-12-1981
Place of birth	Bitterfeld-Wolfen
Gender	masculine
Nationality	German
Address	Arndtstraße 30 B, D-04275 Leipzig, Germany
Correspondence address	Puschkinstraße 37, D-06749 Bitterfeld-Wolfen, Germany

Professional Career

Since 2011	*Helmholtz Centre for Environmental Research – UFZ, Leipzig* Research assistant at the Department Groundwater Remediation
2006 – 2008	*Ingenieurbüro für Grundwasser GmbH – IBGW, Leipzig* Project manager / Research assistant

Education

2008 - 2013	*Martin Luther University Halle-Wittenberg, Halle (Saale)* *Institute for Geosciences and Geography* HIGRADE Scholarship holder – PhD Student Area of expertise: Hydro- and Environmental Geology
2001 – 2006	*University of Leipzig, Inst. for Geophysics and Geology* Subject of study: Geology/Palaeontology Degree: Dipl.-Geol.

Military/Civilian Service

2000 – 2001

School Education

1992 – 2000	Europagymnasium " Walter Rathenau", Bitterfeld Graduate: Allgemeine Hochschulreife
1998 – 1992	Grundschule Anhaltsiedlung, Bitterfeld

Reiner Stollberg